Seafloor seepage in the Black Sea: Mud volcanoes, seeps and diapiric structures imaged by acoustic methods

Dissertation

zur Erlangung des
Doktorgrades der Naturwissenschaften
(Dr. rer. Nat.)

im Fachbereich Geowissenschaften
der Universität Bremen

vorgelegt von
Michelle Wagner-Friedrichs

Bremen, Januar 2007

Gutachter:

Herr Prof. Dr. Volkhard Spieß
Herr Prof. Dr. Gerhard Bohrmann

Termin des Dissertationskolloquiums:

8.3.2007, 16:00 c.t.

Titel des Dissertationskolloquiums:

Seafloor seepage along continental margins: Examples from the Black Sea
(Fluidaustritte an Kontinentalhängen: Beispiele aus dem Schwarzen Meer)

Abstract

The Black Sea is the largest anoxic basin in the world. Organic matter deposited at the continental slopes leads to high gas concentrations within the sediments. Compressive deformation at the margins of the Black Sea due to the collision of Arabia and Eurasia during the Eocene, in combination with a thick sediment coverage forces over-pressured fluids and upward fluid migration towards the seafloor, which is expressed by abundant seafloor seepage along the continental slopes of the Black Sea. Two areas in the Black Sea, the Sorokin Trough (offshore Crimea) and the continental slope offshore Batumi (Georgia) were investigated with high resolution multichannel seismic and additional acoustic data in order to study the distribution, structure and evolution of mud volcanoes and gas seeps and their relation to fluid migration pathways and gas and gas hydrate occurrences in the subsurface. The data of the Sorokin Trough were collected during the Meteor cruise M52/1 and include a 3D seismic dataset across the Sevastopol mud volcano. Offshore Batumi high resolution multichannel seismic data were acquired during the TTR-15 cruise (UNESCO Training Through Research Program).

In the Sorokin Trough, north-south oriented compressive deformation leads to the protrusion of diapiric structures and facilitates fluid/gas migration towards the seafloor, resulting in a large number of mud volcanoes above the diapirs. In total, 25 mud volcanoes with great morphological variability were identified on the seismic data. The mud volcanoes are grouped in three areas of different geological setting, which influences the evolution of the individual mud volcanoes and hence their morphology. Generally, the evolution of the mud volcanoes could be linked to fluid migration along faults developed during the diapiric uplift. In the western Sorokin Trough, low permeability hemipelagic sediments inhibit vertical fluid migration. Seals lead to over-pressured fluids, forcing violent eruptions and forming the collapsed structures common in this area. The homogeneous fan deposits of the Palaeo Don-Kuban Fan in the central and eastern Sorokin Trough are characterized by increased permeability resulting in quiet effusive mud extrusions, reflected by cone-shaped structures. These mud volcanoes partly reach enormous dimensions with diameters up to 2000 m and heights of about 100 m where faults with large offsets allow high mud flow rates.

The new 3D seismic dataset collected during Cruise M52/1 in the Sorokin Trough images the detailed spatial geometry of the collapsed Sevastopol mud volcano and its relationships to diapiric ridges and fluid migration pathways. The seismic data show that the evolution of the Sevastopol mud volcano is related to a diapiric structure with two ridges located beneath the mud volcano. Upward fluid migration is concentrated along a deep fault system, which developed during the growth of the diapiric ridges in a compressional tectonic regime. An initial explosive eruption due to over-pressured fluids generated the collapsed depression of the Sevastopol mud volcano. Several cones observed inside of the

depression were formed by subsequent quiet mud extrusions. High amplitude reflections (Bright Spots) located above one of the diapiric ridges in the direct vicinity to the feeder channel indicate the presence of gas and gas hydrates controlled by focused fluid flow nearby the mud volcano. Bright Spots occur at constant depth, which coincidences with the approximate depth of the base of gas hydrate stability zone (BGHSZ). Therefore, the Bright Spots are interpreted to represent the phase boundary between gas and gas hydrates. Variable fluid flow might lead to temperature variations at the BGHSZ, explaining small depth variations of the Bright Spots. A continuous BSR is not imaged on the data, suggesting either that gas and gas hydrates form locally where fluid flow is focused, as e.g. in the surrounding of mud volcanoes, or that fluid flow is episodically, which would inhibit the formation of a BSR.

The continental slope of Batumi is characterized by a complex E-W trending canyon-ridge system. Numerous gas seeps occur on the top or flanks of ridge structures in water depths of 850-1200 m. In contrast to the Sorokin Trough, the seeps off Batumi are not related to major material upflow. The largest and most active seep is the Batumi Seep located on the Kobuleti Ridge in the central study area. High amplitude reflection patches beneath the surface of the seep indicate massive gas hydrate deposits formed as a result of focused fluid flow. Upward fluid migration at the Batumi Seep is related to faults. Generally, gas seeps off Batumi are associated with shallow gas accumulation, indicated by Bright Spots. A BSR, limited to the Kobuleti Ridge in the area of the Batumi Seep, occurs at abnormal great depth, which could be explained by low salinity pore water of 15‰. The protrusion of diapirs beneath the ridges controls the fluid migration pathways towards the top. Depressions between growing diapirs acted as preferred pathways for turbidity currents, which eroded the deeply incised canyons between the ridges.

Zusammenfassung

Das Schwarze Meer ist das größte anoxische Becken der Welt. Die Ablagerung organischen Materials an den Kontinentalhängen führt zu hohen Gaskonzentrationen in den Sedimenten. Aufgrund der Kollision der arabischen mit der eurasischen Platte im Eozän sind die Ränder des Schwarzen Meeres durch kompressionstektonische Deformation geprägt. In Kombination mit den mächtigen Sedimentablagerungen im Schwarzen Meer führt dies zu unter Überdruck stehenden Fluiden und begünstigt Fluidaufstieg zum Meeresboden. Als Folge existieren zahlreiche Fluidaustrittstellen, so genannte Seeps, an den Kontinentalhängen des Schwarzen Meeres. Zwei Gebiete im Schwarzen Meer, der Sorokin Trog südöstlich der Krim und der Kontinentalhang vor Batumi (Georgien), wurden intensiv mittels hochauflösender Mehrkanalseismischer und hydroakustischer Daten untersucht. Ziel der Messungen ist die Untersuchung der Verteilung, Struktur und Entwicklung von Schlammvulkanen und Gas Seeps. Weiterhin soll die Beziehung zwischen Seeps und Schlammvulkanen an der Oberfläche zu Fluidmigrationswegen, Gas and Gashydratvorkommen im Untergrund analysiert werden. Seismische Daten im Sorokin Trog inklusive eines 3D seismischen Datensatzes im Bereich des Sevastopol Schlammvulkans wurden während der Meteor-Fahrt M52/1 aufgezeichnet. Der hochauflösende Mehrkanalseismische Datensatz am Kontinentalhang vor Batumi wurde während der TTR-15 Fahrt aufgezeichnet (UNESCO Training Through Research Program).

N-S gerichtete Kompressionstektonik führt im Sorokin Trog zum Aufstieg W-E streichender Diapirrücken und fördert Fluidaufstieg zum Meeresboden, der sich in der Entstehung von Schlammvulkanen oberhalb der Diapire äußert. In den seismischen Daten wurden insgesamt 25 Schlammvulkane identifiziert, die eine große morphologische Variabilität aufweisen. Das Auftreten der Schlammvulkane im Sorokin Trog konzentriert sich auf drei Gebiete. Die unterschiedlichen sedimentologischen und geologischen Rahmenbedingungen in diesen Gebieten haben einen direkten Einfluss auf die Entstehungsmechanismen der Schlammvulkane und somit auch auf ihre Morphologie. Die Entstehung der Schlammvulkane ist an Fluidaufstieg entlang von Störungen gebunden, die während des Diapiraufstiegs entstanden sind. Im westlichen Sorokin Trog herrschen hemipelagische Sedimente vor, die nur geringen vertikalen Fluidaufstieg zulassen. Impermeable Lagen bilden häufig Fallen für Gas. Dadurch kommt es zur Bildung unter Überdruck stehende Fluide, die bei explosionsartigen Eruptionen schlagartig freigesetzt werden. Explosionsartige Eruptionen führen zu den Kollapsstrukturen am Meeresboden, die in diesem Gebiet vorherrschen. Die homogenen Fächersedimente im zentralen und östlichen Sorokin Trog weisen eine höhere Permeabilität auf und ermöglichen effusive Schlammextrusionen. Dies äußert sich in der Bildung kegelförmiger Schlammvulkane, die

im Bereich großer Störungen Kegel mit Durchmessern bis 2000 m und einer Höhe bis 100 m bilden.

Anhand des während der M52/1 Fahrt im Sorokin Trog aufgezeichneten 3D Datensatzes kann die dreidimensionale Struktur des Sevastopol Schlammvulkan detailliert dargestellt und in Bezug zu den Untergrundstrukturen gesetzt werden. Der Sevastopol Schlammvulkan liegt oberhalb einer Diapirstruktur mit zwei Diapirrücken. Fluidmigration entlang eines komplexen Störungssystems, das durch den Diapiraufstieg zwischen den Diapirrücken entstanden ist, kontrolliert die Entwicklung des Schlammvulkans. Die Entstehung der Kollapsstruktur lässt sich durch einen explosiven Ausbruch durch unter Überdruck stehender Fluide erklären. Nachfolgende Schlammextrusionen führten zur Bildung mehrerer Kegel innerhalb der Kollapsstruktur. Bright Spots oberhalb einer der Diapirrücken in direkter Nähe zum Förderkanal des Schlammvulkans weisen auf Gas und Gashydratvorkommen hin, die sich aufgrund des fokussierten Fluidflusses im Bereich des Förderkanals gebildet haben. Die Bright Spots liegen in relativ konstanter Tiefe unterhalb des Meeresbodens annähernd in der theoretisch berechneten Tiefe der Basis der Gashydratstabilitätszone (BGHSZ). Die Bright Spots stellen vermutlich die Phasengrenze zwischen freiem Gas und Gashydraten dar. Tiefenvariationen der Bright Spots können durch Temperaturänderungen infolge von variablem Fluidfluß erklärt werden. Das Fehlen eines BSR kann entweder bedeuten, dass Gas und Gashydrate lokal gebildet werden, wo fokussierter Fluidfluß auftritt, z.B. in der Umgebung von Schlammvulkanen, oder dass es aufgrund episodischen Fluidflusses nicht zur Bildung eines BSR kommt.

Der Kontinentalhang bei Batumi ist morphologisch von einem komplexen W-E streichenden Canyon- und Rückensystem geprägt. Mehrere Gas Seeps treten am Top oder an den Flanken der Rückenstrukturen in 850-1200 m Wassertiefe auf. Diapiraufstieg unterhalb der Rücken kontrolliert die Fluidmigrationswege und beeinflusst die Entwicklung des Kanal- und Rückensystems. Im Gegensatz zum Sorokin Trog ist der Materialaufstieg im Batumi Gebiet gering. Das größte und aktivste Seep Gebiet ist das Batumi Seep Gebiet auf dem Kobuleti Rücken. Unterhalb des Meeresbodens deuten Reflexionen hoher Amplitude auf hohe Gashydratkonzentrationen hin, die sich aufgrund fokussierten Fluidflusses im Bereich des Batumi Seep gebildet haben. Im Bereich des Batumi Seep bilden Störungen die Fluidmigrationswege. Bright Spots in der Nähe der Gas Seeps weisen auf einen engen Zusammenhang zwischen Fluidaustritten und Gasansammlungen hin. Ein BSR, der nur entlang des Kobuleti Rückens im Bereich des Batumi Seep zu beobachten ist, liegt in ungewöhnlich großer Tiefe. Die große Tiefe des BSR kann mit Porenwasser geringer Salinität (15‰) erklärt werden. Depressionen zwischen den wachsenden Diapiren stellen bevorzugte Bahnen für Turbiditströme dar, die aufgrund ihrer erosiven Wirkung tief eingeschnittene Canyons zwischen den Diapiren geformt haben.

General outline of the thesis

The thesis is structured into five chapters. Chapter 1 is an introduction into the thesis. The introduction starts with a presentation about the main objectives of the thesis. This part is followed by a general overview about seeps, mud volcanoes, and gas hydrates. Afterwards, the geological setting of the Black Sea in general and of the specific study areas is introduced. At the end of Chapter 1, the applied methods and the processing of the data are described. Special emphasis is drawn on the high resolution seismic data, but the bathymetric and sediment echosounder systems are introduced as well. Three manuscripts (Chapters 2, 3 and 4) are the main part of the thesis. The first paper (Chapter 2) characterizes mud volcanoes in the Sorokin Trough. Chapter 3 presents a detailed analysis of the Sevastopol mud volcano by means of a 3D seismic dataset. Chapter 4 discusses the complex canyon-ridge system offshore Batumi (Georgia). Short outlines of the manuscripts are given below. A summary with the main conclusions of the research work and an outlook on future research interests in the study area form the final Chapter 5.

Chapter 2: Characterization of mud volcanoes in the Sorokin Trough (Black Sea) from hydroacoustic data

M. Wagner-Friedrichs, L. Meisner, S. Krastel, V. Spiess

To be submitted to Marine Geology.

Chapter 2 classifies mud volcanoes in the Sorokin Trough based on a combined interpretation of high resolution multichannel seismic and Parasound echosounder data. The data show that mud volcanoes are associated with near-surface mud diapirs but display a great morphological variability. Based on different structural and sedimentologic environments, the survey area was classified into three areas, which are characterized by different morphological mud volcano types. An interpretation of the morphological features and the subsurface structures provides different evolution models for the three mud volcano areas, related to the development of permeable migration pathways depending on the geological setting. The distribution of the mud volcanoes is put into a regional geological context, and related to deep subsurface structures based on single channel seismic data collected by the SSC “Yuzhmorgeologia” of Gelendzhik in 1979.

Chapter 3: 3D seismic investigations of the Sevastopol mud volcano in correlation to gas/fluid migration pathways and gas hydrate occurrences in the Sorokin Trough (Black Sea)

M. Wagner-Friedrichs, S. Krastel, V. Spiess, M. Ivanov, G. Bohrmann, L. Meisner
Submitted to G-Cubed (in review).

A 3D high resolution multichannel seismic dataset across the Sevastopol mud volcano in the Sorokin Trough allows detailed conclusions about the three dimensional structure of the mud volcano and its spatial relationships to subsurface structures. Based on the data, an evolution model for the mud volcano is presented, which shows that faults acting as potential migration pathways for gas and fluids have great impact on the formation of the mud volcano. Bright Spots near the feeder channel of the mud volcano indicate close interaction of gas/gas hydrates, fluid migration and the evolution of the mud volcano. It is suggested that the Bright Spots are associated with the base of gas hydrate stability zone, which is uplifted due to the rise of warm fluids next to the mud volcano.

Chapter 4: Gas seepage and gas/fluid migration associated with the canyon-ridge system offshore Batumi (Georgia, south-eastern Black Sea) inferred from multichannel seismic data

M. Wagner-Friedrichs, E. Bulgay, H. Keil, S. Krastel, G. Bohrmann, M. Ivanov, V. Spiess
To be submitted to International Journal of Earth Sciences.

In Chapter 4 the distribution of gas seeps and mound structures at a complex canyon-ridge system is analyzed based on high resolution multichannel seismic dataset collected at the continental slope off Batumi (Georgia). All seep locations and subsurface structures, such as diapiric structures and evidences for gas and gas hydrate occurrences, are mapped, showing that gas discharge off Batumi is associated with the ridge structures and related to shallow gas accumulations. It is discussed that diapirs, growing beneath the ridges, control the development of fluid migration pathways and also guide the trend of the canyons by creating pathways preferably used by turbidity currents.

Table of contents

1 General Introduction

1.1 Main objectives of this study

Seafloor seepage in the oceans includes cold seeps on active and passive continental margins, as well as volcanic and hydrothermal hot vents at ocean spreading centers, island arcs and intra-plate volcanoes (Judd, 2003). At cold seeps, great amounts of gas and fluids, dominated by methane, emit to the hydrosphere and atmosphere (Hovland and Judd, 1988; Judd, 1997). Seeps occur worldwide in different water depths outside and within the gas hydrate stability zone (GHSZ). Typically, seeps occur at continental slopes with thick organic rich sedimentary coverage forcing gas generation and fluid migration towards the seafloor (Judd, 2003). Methane is an intensive greenhouse gas with great potential impact on climatic change and carbon budget, thus numerous research projects investigate cold seeps and their impact on methane and carbon budgets of the world oceans and the atmosphere. Seeps are related to focused fluid migration and may indicate shallow gas accumulation and potential hydrocarbon reservoirs at greater depth. Gas can be released in dissolved form with fluids or as free gas bubbles. Seeps are often related to mud volcanoes (Hovland and Judd, 1988), positive or negative geological structures formed by effusive extrusions or violent eruptions of mud, water, and gas (e.g. Dimitrov, 2002). Estimates about the methane emissions through mud volcanoes vary between ~1 and 33 Tg/year and are still uncertain, as estimates are based on simplified analyses of limited data. Estimations, however, show that mud volcanoes are an important source of methane and other hydrocarbons to the atmosphere and the world oceans (e.g. Dimitrov, 2002; Kopf, 2002; Milkov, 2003a). Detailed characterization and studies of mud volcanoes and their subsurface structures are needed to improve the knowledge about their activity and contribution to the atmospheric methane budget, to understand why and how mud volcanoes are formed and what factors control the evolution of mud volcanoes, as well as to identify fluid migration pathways and eventually shallow gas accumulation or indications for deeper hydrocarbon reservoirs.

The Black Sea provides great potentials to study fluid migration and the evolution of mud volcanoes and gas seeps, because the Black Sea contains high concentrations of gas in an anoxic environment. A thick sedimentary coverage in combination with compressive deformation at the margins of the Black Sea due to the collision between Arabia and Eurasia since Eocene time, lead to over-pressured fluids migrating upward towards the seafloor along faults. Numerous seeps and mud volcanoes occur on the continental slopes of the Black Sea. In order to characterize and investigate seep structures and mud volcanoes, as well as the relationship between the evolution of mud volcanoes/gas seeps, near-subsurface diapiric structures, fluid migration pathways, and gas/gas hydrate

occurrences, two regions of the Black Sea were investigated mainly based on high resolution multichannel seismic data:

1) The Sorokin Trough southeast off Crimea (Fig. 1.1)
2) The continental slope off Batumi (Georgia) (Fig. 1.1)

Both selected areas of the Black Sea exhibit gas/fluid discharge at the seafloor in great water depth within the gas hydrate stability zone. In the Sorokin Trough, gas emission is associated with upward material transport and the formation of mud volcanoes above diapiric structures. The seeps off Batumi are associated with ridge structures within a complex canyon-ridge system and mainly represent simple gas/fluid vents without major morphological expression on the seafloor. The canyon-ridge system off Batumi is considered to be guided by diapiric uplift. The diapiric growth influences the sedimentary structure on top and hence also fluid migration pathways towards the seafloor.

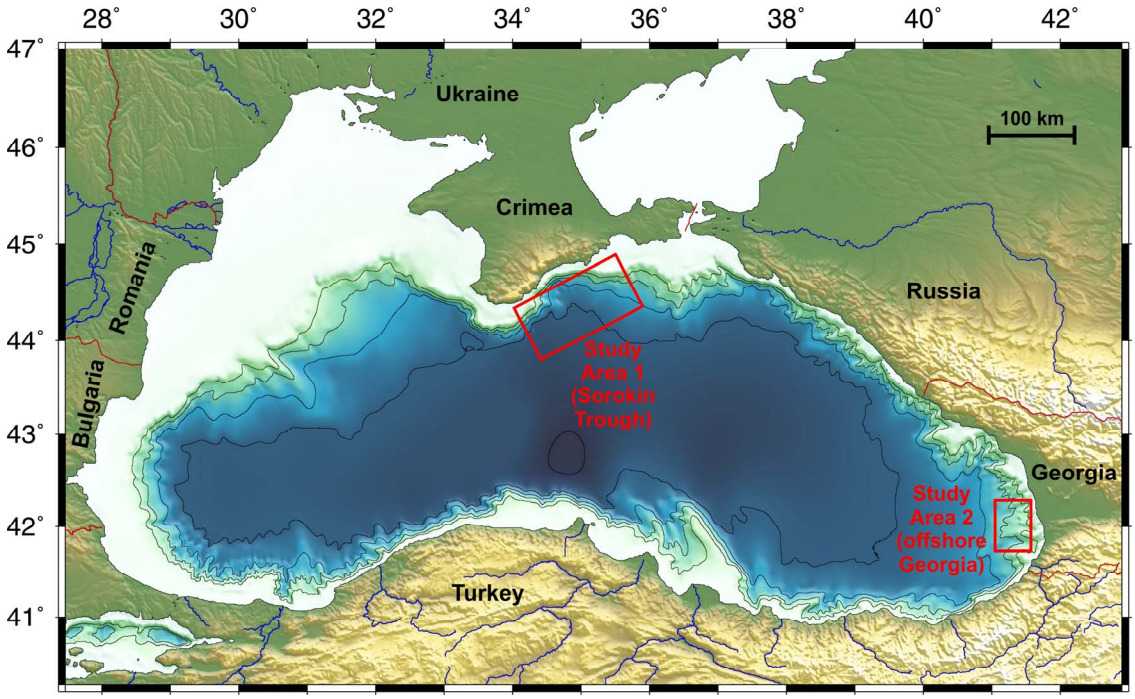

Figure 1.1: *Bathymetric map of the Black Sea and the surroundings (Gebco 1-min grid). The red rectangles show the locations of the study areas.*

The data were acquired during two different expeditions: (a) during RV Meteor cruise M52/1 in January 2002 offshore Crimea, and (b) during the TTR-15 cruise (UNESCO Training Through Research Program) with RV Professor Logache*v* offshore Georgia in June 2005. The data off Crimea include a 3D seismic dataset across the Sevastopol mud volcano.

The specific objectives of this thesis are:

- To map all mud volcanoes and gas seeps together with the subsurface structures
- To integrate the mud volcanoes/gas seeps into the regional tectonic and structural setting
- To study gas/fluid migration pathways related to the mud volcanoes and gas seeps
- To seismically characterize and classify the mud volcanoes in the Sorokin Trough based on morphological features, such as shape and size
- To develop evolution models for the different mud volcano types observed in the Sorokin Trough
- To analyze the three dimensional spatial geometry of the Sevastopol mud volcano, a representative collapsed depression structure in the Sorokin Trough
- To study the development of the canyon-ridge system off Batumi and its relationship to seepage

1.2 Gas and fluids in marine sediments

Gas in marine sediments is mainly dominated by methane of biogenic or thermogenic origin (Schoell, 1988; Floodgate and Judd, 1992). Biogenic methane results from methanogenic processes in shallow sediments, in which CO_2 from organic matter is reduced to methane (Claypool and Kaplan, 1974; Sloan, 1990). Continental margins are characterized by high biogenic productivity and high sedimentation rates, thus the decay of large amounts of organic matter in the sediments might form methane. After formation, the methane either become trapped and buried in the sediments or it may migrate towards the seafloor and discharge at the seabed. At greater depth methane and higher hydrocarbons are generated thermogenically from organic matter by catagenesis at temperatures between 50° and 200°C. Depending on the temperature and pressure conditions, various hydrocarbons are formed (Judd, 2003). Gas and fluids might be mobilized and migrate upward into shallower horizons, if adequate pathways are present. Potential pathways for fluid flow include faults, fractures, dipping permeable stratigraphic horizons, as well as forced folds and mud diapirs, which create pathways by faulting and steepening of sediments (Hovland and Curzi, 1989; Moore et al., 1991; Eichhubl et al., 2000; Orange et al., 2002; Ligtenberg, 2005). The upward rise of fluids is forced by buoyancy, capillary forces and over-pressuring mechanisms, facilitated by sediment compaction and tectonic processes, or a combination of both (Minshull et al., 1994, Gorman et al., 2002).

Upward transport of fluids might occur in solution and as free gas, either diffusive or focused (Ginsburg and Soloviev, 1997; Bouriak et al., 2000). Dispersive fluid flow through the sediment occurs intergranularly and along small-scale fractures, thus leaking out over

large areas, but focused upflow, e.g. along faults, is suggested to be two to three orders more intensive (Moore et al., 1990). Especially in low permeable mudstones, diffusive fluid flow through the sedimentary column is quite slow (Eichhubl et al., 2000). Gas/fluids can be trapped, e.g. at low permeable horizons, leading to increased pore fluid pressure and over-pressured fluids, if fluid flow is sufficiently high. Does the pore fluid pressure exceed the principal stress, fluids might support the creation or widening of fractures by hydraulic fracturing (e.g. Hunt, 1990; Roberts and Nunn, 1995; Luo and Vasseur, 2002; Zühlsdorff and Spieß, 2004).

The direct detection of fluid flow in the subsurface is difficult, but variations in seismic attributes may indicate the accumulation of gas/fluids as the occurrence of fluids and gas changes sediment physical properties such as porosity and p-wave velocity (e.g. Minshull and White, 1989). The scatter of seismic energy at free gas bubbles leads to typical attenuation of seismic amplitudes, indicating free gas occurrences in seismic data (Max, 1990; Wood et al., 2002). Evidence of focused fluid flow through the sedimentary column can be detected as narrow vertical acoustic voids (chimneys) in seismic data, where seismic amplitudes and reflectors are distorted, indicating deeper reservoirs (Heggland, 1998; Gay et al., 2003). Bright Spots, high amplitude reflections resulting from the high impedance contrast between gas-charged and gas-poor strata (Max, 1990), often indicate the accumulation of free gas in seismic data. Indirect evidence of fluid migration is given by the observation of flow-related structures and potential fluid conduits, such as faults and fractures. Trap structures may indicate potential gas accumulation (Brooks et al., 1984; Bray and Karig, 1985; Minshull and White; 1989, MacDonald et al., 1994; Taylor et al., 2000; Zühlsdorff et al., 1999; Zühlsdorff and Spiess, 2004).

Fluid migration towards the seabed may result in seafloor seepage, where fluids are released into the water column in dissolved or gaseous phase. Such seep sites can be associated with different morphological features, such as mud volcanoes and pockmark structures (e.g. Hovland and Judd, 1988; Judd et al., 2002).

1.2.1 Cold seeps

Cold seep sites are characterized by the discharge of cold hydrocarbon fluids, mostly enriched with methane, at the seafloor (e.g. Suess et al., 1985; Hovland and Judd, 1988; Judd et al., 1997; Greinert et al., 2001). Methane is a strong greenhouse gas that absorbs infrared radiation 25 times more efficiently than CO_2 (Lelieveld et al., 1993, 1998). Thus, the emission of significant amounts of methane from seeps to the hydrosphere and atmosphere have great potential relevance on the carbon cycle and the climate change (e.g. Judd et al., 2002). Gas seeps occur where upward fluid migration is focused, e.g. along faults (e.g. Judd, 2003). Gas may be trapped in geological structures building

reservoirs or formed into gas hydrates under certain low temperature and high pressure conditions at sufficient supplies of water. Thus, gas seeps are often associated with shallow gas/gas hydrate accumulations or deeper hydrocarbon deposits (e.g. Wilson et al., 1974; Kvenvolden, 1993; Buffet, 2000). Dissociation of gas hydrates due to changes of p-T conditions may support gas discharge and result in sediment destabilization (Schmuck and Paull, 1993; Bouriak et al., 2000; Bünz et al., 2005). Estimations about the global emission of methane to the atmosphere from seafloor seepage range about 18-48 Tg CH_4/year, which is 4-9% of the global budget (Judd, 2000; Kvenvolden et al., 2001; Judd et al., 2002). An equivalent amount of discharged methane is believed to dissolve in the water column (Kvenvolden et al., 2001).

Methane seepage is globally distributed and occurs from shallow to deep water along most active and passive continental margins in different geological environments (Dimitrov, 2002; Judd, 2003) (Fig. 1.2). Only a small portion of the world seas and oceans have been studied sufficiently, thus the exact distribution and numbers of seep sites remain uncertain (Judd, 2003).

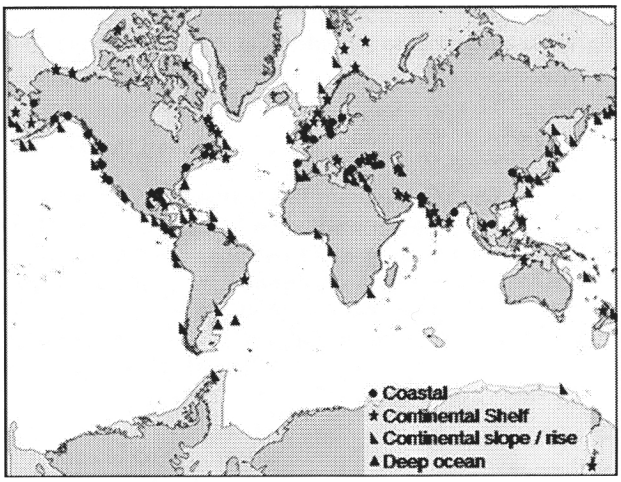

Figure 1.2: *Global distribution of seabed fluid flow correlated to oceanographic settings. Seepage locations are identified by one or more of the following features: gas seeps, chemosynthetic 'cold seep' fauna, methane-derived authigenic carbonates, pockmarks, shallow gas, gas hydrates. The continental shelves are shaded (from Judd, 2003).*

Flow rates at seeps vary between slow, inter-granular and vigorous, even violent eruptions (Judd, 2003). Under normal conditions, most of the methane migrating towards the seabed is dissolved and oxidized (Reeburgh et al., 1993; Boetius et al., 2000; Michaelis et al., 2002). A main sink for methane is the anaerobic methane oxidation (AOM), resulting from microbial activity by a consortium of archaea and sulphate-reducing bacteria and leading to the precipitation of authigenic carbonates (Boetius et al., 2000; Michaelis et al., 2002). At vents with low flow rates, dissolved methane can be completely oxidized by the AOM (Boetius, 2000) according to the following equation (Iversen and Jörgensen, 1985; Boetius, 2000): $CH_4 + SO^{2-}_4 = HS^- + HCO^-_3 + H_2O$. For example, at the Dvurechenskii mud volcano in the Black Sea, the AOM consumes about 80% of the rising methane, so that

during quiescent dewatering periods from an annual transport of 8.9 x 10^{+6} mol CH_4 to the surface, only 1.9 x 10^{+6} mol CH_4/yr is emitted into the water column (Wallmann et al., 2006).

Active cold seeps in deep water are typically colonized by chemosynthetic communities, such as chemoautotrophic clams, tube worms and bacterial mats, at the sediment surface, using the hydrogen sulphide and methane as energy source (Suess et al., 1985; Sibuet and Olu, 1998). At high flux rates, methane is rapidly released in large quantities, generating dense bubble plumes (Michaelis et al., 2002), so that methane oxidation and carbonate precipitation cannot proceed within the surface sediments and methane may pass into the hydrosphere (Luff et al., 2004). Most of the methane released at seep sites, however, is dissolved in the water column (Judd, 2003). The main factors controlling the rate of dissolution are the water depth, bubble size, dissolved gas concentration and temperature (Leifer and Patro, 2002). Released gas bubbles may be protected against rapid dissolution, if they are lined with crude oil (Sassen et al., 2001) or, within the gas hydrate stability field, coated by gas hydrates (Topham, 1984; Suess et al., 2001; Rehder et al., 2002; Greinert et al., 2006). The rise of free gas bubbles through the water column can be detected directly either by video observation or as gas plumes (flares) with hydroacoustic methods, as free gas bubbles give strong backscatter signals (Klaucke et al., 2005, 2006; Greinert et al., 2006) (Fig. 1.3). Rising velocities for bubbles can be determined from visual investigations and hydroacoustic measurements. Observations from Hydrate Ridge indicate rising velocities of 21 to 29 cm/s for bubbles

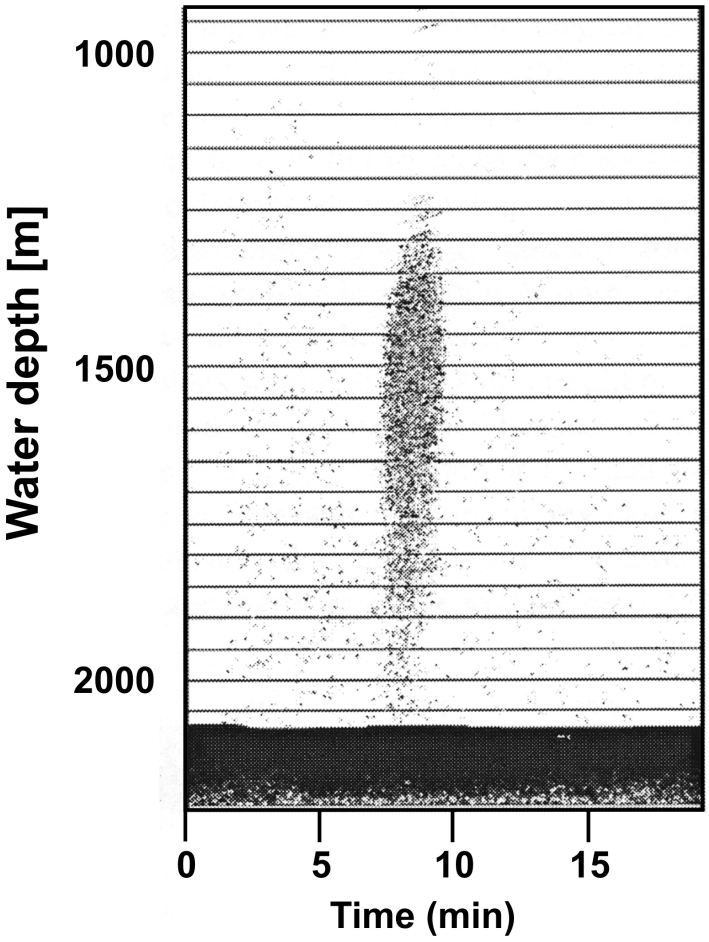

Figure 1.3: *Typical echogram of a gas flare, recorded by Greinert et al. (2006) at the Dvurechenskii mud volcano in the Sorokin Trough (Black Sea).*

with diameters of 4 to 20 mm (Rehder et al., 2002). Greinert et al. (2006) measured rising velocities of 19-22 cm/s near the seafloor and 12-14 cm/s at the top of flares observed at mud volcanoes in the Sorokin Trough (Black Sea).

Many cold seeps are associated with positive morphological structures (mud volcanoes, mud and carbonate mounds) or depressions (Pockmarks) on the seafloor. Such features can easily be recognized on bathymetric, side-scan sonar and seismic data (e.g. Hovland and Judd, 1988; Wever et al., 1998). Seeps without significant morphological relief can be detected in backscatter data. Distinctive backscatter signatures at seeps may indicate seep related biogeochemical processes, such as precipitation of gas hydrates or authigenic carbonates, which generally scatter the acoustic energy and generate typically high backscatter responses, often characterized by circular or flow-like shape (e.g. Anderson and Bryant, 1990; Sager et al., 2003). Acoustic anomalies in seismic data may indicate shallow gas accumulation or columns of focused fluid migration which might refer to seepage.

The Black Sea is well known for the presence of seafloor seepage and seep-related structures, which have been reported from various areas, e.g. at the north-western margins (Shnukov et al., 1995; Peckmann et al., 2001; Michaelis et al., 2002; Mazzini et al., 2004; Naudts et al., 2006), in the central and north-eastern parts (Ivanov et al., 1989, 1998; Ginsburg et al., 1990; Limonov et al., 1994; Woodside et al., 1997; Kenyon et al., 2002; Blinova et al., 2003; Bohrmann et al., 2003; Krastel et al., 2003; Aloisi et al., 2004; Mazzini et al., 2004; Greinert et al., 2006) as well as along the south-eastern slopes of the Black Sea (Kruglyakova et al., 1993; Cifci et al., 2002; Ergün et al., 2002; Klaucke et al., 2006). The distribution of gas flares observed in the Black Sea is imaged in Fig. 1.4. In contrast to most other seep sites, the Black Sea seeps are mainly situated in the anoxic zone, thus typical seep fauna lack. The seeps on the shelf and the slope of the Black Sea are an important source for methane in the water column (Dimitrov, 2002; Schmale et al., 2005). The basin-wide flux of methane from seeps and hydrates to the hydrosphere is estimated to be about 3.6-5.65 Tg/year (Kessler et al., 2006). Gas discharge in the Black Sea is commonly associated with mud volcanism, which is known from different regions of the Black Sea, as e.g. in the Central Black Sea and the Sorokin Trough (Limonov et al. 1994, 1997; Ivanov et al., 1996, 1998; Woodside et al., 1997; Bouriak and Akhmetjanov, 1998; Krastel et al., 2003). The thick sedimentary cover and neo-tectonic compressional deformation at the continental slopes of the Black Sea are the main factor leading to over-pressured pore fluids migrating upward towards the seafloor at faults (Yun et al., 1999). The two working areas investigated in this thesis, the Sorokin Trough in the north-eastern part and the continental slope off Georgia in the south-eastern part of the Black Sea, are known for the presence of abundant seep sites at great water depth between 800 and 2200 m. In

the Sorokin Trough gas discharge is bound to mud volcanism, while the slope off Georgia is characterized by gas seeps dominated by the release of free gas bubbles.

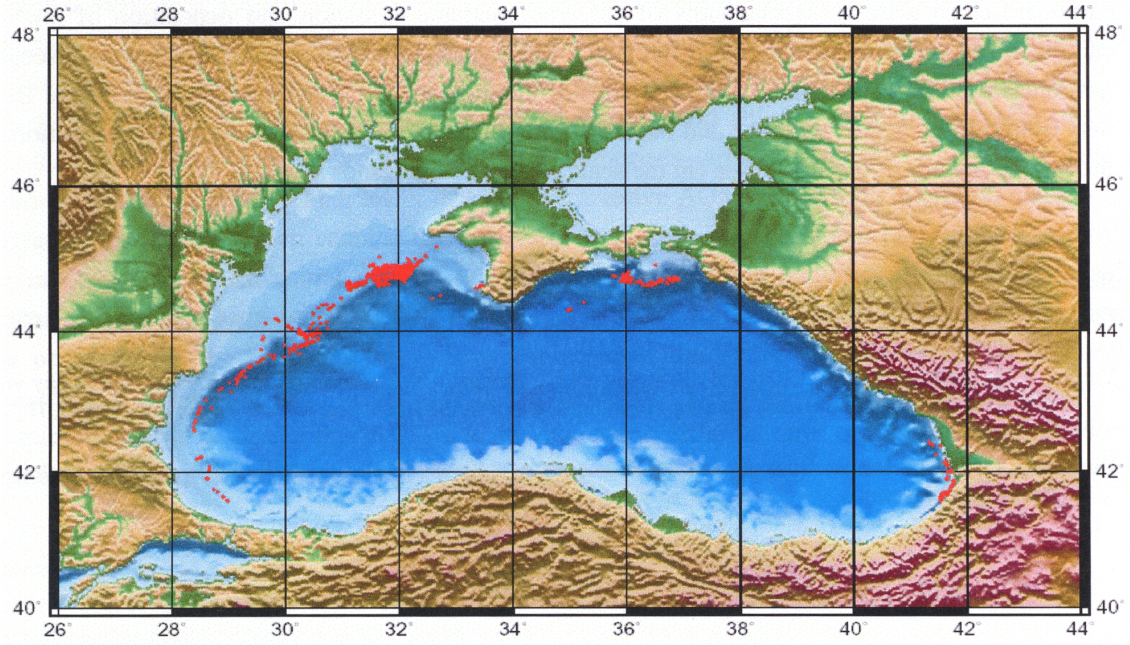

Figure 1.4: *Distribution of gas flares in the Black Sea (from Egorov et al., 2003).*

1.2.2 Mud volcanoes

One major type of seepage is the release of gas by mud volcanism. Mud volcanoes are geological structures formed by the emission of gas, water and sediments (Kopf, 2002; Milkov et al., 2003a), thus providing important information about the subsurface sediments and fluids, which in turn might give evidence of the petroleum potential in the deep subsurface (Guliyev and Feizullayev, 1997; Milkov, 2000). Water and gas are transported within fine-grained muddy sediments forming a semi-liquid and gas enriched matrix and facilitating the mud to rise along adequate pathways towards the seafloor. The outflowing mass, called mud breccia, builds the bodies of mud volcanoes (Dimitrov, 2002, 2003). The origin of gas, water and mud emitted at mud volcanoes is mainly sourced in rocks and muddy sediments at great depth of several km, but shallower biogenic gas may also contribute to the gas discharge. Thus the emitted gas usually shows a mixed composition (Dimitrov, 2002; Kopf, 2002; Milkov et al., 2003a). As gas emissions at mud volcanoes are dominated by methane, mud volcanoes represent an important natural source of methane contribution to the atmospheric carbon budget with great potential impact on the global climatic change (Milkov, 2000; Dimitrov, 2003; Holland et al., 2003).

Gas emissions at mud volcanoes occur during eruptive phases characterized by mostly short periods (hours to days) of quiet mud flows or/and violent mud eruptions, and also continue at different vent sites during long periods of quiescence (years to centuries), when little or no mud is expelled (Hedberg, 1974; Brown, 1990; Bagirov et al., 1996; Guliev and Feizullayev, 1996; Dimitrov, 2002; Kopf, 2002). The emitting gas ascends either as free gas or in dissolved form via fluid flow (dewatering) and mud extrusion. Estimations about the global annual gas flux and the amount of methane contributed to the atmosphere through mud volcanoes vary significantly and have great uncertainties as the number of submarine mud volcanoes is poorly constrained and measurements of gas flux during eruptive periods lack (Milkov et al., 2003a). Milkov et al. (2003a) estimate that the annual global gas flux from mud volcanoes is about ~15.9 Tg during quiescent periods, and ~17.1 Tg during eruptive phases. Large volumes of gas (~27 Tg yr^{-1}) may thereby escape from deep water mud volcanoes (Milkov et al., 2003a). Dimitrov (2002) estimates that the annual amount of methane released from onshore and shallow water mud volcanoes range between 10.2-12.6 Tg. The amount of methane contributed to the atmosphere through mud volcanoes by quiescent and eruptive periods is estimated to be about 5 Tg yr^{-1} (Dimitrov, 2003). Gas flux from onshore and shallow offshore mud volcanoes is the main contributor to the modern atmospheric methane budget, but the contribution of deep-water mud volcanoes to the atmospheric methane budget appears to play not a significant role, as parts of the gases from mud volcanoes are formed into gas hydrates (about 10 % (Ginsburg et al., 1999), or are oxidized and precipitated as authigenic carbonates in the near bottom sediments (Judd et al., 2002). Gas bubbles released into the water column rapidly are oxidized and dissolved (Judd et al., 2002). Mud volcanoes may erupt violently in regular or irregular time intervals or emit mud, fluid and gases continuously. The main gas component released is methane. Minor gas components at mud volcanoes are carbon dioxide and nitrogen (Milkov et al., 2003a), which are the dominant gas phase at mud volcanoes associated with recently active magmatic processes (Motyka et al., 1989; Kopf, 2002).

Mud volcanoes form worldwide in different geological environments, onshore and offshore, primarily occurring in areas of compressional deformation and within sedimentary basins with rapid sedimentation (e.g. Black Sea and Caspian Sea) (e.g. Milkov, 2000; Kopf, 2002). A map with the global distribution of onshore and offshore (known and inferred) mud volcanoes is imaged in Fig. 1.5. Most mud volcanoes (>50% of the total numbers of mud volcanoes identified) are clustered along the Alpine-Himalaya Active Belt with about 650 terrestrial and at least 470 submarine prominent mud volcanoes (e.g. Dimitrov, 2002, 2003). Terrestrial mud volcanoes have been well studied for over 200 years (Ansted, 1866), but research of submarine mud volcanoes started only ~30 years ago (Dimitrov, 2003). During recent studies the number of known submarine mud volcanoes is rapidly increasing, but the

exact number of submarine mud volcanoes is still uncertain; estimations range from 840 to 5000 (Milkov, 2000; Dimitrov, 2002; Kopf, 2002). Areas with well known submarine mud volcano occurrences include the Black Sea and the Caspian Sea (Ginsburg and Soloviev, 1994; Ivanov et al., 1996; Limonov et al., 1997), the Norwegian Sea (e.g. Hovland and Judd, 1988), the Gulf of Mexico (Kohl and Roberts, 1994), the Mediterranean Ridge (Ivanov et al., 1996; Woodside et al., 1997) and the Barbados Ridge (e.g. Hedberg, 1974; Griboulard et al., 1998).

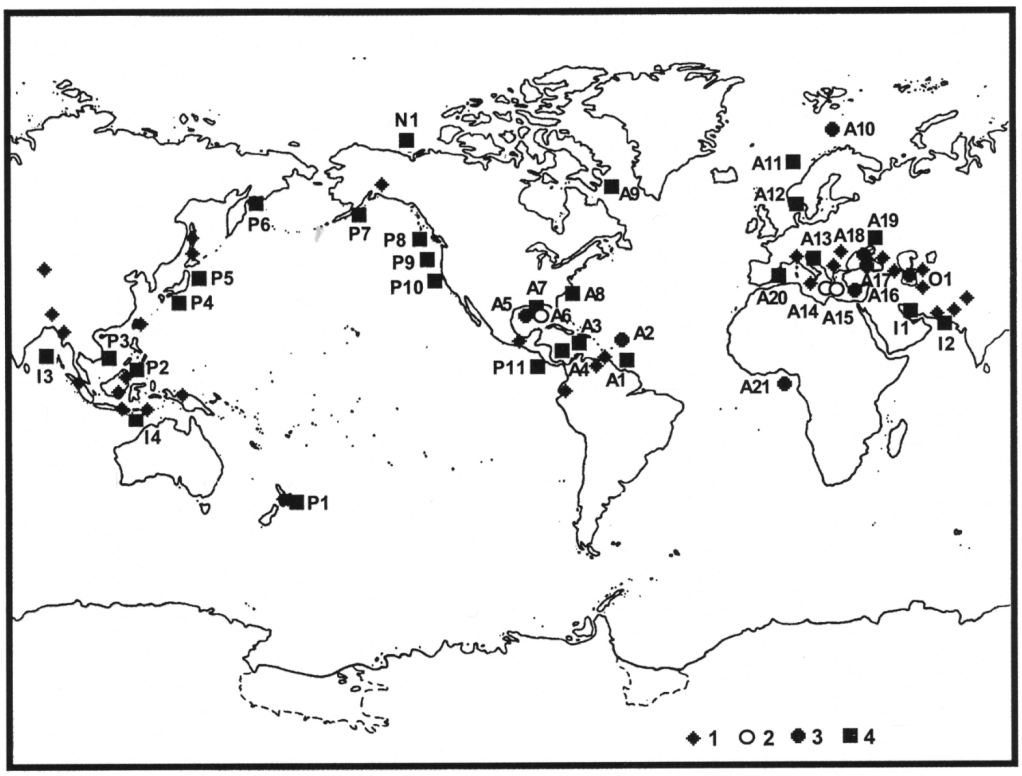

Figure 1.5: *Worldwide distribution of onshore (1), known (2 without gas hydrates, 3 hydrate bearing) and inferred (4) submarine mud volcanoes (after Milkov, 2000).*

Mud volcanism is caused by various geological processes and factors. Individual factors might vary in the different regions, but the occurrence of mud volcanoes is strongly controlled by rapid burial of sediments and compressional tectonic activity. The main formation mechanism leading to mud volcanoes is considered to result from upward fluid migration, forced by high pore fluid pressure due to rapid sedimentation and structural or tectonic compression (Brown, 1990; Milkov, 2000; Dimitrov, 2002).

Mud extrusions building the mud volcanoes form typical circular or elongated morphological structures highly varying in shape, from cone-shaped or flat topped elevations to depression structures. The size might vary from few 10 m² up to 100 km² (Dimitrov, 2002; Kopf, 2002). Heights of mud volcanoes reach from a few meters to several

hundreds of meters (Sturz et al., 1992; Dimitrov, 2002), and diameters range from only a few meters to several kilometers (Jakubov et al., 1971). The outflowing mud breccia sharply contrasts the surrounding host sediments, as the mud breccia represents sediments from greater depth (Dimitrov, 2002). Mud breccia generally comprises a clay mineral-rich mud matrix (as to 99% of the total volume) and a variable quantity of clast and rock fragments with diameters ranging from a few millimeters to over 10 m. The clast and rock fragments are derived from rocks through which the mud has passed (Dimitrov, 2002; Kopf, 2002). Mud extrudes from the main feeder channel, or conduit, forming the central cone or crater, but smaller lateral pipes can split off the feeder channel and lead to vents at the flanks of the mud volcano structure, called griphones (Dimitrov, 2002; Kopf, 2002). The general structure of a mud volcano is imaged in Fig. 1.6. The morphological structures of submarine mud volcanoes can be identified and investigated by side-scan sonar, bathymetric and seismic data, but to specify if the topographic feature observed really represents a mud volcano, sampling has to recover mud breccia and mud flows have to be identified. Mud flows may reach dimensions up to several 100 meters in width and some kilometers in length (Jakubov et al., 1971). Mud volcanoes on seismic data typically show a narrow zone beneath lacking reflections, which represents the feeder channel and is characterized by not stratified sediments.

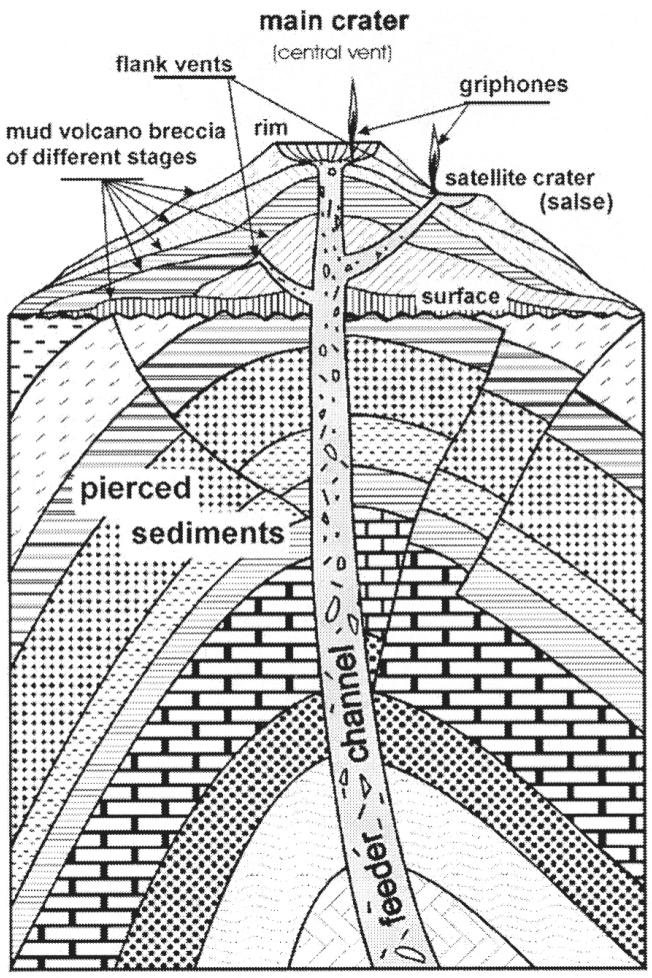

Figure 1.6: *Basic structure and main elements of a cone-shaped mud volcano (from Dimitrov, 2002).*

The morphology of mud volcanoes is directly related to the eruption style and the physical properties of the eruption product. The shape and size of mud volcanoes primarily depend on pore fluid content, frequency and character of activity, and the viscosity and consolidation of the

extruded mud (Brown, 1990; Kopf, 2002). The consistency of the mud and the eruption frequency affect the height of the mud volcano. The dipping angle of the flanks depends on the viscosity and porosity of the material (Kopf, 2002; Yusifov et al., 2004). The more frequent the eruption, the larger the structure. The lower the viscosity, the larger and flatter the body. Highly permeable mud results in domes and pies with relatively steep slopes. High pore fluid pressure, e.g. due to low permeability, probably leads to violent eruptions, which destroy the internal structure of a mud volcano and form pockmarks (Dimitrov, 2002; Kopf, 2002; Yusifov, 2004).

In the Black Sea, mud volcanoes are known since the late 1970's and have been intensively studied and documented during the TTR cruises (UNESCO Training Through Research program) in the 1990's. Well studied mud volcanoes are documented for the Central Black Sea and the Sorokin Trough. About 65 mud volcanoes are known on the shelves (Kerch-Taman shelf) and slopes (off Bulgaria, Ukraine, Russia, Georgia and Turkey) of the Black Sea (Kruglyakova et al., 2002). The Dvurechenskii mud volcano (DMV), located in the Sorokin Trough at about 2000 m water depth, is considered to be a an very active vent site, with estimated high flux rates of 12-24 cm year $^{-1}$ (Bohrmann et al., 2003). Free gas bubbles at the DMV, identified as flares in hydroacoustic data, rise more than 1000 m. These bubble emissions have been observed only periodically, indicating intermittently gas emissions (Greinert et al., 2006). Methane emission rates from the DMV via quiescent dewatering into the water column have been estimated by Wallmann et al. (2006) to be about 1.9 x 10^{+6} mol CH_4/yr. Assuming that the discharge rate of all mud volcanoes in the Black Sea is similar to DMV, the methane emission by quiescent dewatering processes contributes less than 0.1% to the total methane input into the Black Sea (Wallmann et al., 2006). However, large regions of the Black Sea are still unexplored, and the methane emission during active mud eruptions is unknown. Mud volcanoes of the Black Sea in general are related to high sedimentation rates of the Pliocene-Quaternary deposits and are associated with the clays of the Maikopian Formation (Oligocene-Miocene), which is enriched with organic matter, thus containing great potential to generate hydrocarbons leading to over-pressured fluids (Dimitrov, 2002). In the Central Black Sea, mud volcanoes are formed in an extensional regime in combination with a thick sedimentary coverage above potentially mobile beds of the Maikop Formation leading to high overpressure, thus resulting in a fast release of gas/fluids from great depth (Ivanov et al., 1996; Limonov et al., 1997). Mud volcanoes in the Sorokin Trough are related to the diapirism of the Maikopian clay due to the compressive tectonic regime and are formed above diapiric structures from sediments rising with high fluid content along faults towards the seafloor (Woodside et al., 1997).

1.2.3 Gas hydrates

Gas hydrates are ice-like, crystalline solid structures composed of gas molecules occurring in cages of water molecules forming clathrates (Sloan, 1990). Most natural gas hydrates consist of more than 99% methane of the hydrocarbons, known as methane hydrates (Sloan, 1998; Kvenvolden and Lorenson, 2001). Gas hydrates occur in three different crystal structures, named structure I, II or H (Sloan, 1998). Structure I and II crystallize within the cubic and structure H within the hexagonal system. The structure formed depends on the size of the gas molecules. The different structures consist of different cage types forming the cavities, in which the gas molecules are included (Fig. 1.7). Gas hydrates with Structure I crystallography contain natural gases with small molecule sizes. Structure I is most common in marine sediments and mainly comprise methane with minor quantities of CO_2 and H_2S. Gas hydrates with significant amounts of propane and higher carbon gases form Structure II or H. Structure H is a complex structure and is present only with mixtures of small (like methane, nitrogen or carbon dioxide) and very large molecules, such as metylcyclohexane (Sloan, 1998).

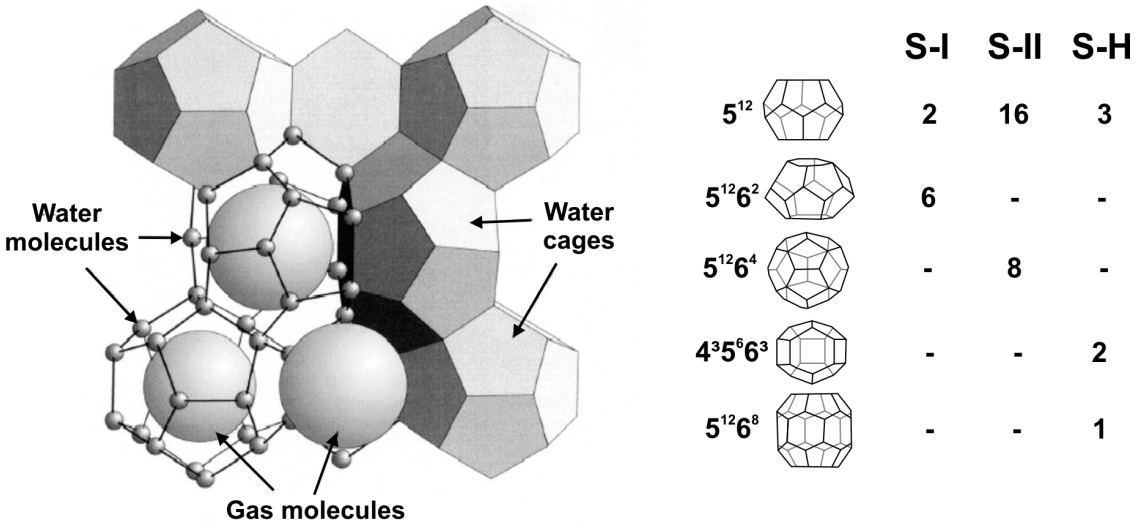

Figure 1.7: *Left: schematic illustration of the cage lattices of gas hydrate structure I. Right: Cage types of the gas hydrate structures I, II, and H (after www.ifm-geomar.de).*

The occurrence of natural gas hydrates is controlled by temperature and pressure, the presence of enough gas, and, to a lesser content, composition of the gases and pore water salinity (Kvenvolden, 1993; Sloan, 1998). Gas hydrates are formed at high pressure and low temperature conditions when water is saturated with gas (e.g. Kvenvolden, 1993; Sloan, 1998). At a given pressure, the presence of CO_2, H_2S and higher hydrocarbons increases the maximum temperature for the stability, higher salinity shifts the stability field to

lower temperatures. At given pressure, seawater salinity of 33.5% would shift the dissociation temperature of methane hydrate about -1.1°C with respect to that of hydrate formation in a pure water system (Dickens and Quinby-Hunt, 1994). A phase diagram of a pure methane-fresh water system is shown in Fig.1.8.

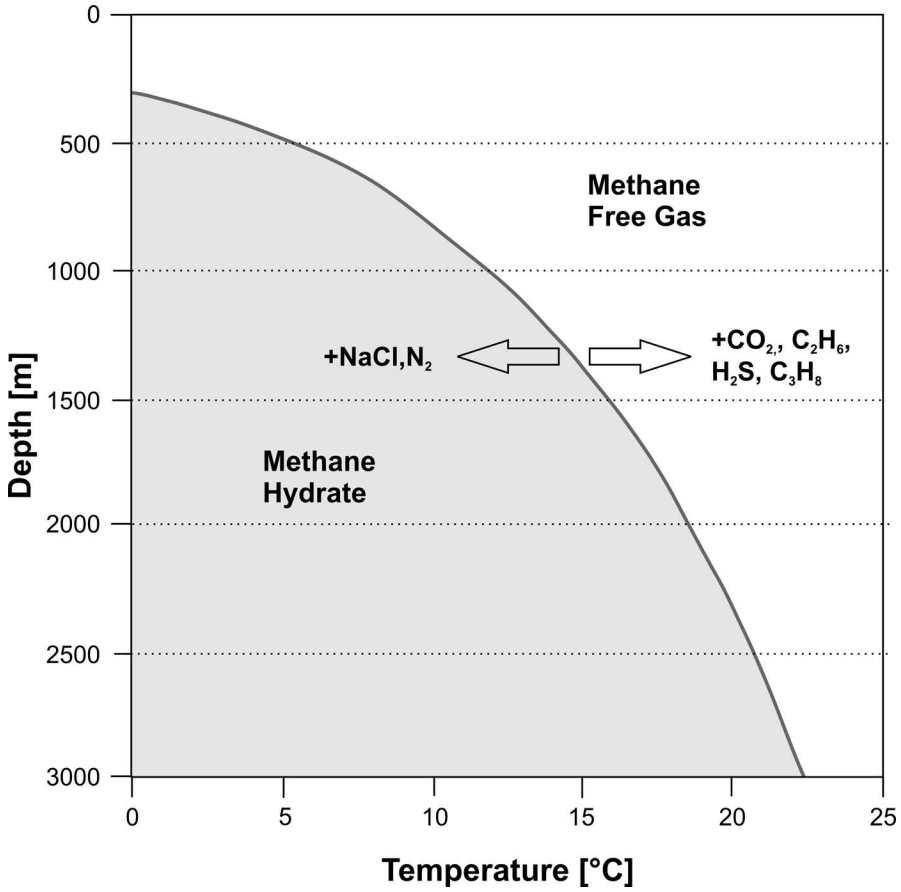

Figure 1.8: *Stability diagram for pure methane hydrates and seawater salinity (after Dickens and Quinby-Hunt, 1994).*

Gas hydrates occur all around the world, but due to their stability field their distribution is restricted to two environments: (1) at permafrost regions on land, and (2) offshore within the upper several hundreds meters of deep water sediments along passive and active continental margins at water depths below about 300 m (Fig. 1.9) (Kvenvolden and Barnard, 1983; Kvenvolden, 1993; Dickens et al., 1997).

The limiting factor for the formation of gas hydrates in most offshore regions is the availability of sufficient gas concentrations, particularly methane, above solubility concentrations, which are thus restricted to the shallow geosphere (Kvenvolden and Lorenson, 2001). The maximal lower boundary of the gas hydrate stability is limited by the temperature gradient, as the stability is primarily influenced by the temperature. Thus, the base of gas hydrate stability (BGHSZ) runs along isotherms (e.g. Kvenvolden and

Lorenson, 2001). Locally increased heat flow will uplift the BGHSZ and thin the gas hydrate stability zone (GHSZ), as e.g. near mud volcanoes and gas seeps. Thereby, the BGHSZ locally can intercept with the seafloor reflection (e.g. De Batist et al., 2002; Van Rensbergen et al., 2002). Other factors influencing the exact depth of the base of gas hydrate stability zone are the gas composition and the salinity of the pore water.

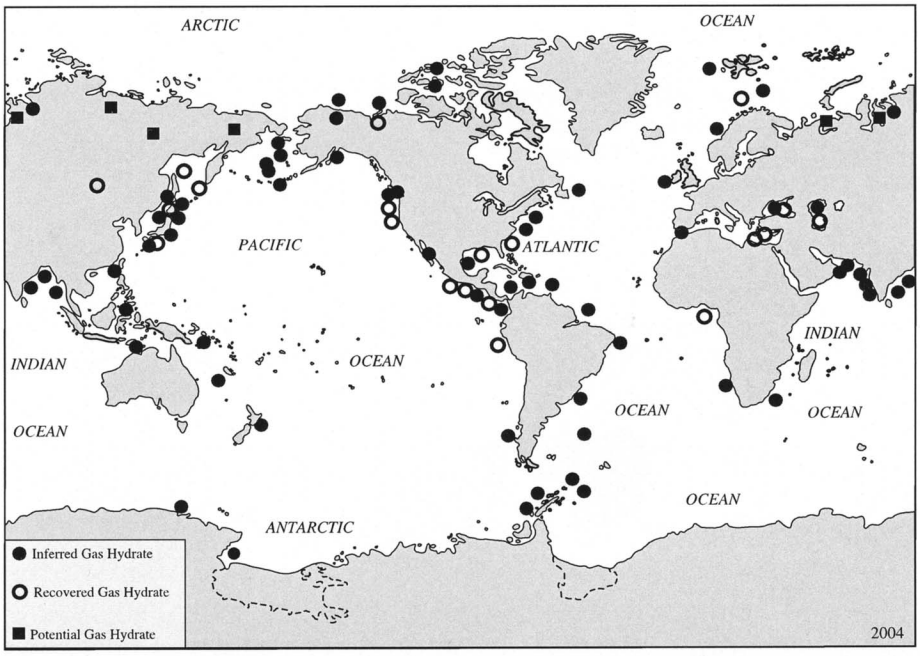

Figure 1.9: *Worldwide occurrences of known and inferred gas hydrates in aquatic sediments and polar continental sediments (after Kvenvolden and Rogers, 2005).*

Gas hydrates are formed in the pore space of sediments (typically a few percent), which leads to a change of the physical properties of sediments (e.g. Kvenvolden, 1993). The p-wave velocity of pure gas hydrate is about 3.3 to 3.8 km/s (Mathews and von Huene, 1985), thus usually the elastic velocity of gas hydrate bearing sediments is increased. The resistivity of gas hydrate cemented sediments is significantly enlarged, as gas hydrates are a good electrical insulator (Collett, 1998). Due to the decreased permeability of gas hydrated layers, free gas is often found beneath the base of the gas hydrate stability zone (Sloan, 1990; Dillon et al., 1994; Holbrook et al., 1996; Ecker, 1998; Sain et al., 2000).

There are several main theories about the origin of the methane forming methane hydrates in sediments at continental margins: (1) in situ biogenic methane generation within the hydrate stability zone (Claypool and Kaplan, 1974), (2) biogenic methane formation below the stability field with subsequent upward migration of dissolved methane in rising pore fluids into the GHSZ (Hyndman and Davies, 1992), (3) recycling of methane during the process of hydrate dissociation accompanying sedimentation (Paull et al., 1994), and (4)

upward migration of thermogenic methane generated at greater depth (Kvenvolden and McDonald, 1985).

The presence of gas hydrates in marine sediments is most commonly inferred from the observation of a BSR (*bottom-simulating reflector*) in seismic reflection profiles (Stoll et al., 1971; Shipley et al., 1979; Kvenvolden and Barnard, 1983; Hyndman and Spence, 1992) (Fig. 1.10). As the BSR is considered to reflect the chemical phase boundary of gas hydrates, the BSR runs along isotherms, thus generally following the seafloor and typically crosscutting the strata (Shipley et al., 1979).

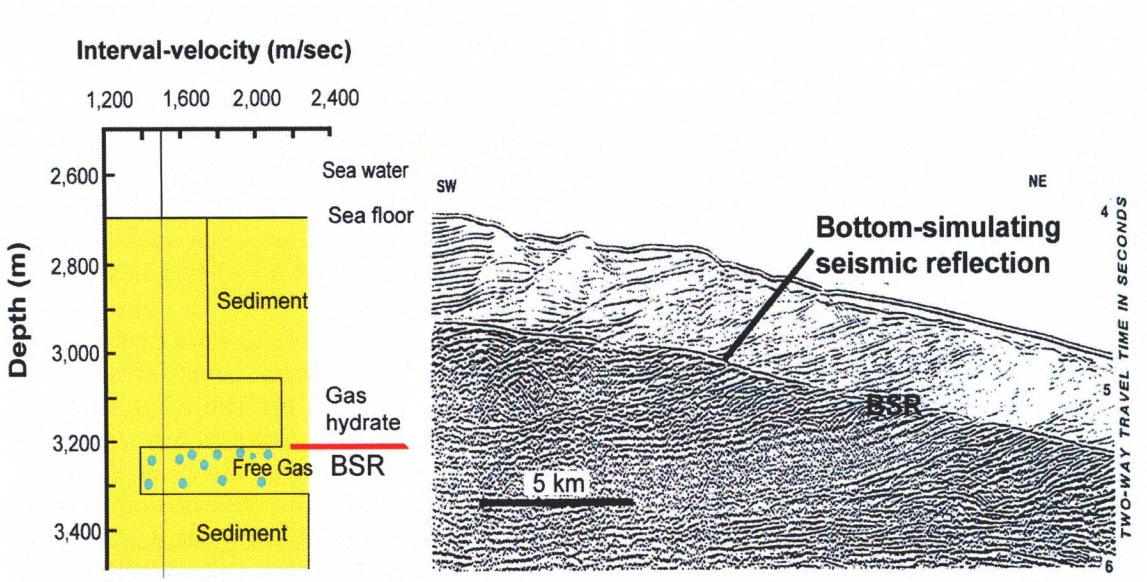

Figure 1.10: *Most famous BSR at the eastern flank of the Blake Ridge (Shipley et al., 1979) (right). A seismic velocity model shows the significant velocity decrease below the BSR marking free gas (left) (after Bohrmann and Torres, 2006).*

The BSR is a strong reflector with reversed polarity relative to the seafloor due to a p-wave velocity inversion across the stability boundary from the high velocity gas hydrate bearing sediments above to the lower velocity of gas bearing sediments beneath (Dillon and Paull, 1983; Miller et al., 1991; Hyndman and Spence, 1992; Singh et al. 1993) (Fig. 1.10). P-wave velocities of gas hydrated sediments range between 1700-2400 m/s (Katzmann et al., 1994; Minshull et al., 1994; Lee et al., 1994), while velocity values below 1500 m/s indicate the presence of free gas in the pore space. The BSR could also be caused by the increased seismic impedance contrast of hydrate cemented sediments relative to hydrate-free sediments beneath (Hyndman and Davis, 1992). Detailed velocity models crossing BSR structures, however, suggest that the BSR results from the presence of free gas beneath (Holbrook et al., 1996). The presence of free gas beneath the BSR is proved by drilling, e.g. on the Blake Ridge during ODP Leg 164 (Holbrook et al., 1996). The amplitude of the BSR depends on the degree of saturation of sediments by hydrates above and by gas

below (Sain et al., 2000). BSRs are common in hydrate-bearing sediments, but gas hydrates can be present, even where BSRs lack (Mathews and von Huene, 1985; Holbrook et al., 2002). Based on the depths of BSRs in combination with the bottom water temperature, the temperature geothermal gradient and heat flow can be estimated (Shipley et al., 1979, Yamano et al., 1982).

As gas hydrates change the physical properties of sediments, seismic reflection amplitudes can be affected by the presence of gas hydrates, depending on the amount of gas hydrate concentration leading to reduced or enhanced reflectance (Lee and Dillon, 2001). Gas hydrates preferentially form in more porous (lower velocity) sediments increasing the velocity relative to the less porous (higher velocity) layers. This reduces the impedance contrast between high and low porous strata at low gas hydrate saturations, suppressing the seismic reflectance. High hydrate saturated layers, however, can have significantly increased velocity, generating enhanced reflectance within the GHSZ (Holbrook, 2002).

Gas hydrates are commonly associated with deep water mud volcanoes, as gas rising at mud volcanoes often is captured in the near-subsurface sediments in gas hydrates (Reed et al., 1990; Woodside et al.; 1998, Ginsburg et al., 1999; Milkov, 2000). Estimations from Milkov (2000) show that globally about 10^{10}-10^{12} m³ of methane are associated with mud volcanoes at standard temperature and pressure. Gas hydrate accumulation at mud volcanoes is found in a concentric zone around the conduit for the fluid upflow (Ginsburg et al., 1997, 1999; Milkov, 1998). The dissociation of gas hydrates might play a significant role in mud volcano processes (Milkov, 2000). Warm fluids migrating at mud volcanoes towards the seafloor might lead to decomposition of gas hydrates (De Lange and Brumsack, 1998; Aloisi et al., 2000). Otherwise gas hydrates may be formed near mud volcanoes when gas/fluids pass through the GHSZ (Kopf, 2002).

Recently, gas hydrates have become of great interest, due to (a) their potential as a future energy resource, as great amounts of methane are stored in gas hydrates, considered to form the largest reservoir type of natural gas (MacDonald, 1990; Kvenvolden, 1993), (b) their role in climate change, as methane is a very strong greenhouse gas and release of methane from decomposed gas hydrates might significantly influence the atmospheric composition and thus impacting the global warming (Kvenvolden, 1988), and (c) their potential impact on slope stability after dissociation of gas hydrates (Kvenvolden, 1993). In a saturated methane hydrate, with a molecular ratio of methane:water = 1:5.75, one m³ of methane hydrate contains 164 m³ of methane gas at standard conditions (Kvenvolden, 1993). Estimations about the amount of methane resources in global gas hydrate occurrences vary by several orders of magnitude and are highly uncertain and speculative due to heterogeneous gas hydrate distribution and incomplete knowledge about

gas hydrate content in sediments (e.g. Lerche, 2000). In the 1990s, estimations about the global hydrate-bound gas converge at about 10 teratonnes of methane carbon, a value, which was established from several independent estimations (Holbrook et al., 1996; Dickens et al., 1997; Makogon, 1997; Kvenvolden and Lorenson, 2001). Formation of gas hydrate impacts the slope stability, as gas hydrates decrease the sediment permeability and may form a barrier for fluids, which inhibits diagenetic processes during the burial and might lead to the formation of excess pore pressures (Sloan, 1990). Dissociation of gas hydrates then produces a fluidized layer at the base. This locally reduces the shear strength at the former boundary facilitating submarine slope failures, accompanied by the release of gas into the water column (Kvenvolden, 1993).

The distribution of gas hydrates and the content of gas hydrate occupying the sediment pore space highly vary and are poorly understood yet. First estimations about gas hydrate occupation from drilling during ODP Leg 164 at Blake Ridge show that gas hydrate distribution is heterogeneous and that gas hydrate occupies 1-10% of the pore space (Paull et al., 1996). Recent investigations from ODP Leg 204 and IODP Leg 311 on the three-dimensional distribution of gas hydrate within Hydrate Ridge, Cascadia Margin, provided new insights about the gas hydrate content and distribution in sediments, as well as about the presence of free gas within the GHSZ (Tréhu et al., 2003; Riedel et al., 2006; Tréhu et al., 2006). These studies confirm a highly heterogeneous distribution of gas hydrates in marine sediments (Tréhu et al., 2003, 2004a). The average amount of gas hydrate is estimated to be 1-2% of the sediment pore space (Milkov et al., 2003b; Tréhu et al. 2004a). Patchy zones of locally high concentration occur below 40 m occupying up to 20% of the pore space. Very high gas hydrate content with 30-40% of pore space is limited to the upper 30-40 meter below seafloor (mbsf) at the southern summit of the ridge near seep sites (Tréhu et al., 2004a), resulting from focused fluid migration into and through the GHSZ towards seafloor vents (Torres et al., 2004). The massive gas hydrate deposits coexist with brines (Torres et al., 2004) formed during formation of gas hydrates by exclusion of dissolved ions, which are too large to fit into hydrate cages. Over time, the excluded ions are removed by advection or diffusion (Ussler and Paull, 2001). Thus, the co-existence of high gas hydrate deposits and brines indicates rapid gas hydrate formation. Recent modeling by Torres et al. (2004) shows that the rapid growth of hydrates could only be explained by upward transport of abundant free gas, since the observed chloride enrichment cannot be generated from the transport of methane dissolved in the pore fluids. Anomalous high and massive shallow gas hydrate concentrations due to focused fluid flow may form in other areas of fluid venting as well.

Free gas migration within the GHSZ has been previously inferred from the observation of bubble plumes, seismic data and critical pressure models (Gorman et al.,

2002; Flemings et al., 2003). The presence of free gas within the GHSZ is not fully understood, since seafloor sediments are generally very porous and contain abundant water, so that gas hydrates should be formed. Several mechanisms whereby free gas migrates through the GHSZ have been suggested, such as hydrate or oil coatings around gas bubbles isolating the free gas phase from the pore water (Suess et al., 2001), high pore water salinity or increased heat flow that locally shift the stability field of gas hydrates down, local dehydration of sediments, and inhibition of hydrate formation because of capillary forces (Ginsburg and Soloviev, 1997; Clennell et al., 1999; Bohrmann et al., 2003; Milkov et al., 2004). Milkov et al. (2004) argue that free gas can move through the GHSZ in association with high salinity water. Co-existence of gas hydrate and free gas could occur when gas hydrate formation is faster than removal of ions excluded during hydrate formation, so that pore waters may become too saline for further gas hydrate formation.

The recent studies at Hydrate Ridge show that critically pressured free gas beneath the GHSZ provides a driving force for gas migration (Tréhu et al., 2004b).

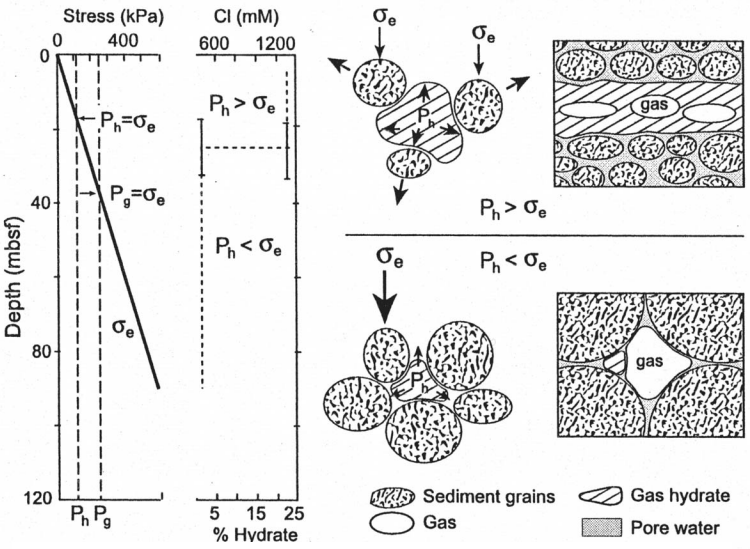

P_h= pressure of hydrate crystallite. P_g= pressure of gas bubbles. σ_e= effective overburden stress

Figure 1.11: *Schematic illustration of the effect of geochemical and physical properties of the sediment on gas hydrates and bubbles. Left: Increase of effective overburden stress with depth. Above 20 mbsf, internal pressures are large enough to push aside the sediment grains and result in enhanced gas hydrate contents and brine formation (from Torres et al., 2004).*

High gas hydrate saturations reducing sediment pore space may form a critically pressured gas column beneath the GHSZ and drive gas migration through the GHSZ towards the seafloor (Tréhu et al., 2004b). Gas transport through the GHSZ results in gas hydrate formation, which is enhanced in the upper tens mbsf, where the overburden stress is less than the internal pressures of growing hydrate crystals and gas bubbles (Torres et al., 2004) (Fig. 1.11). Torres et al. (2004) demonstrated that the depth at which gas hydrates can form by pushing away sediment grains corresponds to the depth at the base of shallow massive

gas hydrate deposits. This means that below ~30 mbsf capillary effects inhibit hydrate formation, and allow methane gas to coexist with gas hydrate (Clennell et al., 1999) (Fig. 1.11).

1.3 Geological setting of the Black Sea

The Black Sea is a large intercontinental basin with anoxic conditions below a water depth of 100-150 m located within the Alpine orogenic belt on the western flank of the active Arabia-Eurasia Collision and north of the North Anatolian Fault (e.g. Rangin et al., 2002). It is surrounded by the Balkanides in the west, the Crimean Mountains in the north, the Caucasus in the east and the Pontides in the south (Fig. 1.12).

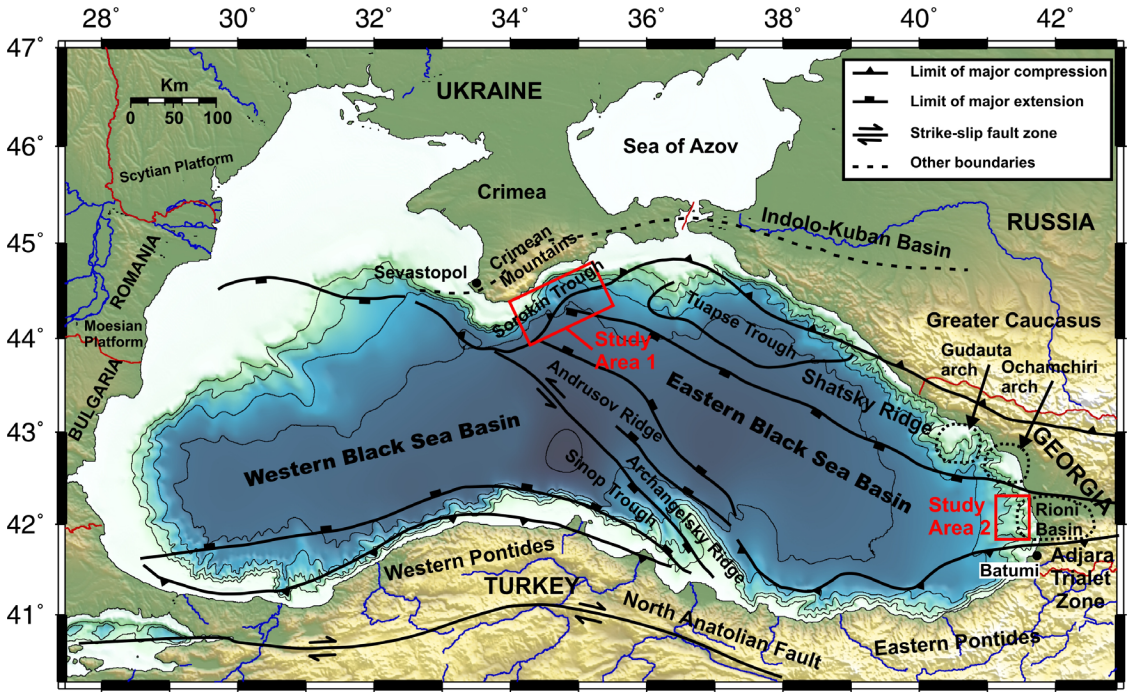

Figure 1.12: *Bathymetric map of the Black Sea and the surroundings (Gebco 1-min grid) together with the general geological structures and tectonic elements of the Black Sea (modified after Robinson et al., 1996). The locations of the study areas are marked as red rectangles.*

The Black Sea is connected by the Kerch Street to the Sea of Azov in the north and via the narrow Bosporus and the Sea of Marmara with the Mediterranean in the south-west (Ross et al., 1974). Thus, the Black Sea has only a restricted exchange with the global oceans. The northern and north-western continental shelves of the Black Sea are wide due to a large sedimentary influx through several major rivers, such as the Danube, Dniester, Dnieper and Don, but become narrower in the remaining parts of the Black Sea with only a

few small rivers draining into the Black Sea from the south. The shelf break occurs at a water depth between 110 and 150 m; the slope is dipping steeply (5-9°) to the floor of the Black Sea basin at about 2200 m (Duman et al., 2006). Most parts of the basin floor of the Black Sea are recently characterized by a flat abyssal plain at water depths of about 2000-2200 m (Robinson et al., 1995).

The Black Sea is considered to be originated during the Cretaceous by a back-arc extension due to the northward subduction of the Tethys Ocean (Okay, 1994; Nikishin et al., 2003), now closed at a suture passing E-W through Northern Turkey (Robinson et al., 1996). In spite of its extensional origin, the tectonic setting changed to a compressional system due to the collision between Eurasia and Arabia in Eocene times, so that the margins of the Black Sea are recently characterized by compressive deformation (Robinson et al., 1995; Spadini et al., 1996).

Although the basin recently reflects a single depocenter it comprises two extensional basins, the W-E trending Western and the NW-SE trending Eastern Black Sea Basin (Tugolesov et al., 1985; Finetti et al., 1988; Okay et al., 1994). The Western and Eastern Black Sea Basin are separated by the complex NW-SE trending Mid Black Sea Ridge consisting of thinned continental crust (Finetti et al., 1988; Robinson et al., 1996). The Mid Black Sea Ridge is subdivided into the Archangelsky and Andrusov Ridge (Robinson et al., 1996) (Fig. 1.12). The basins have kinematics of separate origin with different formation timing, which is still discussed especially for the Eastern Black Sea Basin (Okay et al., 1994; Rangin et al., 2002). Currently, it is believed that the Western Black Sea Basin opened by the separation of the Western and Central Pontides (North Turkey) from the Moesian Platform (Romania and Bulgaria) in the Mid-Cretaceous (e.g. Robinson et al., 1996). The Eastern Black Sea Basin is younger than the Western Basin and opened by the separation of the Shatsky Ridge and the Mid Black Sea High by rotation about a pole west of Crimea. The age of Eastern Black Sea Basin opening is not as well documented, thus interpretations vary from Jurassic time (Golmshtok et al., 1992), over end-Cretaceous (Nikishin et al., 2003) to a Paleocene/Eocene opening (Robinson et al., 1996; Spadini et al., 1996; Cloething et al., 2003). The Eastern Black Sea Basin is flanked by several ridges (Shatsky, Gudauta, Ochamchiri) and troughs (Sorokin, Tuapse, Sinop) (Fig. 1.12), which developed in the Oligocene-Miocene age due to orogenic activity (Tugolesov et al., 1985; Kutas et al., 1998; Starostenko et al., 2004) and are intersected by several deep faults (Finetti et al., 1988). An enormous post Mesozoic sedimentary coverage in both basins is characterized in seismic data by highly reflective, well stratified and intensively faulted strata. The sedimentary cover is deformed into several diapiric folds in the easternmost part of the Black Sea and south-east of Crimea (Tugolesov et al., 1985). The Western Black Sea Basin is thought to be underlain by oceanic crust covered by up to 19 km thick sediments

(Tugolesov et al., 1985; Nikishin et al., 2003). The basement of the Eastern Basin is thinned and it is still debated whether it consists of oceanic (Belousov et al., 1988; Finetti et al., 1988; Rangin et al., 2002) or continental crust (Tugolesov et al., 1985). The crust in the Eastern Basin is overlain by up to 12 km thick post-rift sediments (Tugolesov et al., 1985; Rangin et al., 2002).

Five main seismic sedimentary units have been distinguished for the Black Sea: (1) the upper Cretaceous with a thickness of 3-6 km and dominated by carbonates, (2) the 3-5 km thick Paleocene-Eocene unit of terrigeneous siliciclastic and carbonate composition, (3) the Oligocene-Lower Miocene clays of the Maikopian Formation with a thickness of 4-5 km, (4) the Middle-Upper Miocene unit composed of siliciclasts with a thickness varying from several hundred meters to 3 km, and (5) the Pliocene-Quarternary consisting mostly of clays with a thickness of 2-3.5 km (Tugolesov et al., 1985; Nikishin et al., 2003). All sequences consist of nearly horizontal and undeformed layers within the basin. The basement beneath is disrupted by several normal faults supporting the extensional origin of the basins (Tugolesov et al., 1985; Zonenshain et al., 1986). During the Quarternary, increased sediment supply led to significant subsidence and high sedimentation rates, but the water depth decreased only slightly to the present depth of 2200 m (Robinson et al., 1995). Sedimentation rates for the Pliocene-Quarternary varies, but are estimated to be not less than 10 cm/kyrs (Limonov et al., 1994). The modern sediment facies deposited during the last 25.000 years is recognized in most parts of the Black Sea with a maximum thickness in the central Black Sea and is characterized by three units (Ross and Degens, 1974). Coccolithic ooze in alternation with clay sediments (unit 1) overly sapropel layers with coccolithic ooze laminae (unit 2), which in turn are underlain by a lacrustine facies consisting of laminations of terrigeneous clayey material (unit 3) (Ross and Degens, 1974).

The organic-rich sediments of the Black Sea are characterized by high gas concentrations (Hunt and Whelan, 1978), manifested in the observation of abundant cold vents along the continental margins, mud volcanoes, and gas hydrate occurrences. Gas hydrates in the Black Sea were sampled in 1974 for the first time. This recovery was the first proof for natural gas hydrates in marine sediments on the world (Yefremova and Zhizhchenko, 1974). Most parts of the Black Sea are located within the gas hydrate stability zone. Typical bottom water temperatures of 9°C, result in stable gas hydrates below a water depth of 700 m (Ginsburg et al., 1990).

In the Sorokin Trough and along the continental slope off Batumi (Georgia) cold vent sites are common. In the Sorokin Trough seepage is associated with the formation of mud volcanoes at water depth of 1500 to 2200 m (Limonov et al., 1994; Woodside et al., 1997). Offshore Georgia, gas seeps and free gas bubbles were observed at > 800 m water depth within the gas hydrate stability zone (Klaucke et al., 2005, 2006).

1.3.1 The Sorokin Trough

The Sorokin Trough forms a structural depression with a length of 150 km and a width of 50 km, stretching along the south-eastern margin of the Crimean Peninsula in the northernmost part of the Eastern Black Sea Basin. The water depths in the Sorokin Trough range from 800 m to 2200 m (Fig. 1.13) (Tugolesov et al., 1985).

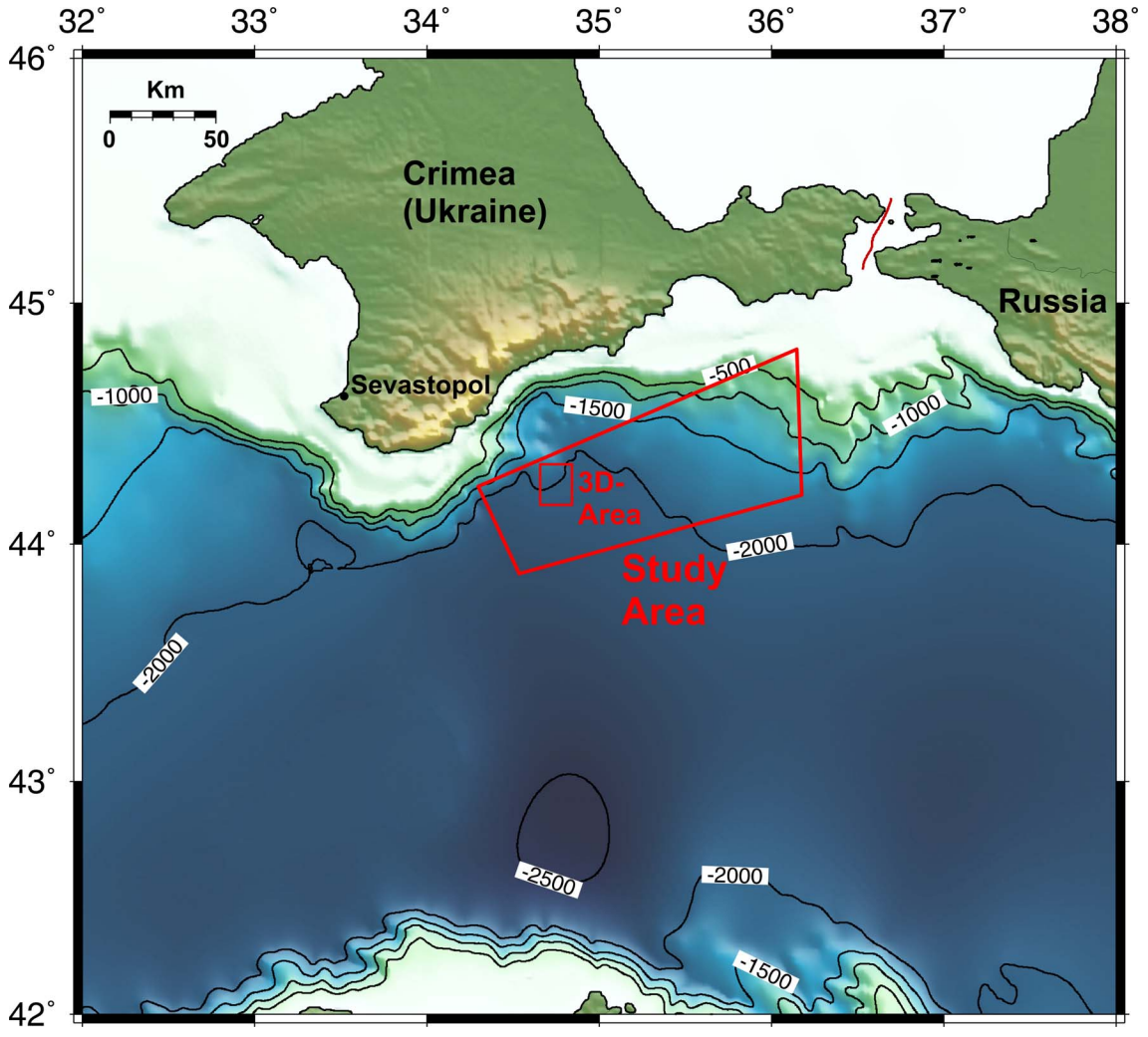

Figure 1.13: *General bathymetric map of the slope south-east of Crimea (Gebco 1-min grid, contours at 500 m) showing the study area (red box).*

The major part of the Sorokin Trough is situated on a flat platform complex at water depths of around 2000 m. In the south and the south-east, the trough is bordered by the buried Cretaceous-Eocene Tetyaev Rise and Shatsky Ridge, and in the north and the west by the marine continuation of the Crimean Mountains (Fig. 1.12). The trough is considered to be the southern foredeep of the Crimean Mountains and is originated during the Oligocene associated with the loading of the Crimean Mountains (Andreev, 1976). A succession of

more than 8 km thick post Oligocene sediments has been deposited in the trough with the Crimean Mountains being the main source (Limonov et al., 1997).

The sedimentary cover of the Sorokin Trough has been divided into two main units based on seismic data collected during the TTR-6 cruise (Woodside et al., 1997). The lower unit comprises the Pliocene deposits and the upper part of the Maikopian Formation (Oligocene-Lower Miocene), which represents the main portion of the deposits in the Sorokin Trough. The Maikop Formation is primarily composed of clay sediments, inter-bedded by marlstones, sand and siltstones, with an average thickness of 3-5 km (Limonov et al., 1997). The Middle Miocene-Pliocene deposits have a maximal thickness of 1 km (Woodside et al., 1997). The sediments of this unit are intensively folded and disrupted by numerous faults, traceable into the upper unit and partly almost reaching the seafloor (Limonov et al., 1997). The upper unit consists of Quarternary sediments characterized by subparallel, rarely faulted bedding, forming a blanket above the lower unit with synclines between the diapiric structures (Limonov et al., 1997). The Quarternary deposits are laterally subdivided into fan deposits of the Pleistocene Palaeo Don-Kuban Fan and basinal deposits, comprising hemipelagic sediments and turbidites with origin in the Crimean Mountains (Limonov et al., 1997). Turbidity currents formed a system of narrow channels in the western Sorokin Trough (Akhmetzhanov et al., 2002). The fan deposits are characterized by several channel-levee systems forming an accumulative structure with complex relief in the East (Volkonskaya, 1997). Due to a significant subsidence in the Pleistocene high sedimentation rates of 25 to 75 cm/kyrs are documented for the Quarternary sediments (Limonov et al., 1997; Akhmetzhanov et al., 2002).

The Sorokin Trough is characterized by compressive deformation due to the tectonic loading of the southward oriented Crimean Mountains and the northward moving Shatsky and Tetyaev Ridges (Limonov et al., 1997). The compressive tectonic regime, in combination with the weight of the thick overburden result in the protrusion of plastic and water saturated Maikopian clays forming diapiric structures, which reach up to several 100 mbsf and mainly strike in the E-W direction (Limonov et al., 1997; Woodside et al., 1997) (Fig. 1.14). The thickness of the overlying Quarternary unit varies from several 100 m up to 2.5 km, which is controlled by the growths of diapirs, and increases progressively towards the north-east (up to 3 km), where the thick Palaeo Don-Kuban Fan deposits dominate. Westward, the fan deposits merge with the turbiditic and hemipelagic deposits (Limonov et al., 1997). Forced by the compressive deformation, fluid/gas migration towards the seafloor and over-pressured fluids lead to the formation of numerous mud volcanoes, mostly located above the near-subsurface diapiric structures (Fig. 1.14) and primarily associated with faults acting as migration pathways for rising fluidized mud (Woodside et al., 1997).

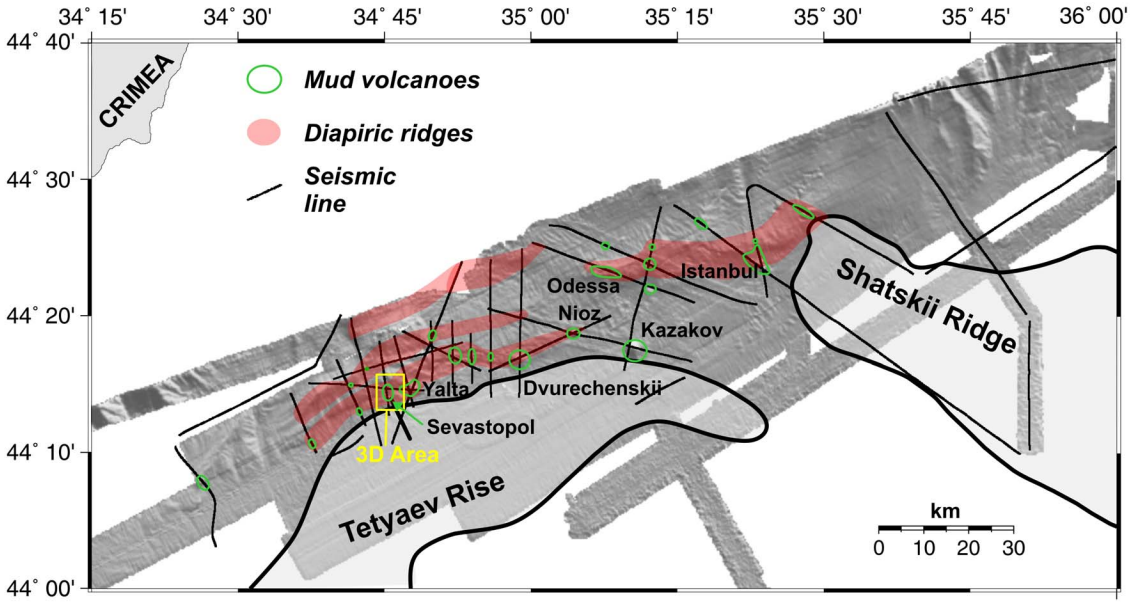

Figure 1.14: *Grey-shaded bathymetric map of the Sorokin Trough together with the locations of the seismic lines collected during the Meteor Cruise M52/1 and the main structures. The bathymetry combines Hydrosweep data acquired during Meteor-Cruise M52/1 with multibeam data collected during the TTR-6 Cruise in 1996 using a Simrad EM-12 system. The green circles show the mud volcanoes identified during the Meteor Cruise M52/1, the red zones give the trend direction of the near-subsurface diapiric structures.*

Fig. 1.14 shows the distribution of the mud volcanoes and the location of the diapiric ridges in the Sorokin Trough. Mud volcanoes in the Sorokin Trough were discovered during the last three decades and have been intensively studied since the TTR cruises in the 1990s (Limonov et al., 1994, Ivanov et al., 1998; Kenyon et al., 2002, Krastel et al., 2003). The mud volcanoes can be classified into three morphological types: most of the mud volcanoes are cone-shaped, some are collapsed structures (pockmarks), and one, the Dvurechenskii mud volcano, is flat-topped (Krastel et al., 2003). The mud volcanoes are concentrated at the northern edges of the Tetyaev Rise and the Shatsky Ridge (Fig. 1.14). Mud volcanism in the Black Sea in general and specifically in the Sorokin Trough is related to the Maikopian Formation, as most clasts cored are derived from the Maikop clay (Woodside et al., 1997).

The sediments of the Sorokin Trough are characterized by high gas content in the form of both free gas and gas hydrate accumulations (Ivanov et al., 1998). Gas measurements showed that methane is the dominated gas with 98-99.9% of the total content of hydrocarbons (Stadnitskaya, 1997). The composition of the hydrocarbons shows a thermogenic component indicating that the high gas content in the Sorokin Trough is contributed to upward fluid migration from sources at greater depth (Ivanov et al., 1998).

Gas hydrates were recovered from several mud volcanoes (e.g., Ginsburg et al., 1990; Bouriak & Akhmetjanov, 1998; Ivanov et al., 1998, Kenyon et al., 2002; Bohrmann et al., 2003), but no BSR is present on seismic images of the Sorokin Trough.

1.3.2 The continental slope offshore Georgia

The Georgian Continental Slope is located at the south-eastern margin of the Eastern Black Sea Basin, and is bordered by the Shatsky Ridge in the north-east and limited in the south-east by the Eastern Pontides thrust belt (Robinson et al., 1995) (Fig. 1.15).

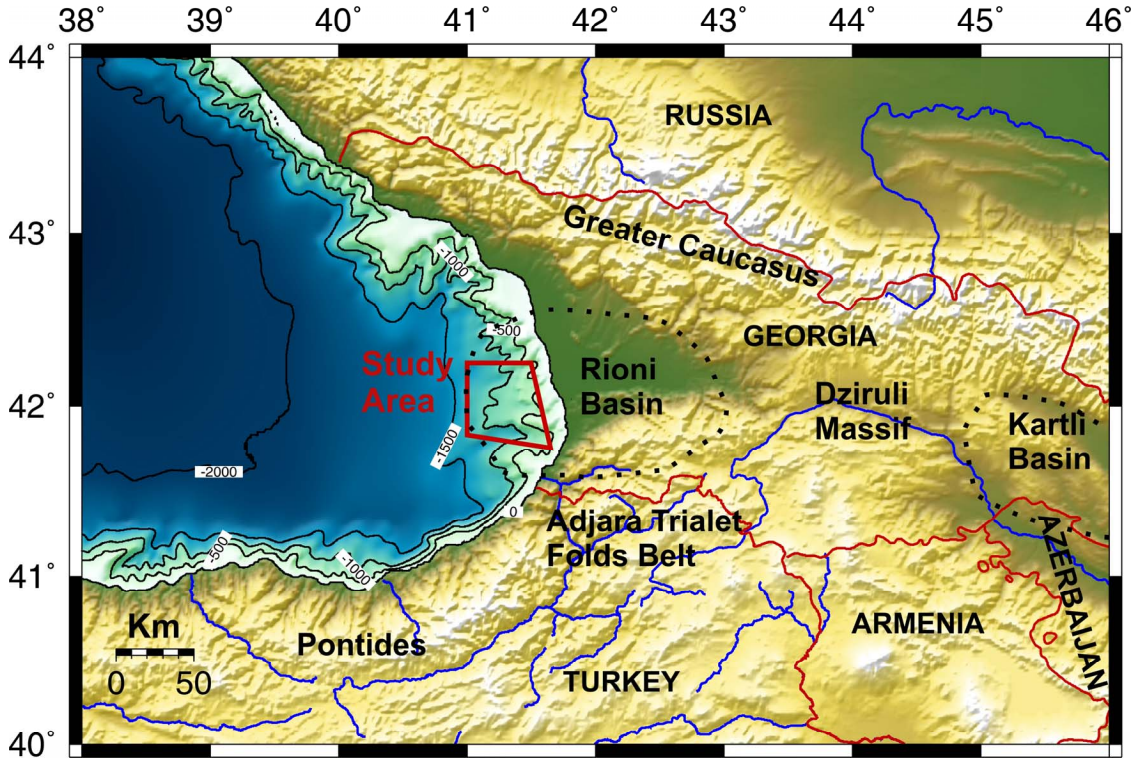

Figure 1.15: *General bathymetry (Gebco 1-min grid, contours at 500 m intervals) of the continental slope off Georgia showing the location of the study area off Batumi (red box).*

The ~20 km wide Shatsky Ridge trends from offshore Crimea in ESE direction towards Georgia, crossing the coast near Poti, and is interpreted to be the northern rift margin of the Eastern Black Sea Basin (Robinson et al., 1996). Two major thrust belts affect the geology of Georgia: the east-southeast trending Greater Caucasus Thrust Belt in the north and the E-W trending north vergent Adjara Trialet Fold Belt in the south (Figs. 1.12, 1.15). The Adjara Trialet Belt is originated in the Paleogene as an extensional basin closed during the Late Eocene or Oligocene and deformed during the Miocene (Robinson et al., 1997). In

eastern Georgia, the Adjara Trialet Belt becomes overriden by the Greater Caucasus (Banks et al., 1997; Robinson et al., 1997). In the west, the Adjara Trialet Belt is linked to the on- and offshore structures of the Eastern Pontides; in the north the Adjara Trialet Belt overrides the Shatsky Ridge, which is flexed down to the south (Banks et al., 1997; Robinson et al., 1995;). The thrust belts of Georgia are separated by two W-E trending foreland basins, the Rioni Basin extending to the Black Sea in the west and the Kartli Basin in the east extending into the Caspian Sea (Banks et al., 1997) (Figs. 1.12, 1.15).

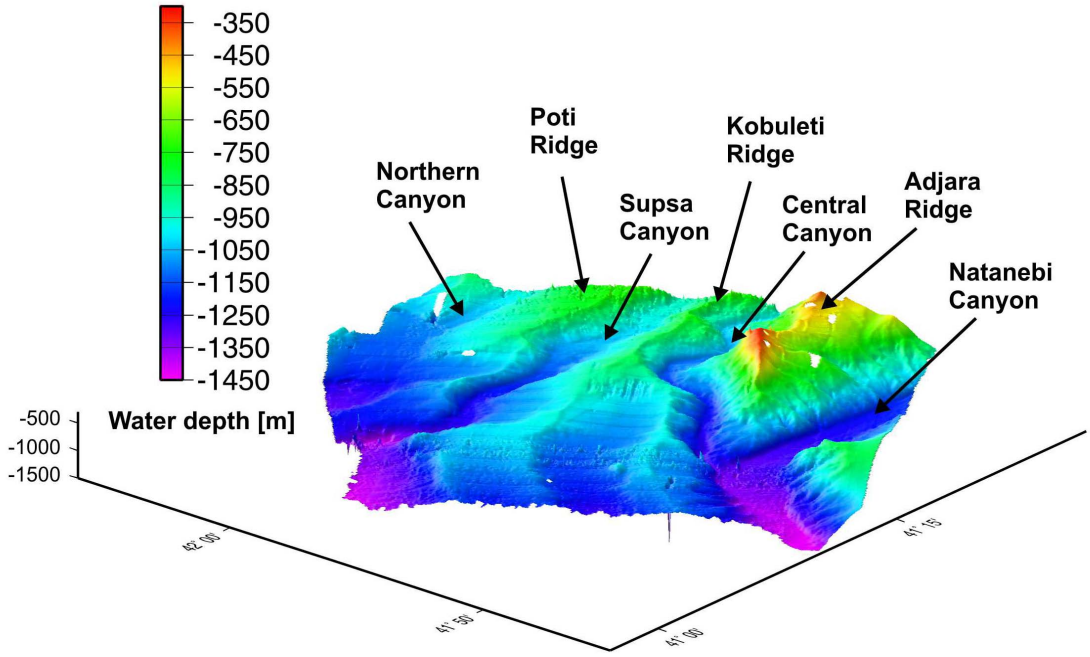

Figure 1.16: *Three-dimensional bathymetric map of the central study area off Batumi (Georgia) collected during the P317 cruise by using a 50 kHz ELAC Bottomchart Mk-II multibeam with a grid cell size of 50 m (Klaucke et al., 2005).*

The Jurassic-Cretaceous sequences below the onshore part of the Rioni and Kartli Basin are considered to represent the continuation of the Shatsky Ridge (Banks et al., 1997). The Rioni and Kartli Basin are of flexural origin developed mainly during the Miocene through the loading of the Adjara Trialet Fold Belt (Banks et al., 1997; Robinson et al., 1997). The basins are separated by the Dziruli Massif (Fig. 1.15), a basement high of the Middle Jura to Lower Cretaceous, acting as the main source of the deposits in the Rioni and Kartli Basin (Robinson et al., 1997). The thick Upper Miocene to Quarternary sediments deposited in the Rioni Basin onlap the Shatsky Ridge in the north and merge eastward with the post-rift fill of the Eastern Black Sea Basin (Banks et al. 1997; Robinson et al., 1997). Numerous unconformities within the sequence reflect the development of submarine canyons transferring sediment to the Black Sea (Banks et al., 1997). In the south and the

east, the Rioni Basin is overridden by the Pontides leading to obscured margins (Rangin et al., 2002).

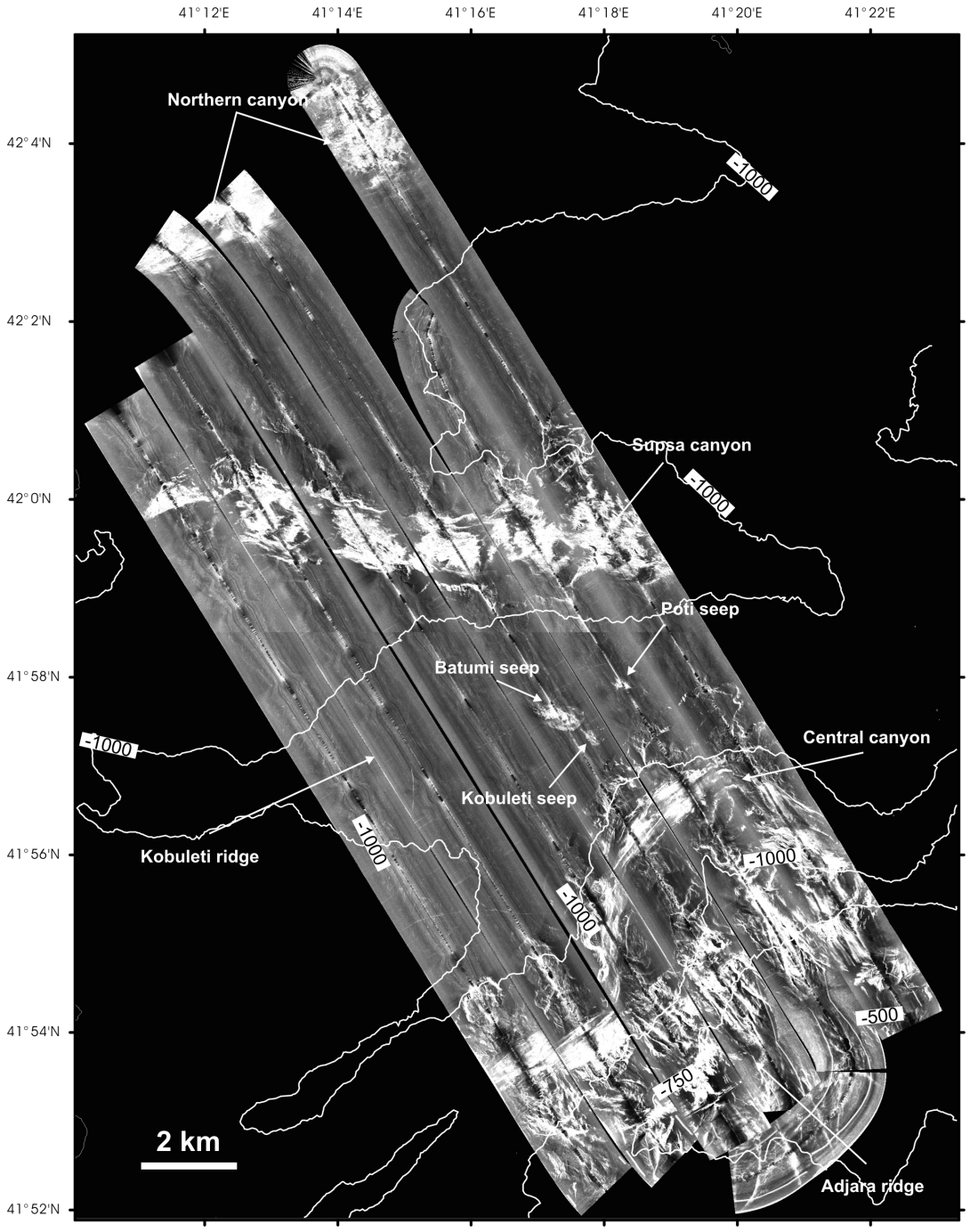

Figure 1.17: *Mosaic of 75 kHz DTS-1 side-scan sonar profiles showing the canyon-ridge system offshore Batumi and several seep locations. White represents high back scatter intensity (after Klaucke et al., 2006).*

The study area offshore Batumi, located at the offshore extension of the Rioni Basin, is characterized by a complex system of W-E striking canyon and ridge structures (Fig. 1.16). Within the Rioni Basin the Maikopian Formation is deformed into several W-E trending anticlinal structures (Tugolesov et al., 1985), but is not related to mud volcanoes as in other parts of the Eastern Black Sea Basin (e.g. the Sorokin Trough). Numerous gas seeps occur off Batumi, which are associated with the ridge structures. The seeps have been identified as acoustic anomalies in the water column and as high backscatter patches on the seafloor on side-scan sonar records collected during the P317 cruise in 2004 (Klaucke et al., 2005, 2006) (Fig. 1.17).

1.4 Materials and methods

The high resolution multichannel seismic data presented in this thesis were collected during to cruises: Seismic data in the Sorokin Trough were collected during Meteor cruise M52/1 in January 2002 in the frame of the MARGASCH project (Marine gas hydrates of the Black Sea). The continental slope off Batumi (Georgia) was investigated in the frame of the METRO project (Methane and methane hydrates within the Black Sea: Structural analyses, quantification and impact of a dynamic methane reservoir) during TTR-15 cruise with R/V Professor Logachev in June 2005. Additionally, data include Parasound sediment echosounder and Hydrosweep multibeam swathsounder data recorded during the M52/1 cruise simultaneously to the seismic profiling. The Hydrosweep data has been combined with Simrad EM-12 multibeam data acquired during the TTR-6 cruise (Woodside et al., 1997). Bathymetric data offshore Batumi shown in Chapter 4 represents ELAC Bottomchart Mk-II multibeam data collected during the Poseidon cruise P317 (Klaucke et al., 2005). In the Sorokin Trough the seismic survey was divided into 2 parts: initially 2D overview profiles were shot and then a 3D survey was shot based on the results of the overview lines in order to resolve the structural variability of the Sevastopol mud volcano. For this study ~570 km of 2D seismic lines and ~620 km of 3D seismic data off Crimea as well as 324 km of seismic profiles off Georgia have been processed and analyzed.

1.4.1 The Bremen high resolution multichannel seismic system

The seismic data used for this study were collected with the Bremen high resolution multichannel seismic system, which is specifically designed to acquire high resolution seismic data through optimizing all system components and procedural parameters. Different seismic system setups were used during the M52/1 and TTR-15 cruises, both described in detail below. The principal setups of the seismic surveys are outlined in Figs. 1.18 and 1.19.

1.4.1.1 Data acquisition

During the M52/1 cruise three different seismic sources, two different GI-Guns with chamber volumes of 2 x 1.7 l and 2 x 0.4 l, respectively, and one Watergun with 0.16 l chamber volume, were used for generating the seismic signal. The guns were operated in a quasi-simultaneous mode at a time interval of 9 s. Only GI-Gun data are analyzed in this thesis. The main frequencies of the used GI-Gun range from 50Hz to 500Hz. During the first 12 profiles the GI-Guns were triggered in an alternating mode and only one GI-Gun was shot each time interval leading to a shot repetition time of 18 s for the different GI-Guns. This setting results in a shot distance of 60-70 m for the individual GI-Guns. Along all further profiles only the 0.4 l GI-Gun was shot in order to increase the coverage. The 0.4l GI-Gun was selected due to its slightly higher frequency content, because the aim of the survey was to record high resolution images of the near-subsurface. The acquisition geometry of the 3D seismic survey consists of 81 parallel 2D lines with a line spacing of 25 m. Additionally, 24 profiles with a line separation of 50-100 m were collected at the margins of the 3D grid and 11 cross profiles were shot as connecting lines to the overview profiles.

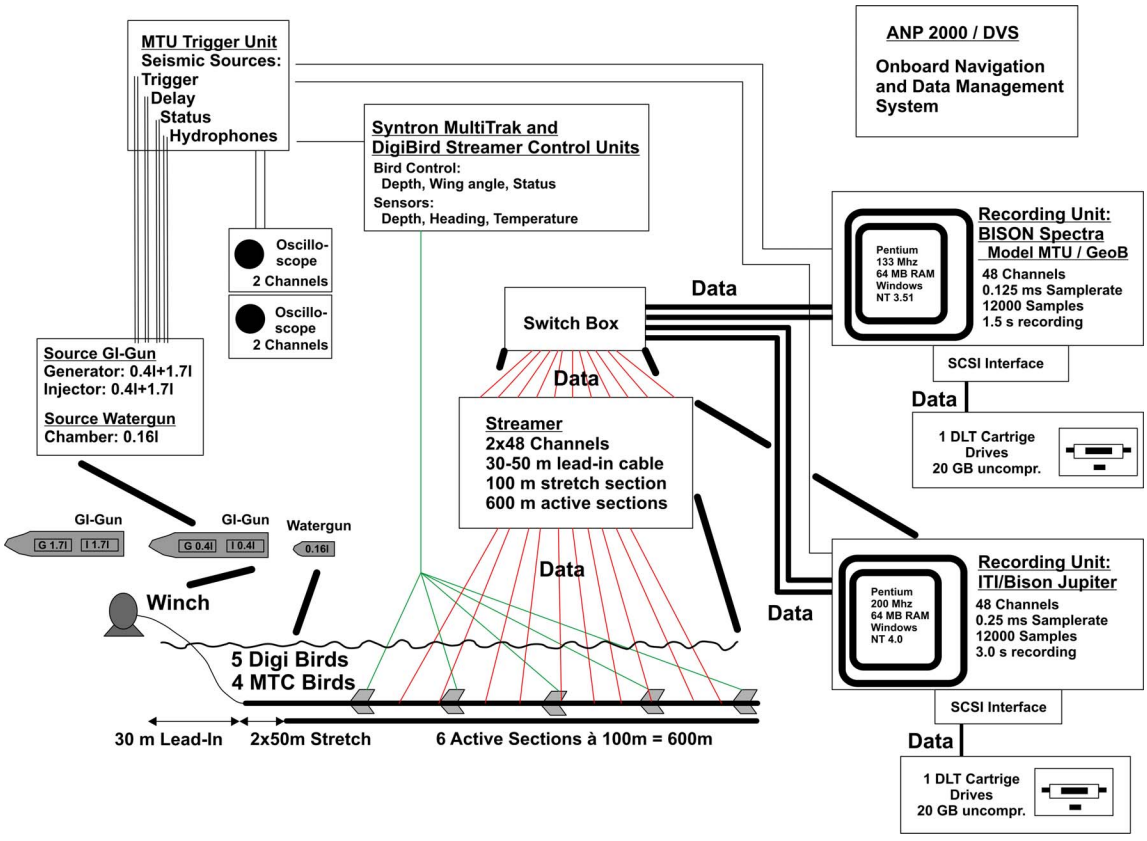

Figure 1.18: *Outline of the high resolution multichannel seismic data acquisition system used during the Meteor cruise M52/1 off Crimea (after Bohrmann and Schenk, 2002).*

During the TTR-15 cruise only the 2 x 1.7 l GI-Gun was used in harmonic GI mode with main frequencies of 50-400 Hz at a shot interval of 10-12 s, depending on the availability of high-pressure air, which was provided by two shipboard compressors. Only for one line, GeoB05-057, a Mini-GI-Gun with a chamber volume 2 x 0.18 was deployed at 5 seconds shot interval to get a high resolution image of the uppermost 500 ms TWT. The seismic profiling during the TTR-15 cruise was either deployed parallel to the OKEAN or the deep towed MAK side-scan sonar and the subbottom profiler system of the R/V Logachev. The average shot point distance was about 25-31 m at 5 knots ship speed during the operation parallel to the OKEAN system and about 10-12 m at 2 knots ship speed at the operation parallel to the MAK system.

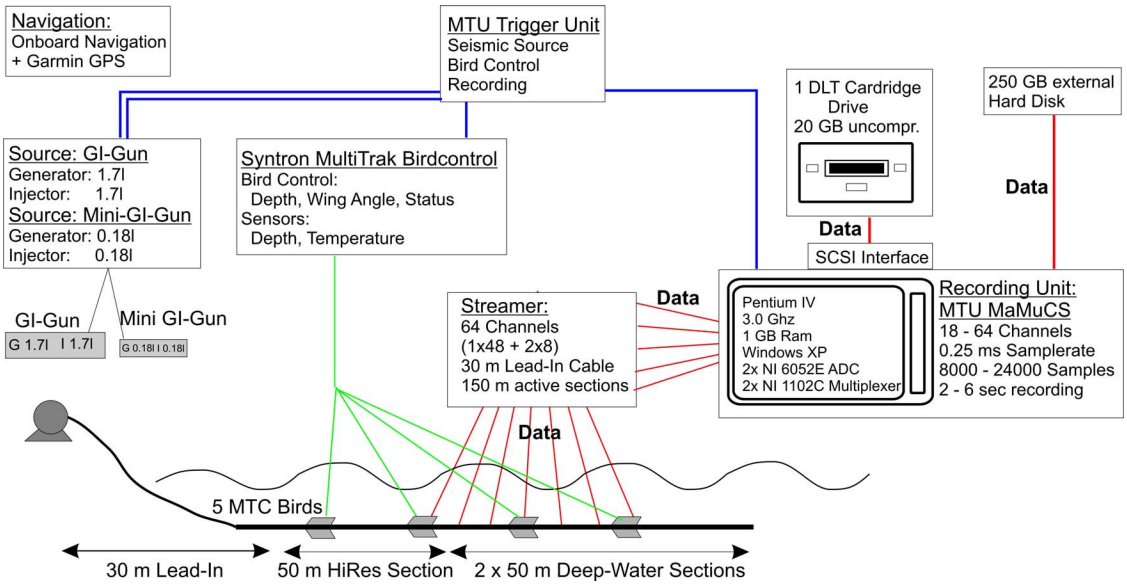

Figure 1.19: *Outline of the high resolution multichannel seismic data acquisition system used during the TTR-15 cruise off Batumi.*

During both cruises the signal was recorded by using an oil-filled SYNTRON streamer, equipped with separately programmable hydrophone subgroups of different lengths in order to optimize resolution and bandwidth of the received signals. During the M52/1 cruise the streamer was employed with a 35 m long lead-in cable, a 50 m long stretch section and six active sections of 100 m length each, while during the TTR-15 cruise the streamer had a 30 m tow-lead and three active sections of 50 m length each. Offshore Crimea, 48 channels of 6.25 m length and a group distance of 12.5 m recorded the GI-Gun data. Offshore Georgia, the first active streamer section used was especially designed for high resolution imaging at shallow water, containing 48 channels at a channel spacing of 1 m. This configuration was of reduced performance for greater water depths, and hence this section was not used for processing and interpretation. The second and third active sections

(SYNTRON) are subdivided into 16 hydrophone groups with a length of 6.25 m. Generally, the streamer was kept in a water depth of 3 m (+/- 0.5 m) by the attachment of four MultiTrak Remote Units (MTC Birds) and five DigiCourse Birds (DigiBirds) during the M52/1 cruise and the use of five MTC Birds during the TTR-15 cruise. The birds contain a depth sensor and adjustable wings, which could be remotely controlled with a PC-based control-unit. Magnetic compass readings allowed for the determination of the position of each hydrophone group relative to the ship course.

The streamer was connected with a deck cable via a switch box to the recording system. On the M52/1 cruise the GI-Gun data were digitally recorded by a Jupiter/ITI/Bison seismograph, which allows online display of the shot gather and demultiplexing of the data. The GI-Gun data were recorded at a sampling frequency of 4 kHz over an interval of 3 seconds. Pre-amplifiers were set to 48 dB, low-cut filter to 16 Hz. A delay was adjusted depending on the current water depth. The data were stored on DLT 4000 cartridge tapes (20 GB) in SEG-Y format. During the TTR-15 cruise a newly in house designed data acquisition system, consisting of a Pentium IV based PC with two NI6052E 16 bit AD converters, was used for the first time. Each ADC is connected to a 32-channel multiplexer with onboard pre-amplification and anti-alias filter. The custom developed acquisition software permits a continuous recording of maximum 64 channels and allows storing the data in demultiplexed SEG-Y format on hard disk, as well as online display of the shot gathers and online profile plot using brute channel stacks of arbitrary channels. Data were recorded at a sampling frequency of 4 kHz over an interval of 5 seconds with a delay of 0 seconds.

1.4.1.2 Data processing

The processing of the multichannel seismic data was applied by using the custom developed software package GeoApp for the geometry processing (Zühlsdorff, 1999) and the commercial VISTA software (Seismic Image Software Ltd.) for the main processing steps.

The geometry processing includes the calculation of the shot and receiver positions, the CMP-sorting and the static correction to correct vertical movements of the streamer recorded by the birds. The input data for the geometry processing contains the following information: (1) shot number and time information, (2) navigation information, (3) depth data of the birds and (4) heading data of the birds. For all datasets, initially all information of the data were resampled to the same time interval by a time interpolation. As the further processing procedures of the 2D and 3D seismic data differ, the single steps for both are described separately below. All seismic data were displayed and interpreted by using the commercial software package Kingdom Suite (Seismic Micro Technology, Inc.).

Processing of the 2D seismic data

Only the GI-Gun data collected during the M52/1 cruise and only the data recorded with the second and third streamer section collected during the TTR-15 cruise were processed and analyzed in this study. First, the reflection midpoints between the source and the receiver (CMPs) were calculated for each trace based on the information of the navigation and heading data. The CMPs were defined as small circles, so-called bins, with distinct sizes and distances along the cruise track. Each midpoint was assigned to one bin with the minimum distance to the center of the bin. Based on this procedure, a CMP number was determined for each shot-receiver pair. A calculation of the static correction time was then applied for each trace using lateral linear interpolation of the depth information of the birds for each receiver. The static correction time and CMP number were exported as ASCII files and imported into Vista. After delay correction a velocity analysis was utilized to obtain the velocities for NMO corrections and stacking. The velocity analysis showed that a constant velocity of 1500 m/s could be used for the data due to the relatively short streamer length and water depths >1000 m. The data collected during the M52/1 cruise were stacked at a bin distance of 10 m leading to 7-8 fold coverage, while the data of the TTR-15 cruise were stacked at a bin distance of 10, 15 or 20 m leading to 10 fold coverage on average. The stacked sections were bandpass frequency filtered with a frequency content of 55/110 - 600/800 for the M52/1 data and 20/40 - 200/400 for the TTR-15 data and finally time migrated. For the TTR-15 data, coherent noise with main frequencies at 50 Hz, which is believed to be caused by mechanical vibrancy of the ship or streamer, was reduced by fk-filtering with a wave number between -0.25 and +0.25 before stacking.

Processing of the 3D seismic data

The 0.4 l GI-Gun data collected during the 3D seismic survey across the Sevastopol mud volcano were processed and analyzed in this study in order to image the uppermost 500 ms of the sediments with best possible resolution. A processing flow of the 3D seismic data is shown in Fig. 1.20. For the processing of the 3D dataset initially a 3D grid with specified coordinate edges and a given inline spacing of 25 m and a crossline spacing of 12.5 m was created for the survey area. This grid was used to calculate the coordinates for each cross point of the gridlines. The traces of each line were sorted to common cell gathers with a cell width of 12.5 m in the inline direction and 25 m in the crossline direction. Traces assigned to the same cell could derive from different profiles and traces from the same profile could be assigned to cells on different inlines. Thus, the trace coverage of the cells varies. Mostly 2-3, but partly up to 4 different profiles, were adjusted to one inline. Static corrections were applied as for the 2D data. The information about the cell number,

the inline and crossline number, as well as the static correction time were exported to VISTA and written into the trace headers for each shot-receiver pair.

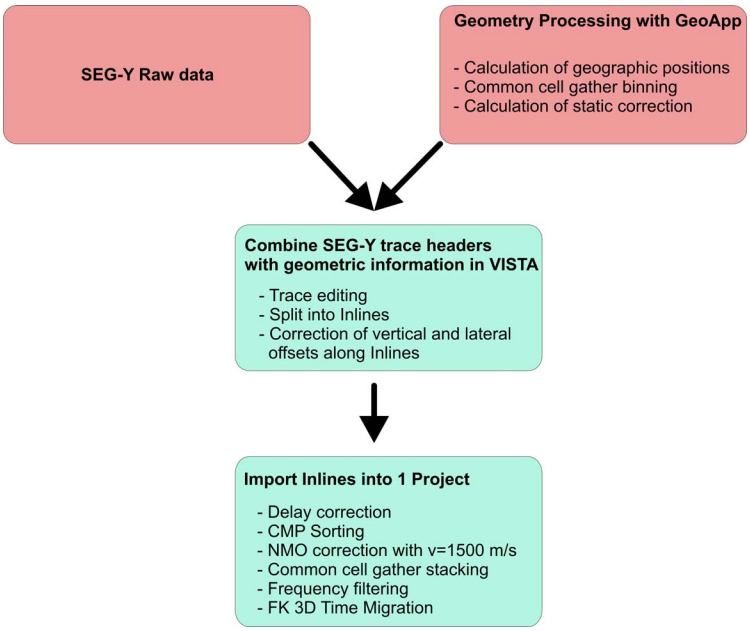

Figure 1.20: *Processing flow applied for the 3D seismic data.*

Profiles were split according to their inline number, and then plots were created showing the data of an inline measured with one profile. After that, lateral and vertical offsets between adjacent profiles binned on the same inline were adjusted. Inaccuracies in the measurement of the equipment outlay lead to inexact geometry and result in lateral offsets between opposite shot profiles. This would cause a constant offset between adjacent profiles with opposite headings. Trigger errors might lead to small vertical offsets. The parts of the acquired profiles belonging to one specific inline were NMO-corrected, filtered and stacked in order to determine the offsets between the measured profiles. As traces of one acquired profile could be binned on different inlines, the coverage of the profile representing one inline could be incomplete. Therefore, missing CMPs were filled with empty-traces, which allows to compare the different measured profiles binned to a specific inline at the same scale. Characteristic morphological structures were used to compare and adjust the profiles on a light table. In the central grid, the lines could be adjusted based on the structure of the Sevastopol mud volcano. The comparison for the lines at the margins of the grid was more complicated as the study area is characterized by a smooth dipping slope without great relief. Here, a slight edge at the seafloor was chosen as structure for comparison. Uncertainties occurred only at locations where comparability of different profiles lacks due to low coverage of several lines. Due to the low line spacing at the margin

of the 3D grid the bin coverage decreases towards the edges of the grid. Fig. 1.21 shows a stacked inline at the margin of the grid with fragmentary coverage and a stacked inline with good coverage in the central grid area.

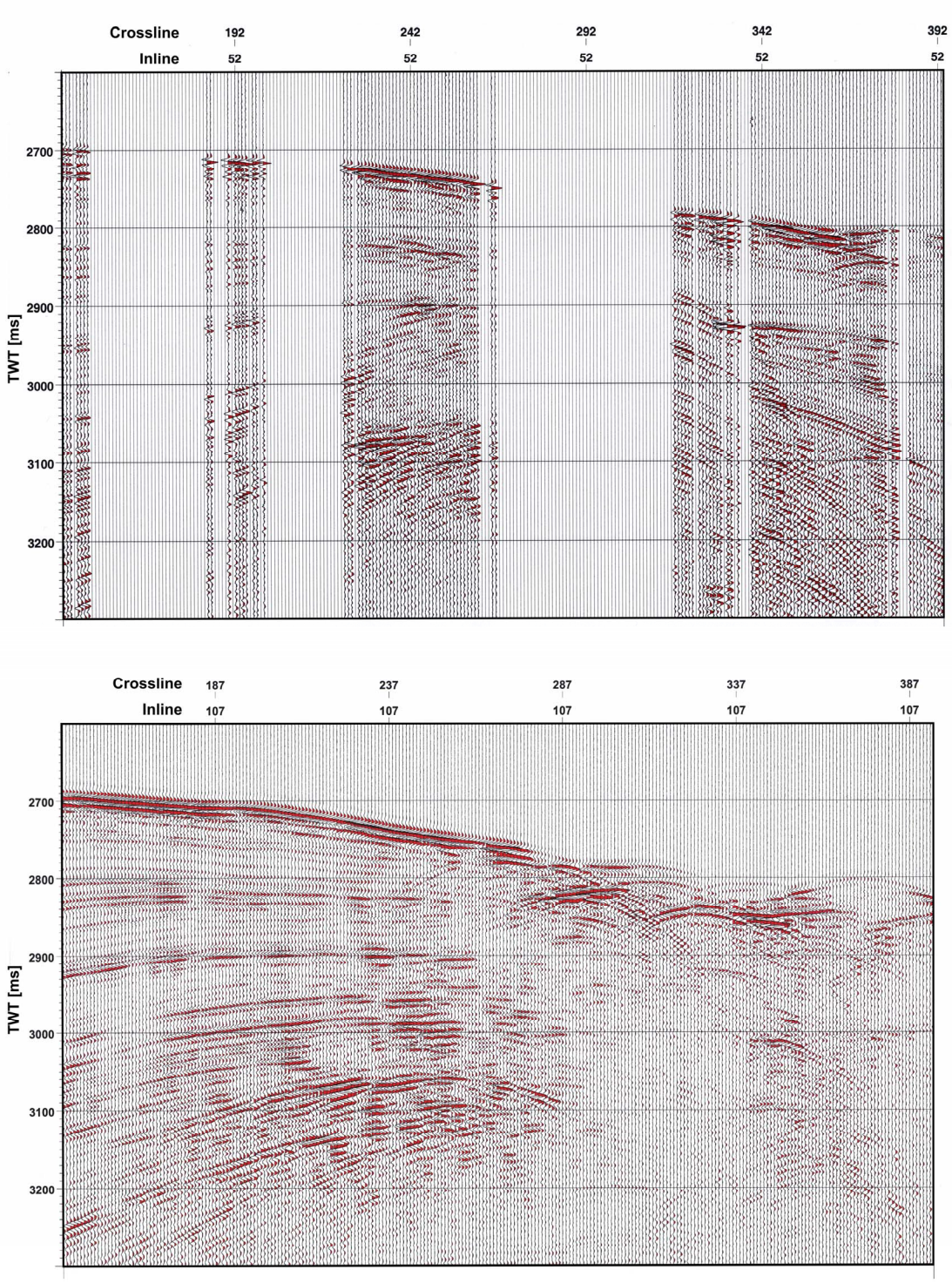

Figure 1.21: *Stacked images of inline 52 at the western margin of the grid area with low coverage (top) and inline 107 in the central grid area with good coverage (bottom).*

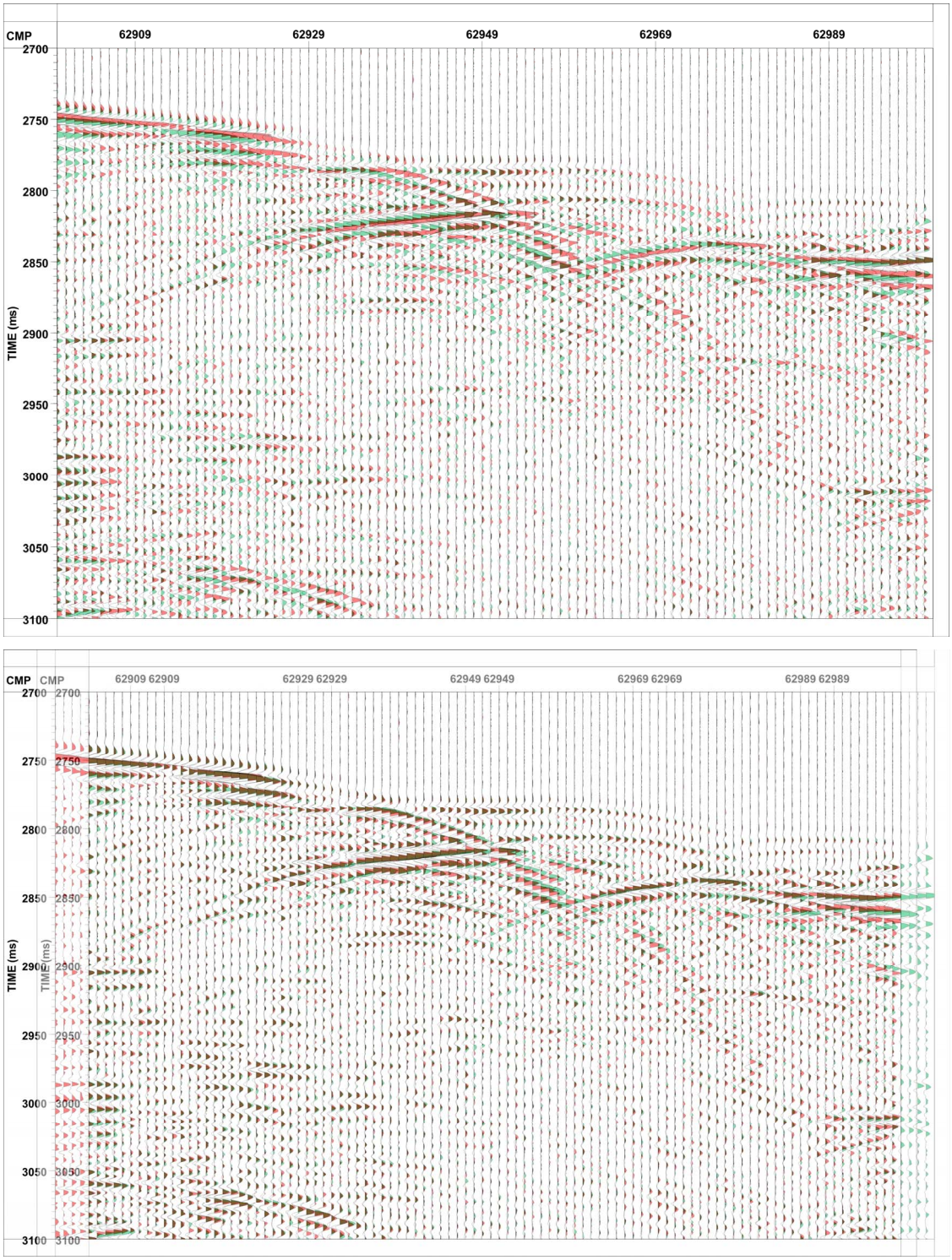

Figure 1.22: *Overlay of stacked profiles 066 and 113 with opposite heading binned on inline 107. Top: Distinct discrepancy between the profiles due to lateral offset. Bottom: Best adjusting of the lines.*

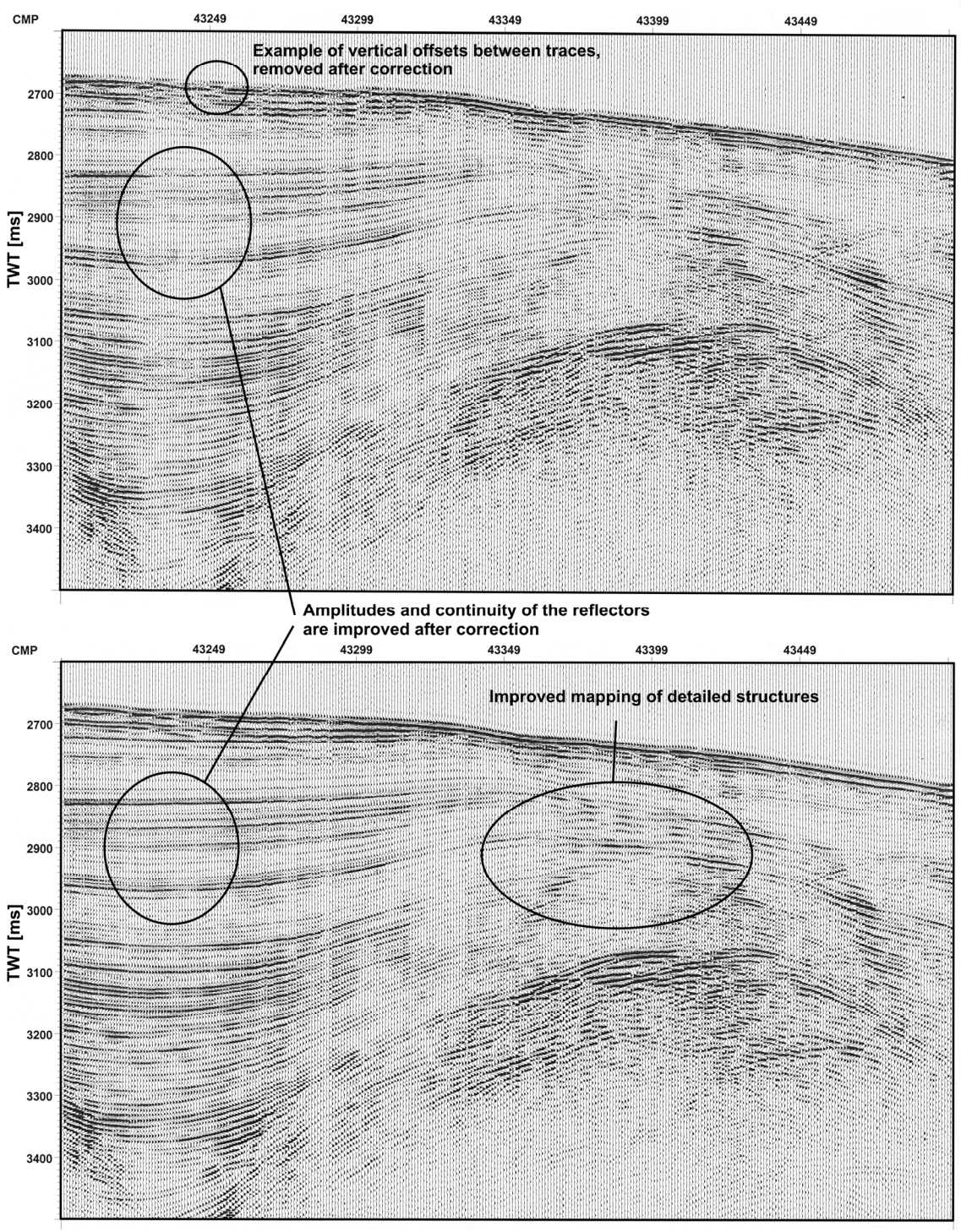

Figure 1.23: *Stacked seismic inline 107, composed of three profiles, before (top) and after (bottom) correction of the lateral and vertical offsets.*

The detailed comparison off all profiles shows that measured profiles with the same heading do not show any offset, but profiles shot in opposite direction show a constant lateral offset of four CMP numbers. This is visualized on Fig. 1.22 showing inline 107. Two acquired profiles (Profiles GeoB02-066 and GeoB02-133) shot in opposite directions were

binned on this inline. The overlay of these two profiles show an lateral offset, which can be corrected by a constant shift of one of the profiles (Fig. 1.22).

The lateral offsets for all profiles was corrected by shifting the even numbered acquired profiles with a heading of about 165° four CMPs to the NNW. Additionally, the profiles between 95 and 112 show a vertical offset of 4 ms TWT, thus these lines were upward corrected with respect to the other lines. The corrections were applied on the raw data for each profile. Afterwards, profiles representing the same inline were combined. On Fig. 1.23, the stacked inline 074, measured by three profiles (062, 105, 134) is imaged before (top) and after (bottom) correction. The quality of the inline is significantly improved after corrections, so that detailed structures and reflectors are more distinctly imaged. For example: before correction numerous vertical offsets between traces of different profiles occur along the inline (top), which are removed after correction (bottom). The corrected inline is characterized by enhanced continuity and reflectivity of the reflectors.

After correction, all inlines were loaded to one project and delay corrected. Based on the results of the velocity analysis applied on the 2D data a constant velocity of 1500 m/s was used for NMO correction. The data were stacked at a common cell gather distance of 12.5 m in the inline direction and 25 m in the crossline direction, leading to 6-7 fold coverage. The stacked grid was bandpass frequency filtered with a frequency content of 55/110 - 600/800 and finally a FK-3D time migration at a constant velocity of 1500 m/s was applied. Locally low and irregular bin coverage along several inlines, particularly at the margins of the grid, and the limited crossline extension affect the quality of the 3D migration, thus only the central grid area, comprising inline 60-140, was used for 3D migration.

1.4.2 The Parasound sediment echosounder

Parasound data of the Sorokin Trough were used for the analysis of mud volcanoes in the Sorokin Trough (Chapter 2). The hull-mounted narrow beam Parasound sediment echosounder is permanently installed on the R/V Meteor. It uses the so-called parametric effect by the emission of two high amplitudes, high frequency sound waves to generate an operational secondary sound wave of the difference frequency lying between 2.5 and 5.5 kHz. This secondary operational signal is focused within a cone with 4° as opening angle, resulting in a footprint diameter of only ~7% of the water depth. Thus, lateral resolution is significantly improved compared to conventional 3.5 kHz systems; vertical resolution is in the order of a few decimeters. Penetration varies between 0 - 200 m, depending on the type of sediment and attenuation (Grant and Schreiber, 1990).

During the M52/1 cruise the data were collected with a difference frequency of 4 kHz. The Parasound data were permanently acquired and digitally recorded and stored by

the ParaDigMa System (Spiess, 1993). To remove acoustic and electronic noise, the data were bandpass filtered from 2-6 kHz.

1.4.3 The Hydrosweep swath bathymetry system

Bathymetric data during cruise M52/1 were recorded using a Hydrosweep multibeam echosounder. The system maps the seafloor by generating 59 pre-formed beams over an angle of 90° at an operating frequency of 15.5 kHz, providing seafloor information of a swath with a width of twice the water depth (Grant and Schreiber, 1990). The lateral resolution depends on the water depth and the slant angle and was about 80 to 200 m at water depths of 2000 to 2500 m.

The data were processed with the public domain software package MultiBeam (Caress and Chayes, 1996), including the correction of the navigation data and the depth values. For removing bad outer beams and abnormal depth values automatic tools were used and remaining artifacts were deleted by interactive editing. Gridding and imaging the data were carried out with the public domain software package GMT (Wessel and Smith, 1998). The Hydrosweep data recorded during the overview profiles in the Sorokin Trough were merged with multibeam data collected with a Simrad EM-12 system during the TTR-6 cruise (Woodside et al., 1997).

2 Characterization of mud volcanoes in the Sorokin Trough (Black Sea) from hydroacoustic data

Michelle Wagner-Friedrichs, Leonid Meisner, Sebastian Krastel and Volkhard Spiess

To be submitted to Marine Geology

2.1 Abstract

High resolution multichannel seismic data collected during the Meteor cruise M52/1 in the Sorokin Trough (Black Sea) south-east of the Crimean peninsula in early 2002 reveal numerous mud volcanoes of various morphology, such as depression, cone-shaped and flat topped structures. The evolution of the mud volcanoes is associated with near-subsurface diapiric structures grown in a compressional tectonic regime. The mud volcanoes are concentrated in three areas of different sedimentological environments and structural features resulting in different evolutions and eruption styles. Generally, the formation of the mud volcanoes in the Sorokin Trough is controlled by fluid migration along faults developed during the protrusion of the diapiric ridges. In the western Sorokin Trough over-pressured fluids are sealed by impermeable or gas hydrate bearing layers in the dominating hemipelagic sediments leading to violent eruptions forming the collapsed depression structures of this area. Trapped gas is indicated by numerous Bright Spots limited to this area. In the central and eastern Sorokin Trough, homogeneous fan deposits of the Palaeo Don-Kuban Fan are characterized by enhanced permeability due to the lack of seals, hence reducing the pore fluid pressure. This is reflected by more quiet effusive eruptions forming cone-shaped structures of partly enormous dimensions with diameters up to 2000 m and heights of 100 m. In the easternmost Sorokin Trough the mud volcanoes additionally are supplied by absorption of the gas saturated fan deposits due to lateral fluid migration towards a morphological high leading to increased fluid content and moussy consistence of the erupted mud.

2.2 Introduction

Mud volcanoes are positive or negative geological structures related to mass and fluid discharge, representing an important source of methane and subordinately carbon dioxide emissions to the hydro- and atmosphere with a high potential relevance to climate change (Milkov, 2000; Holland et al., 2003). The total annual methane emissions to the atmosphere through mud volcanoes are estimated to be about 5 Tg (Dimitrov, 2003). Mud volcanoes are observed all over the world, onshore and offshore, but predominantly occur at compressional systems, as at accretionary complexes, convergent plate margins and thrust belts, but are observed at sedimentary basins with great sediment thickness as well

(e.g. Black Sea and Caspian Sea) (Kopf, 2002; Dimitrov, 2003). Most mud volcanoes occur along the Alpine Himalaya Active Belt with about 1200 terrestrial and offshore mud volcanoes (Dimitrov, 2003). Onshore, mud volcanoes have been intensively studied since several 100 years, but less is known about submarine mud volcanoes. Since the studies of submarine mud volcanoes started during the last three decades, the number of newly discovered mud volcanoes increases yearly, but nevertheless probably there will be yet a great number of submarine mud volcanoes not identified. Milkov (2000) estimated that the number of large seafloor mud volcanoes might exceed 5000.

There are different reasons and factors controlling the formation of mud volcanoes, which are still intensively discussed. Two key reasons for the formation of mud volcanoes were defined by Milkov (2000): (1) high sediment accumulation rate at passive margins and abyssal plains, (2) lateral compression at active margins. Further conditions necessary for the formation of mud volcanoes as density inversion, faulting, over-pressured fluids and fluid migration result from these two key factors listed above (Milkov, 2000).

Mud volcanoes show a great morphological diversity in size and shape, which is directly linked to the formation mechanisms and the physical properties of the eruption product (Brown, 1990; Kopf, 2002). The morphological expression of mud volcanoes is primarily controlled by the fluid content, viscosity and consolidation of the extruded material (e.g. Brown, 1990).

Thick organic rich sedimentary sequences in the Black Sea represent excellent conditions for the evolution of mud volcanoes. In the central Black Sea (Ivanov et al., 1996; Limonov et al., 1997) and in the Sorokin Trough (Woodside et al., 1997; Kenyon et al., 2002; Krastel et al., 2003; Wagner-Friedrichs et al., in review) mud volcanoes are known since the late 1970's and have been intensively studied and documented, particularly since the TTR (UNESCO/IOC Training Through Research Program) cruises during the 1990's. Mud volcanoes in the Sorokin Trough are related to the diapirism of the Maikopian clay and result from the rise of sediments with high fluid content along faults to the seafloor (Woodside et al., 1997).

In this study we present a characterization of mud volcanoes in the Sorokin Trough obtained from high resolution seismic, sediment echosounder and bathymetric data carried out during Meteor cruise M52/1 in January 2002. The data reveal 25 mud volcanoes of varying morphology, size and shape reflecting different driving and evolution mechanisms. The mud volcanoes, located at water depth between 1700 and 2200 m, were cataloged in shape, height, and diameter, and were related to subsurface structures. Accordingly, the mud volcanoes were attributed to three areas characterized by different depositional and structural environments. The main objective of the study is to explain the variability of the mud volcanoes.

Key questions are:

- Are the morphological features related to different subsurface structures influencing the evolution of the mud volcanoes and can the shapes of the mud volcanoes be related to eruption styles?
- What are the fluid migration pathways and are there differences between individual mud volcanoes concerning the fluid migration pathways?
- What is the effect of the sedimentologic environments on the evolution of the mud volcanoes?

Based on the analysis of the above mentioned questions we propose different loading models for the evolution of the mud volcanoes in the various areas of the Sorokin Trough depending on the migration pathways and driving forces.

2.3 Geological overview of the Black Sea and the Sorokin Trough

The Black Sea is generally considered to be originated by a backarc extension due to the subduction of the Tethyan Plate in end-Cretaceous (Dewey et al., 1973; Robinson et al., 1995; Nikishin et al., 2003). This collision of Arabia with Eurasia lead to a compressional tectonic regime during the Eocene (Nikishin et al., 2003), thus in particularly the margins of the Black Sea are characterized by deformation (Robinson et al., 1995). The Black Sea is enclosed by Cenozoic orogenic belts, such as the Pontides in the south, the Caucasus in the east, the Balkanides in the west and the Crimean Mountains in the north (Fig.2.1). The Andrusov and the Archangelsky Ridge separate the Black Sea structurally into two basins, the Western and the Eastern Black Sea Basin (Fig. 2.1), both containing a 10-19 km thick sediment cover, which is underlain either by oceanic or thinned continental crust (Tugolesov et al., 1985). The Eastern Black Sea Basin is characterized by a number of troughs and barriers developed in the Oligocene-Miocene age, such as the Sorokin Trough, Kerch-Taman Trough and Indolo-Kuban Trough (Fig. 2.1).

The Sorokin Trough is located in the northern part of the Eastern Black Sea Basin stretching along the south-eastern continental margin of the Crimean Peninsula with a length of 150 km and a width of 50 km at water depths between 800-2200 m (Fig.2.1) (Tugolesov et al., 1985). The main part of the Sorokin Trough is located on a flat platform complex at water depths of around 2000 m, bordered in the south and the south-east by the buried Cretaceous-Eocene Tetyaev Rise and Shatsky Ridge and in the north and the west by the marine continuation of the Crimean Mountains (Fig. 2.1).

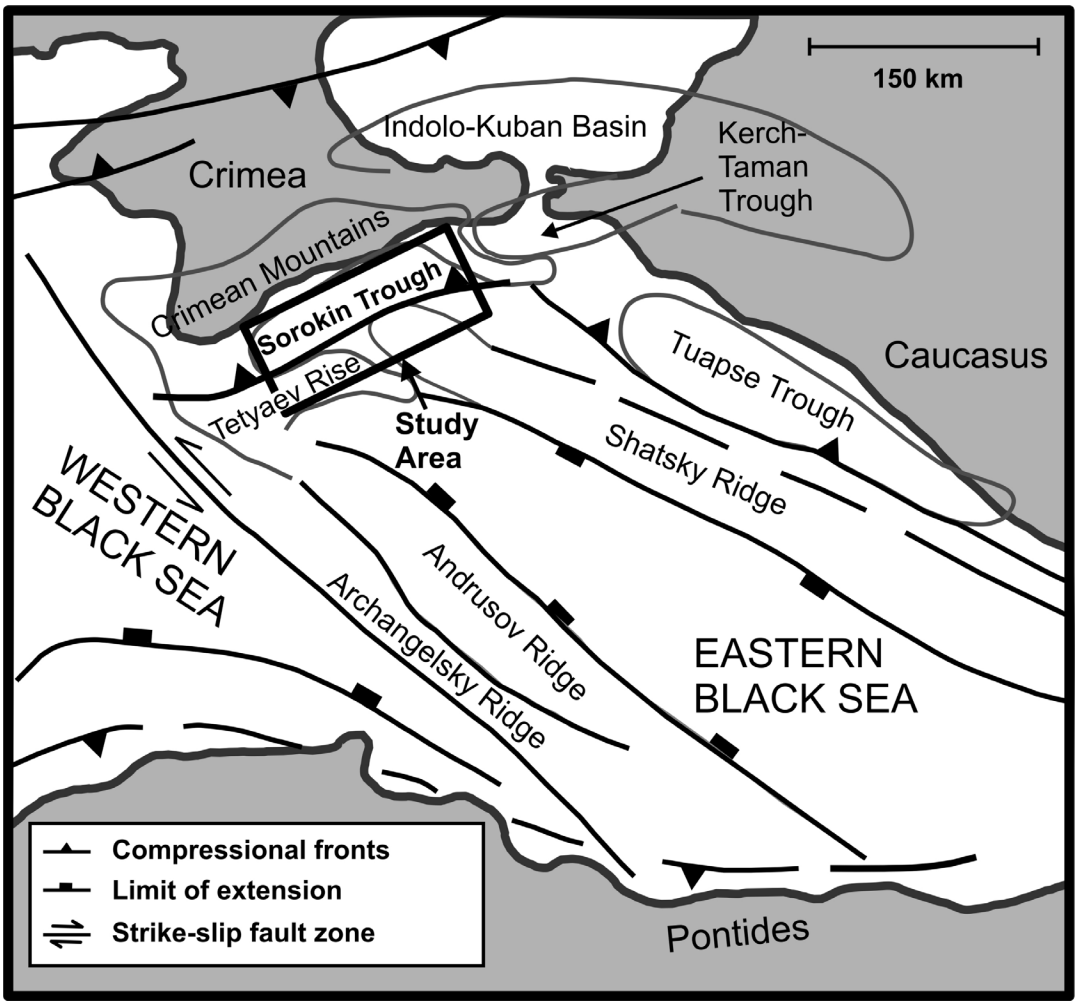

Figure 2.1: *Schematic overview of the structural and tectonic units of the Eastern Black Sea Basin (modified after Robinson et al., 1996). The working area is shown as black box.*

The Sorokin Trough is considered to be a southern foredeep of the Crimean Mountains, which grew in Oligocene times (Andreev, 1976). The Crimean Mountains are the main source for the deposition of the more than 8 km thick succession of Oligocene to Quarternary sediments in the Sorokin Trough. The main part of the deposits is represented by the 3-5 km thick clayey sediments of the Maikop Formation (Oligocene-Lower Miocene) (Limonov et al., 1997). The Miocene-Pliocene deposits are of low thickness (less than 1 km) (Woodside et al., 1997). A significant subsidence in the Pleistocene is documented by high sedimentation rates, leading to thick Quarternary sediments in the Sorokin Trough with an average thickness of 1 km. The Quarternary deposits can be laterally subdivided into fan deposits of the Pleistocene Palaeo Don-Kuban Fan and basinal deposits, consisting of hemipelagic sediments and turbidites with origin in the Crimean Mountains (Limonov et al.,

1997). The north-eastern part of the Sorokin Trough is dominated by the fan deposits leading to increased thickness of the Quarternary sediments up to 2.5 km.

Compressive deformation due to movements of the Crimean Mountains on the one hand and the Shatsky and Tetyaev Ridges on the other hand in combination with the overburden of thick post-Miocene sediments result in the protrusion of the plastic and water saturated Maikop clay forming diapiric structures up to several 100 meter below seafloor (mbsf). The diapiric ridges are mainly striking in the E-W direction, changing towards the east and the west following the flanks of the buried Tetyaev Rise and Shatsky Ridge (Woodside et al., 1997). Fluid flow to the seafloor, forced by the compressive tectonic regime, leads to the formation of mud volcanoes above the top and the edges of the near-surface mud diapirs.

2.4 Previous acoustic studies in the Sorokin Trough

Hydroacoustic studies during the last decades showed the presence of numerous mud volcanoes above diapiric structures in the Sorokin Trough (Limonov et al., 1994; Meisner et al., 1996; Woodside et al., 1997; Ivanov et al., 1998; Kenyon et al., 2002; Krastel et al., 2003). The mud volcanoes are characterized by a highly variable morphology and could be distinguished into three types: cone-shaped mud volcanoes dominate, some are collapsed structures (pockmarks), and one, the Dvurechenskii mud volcano, is flat-topped (Ivanov et al., 1998; Kenyon et al., 2002; Krastel et al., 2003). Gas hydrates in the Sorokin Trough were sampled at several mud volcanoes (e.g., Ginsburg et al., 1990; Bouriak & Akhmetjanov, 1998; Ivanov et al., 1998; Kenyon et al., 2002; Bohrmann et al., 2003), but, despite the sampled near-surface gas hydrates BSRs (bottom-simulating reflector) have not been identified in seismic data. Bright Spots at the top and flanks of several diapiric ridges in the direct vicinity to mud volcanoes are interpreted to represent the base of the gas hydrate stability zone (Krastel et al, 2003; Wagner-Friedrichs et al., in review). Gas hydrates are believed to occur locally where upward fluid migration is focused towards the seafloor, i.e. at the top of the diapirs and/or in direct vicinity to the feeder channels of the mud volcano (Ginsburg et al., 1990; Bouriak & Akhmetjanov, 1998; Wagner-Friedrichs et al., in review). Evidences for extensive fluid venting through the seafloor were found during the TTR-6 cruise, indicated by mud volcanoes, pockmarks and acoustic anomalies (Ivanov et al., 1998). Recently, gas flares have been observed at three mud volcanoes in water depths of about 2080 m using hydroacoustic methods (Greinert et al., 2006). The gas bubbles arise about 1300 m to a water depth of 770 m, which is ~75m below the phase boundary of pure methane hydrate in the Black Sea. The flares appear to be temporal variable, as the Dvurechenskii mud volcano (DMV) was inactive during the Meteor cruise M52/1 in early 2002, but high gas flares were observed in June 2002, May-June 2003 and May 2004. In

June 2004 the flares vanished and the DMV remained inactive in August 2004. At the other surveyed mud volcanoes activity slightly decreased with time, indicated by lower flare heights during the last observations in 2004 (Greinert et al., 2006).

2.5 Materials and methods

The acoustic data used for this study were collected during Meteor-cruise M52/1 in January 2002. Sediment echosounder data were acquired using the hull-mounted narrow beam Parasound System. By utilizing the so-called parametric effect, the system generates an operational signal of 4 kHz focused within a cone of only 4° opening angle, resulting in a footprint diameter of ~7% of the water depth. Thus lateral resolution is significantly improved compared to conventional 3.5 kHz systems. Vertical resolution is in the order of a few decimeters. Penetration varies between 0-200 m, depending on the type of sediment and attenuation (Grant and Schreiber, 1990). The Parasound data were permanently acquired and digitally recorded and stored by the ParaDigMa System (Spiess, 1993).

Multichannel seismic data (MCS data) were acquired using a 0.4l GI-Gun and a 600 m long streamer. For recording we used 48 channels with a group length of 6.25 m at a group distance of 12.5 m. The GI-Gun data were digitally recorded at a sampling frequency of 4 kHz over an interval of 3 s. Remotely controlled birds kept the streamer depth within a range of 1 m. Standard processing procedures were applied to the MCS data with ‘in house’ and the ‘Vista’ (Seismic Image Software Ltd) softwares, including trace editing, geometry processing, static and delay corrections, NMO-corrections, bandpass frequency filtering with a frequency content of 55/110 - 600/800, stacking with a CMP distance of 10 m and time migration. In total we collected about 570 km of 2D seismic profiles. The location of the seismic lines is shown in Fig. 2.2 together with the bathymetric data. The presented bathymetric map is a combination of Hydrosweep data acquired during Meteor cruise M52/1 (Bohrmann and Schenk, 2002) with multibeam data collected during the TTR-6 cruise in 1996 using a Simrad EM-12 system (Woodside et al., 1997).

2.6 Results

2.6.1 Distribution of the mud volcanoes in the Sorokin Trough

The seismic and bathymetric data collected during the Meteor cruise M52/1 reveal numerous mud volcanoes of varying morphology and size. The location of the mud volcanoes is mapped on Fig. 2.2. In total, 25 mud volcanoes were observed, 14 are cone-shaped, 10 are depression structures and one mud volcano is flat topped (Table 1).

The cone-shaped mud volcanoes often consist of several cones (up to three) and most of the depression structures contain small cones inside (Table 1). Several mud volcanoes have been known from previous cruises (TTR-6+11 cruises) (Woodside et al., 1997; Bouriak et al., 1998; Ivanov et al., 1998; Kenyon et al., 2002), but also new mud volcanoes were identified. With exception of the Kazakov mud volcano all mud volcanoes are located above the top or the edges of near-surface diapiric structures. Thus, the mud volcanoes are relatively linear distributed conform to the W-E strike direction of the diapiric ridges (Fig. 2.2). The mud volcanoes are concentrated at the northern edges of the Tetyaev Rise and the Shatsky Ridge and can be grouped into three areas, based on the different geological and depositional environments in the Sorokin Trough. The only mud volcano not included in any group is the M10 mud volcano observed in the westernmost part of the Sorokin Trough (Fig. 2.2, Table 1).

Mud volcano Area 1 runs along the northern margin of the Tetyaev Rise and is characterized by a morphological step on the seafloor extending over 25 km in the W-E direction, at which most of the mud volcanoes are located (Fig. 2.2). The mud volcanoes in this area reveal a great morphological variety, but collapsed mud volcanoes with caldera-like structures, often including one or more cones inside, and small cone-shaped mud volcanoes dominate (Table 1). The second mud volcano area (Area 2) stretches in the NW-SE direction along the north-eastern edge of the Tetyaev Rise and includes only two single large cone-shaped mud volcanoes, the Nioz and the Kazakov mud volcano (Fig. 2.2). These mud volcanoes are thrice as large as the mud volcanoes of Area 1 and double as large as the mud volcanoes of Area 3. The mud volcanoes are located at the flat plain of the Sorokin Trough in water depths of 1950 to 2100 m. In Area 3, located at the north-western edge of the Shatsky Ridge, ten mud volcanoes were identified in the seismic and echosounder data, most located on a morphological high at water depths of 1700-1800 m (Fig. 2.2). Small cone-shaped mud volcanoes predominate, but some larger sized structures consist of several cones, partly located within a depression structure (Table 1).

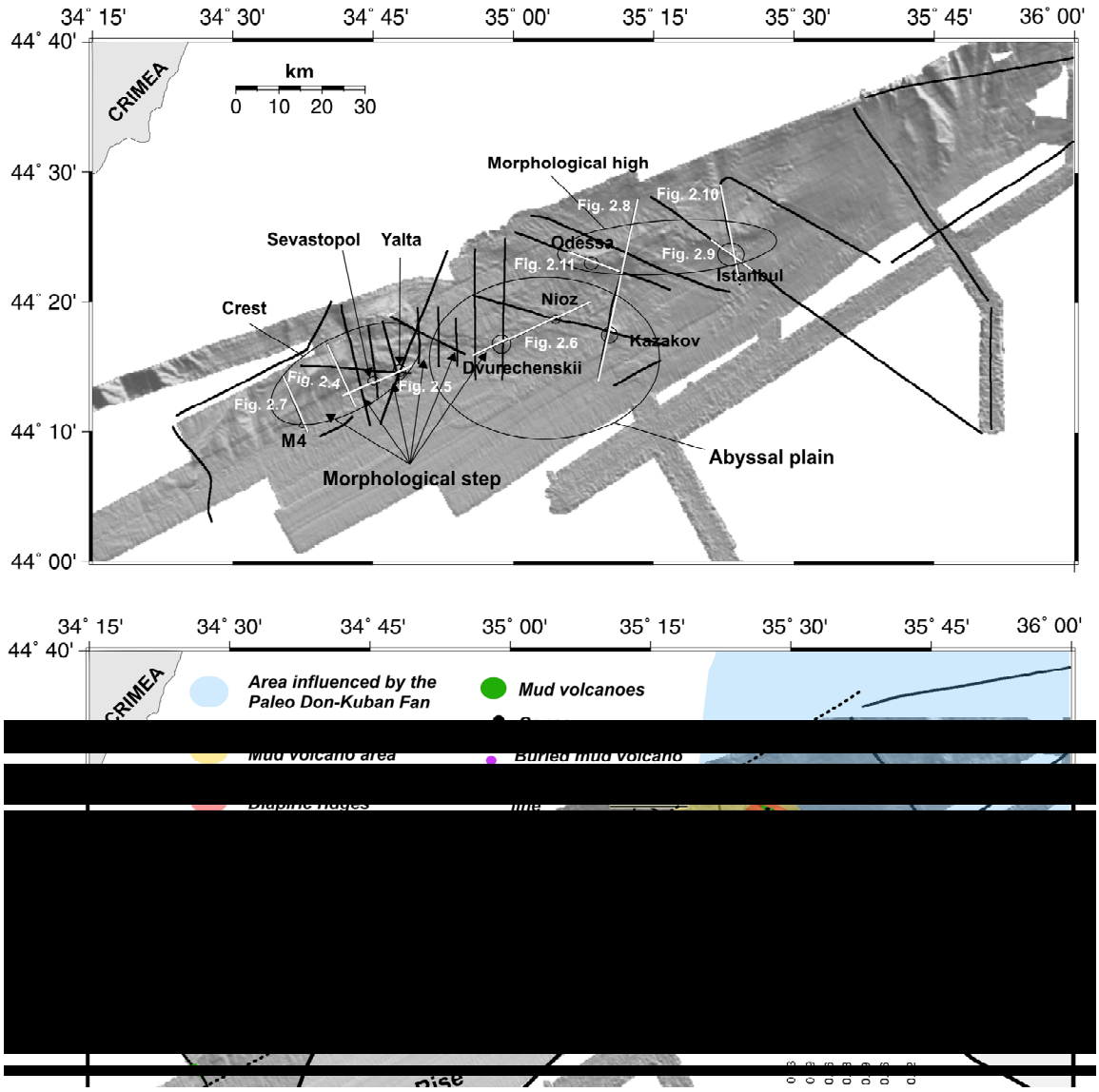

Figure 2.2:
Top: Grey-shaded bathymetric map of the Sorokin Trough. The larger mud volcanoes are distinctly imaged on the bathymetry, as the Dvurechenskii, M4, Yalta, Sevastopol, Odessa and Istanbul mud volcano, outlined by black circles. The structural features of the seafloor (morphological high, morphological step and abyssal plain) are encircled in black.
Bottom: Distribution of the mud volcanoes and subsurface structures, as diapiric ridges, faults and Bright Spots, mapped from the seismic data. The area influenced by the Don-Kuban Fan sediments is marked in blue. The dashed line running through the Sorokin Trough in the SW-NE direction represents the seismic cross-section recorded by the SSC "Yuzhmorgeologia" of Gelendzhik in 1979 shown in Fig. 2.16.

Mud volcano	Line	Depression		Cones			Feeder channel		Shape	Characterization
		width [m]	depth [m]	width [m]	height [m]	dipping angle [°]	width [m]	penetration [m]		
Area 1										
Dvurechenskii	43			2000	80	3-7°	600		flat topped	Flat topped mud volcano. Influenced by the deposits of the Don-Kuban fan. Strong seafloor reflection of the top. Above diapiric structure.
	13			2000	30					
M1	25	2400	30	400	20	8-9°	500	430	depression structure with 2 cones	Two cones within depression, one steep flanked, one smoothed. Next to a fault. Indistinct feeder channel but diffuse zone of signal penetration. Diapiric structure at 350 ms TWT bsf.
				300	25	11°				
M2	24	2550	19	1000	42	9.5°	1600	270	Cone-shaped within depression	Cone with steep flanks within depression. The old cone was destroyed and a new cone grew up. Above top of diapiric structure. No clear feeder channel, but a wide zone of signal attenuation. Weak seafloor reflection of the cone.
	14	1100	5	520	40	12°				
Yalta	22	2300	15	350	22	7°			3 cones within depression	Three cones are observed within a collapse syncline. The small cone has steep flanks. No clear feeder channel.
	15			600	45					
	41			1190	30		800	360		
	50	2400	15	500	30		2300			
				490	30					
				650	45					
Sevastopol	17	1700	22	450	37	7-12°	500	320	3 cones within depression	Three cones within depression. The depression can be traced down to 3.3 s TWT. The feeder channel is not clear seen, but a wide zone of signal attenuation. Low seafloor reflection.
				400	35					
	50	1100	25	400	37					
	22	300	12							
M3	19			550	20	5-8.5°	700	480	cone-shaped	Small cone-shaped mud volcano with strong seafloor reflection. Several reflection patches at the margin of the feeder channel.
M4	21			500	37	not measurable	600	480	cone-shaped	Pillar like structure, extruding from conduit. Strong reflector on top. Faults south and north of the mv.
M5	22			250	15	7.5°	20	390	cone-shaped	Small cone-shaped mud volcano with weak seafloor reflection above diapiric structure. Most likely a fault is located beneath.
M6	41	900	25	400	20	6-7°	19		Cone-shaped within depression	Eastern periphery of the mud volcano. Two cones are divided by a small cavity.
	23			350	12	3-5°				
M7	42	1900	7-30	700	40	2-7°			Cone-shaped within depression	Periphery or begin of mv = sea mound. Beginning of formation of feeder channel, not yet reaching up to the seafloor. Several faults beneath the mound.
M8	45	330	10				250	330	depression structure	MV with depression structure above the top of a diapir.
M9	13			200	13	9.5			cone-shaped	2 Cones in the direct vicinity to the Dvurechenskii mud volcano
				190	18	14				
Seperated mud volcano										
M10	37			900	22	2-4°	250	200	cone-shaped buildup	Above anticlinal. Cone-shaped buildup, most probably beginning of mv. Begin of feeder channel not reaching the seafloor.
Area 2										
Nioz	13			1200	90	11°	1200	510	Cone-shaped	Big single cone-shaped mud volcano. Diapiric crest is observed beneath. The surrounding sediments are significantly influenced by the Don-Kuban fan. Circular shaped. Steep flanks.
	1			800	22		8000			
Kazakov	1			1700	105	14°	1000		Cone-shaped	Big single cone-shaped mud volcano. Without a diapiric structure beneath, hence no root of feeder channel. Strong influence of the Don Kuban fan. Circular shaped.
	3			2200	75	13°	1540			
Area 3										
Odessa	44			500	40	12°	400	540	2 cones within depression	Two cones within a depression, showing dome lifting between the cones. Located above diapiric structure.
		2500	10	1000	45-50	5-10°				
M11	44	1000	22				600	750	depression	Periphery of the mud volcano, containing a small collapsed syncline, which can be traced down to 580 m bsf. Above the eastern edge of a diapir.
M12	3			1000	45	15°	1100	400	cone-shaped	The cone with steep flanks is complicated by a small caldera. Located at morphological break, at the swell. Feeder channel can be traced down to a diapiric structure at 2.7 s TWT. Probably a fault beneath.
	12			800	45	16°	400	350		
M13	3			400	12	13°	540	360	cone-shaped	Small cone-shaped mud volcano. The feeder channel can be traced down to the diapiric structure at 2.7 s TWT.
Istanbul	4			600	30	9-13°			cone-shaped 3 cones	The mud volcano is represented by three cones with a feeder channel beneath each top respectively characterized by transparent turbiditic deposits. Strong influence of Don-Kuban fan. Above the southern edge of a diapiric structure at 450 ms TWT bsf. Steep flanks of the southern cone.
				800	60	18°				
				200	15	13°	2800	550		
	11			800	80	11°				
				900	15	5°	600			
M14	4			1300	30	3.5°	-	-	cone-shaped	Developed as a local uplift, most probably representing the margin of a mud volcano. Above anticlinal structure at 2.8 s TWT.
M15	11			200	15	not measurable			cone-shaped	Small hill at the southern edge of a small depression, located above a large anticlinal structure. No feeder channel is visible beneath. Strong influence of Don Kuban fan deposits.
M16	10			600	15	10°			cone within depression	Two turbiditic cones with smooth surface reflection are observed within a collapsed depression. Located above diapiric structure at 400 ms TWT bsf. Strong influence of the Don-Kuban fan.
		2200	20	500	20	15°				
M17	echo sounder			700	25	2.6°			cone-shaped	Cone with weak reflectance
M18	echo sounder			880	30	4°			cone-shaped	Cone with weak reflectance
Buried mud volcano features										
BMV	12	1600	30						depression	Buried collapse syncline at a depth of 50 m bsf, which can be traced down to 440 m bsf. The dome of an anticline is observed at 440 m bsf.

Table1: *Morphological characteristics and description of the mud volcanoes in the Sorokin Trough.*

2.6.2 Characterization of the mud volcanoes

Table 1 summarizes the morphological characteristics of the observed mud volcanoes. As seismic lines are not closely spaced the individual profiles might cross only the periphery of the mud volcano, hence additionally the bathymetry was used to determine the spatial morphology of the mud volcanoes.

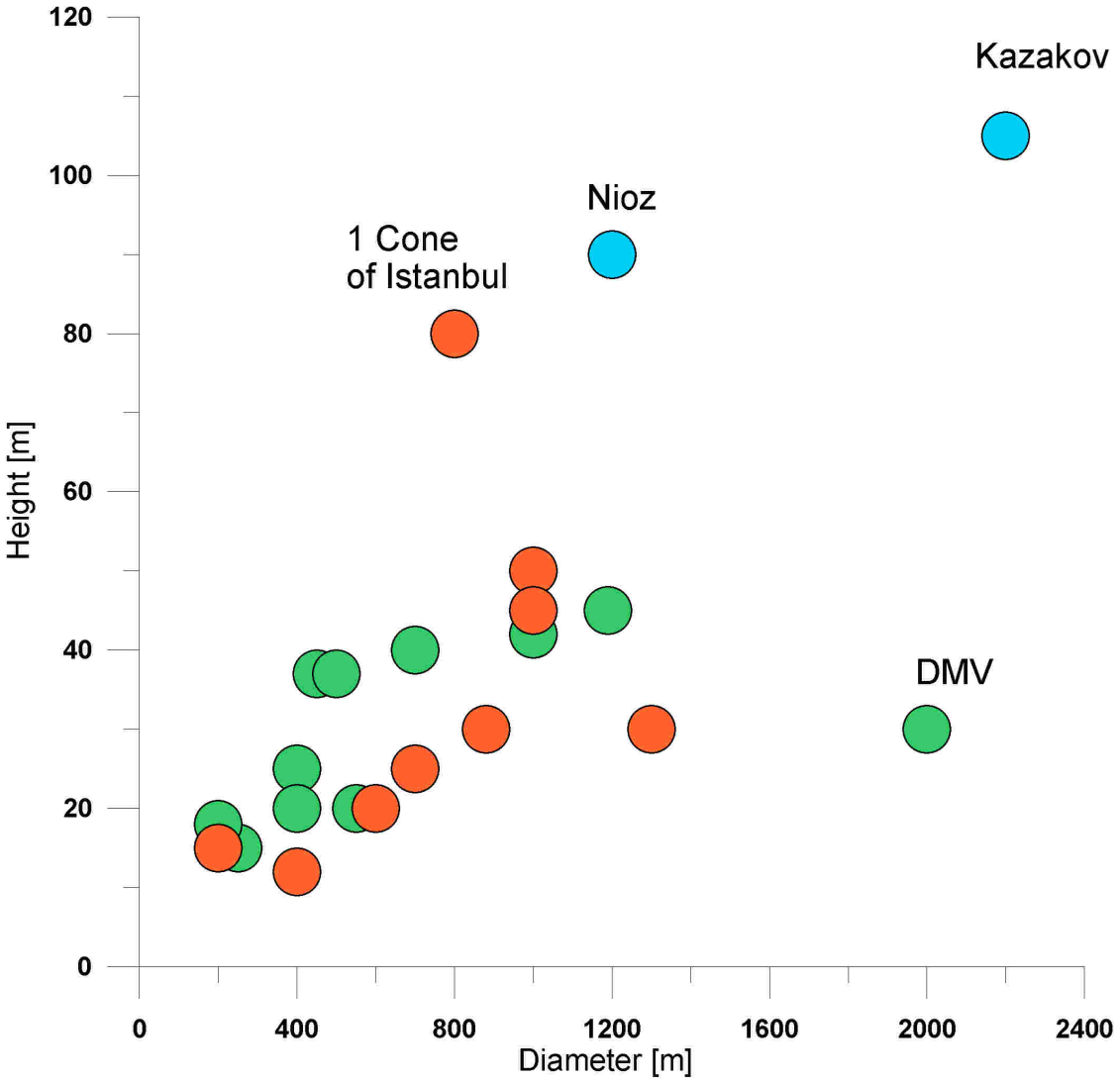

Figure 2.3: *Heights of the mud volcanoes versus their diameters. The green circles represent the mud volcanoes of Area 1, the blue circles are the Nioz and Kazakov mud volcano of Area 2, and the red circles represent the mud volcanoes of Area 3. With exception of Area 2, comprising the largest mud volcanoes, the mud volcanoes of Area 1 and 3 can not be related to defined dimensions, but show great variations. The mud volcano M10 outside of the Areas 1-3 is not included.*

Fig. 2.3 images the heights of the cone-shaped mud volcanoes (including the flat-topped mud volcano and the cones within the depression structures) versus their diameters. From mud volcanoes comprising several cones, only the largest one was used. In total, the

diameters of the cones vary between 200 and 2000 m, their heights range from 10-105 m. Most mud volcanoes have diameters of several 100 m up to 1000 m and heights between 15-50 m. The cones of four mud volcanoes have significant increased dimensions, i.e., the DMV (Area 1), the Istanbul (Area 3), and particularly the Nioz and Kazakov mud volcano (Area 2).

The characteristics of the different mud volcanoes and the typical features of each area are described below.

Mud volcanoes of Area 1

In the western Sorokin Trough two main diapiric ridges strike parallel to the Tetyaev Rise in the WSW-ENE direction. They separate sedimentary basins with continuous strong reflectors of most probably hemipelagic sediments onlapping the flanks of the diapirs and bulging above their tops (Fig. 2.4). Nine of twelve mud volcanoes imaged on the seismic lines are located above the steep southern flank of the southernmost diapiric ridge aligned along the morphological seafloor step, which marks the transition between a crest in the north-west and the flat abyssal plain in the south-east (Fig. 2.2). Concerning the morphology of the mud volcanoes there is a trend to pockmark structures: 7 mud volcanoes are depression structures, of which 6 include cones inside, 4 of the mud volcanoes are cone-shaped and one mud volcano, the Dvurechenskii mud volcano, has a flat top (Table 1).

Typical pockmark structures are the Sevastopol and the Yalta mud volcano, two larger sized mud volcanoes of this area with diameters of 2400 and 1700 m and depths of 15 and 25 m, respectively (Fig. 2.5, Table 1). The Yalta mud volcano was imaged by six seismic lines providing detailed information about its structure. The elliptic shaped SW-NE trending depression structure includes three cones with steep flanks of about 7° in average. The westernmost cone is characterized by a weak seafloor reflection, while the others show higher seafloor reflection amplitude. The interior of all cones is characterized by acoustic transparency (Fig. 2.5). On the Parasound image in Fig. 2.5, low seafloor reflection amplitudes and weak reflectors within the upper 25 - 30 m characterize the cones of Sevastopol and Yalta mud volcano. The seismic data show a zone of strong signal attenuation beneath the Yalta mud volcano including several short reflection patches. This zone is as wide as the depression and reaches down to the diapir (Fig. 2.5). Between the Sevastopol and the Yalta mud volcano a package of Bright Spots is observed at a depth of about 300 ms TWT bsf (Fig. 2.5). Bright Spots are widely distributed in the western Sorokin Trough, generally occurring on the top or the edges of the diapiric ridges at +/- constant depth (Figs. 2.2, 2.4, 2.5). The Bright Spots are limited to an area west of the Yalta mud volcano concentrated northwest of the Sevastopol mud volcano (Fig. 2.2).

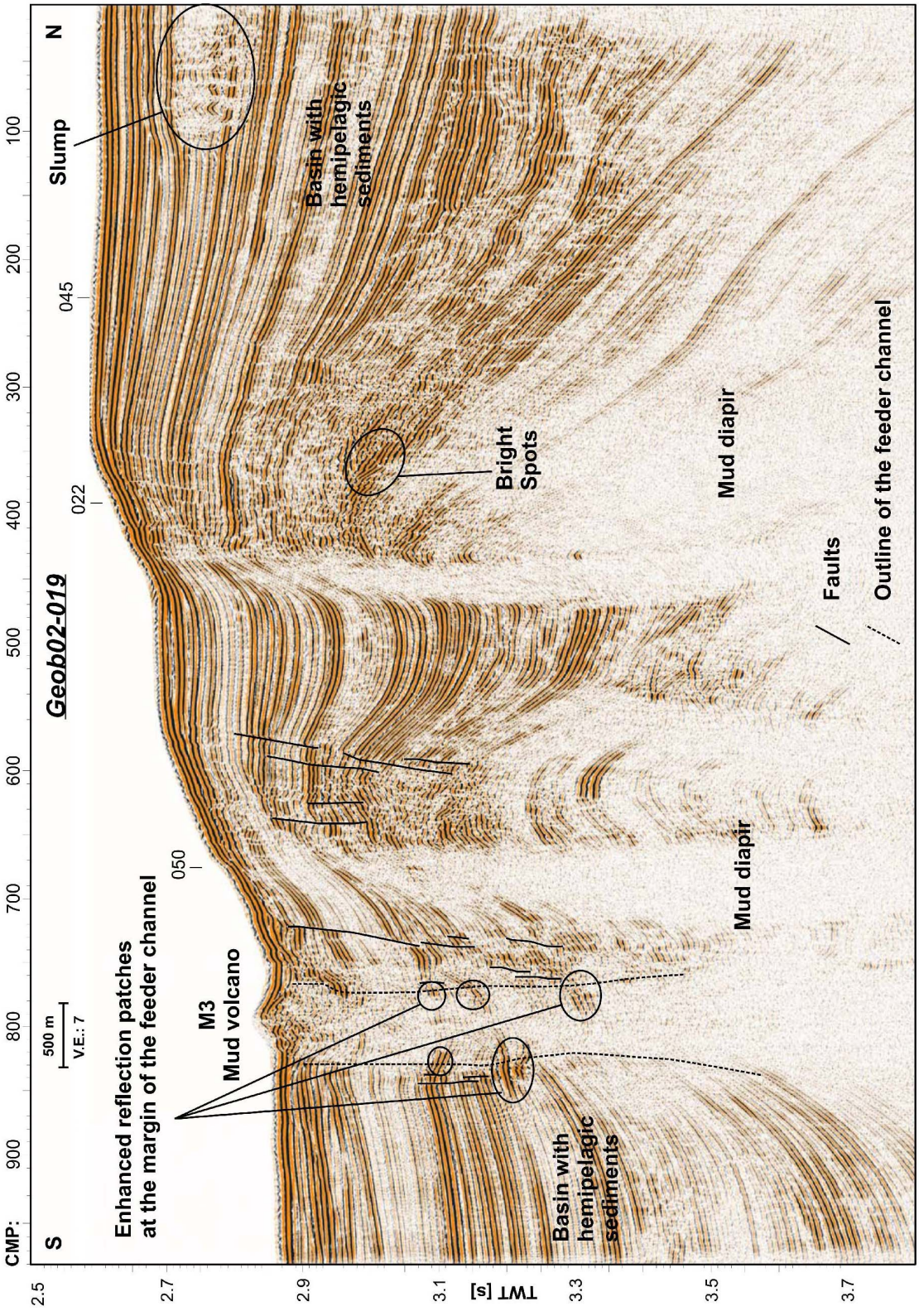

Figure 2.4: *Time migrated seismic profile GeoB02-019 showing the general structures of mud volcano Area 1. The M3 mud volcano is a typical small cone-shaped mud volcano above the steep southern flank of the southernmost diapiric ridge structured by several near vertical faults. The location of the line is shown in Fig. 2.2.*

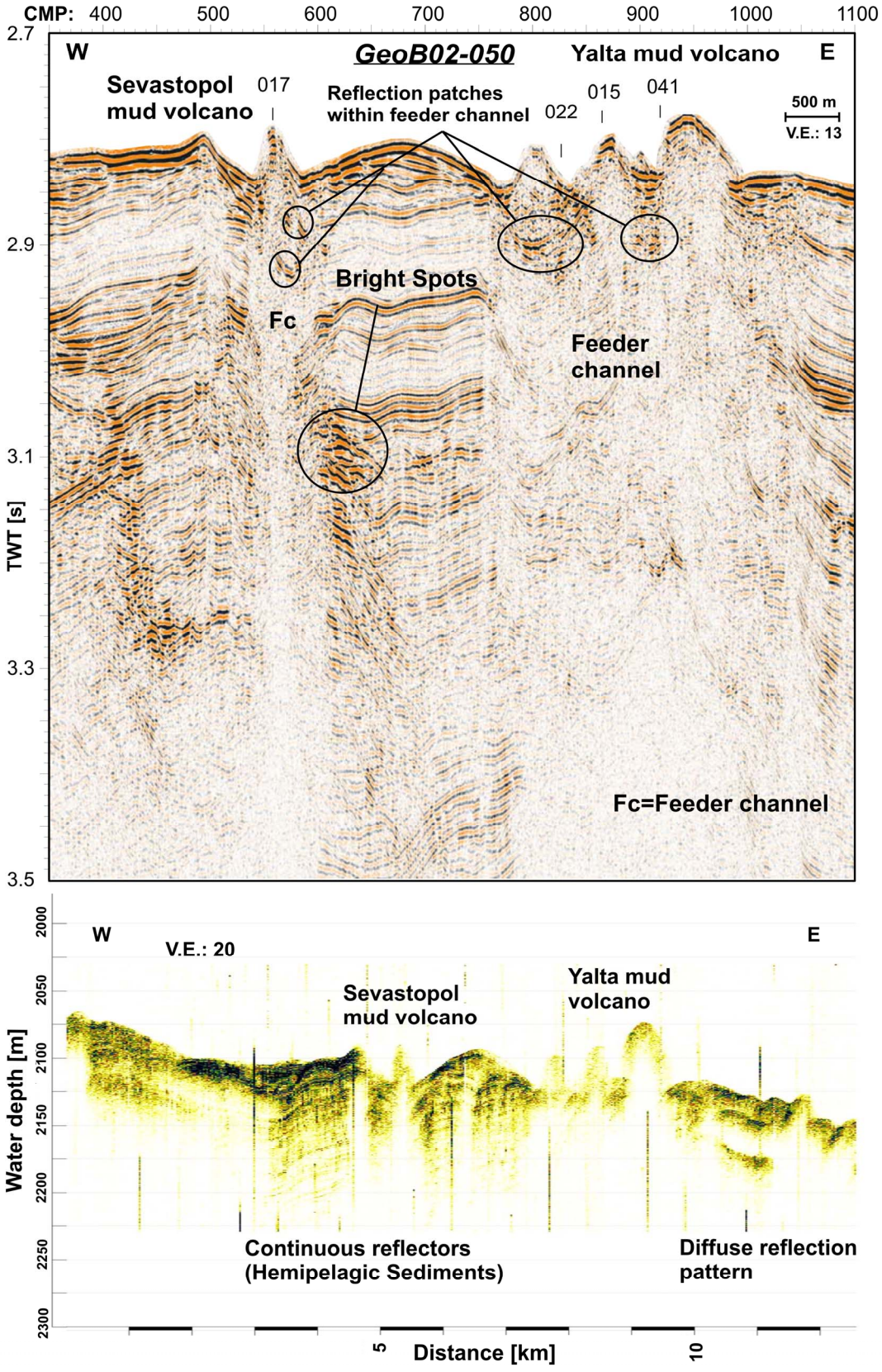

Figure 2.5: *Close-up of time migrated seismic section (top) and Parasound image (bottom) of line GeoB02-050 crossing the Sevastopol and Yalta mud volcano. The location of the line is shown in Fig.* 2.2.

A typical cone-shaped mud volcano with weak diffusive disrupted seafloor reflection is the circular M3 mud volcano located above the flank of the southernmost diapiric ridge at a water depth of ~2130 m (Fig. 2.4). The feeder channel has blurred outlines and several strong reflection patches are observed in particularly at the margin of the channel. Near vertical faults with vertical offsets of up to 25 ms TWT occur in the surrounding of the feeder channel and above the diapirs (Fig. 2.4). In the north, further acoustic transparent zones arise along the flanks of diapirs up to 130 ms TWT bsf, but no mud volcano is observed on the seafloor (Fig. 2.4).

The Dvurechenskii mud volcano (DMV) located at the eastern edge of the area shows a completely different shape and a large size. The flat cone has a width of 2000 m and a height up to 80 m (Fig. 2.6, Table 1).

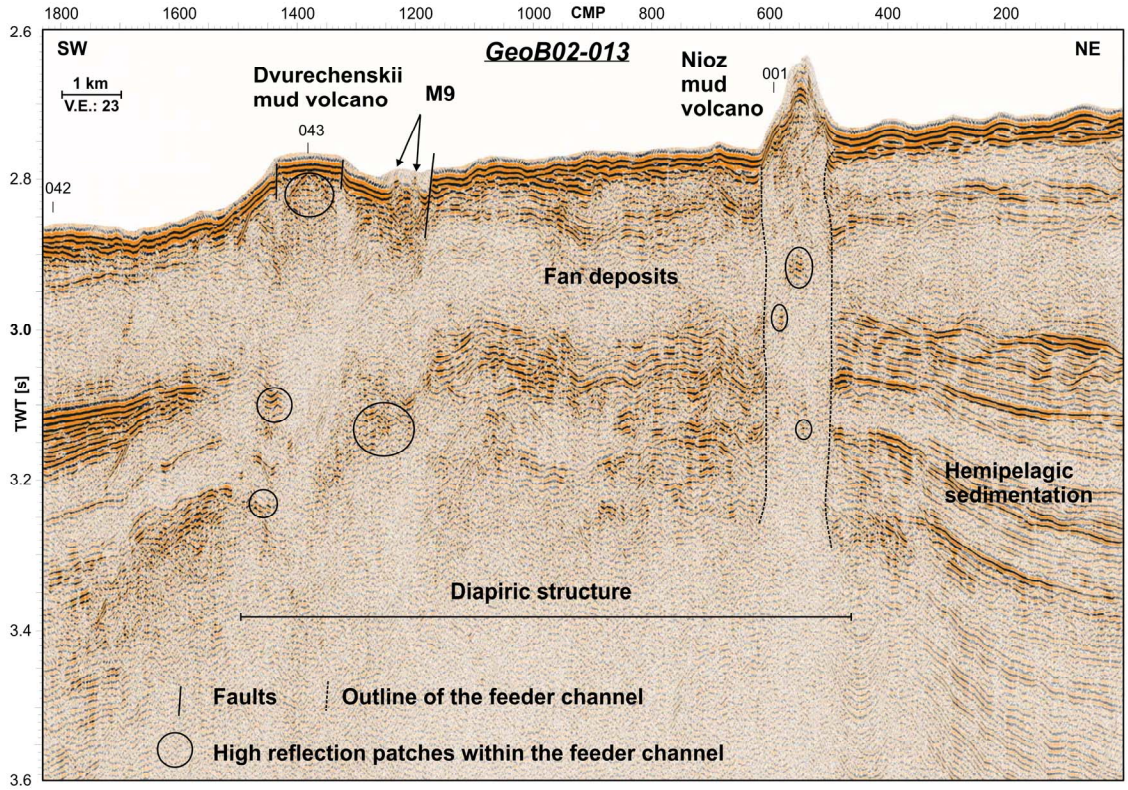

Figure 2.6: *Time migrated seismic section GeoB02-013 crossing the Dvurechenskii, the M9 and the Nioz mud volcano, surrounded by fan sediments. The black lines give the outline of the feeder channel, which boundaries are diffuse at the DMV and M9 mud volcano. The location of the line is shown in Fig. 2.2.*

Acoustic transparent units separated by bands of high amplitude reflectors dominate the subsurface sediments around the DMV. The feeder channel has a sharp outline to its northern and southern margin, but diffusive boundaries to the south-west and north-east (Fig. 2.6). The reflectors south-west and north-east of the feeder channel are displaced by

40 ms TWT (Fig. 2.6) indicating a fault beneath the DMV, as also suggested by Krastel et al. (2003). Beneath the top of the DMV short weak reflection patches are imaged within the upper 100 ms TWT. The flanks of the DMV show varying dipping angles and heights. The southern flank has a height of ~ 80 m with a slope angle of ~ 2.7°, while the northern flank is only 15 m high with a slope angle of 7.7°. There is a vertical offset of 4-9 m between the top and the flanks of the mud volcano (Fig. 2.6).

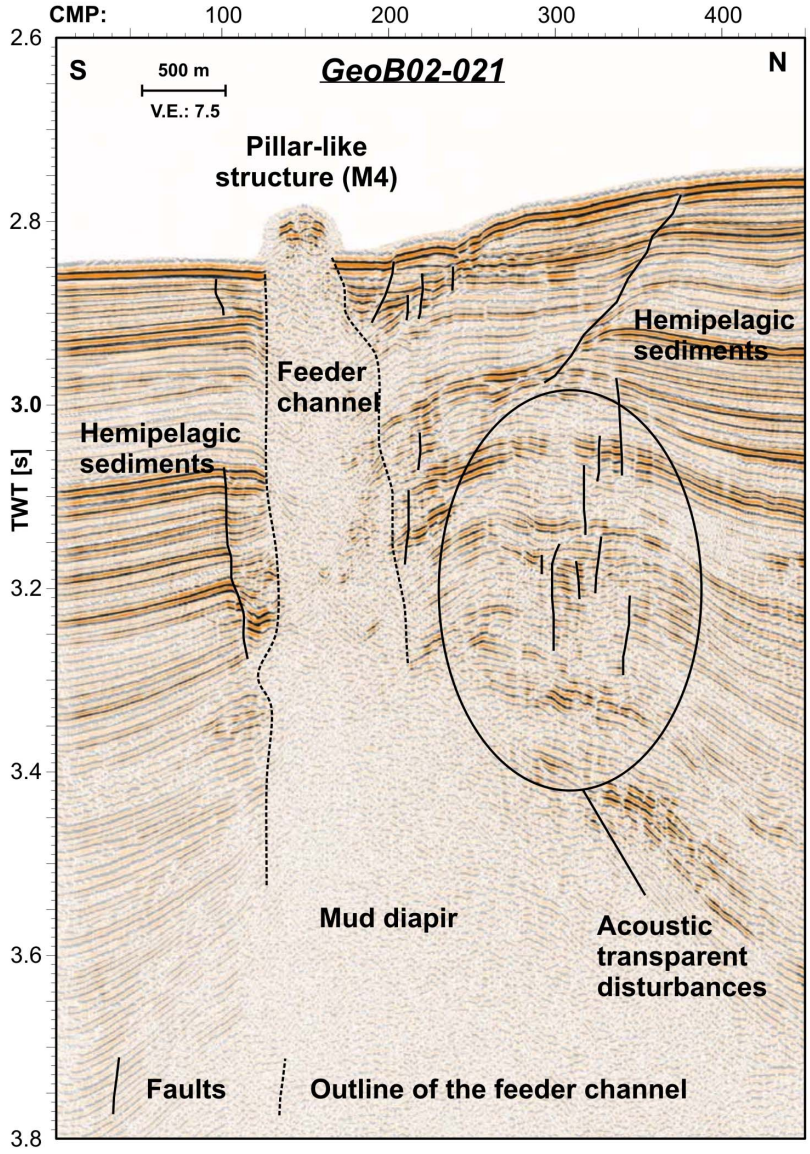

Figure 2.7: *Close-up of the time migrated seismic line GeoB02-021 (location of the line is shown in Fig. 2.2). The special shape of the M4 mud volcano with steep flanks let us presume that the eruption product is more porous and might consist of presumably sand. Acoustic transparent disturbances at faults above the diapiric top are interpreted as fluid escape structures due to fluid migration along these faults.*

A special structure is the M4 mud volcano located at the westernmost periphery of the area, with a shape varying significantly from the other cone-shaped mud volcanoes (Fig. 2.7). The M4 mud volcano has a pillar-like shape and the top is slightly convex with a strong seafloor reflection. No reflections are seen at the southern and northern flanks of the cone due to high slope angles. The feeder channel is characterized by acoustic transparency and can be traced down to a mud diapir at 450 ms TWT bsf.

Mud volcanoes of Area 2

Area 2 is located at water depths of around 2000 m at the flat plain of the Sorokin Trough (Fig. 2.2). The sediments are influenced by the distal fan deposits of the Palaeo Don-Kuban Fan characterized by an alternation of thick acoustic blank units (100 - 200 ms TWT) and few bands of strong reflectors (Figs. 2.6, 2.8).

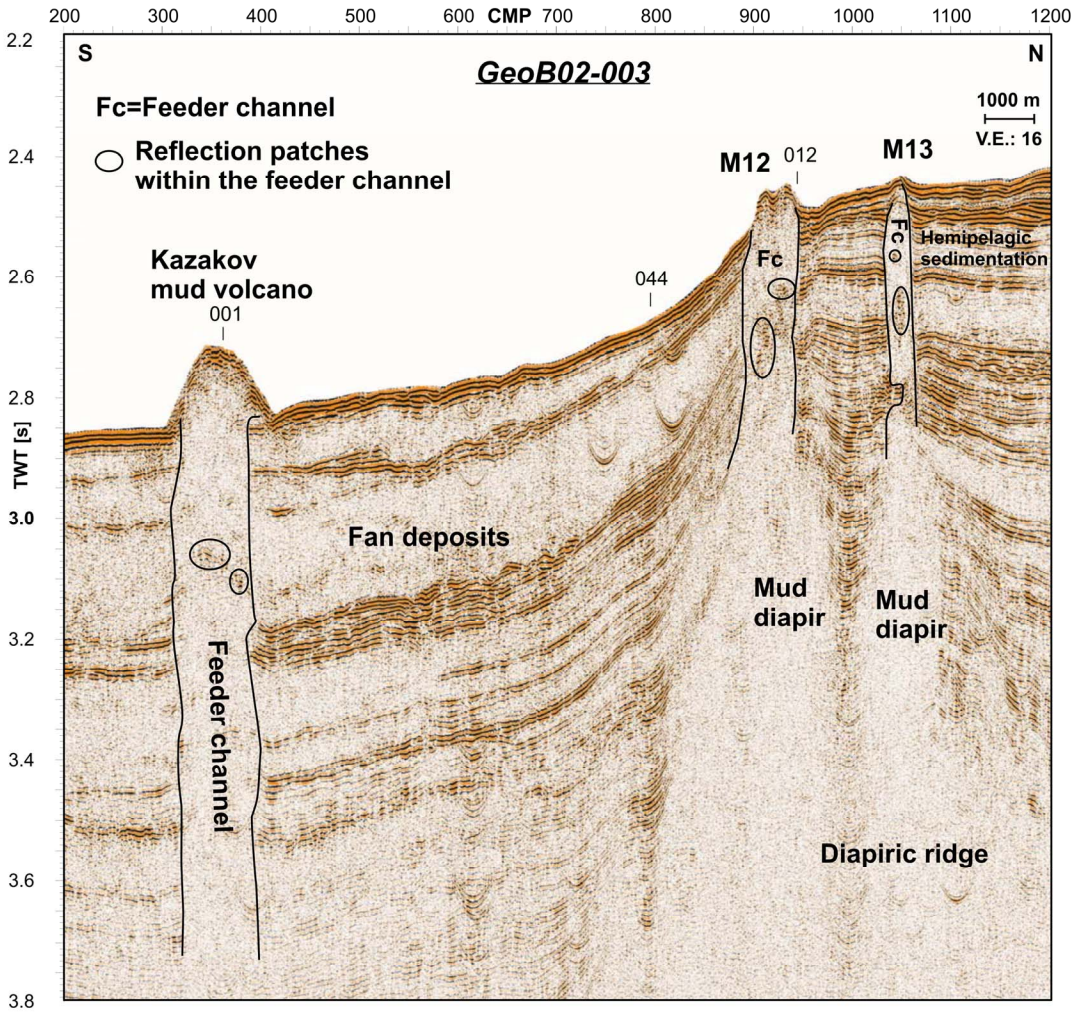

Figure 2.8: *Time migrated seismic line GeoB02-003 imaging the large Kazakov mud volcano of Area 2 and the two small-sized M12 and M13 mud volcanoes on the morphological high within Area 3. The feeder channels are outlined by black lines. See Fig. 2.2 for location of line.*

The two largest cone-shaped mud volcanoes of the Sorokin Trough, the Kazakov and the Nioz mud volcano, are found in this area, both distinctly imaged on the bathymetric data (Fig. 2.2). They have enormous dimensions with heights of about 100 m and diameters of 1200 m for the Nioz and 2000 m for the Kazakov mud volcano (Figs. 2.6, 2.8, Table 1). The Kazakov mud volcano has steep slope angles with about 14°. No diapiric structure is observed beneath and the feeder channel can be traced down to the maximal signal penetration at 4 s TWT (Fig. 2.8). Contrary, the Nioz mud volcano is located above the eastern edge of the southern diapiric ridge observed in Area 1. Both mud volcanoes are characterized by a strong seafloor reflection, but the internal structure is masked by acoustic transparency, with exception of some short weak reflectors inside the Nioz mud volcano (Fig. 2.6). At both mud volcanoes the seafloor reflection is vertically displaced, the southern seafloor reflection being about 20 m deeper than the northern one (Figs. 2.6, 2.8). The few subsurface reflectors observed beneath the Kazakov mud volcano are also vertically displaced by about 10-20 m (calculated with a sediment velocity of 1600 m/s).

Mud volcanoes of Area 3

Area 3 can be subdivided into 2 sub-regions: In the south-east the sediments are characterized by acoustic blank units, which are partly divided either by single distinct reflectors (Fig. 2.9) or by several continuous bands of strong reflectors (Fig. 2.10). The sediments in the north-west are characterized by well stratified continuous high amplitude reflectors, separated by single acoustic transparent zones of smaller thickness (Figs. 2.9, 2.10). These different deposition sub-regions are separated by an E-W striking morphological seafloor high, underlain by a diapiric ridge at a depth of about 350-400 mbsf. Seven mud volcanoes of this area occur on that morphological high, and all ten mud volcanoes are located above a diapiric structure (Fig. 2.2, 2.9, 2.10).

Most of the mud volcanoes (7) are cone-shaped and three mud volcanoes are pockmark structures, of which two include cones inside (Table 1). Additionally, a buried pockmark structure is observed at a depth of 80 ms TWT bsf in this area (Fig. 2.2, Table 1). The cone-shaped M17 and M18 mud volcanoes are not covered by seismic lines, but have been crossed by echosounder profiles (Fig. 2.2). All except one mud volcano (M15) show feeder channels beneath their tops. The largest mud volcanoes in this area are the depression of the Odessa and the cone-shaped Istanbul mud volcano with widths of about 2500 and 1700 m respectively (Fig. 2.9-2.11, Table 1).

The elliptical shaped NW-SE trending Istanbul mud volcano is located at the distal area of the fan deposits and contains 3 cones with weak seafloor reflections and acoustic transparency inside. Between the central and the north-western cone a flat platform with strong seafloor reflection is developed, while a narrow basin is formed between the central

and south-eastern cone. A Parasound line crossing the Istanbul mud volcano (Fig. 2.11) shows that the subbottom is characterized by diffuse reflectors and low signal penetration of several m to max. 25 m. The Odessa mud volcano is a big pockmark structure including two cones surrounded by non fan sediments (Fig. 2.10). Contrary to the structures of Area 1 the depression of the Odessa mud volcano is less deep (~10 m) and shows a continuous strong seafloor reflection, broken by the cones, which are characterized by washed out reflections and a weak seafloor reflection. Beneath each cone a feeder channel can be traced down to the diapir (Fig. 2.10). The chaotic discontinuous sediments above the diapir, disconnected by the feeder channels, are dissected by several faults.

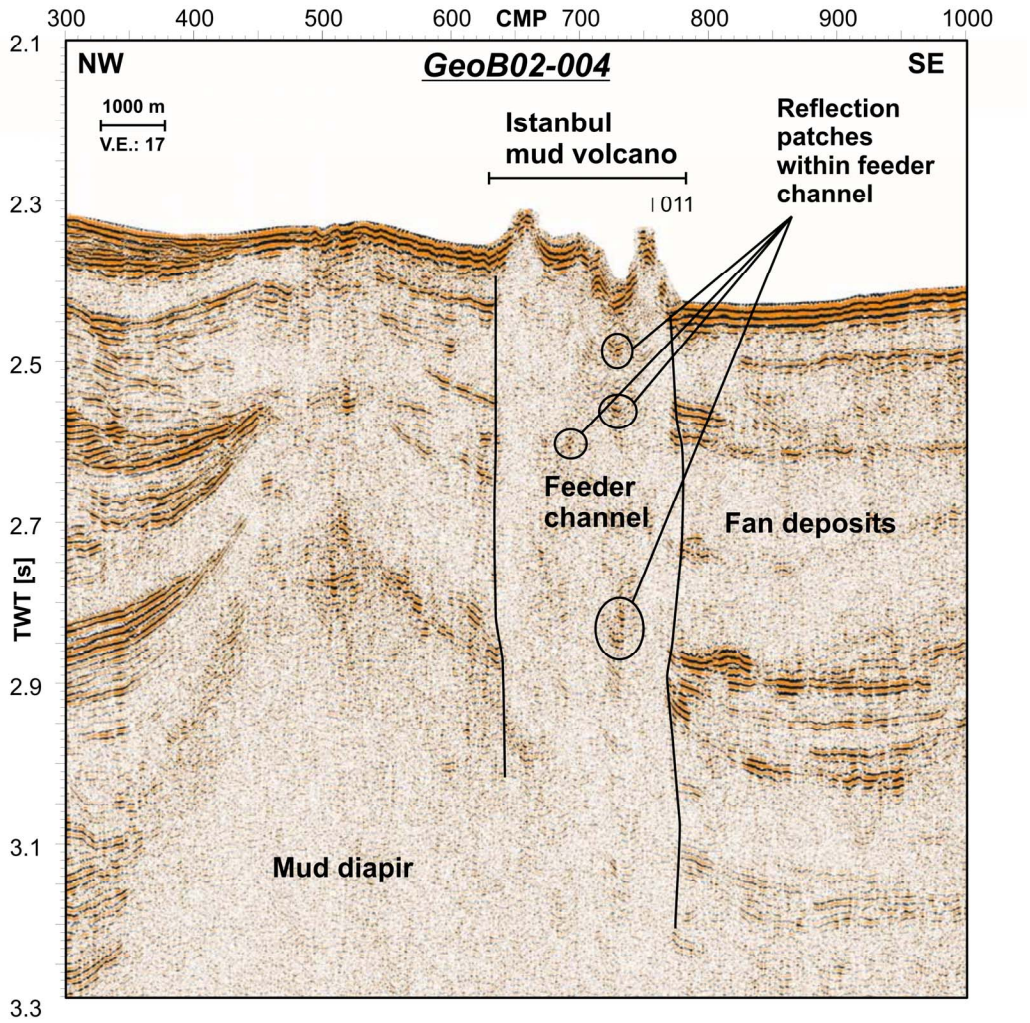

Figure 2.9: *Close-up of the time migrated seismic section GeoB02-004 imaging the Istanbul mud volcano. The surrounding of the mud volcano and the south-east are characterized by fan deposits. The acoustically masked feeder channel is as wide as the mud volcano and reaches down to the diapiric ridge at 2.9 s TWT. Several reflection patches are observed within the feeder channel. The location of the line is shown in Fig. 2.2.*

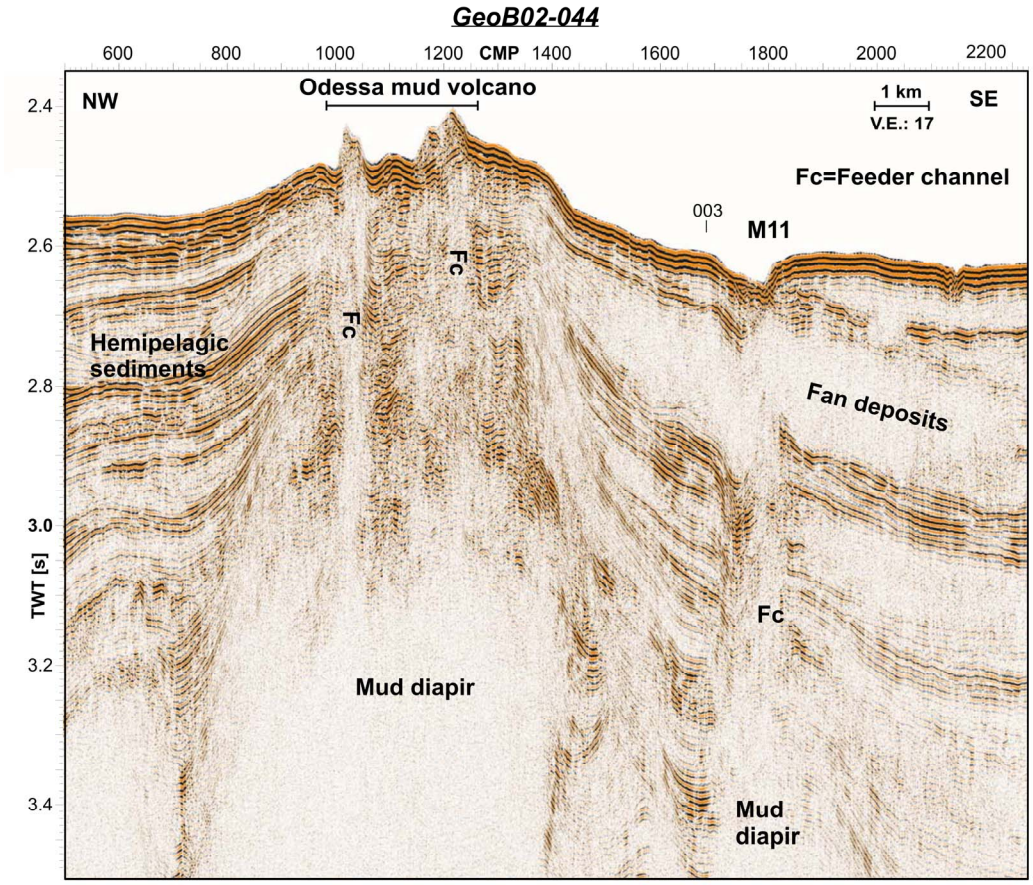

Figure 2.10: *Close-up of the time migrated seismic profile GeoB02-044 imaging the Odessa and the M11 mud volcano. The south-east is influenced by fan deposits, but changing to the north-west into well stratified bedding of hemipelagic sediments. The location of the line is shown in Fig. 2.2.*

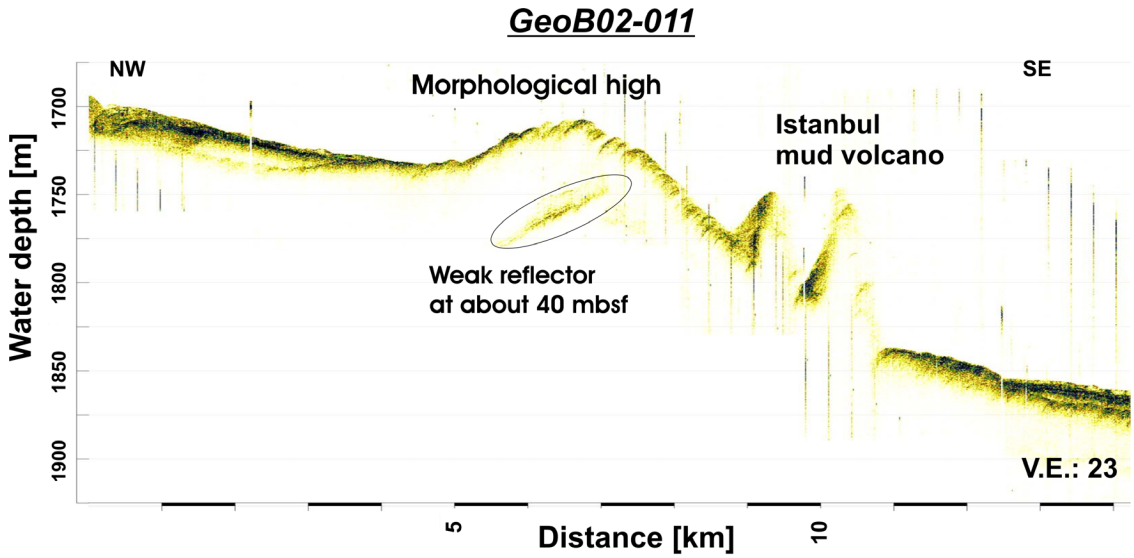

Figure 2.11: *Parasound image of the line GeoB02-011. At the morphological high the seafloor reflection shows reduced amplitudes and the subsurface is characterized by a weak reflector at about 40-70 mbsf. The location of the line is shown in Fig. 2.2.*

The M12 and M13 mud volcanoes north of the Kazakov mud volcano are two typical small cone-shaped mud volcanoes (Fig. 2.8). The M12 mud volcano, consisting of 2 tops with weak seafloor reflection, is directly located at the edge of the morphological high. Reflections in the interior of the mud volcanoes are masked by acoustic transparency. Both mud volcanoes are connected via individual feeder channels to mud diapers.

2.6.3 Diapiric structures in the Sorokin Trough

Several WSW-ENE striking diapiric ridges and single mud diapirs, which could not be attributed to a ridge, were identified in the seismic sections. In the western Sorokin Trough three diapiric ridges stretch along the northern margin of the Tetyaev Rise (Fig. 2.2). The southernmost diapiric ridge can be traced over 40 km from the M4 mud volcano in the west to the Nioz mud volcano in the east; the central diapiric ridge runs over 34 km from seismic line 21 to line 43 (Fig. 2.2). The northernmost diapiric ridge is imaged only on few seismic lines in the central Sorokin Trough and can not be traced over a great distance due to missing seismic data coverage (Fig. 2.2). The tops of the central and the southern ridge protrude up to 350-400 ms TWT bsf showing a relatively constant subsurface depth, whereas the top of the northern ridge is located at greater depth of 500-700 ms TWT bsf with more variations in depth. The diapirs are characterized by acoustic transparency. Continuous reflectors of the surrounding sedimentary basins are onlapping the flanks of the diapirs and are bulged above their tops. The ridges are asymmetric with a steeper southern flank. In the surrounding of the M3, Sevastopol and Yalta mud volcano the southern diapiric ridge splits into two tops separated by a syncline with continuous parallel reflectors (Fig. 2.2). Near vertical faults with offsets of about 3-7 ms TWT disrupt the sediments above the diapiric ridges leading to a disturbed and chaotic reflection pattern (Fig. 2.4).

Numerous high amplitude reflection packages (Bright Spots) are observed in the westernmost Sorokin Trough along the top or the flanks of the central and southern diapiric ridge (Fig. 2.2). The depth of the Bright Spots varies for about 200 ms TWT from 220 to 430 ms TWT bsf with an average depth at about 300 ms TWT bsf. The Bright Spots are local amplitude anomalies with a limited lateral extension of maximal 1500 m in the N-S direction. In an area north-west of the Sevastopol mud volcano the Bright Spots could be traced over a maximal distance of 4.8 km in the E-W direction (Fig. 2.2).

In the eastern Sorokin Trough it is more difficult to identify mud diapirs due to the acoustic blank units of the fan deposits. Contrary to Woodside et al. (1997), who observed N-S striking diapiric zones north-east of the Shatsky Ridge we could not identify diapirs at this margin of the survey area. At the north-western edge of the Shatsky Ridge, however, one diapiric ridge stretches in the WSW-ENE direction along a morphological high. The

ridge rises to a depth of about 400-500 ms TWT bsf. Several single mud diapirs were identified north and south of this ridge but could not be attributed to a ridge.

2.7 Discussion

2.7.1 Feeder channels

The feeder channels of the mud volcanoes are seismically characterized by acoustic transparent zones connected to the diapirs beneath with widths similar to the mud volcano structure. The resulting diameters of the conduits are in the range of several 100 m to maximum 2400 m at the Yalta mud volcano (Figs. 2.4-2.9, 2.11). Although information about the dimensions of ancient and recently active feeder channels are marginal, surface observations indicate that diameters of conduits range from 15 cm at Taiwan (Yassir, 1989) to 3 m at the Mediterranean Ridge (Stamatakis et al., 1987; Pascoe, 1912; Gorkun and Siryk, 1968; Kopf and Behrmann, 2000). Cemented chimneys at the ancient Verrua mud volcano in Italy also consist of diameters of only several 10 cm (Cavagna et al., 1998). Contrary observations on seismic data show conduits of several 100 m to 1.5-3.5 km in the Black Sea (Ivanov et al., 1996; Limonov et al., 1997; Krastel et al., 2003) at the Barbados Ridge (Griboulard et al., 1998) and in the Alboran Sea (Perez-Belzuz et al., 1997). 3D seismic investigations of mud volcano provinces, however, demonstrate that the width of the feeder channels is probably much smaller than the zone affected by acoustic blanking (Van Rensbergen et al., 1999). Kopf (2002) argued that conduit diameters of hundreds or thousands meters would be only reasonable for slowly ascending diapiric intrusions without considerable over-pressure, otherwise astronomic flow rates have to be expected, even if only small density contrasts exist as driving force. Krastel et al. (2003) proposed for the Dvurechenskii mud volcano that the transparent zone corresponds to an area riddled with smaller conduits, which cannot be resolved by the seismic system. This interpretation is based on short reflection patches within the feeder channel. We observed such weak chaotic reflections within the feeder channel of most of the mud volcanoes in the Sorokin Trough, but they might reflect disturbed sediments as well (Figs. 2.4-2.9, 2.11). The acoustic transparent zone imaged beneath the mud volcanoes is probably much wider than the real conduit, most likely due to generally increased gas content in the sediments surrounding the conduit. Although the main mass transport in the feeder channels is vertically, lateral transport from the channel into the surrounding sediments and vice versa occurs as well. Such lateral flows can explain the blurred margins of most of the feeder channels.

2.7.2 Evolution of the mud volcanoes at the different areas

Previous studies showed that mud volcanism in the Sorokin Trough is associated with the diapirism of the Miocene Maikop plastic clay formation (e.g. Ivanov et al., 1998) by forming diapiric protrusions due to the compressional deformation between the Crimean Mountains and the buried Tetyaev and Shatsky Ridges. The formation and evolution of the mud volcanoes in the Sorokin Trough is controlled by fluid migration along faults and fractures (Woodside et al., 1997).

The morphological shape of mud volcanoes is directly related to the evolution of the mud volcano and the physical properties of the material erupted, primarily depending on the viscosity, the porosity and consolidation of the extruded mud (Brown, 1990; Ivanov et al., 1996; Kopf, 2002; Yusifov et al., 2004). The height of the mud volcano reflects the consistency of the mud and the eruption frequency. The viscosity and porosity of the material influence the dipping angle of the flanks (Kopf, 2002; Yusifov et al., 2004): Mud flows with low viscosity form big and flat cones with low slope angles, while high viscose mud extrusions form cones with steep flanks. High permeable mud results in domes and pies with relatively steep slopes. High pore fluid pressure, e.g. due to fluids sealed by low permeable material, leads to violent eruptions. The great morphological variety of the mud volcanoes observed in our data indicates that different factors control the eruption process and development of the mud volcanoes in the Sorokin Trough, depending on the driving force, eruption mechanism and the physical properties of the material. Concerning to their distribution and morphology, the mud volcanoes have been distinguished into 3 areas (Fig. 2.2). Variations in sedimentary characteristics and subsurface structures most probably influence the factors controlling the evolution of the mud volcanoes in the individual areas.

Evolution model of the mud volcanoes of Area 1

In the western Sorokin Trough the WSW-ENE striking diapiric ridges reflect the S-N oriented compressional tectonic regime due to the northward movement of the Tetyaev Rise. The sedimentary basins contain hemipelagic deposits as well as slumps and turbidity currents from the steep Crimean slope, which formed a system of narrow channels of less than 10 m in depth (Akhmetzhanov et al., 2002). The mud volcanoes of this area are elongated along a morphological step on the seafloor located above the southernmost diapiric ridge (Fig. 2.2). The seafloor step reflects the morphology of the subsurface structures and can be correlated to steep dipping sediments bulging above the diapir (Fig. 2.4). Numerous faults striking parallel to the Tetyaev Rise, perpendicular to the main strain direction, occur at the steep southern flank of the diapir in the surrounding of the feeder channels as well as above the top of the diapir, but lack at the northern diapir flank (Figs. 2.4, 2.7). However, only the M7 mud volcano could be directly linked to a fault underneath,

as mostly sediments beneath the mud volcanoes are acoustically masked in the range of the feeder channel. Reflectors north and south of the feeder channels are difficult to correlate, but at the M3 mud volcano a strong reflector at about 3 s TWT is displaced by 10 ms TWT (Fig. 2.4), and at the DMV the reflectors south-west and north-east are also displaced by about 40 ms TWT (Fig. 2.6), indicating that faults appear to be common beneath the mud volcanoes. Thus, we suggest that the mud volcanoes are associated with faults developed at the steep southern flank of the diapir providing excellent fluid migration pathways towards the seafloor. Acoustic transparent disturbances observed at numerous faults above and at the flank of the diapir are interpreted as fluid escape structures (e.g. Figs. 2.4, 2.7), supporting that fluid migration is fault-controlled. The evolution of the faults probably is mainly forced by the growth of the diapirs, destroying the overlying sediments and leading to over-steepened sediments at the diapir flanks. Thus faults developed above and at the flanks of the diapirs. In the study area, the southern flank of the diapir is significant steepened and faults are limited to this side (Fig. 2.4). This supports that fluid migration and evolution of mud volcanoes is concentrated at the southern flank of the diapir.

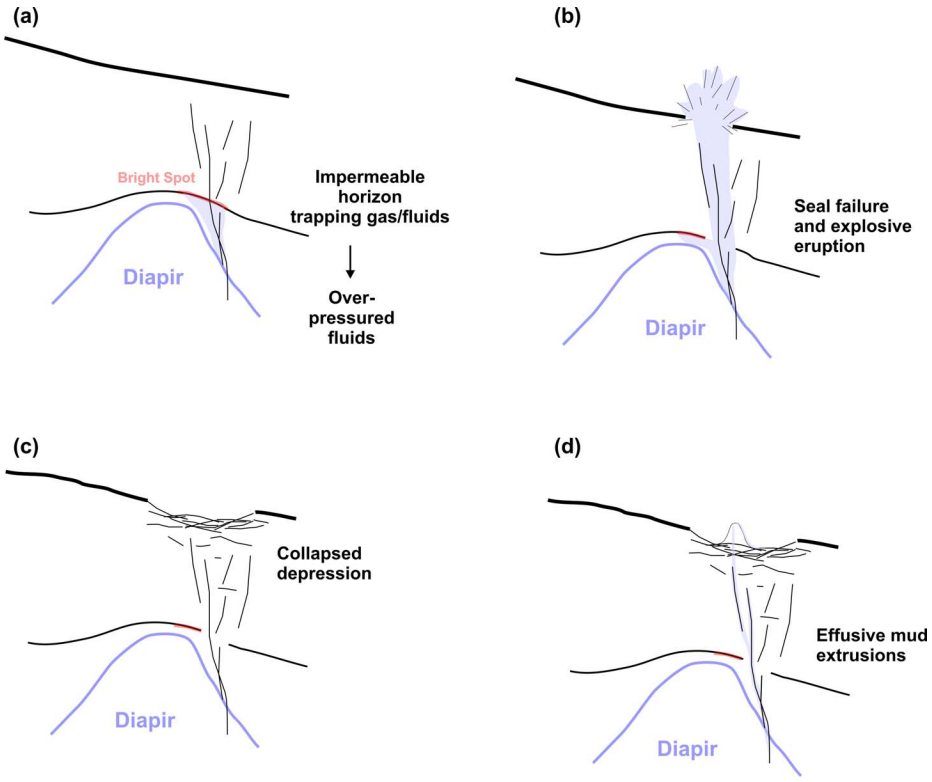

Figure 2.12: *Sketch of the explosive eruption model in Area 1 leading to collapsed depressions. (a) Gas is trapped at horizons with decreased permeability indicated by Bright Spots. (b) If pore pressure exceeds the fracture pressure, gas and sediments are sudden released by gaseous explosion. (c) The material collapses back into the depression. (d) After seal failure the permeability is increased, leading to quiet mud extrusions forming cones.*

The morphological expression of the mud volcanoes in this area greatly varies reflecting different settings concerning the driving mechanism. Most mud volcanoes are depression structures, which are interpreted to represent collapsed structures formed by explosive eruptions. A model for the explosive evolution of the depression structured mud volcanoes is imaged in Fig. 2.12.

The most driving forces for violent eruptions are over-pressured fluids, which can be sealed either by impermeable layers or by gas hydrates (e.g. Brown, 1990). The hemipelagic sediments probably contain predominantly fine grained low permeable clayey sediments in alternation with more permeable silty and sandy sediments, hence prohibiting vertical fluid migration. In addition, gas hydrates have been sampled at several mud volcanoes in the Sorokin Trough (Bohrmann et al., 2003) which decrease the permeability of sediments as well (e.g. Kvenvolden, 1993) and hence possibly lead to excess pore pressures (Sloan, 1990). An evolution model of the mud volcanoes of Area 1 is presented in Fig. 2.13.

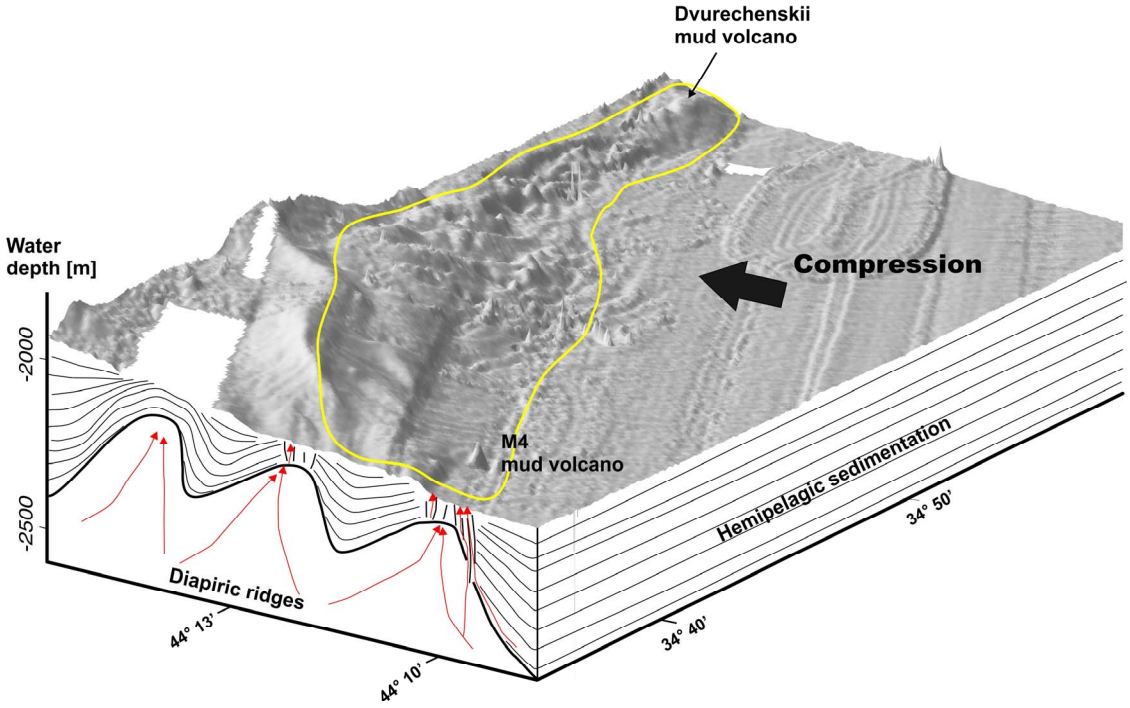

Figure 2.13: *Schematic evolution model of the mud volcanoes in Area 1. Fluid migration is bound to faults developed during the diapiric uplift at the top and the flanks of the diapirs.*

Bright Spots at the approximate depth of the base of the gas hydrate stability zone are widespread in the mud volcano Area 1, especially in the surrounding of the mud volcanoes (Figs. 2.2, 2.4, 2.5). Bright Spots are absent in Area 2 and 3 indicating different mechanisms for the formation of the mud volcanoes. Krastel et al. (2003) and Wagner-

Friedrichs et al. (in review) interpreted these Bright Spots as local free gas accumulation trapped either by impermeable horizons or gas hydrates above. The Bright Spots are probably limited to local areas where fluid migration occurs, associated with mud volcanism. Lateral gas migration from the feeder channel into porous sediment layers might be an explanation why Bright Spots often occur next to feeder channels. The occurrence of the Bright Spots supports that gas is trapped in this area. If the pore pressure exceed the fracture pressure the seal fails and the sudden release of pressure leads to gas expansion and explosive escape of gas/fluids and fluidized material to the seafloor resulting in violent explosions forming collapsed depressions, calderas and craters (Hovland et al, 1997). Over-pressured fluids would be presumably released at cracks and faults, and hydraulic fracturing could play an important role in the development of faults representing an early phase of the formation of the feeder channel. Several authors showed that fluid flow along faults often is associated with hydraulic fracturing (Behrmann, 1991; Brown et al., 1994) though 3D-seismic data would be necessary to prove this hypothesis for our working area. After the burst the collapsed material falls back into the depression (Hovland et al., 1997). Our seismic data show irregular seabed reflections and diffuse discontinuous reflection pattern within the feeder channel, which we interpret as material deposited in the depression after the burst (e.g. Fig. 2.5). After the first violent eruption, the conduit is open for successive more quiet mud extrusions building up the cones within the collapsed structures. Accumulation of gas probably increases the fluid content and decreases the viscosity, thus subsequent fluid-rich mud flows form cones with flat angles, as e.g. at the Dvurechenskii mud volcano (Fig. 2.6).

The simple cone-shaped mud volcanoes indicate less violent and more effusive mud extrusions, fed by continuous fluid flow from the diapir, where permeability is increased, e.g. due to well developed faults, and open unsealed conduits. No Bright Spots are found in the vicinity of these mud volcanoes supporting the idea that no seals exist for these mud volcanoes.

Two special structures occur at the eastern and western edge of the study area: The flat topped Dvurechenskii mud volcano (DMV) (Figs. 2.2, 2.6) with low slope angles indicates extrusions of low viscous fluidized mud, which is supported by sampled mousse like mud breccia with high gas content (Bohrmann et al., 2003). Similar flat-topped mud volcanoes correlated to fluid-rich mud extrusions have been observed e.g. in the Barbados accretionary prism (Henry et al., 1996). The huge dimension of the DMV indicates high frequently mud eruptions (e.g. Yusifov et al., 2004). The DMV is interpreted to be a presently active seep site and seems to be the most active mud volcano in the Sorokin Trough with calculated high flux rates of 12-24 cm year $^{-1}$ and recent mud flows observed on video images at the western rim of the mud volcano (Bohrmann et al., 2003). Gas bubbles

above the DMV, however, have not been observed during the M52 cruise (Bohrmann et al., 2003), but were recorded during the CRIMEA cruise in 2002 as acoustic flare images in echosounder data (Greinert et al., 2006), indicating that gas emission at the DMV is episodically. The Pillar-like structure of the M4 mud volcano characterized by steep flanks is interpreted to represent a high porous sandy mud volcano (Fig. 2.7). Such morphological structures have been observed at onshore sand mud volcanoes cemented by clay and silt-breccia. The origin of the sand might be associated with the basis of the Maikop Formation containing sandstones, which partly have been eroded and washed out forming sand lenses within the Maikop formation (Golubnichaya, 1969).

Evolution model of the mud volcanoes of Area 2

The mud volcanoes located at the flat plain of the Sorokin Trough have a completely different character to those of Area 1 implying a different eruption style. The big Nioz and Kazakov mud volcano are simple cone-shaped indicating quiet effusive mud extrusions, which are proposed either to occur more frequently or to contain huge amounts of mud resulting in such large structures. The deposits of the Don-Kuban Fan, which might affect the migration pathways controlling the evolution of the mud volcanoes, intensively influence this area. The gas and water saturated fan deposits are correlated to mass movements along canyon systems at water depths above 1200 m in the north-east (Akhmetzhanov et al., 2002) resulting in homogeneous mixed sediment units without internal structure, seismically characterized by an acoustically transparent facies (Figs. 2.6, 2.8). As this area represents the distal fan province, the fan deposits are merged with hemipelagic sediments, which are characterized by bands of strong reflectors separating the transparent fan units (Figs. 2.6, 2.8). The lack of layered horizons within the fan sediments provides less seals for ascending gas, which increases permeability. Therefore no trapping of gas and fluids occur, resulting in more quite eruptions characterized by ductile mud extrusions forming simple cone-shaped structures. The displacement of the seafloor and subsurface reflections east and west of the Nioz and Kazakov mud volcano implies that the upward mass transport to them is fault-controlled as already discussed for Area 1 (Figs. 2.6, 2.8). An evolution model for this area is imaged in Fig. 2.14. The Nioz mud volcano is associated to a diapiric ridge beneath, but no root of the feeder channel is visible beneath the Kazakov mud volcano in our high resolution seismic data. There might be a diapiric protrusion at greater depth. Otherwise the mud volcano could be directly fed from the Maikop Formation. Such structures have been observed in the Central Black Sea, where feeder channels could be traced down to 7-9 km terminating in the Maikopian Formation (Meisner et al., 1996). It is believed that the Maikop Formation is the source of the mud volcanoes in the Sorokin Trough, as clasts recovered from mud breccia sampled at the Dvurechenskii mud volcano

could be correlated to the Maikopian Formation, which is located at a depth of 4-5 km (Bohrmann et al., 2003). Upward bending reflectors at 3.0 - 3.1 s TWT at the margins of the feeder channel of the Kazakov mud volcano could either be related to velocity pull-ups due to the presence of gas hydrates with higher velocities, or represent uplifted and tilted sediments caused by the upward transport of material.

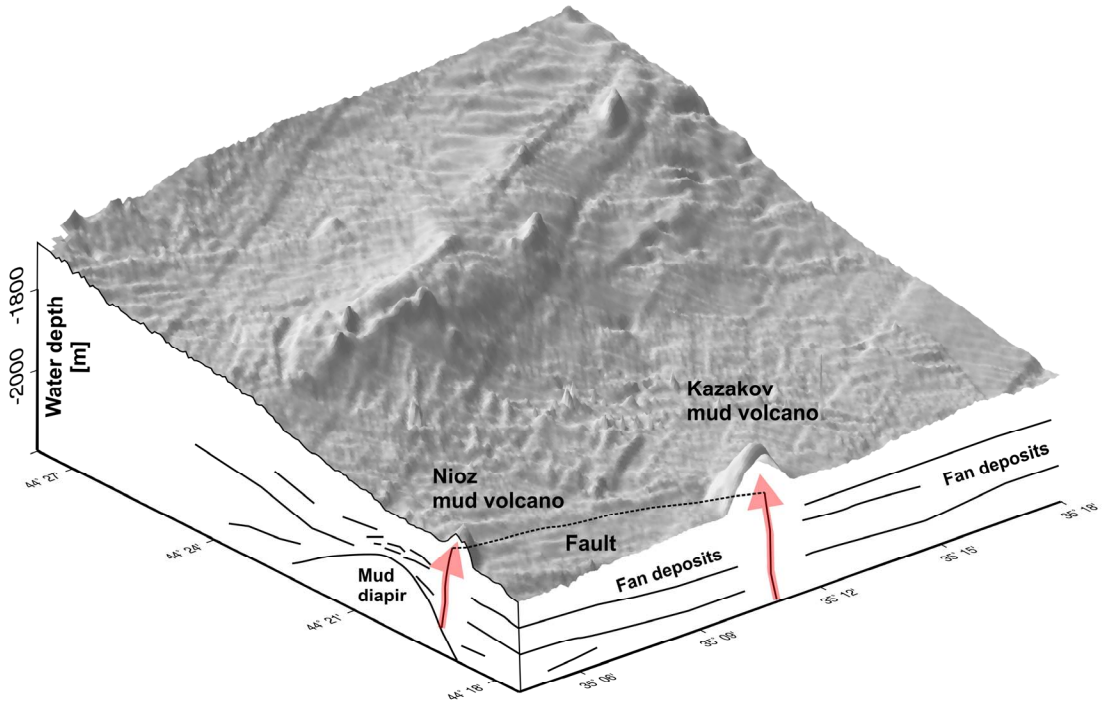

Figure 2.14: *Schematic model of the evolution of the mud volcanoes in Area 2. The Nioz and Kazakov mud volcanoes are fed by fluid migration along major faults.*

Evolution model of the mud volcanoes of Area 3

In this area the formation of the mud volcanoes is related to the diapiric ridge stretching along the morphological high north-west of the Shatsky Ridge, representing the south-western edge of the Paleocene-Eocene Pallas-Uplift. The Pallas-Uplift is covered by mainly Quarternary sediments of the Don-Kuban Deep Sea Fan, forming a thick accumulative structure with complex relief (Tugolesov et al., 1985; Volkonskaya, 1997; Akhmetzhanov et al., 2002). Half of the mud volcanoes concentrated on this high is surrounded by well stratified hemipelagic sediments in the north-west, while the other mud volcanoes are located within the unstructured acoustically transparent facies of the fan deposits in the south-east (Figs. 2.2, 2.9, 2.10).

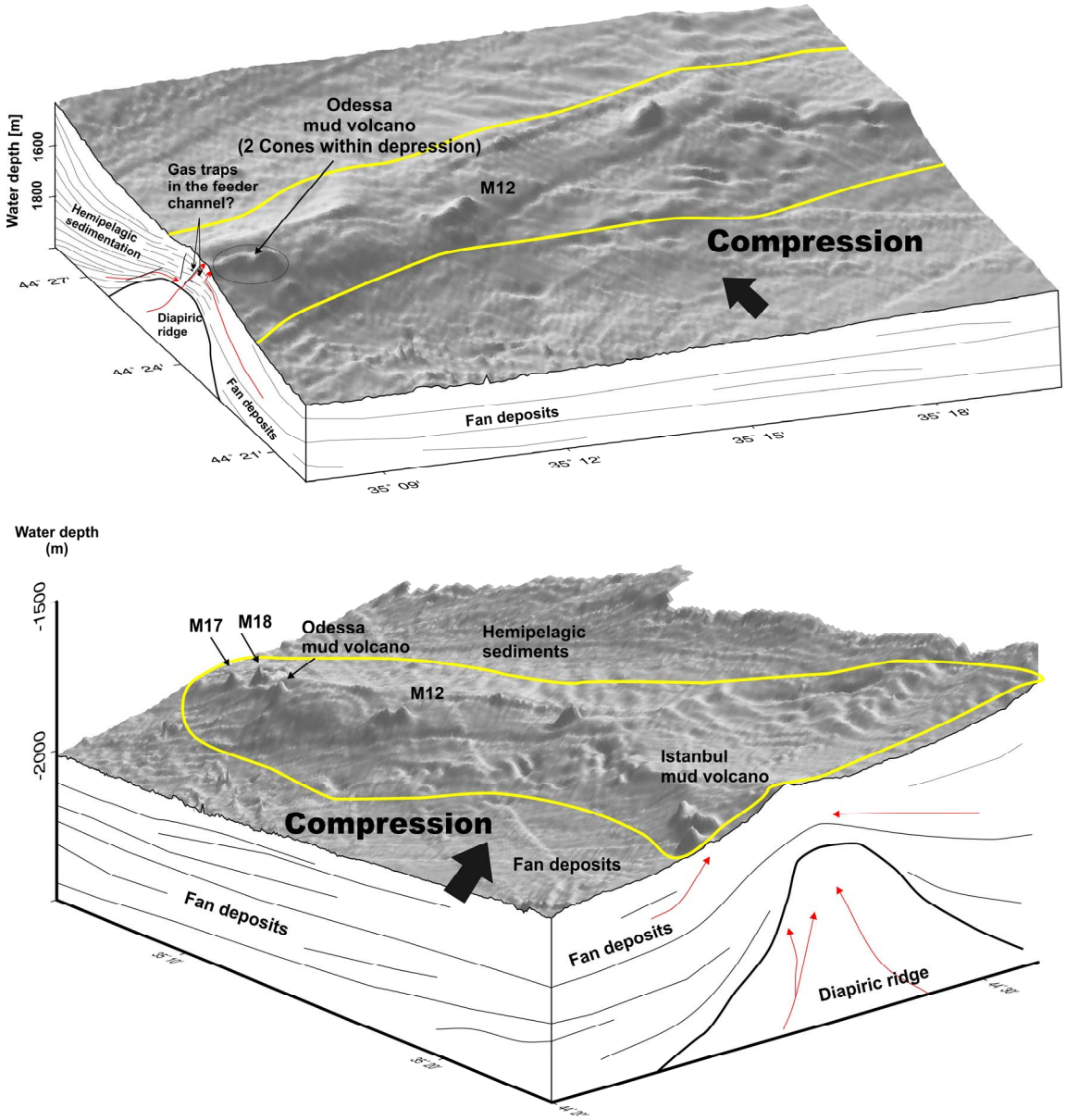

Figure 2.15: *Schematic model of the evolution of the mud volcanoes in Area 3. a: At the sub-region dominated by hemipelagic sediments the mud volcanoes are fed by fluid migration along faults. b: In the south-eastern sub-region lateral fluid migration within the fan horizons towards the morphological high might play a key role in supplying the mud volcanoes.*

Analogue to Area 2 cone-shaped mud volcanoes are the most typical structures in Area 3 indicating a dominance of quiet eruptions, which probably occur less frequently than in Area 2 due to the generally smaller size of the mud volcanoes. Explosive gas/fluid expulsion due to over-pressured fluids plays a minor role in this area, as only few collapsed structures were observed in both sub-regions (M11, M16 and Odessa mud volcano; Table 1). Bright Spots, which are common in Area 1 and indicate trapped free gas, are absent in this area. Asides, breccia or gas hydrates in the conduits might act as seal as well, inducing

increased pore pressure and leading to explosions in case of seal failure. Gas hydrates and clasts would affect seismic amplitudes, as they create high impedance contrast to the surrounding gassy material of the conduit (Holbrook et al., 2002). High amplitudes reflection patches are often observed in the feeder channels, in Area 1 as well as in Area 2 and 3 (Figs. 2.5, 2.6, 2.8, 2.9), and might be an indication for potential seals. As the dimension of these patches is small, their impact on great explosions probably is very low. The different depositional environments in the two sub-regions of Area 3 suggest different evolution models (Fig. 2.15a+b). In the north, faults imaged above the diapiric top in the surrounding of the mud volcanoes let us presume that fluid migration along faults probably fed the mud volcanoes from the diapiric ridge as in Area 1. Continuous upward migration of fluids and fluidized mud forms cones and domes depending on the density and consistency of the material. In the south-east faults could not be identified within the transparent units of the fan deposits, but are suggested to be present due to the diapiric protrusion beneath. Here, additionally to vertical fluid migration along faults the mud volcanoes might be supplied by absorption of material from the fan deposits. The northward oriented tectonic stress initiates lateral fluid migration towards the morphological high. Passing into the feeder channel these fluidized material can be periodically expelled at the mud volcano due to the upward fluid migration absorbing and raising them to the mud volcano. This process increases the fluid content at these mud volcanoes, which is supported by mousse like breccias sampled during the TTR cruises (Woodside et al., 1997). The higher fluid content, however, is not reflected in the morphology of the mud volcanoes.

2.7.3 Correlation of the mud volcanoes to deep subsurface structures and the regional geological and tectonic framework

The seismic data collected during Meteor cruise M52/1 does resolve a maximum of 1000 m of sediment coverage, which means that only Quarternary sediments and the tops of the diapiric ridges are imaged. We do not penetrate down to the root of the diapirs, which are considered to be located at the Maikopian Formation in 4-5 km depth (Woodside et al., 1997; Ivanov et al., 1998). Our access to single channel seismic data collected by the SSC “Yuzhmorgeologia” of Gelendzhik in 1979, penetrating the deeper structures of the Sorokin Trough, enabled conclusions about the evolution of the mud volcanoes with respect to the regional geological framework. An interpreted image of the SW-NE striking cross section covering the Sorokin Trough along the general trend of the structures is shown in Fig. 2.16.

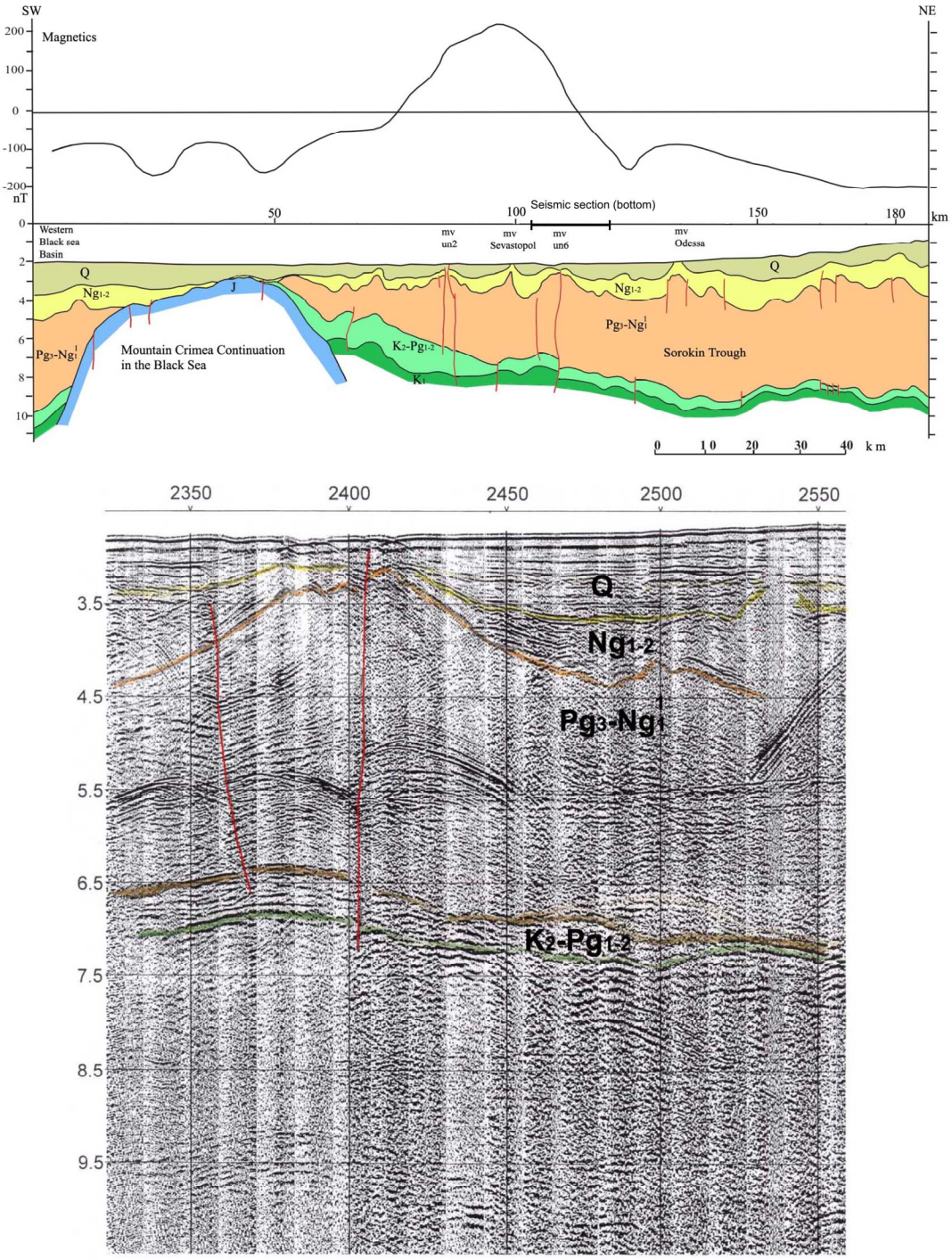

Figure 2.16:
Top: Interpretation of the seismic cross section of SSC "Yuzhmorgeologia" of Gelendzhik through the Sorokin Trough together with the residual magnetic data (upper part). See Fig. 2.2 for location of the line. The positive anomaly of the magnetic data corresponds with fault systems.
Q=Quaternary, Ng_{1-2}=Miocene-Pliocene, Pg_3-Ng_1^1=Oligocene-Lower Miocene (Maikop), Pg_{1-2}=Palaeocene-Eocene, K_1=Lower Cretaceous, K_2=Upper Cretaceous, J=Jura
Bottom: Close up of the seismic cross section. A mud volcano is located above a diapiric structure showing faults inside probably acting as fluid migration pathways.

The Maikop Formation shows varying thickness defined by subsurface structures, but generally thins towards the offshore continuation of the Crimean Mountains, which is composed of Triassic-Jurassic terrigeneous flysch and forms a barrier west of the Sorokin Trough. Above the marine continuation of the Crimean Mountains the Maikop Formation is found to be absent in the seismic data (Fig. 2.16). In the range of the diapiric folds the thickness of the Maikop formation is increased to almost 7 km. The cross section shows that the diapiric structures are rooted in the Maikop Formation, but do not reflect the topography of the Maikopian basis (Fig. 2.16). Four mud volcanoes (M4, Sevastopol, M6 and Odessa) are covered by the cross section, all underlain by a diapir. The M4 and M6 mud volcano have not been imaged on this seismic line, but could be identified on our high resolution seismic data (Fig. 2.2). Our observation that the mud volcanoes are related to fluid migration along faults is supported by the Gelendzhik seismic data revealing numerous deep faults, concentrated beneath the mud volcanoes, within the Miocene/Pliocene sediments and the Maikop Formation. The faults partly reach down into older rocks underneath the Maikop (Fig. 2.16). We suggest that the near-subsurface faults observed in the high resolution seismic data are connected to the deeper faults acting as fluid migration pathways to the seafloor.

Why are the mud volcanoes concentrated at the northern edges of the Tetyaev Rise and Shatsky Ridge? The source of the fluids is considered to be at greater depth within the Maikop Formation, released under great pressure and temperature conditions due to the transformation of smectite to illite, which is expected to be completed in a depth of about 3.7 km (Kholodov, 1983). The evolution of faults within the Maikop Formation probably is related to over-pressured fluids. The Maikop clay contains less migration pathways due to its low permeability leading to over-pressured fluids. This forces primary lateral fluid migration together with the general mass movements from north to south, mobilized by the overburden and lateral compression. The Tetyaev Rise and the Shatsky Ridge south of the Sorokin Trough represent uplifts of Mesozoic and Palaeogene rocks, acting as a barrier for the mass and fluid migration. Fluids accumulate and get over-pressured preferably released at cracks and faults. The origin of the deeper faults can be attributed to a Gabbro Intrusion in Jurassic time, proved onshore on Crimea and in Georgia (Zaridze et al., 1964, Lebedinsky, 1969). Offshore, a positive magnetic anomaly with a width of 40-50 km extending from the Crimean slope through the Sorokin Trough and along the Shatsky Ridge to Georgia is considered to represent the same intrusion (Fig. 2.16). The Gabbro probably has intruded along existing faults and forced the evolution of further faults, which proceeded into younger layers. The fluids are released at pre-existing weakness zones, such as cracks and faults.

As described above we think that the origin of the gas emitting at the mud volcanoes is sourced at greater depth within the Maikop Formation migrating upward along faults, but to a minor degree the gas additionally could be originated by in situ microbial transformation of organic matter into hydrocarbons. The molecular components of the hydrocarbon gases measured at several mud volcanoes suggest a deep source of the venting fluids (Blinova et al., 2003). However, the isotopic composition of the methane, which is the dominating component of the gas extracted by dissociation of gas hydrates, with an average delta ^{13}C value of -64 ‰ indicates a mainly biogenic origin with an admixture of thermogenic gas (Blinova et al., 2003).

2.8 Conclusions

Based on new acoustic data collected during the Meteor cruise M52/1, 25 mud volcanoes were identified in the Sorokin Trough associated with diapiric structures of the Maikopian Formation mainly trending in the WSW-ENE direction due to an N-S oriented compressional tectonic regime. The single channel seismic data from 1979 show that the deep subsurface of the Sorokin Trough is structured by numerous faults within and beneath the Maikop Formation, which can be traced also into the Pliocene and Quaternary sediments, suggesting that fluid migration towards the mud volcanoes is controlled by faults and sourced at great depth. The Shatsky and Tetyeav Ridge act as a barrier for lateral fluid migration, leading to over-pressured fluids, preferentially released at cracks and faults, thus mud volcanoes are clustered at the northern edges of these buried ridges.

The new high resolution seismic data show that most mud volcanoes are related to near-subsurface faults developed during the growth of the diapirs and acting as fluid migration pathways. The mud volcanoes show a great variety in shape and size reflecting different driving mechanisms. Four different morphological types of mud volcanoes were identified: cone-shaped mud volcanoes, collapsed structures, collapsed structures including cones and one flat topped mud volcano. Based on different geological and depositional settings, the study area was subdivided into three areas dominated by different mud volcano types: In Area 1 the mud volcanoes are elongated along a morphological step with predominately collapsed structures. Layered hemipelagic sediments provide efficient seals for gas/fluids rising along growth faults at the steep southern flank of the southernmost diapir, which lead to high pore pressure. Seal failures cause gaseous explosions and abrupt release of fluids and material collapsing back into the vent and forming caldera-like structures. Traps of gas are indicated by the local distribution of Bright Spots near the mud volcanoes. Area 2, located at the deep plain of the Sorokin Trough, comprises two big simple cone-shaped mud volcanoes, formed by quiet effusive mud extrusions due to increased vertical permeability of the dominating homogeneous fan deposits. The mud

volcanoes are located above faults with great vertical offsets of about 20 m, indicating that high mud flow rates seem to be related to prominent faults. The small cone-shaped mud volcanoes of Area 3, aligned along a morphological high, are built by quiet ductile mud flows as in Area 2. Lateral fluid migration towards the morphological high might supply the formation of the mud volcanoes leading to very moussy eruption products.

2.9 Acknowledgements

We would like to thank the crew of the R/V Meteor and the scientists participating the M52/1 cruise (MARGASCH Project) for the successful data acquisition facilitating this study. This research was funded by grants from the Deutsche Forschungsgemeinschaft (code Kr2222/4).

3 3D seismic investigations of the Sevastopol mud volcano in correlation to gas/fluid migration pathways and gas hydrate occurrences in the Sorokin Trough (Black Sea)

Michelle Wagner-Friedrichs, Sebastian Krastel, Volkhard Spiess, Michael Ivanov, Gerhard Bohrmann, Leonid Meisner

Submitted to G-Cubed (in review)

3.1 Abstract

New 3D seismic investigations carried out across the Sevastopol mud volcano in the Sorokin Trough firstly represent 3D seismic data of a mud volcano in the Black Sea. The studies allow us to image the complex three dimensional morphology of a collapsed structured mud volcano and to propose an evolution model. The Sevastopol mud volcano is located above a buried diapiric structure with two ridges and controlled by fluid migration along a deep fault system, which developed during the growth of the diapirs in a compressional tectonic system. Over-pressured fluids initiated an explosive eruption generating the collapsed depression of the Sevastopol mud volcano. Several cones were formed within the depression by subsequent quiet mud extrusions. Although gas hydrates have been recovered at various mud volcanoes in the Sorokin Trough, no gas hydrates were sampled at the Sevastopol mud volcano. A BSR (bottom-simulating reflector) is missing in the seismic data, however, high amplitude reflections (Bright Spots) observed above the diapiric ridge near the mud volcano correspond to the approximate depth of the base of the gas hydrate stability zone (BGHSZ). Thus, we suggest that gas hydrates are present locally where gas/fluid flow occurs related to mud volcanism, i.e. above the diapir and close to the feeder channel of the mud volcano. Depth variations of the Bright Spots of up to 200 ms TWT might be caused by temperature variations produced by variable fluid flow.

3.2 Introduction

Mud volcanoes are structures related to fluid discharge and are considered to be one of the most significant natural sources of carbon emission to the hydrosphere and atmosphere. Emission is dominated by methane gas, which contributes to the modern atmospheric methane budget (Dimitrov, 2003; Milkov et al., 2003a). The emitted greenhouse gases have a great relevance to the carbon budget and climatic change, which lead to increased interest in the study of mud volcanoes since the last decades (e.g. Milkov, 2000). Mud volcanoes are formed by the emission of gas, water and sediments, which

might occur by violent eruptions, but mostly occur by semi-liquid effusive mud flows (Dimitrov, 2002; Milkov et al., 2003a). Thus, the extruded material at mud volcanoes gives information about sediments and fluids in the shallow and deep subsurface (e.g. Guliyev and Feizullayev, 1997). Estimates about the amount of methane emitted to the atmosphere through mud volcanoes vary significantly: Milkov et al. (2003a) establish that the global methane flux through mud volcanoes is about ~ 33 Tg year $^{-1}$, while Kopf (2002) suggests that only 0.08-1.41 Tg year $^{-1}$ of methane are released through mud volcanoes. Dimitrov (2003) estimates that the annual amount of methane released from onshore and shallow water mud volcanoes range between 10.2-12.6 Tg. The annual contribution of methane to the atmosphere through mud volcanoes is estimated to be about 5 Tg year $^{-1}$ (Dimitrov, 2003). Mud volcanoes occur worldwide onshore and offshore, predominantly in areas of compressive tectonic regimes facilitating fluid/gas and mud flow towards the surface (Kopf, 2002). Almost 2000 mud volcanoes have been observed worldwide, most located along the Alpine-Himalaya Active Belt (Dimitrov, 2003). The distribution, activity, eruption products and formation mechanisms of terrestrial mud volcanoes have been well studied for over 200 years. The investigation of submarine mud volcanoes, however, only started ~30 years ago and the exact number of submarine mud volcanoes is uncertain, but the number of described submarine mud volcanoes is increasing rapidly (Dimitrov, 2003). The formation of mud volcanoes has been intensively discussed and is affected by several factors and processes. Woodside et al. (1997) distinguished 2 main mechanisms for the formation of mud volcanoes: (1) fluid migration associated with a shale diapir and (2) rise of fluidized mud along faults and fractures. Mud volcanoes show a great variety in size and geometry (Kopf, 2002). Morphological and structural characteristics of submarine mud volcanoes are mainly investigated by hydroacoustic methods. The morphology of mud volcanoes reflects directly the eruption style and the physical properties of the material erupted, primarily depending on the fluid content, the viscosity and consolidation of the extruded mud (Brown, 1990; Kopf, 2002).

The Black Sea, containing thick sedimentary sequences with high methane concentrations, provides an excellent area to study mud volcanism. Well studied mud volcanoes occur in the central part of the Black Sea (Ivanov et al., 1996; Limonov et al., 1997) and in the Sorokin Trough (Ginsburg et al., 1990; Woodside et al., 1997; Krastel et al., 2003). The mud volcanoes in the Sorokin Trough show varying morphology and are generally connected to near-subsurface diapiric structures (Woodside et al., 1997). The evolution of the mud volcanoes in the Sorokin Trough is primarily linked to faults acting as migration pathways for rising fluidized mud (Woodside et al., 1997). Generally, deep water mud volcanoes are often associated with gas hydrate occurrences (Woodside et al., 1997) as first discussed by Ginsburg et al. (1984). In the Sorokin Trough gas hydrates near

numerous mud volcanoes have been sampled since the 1980s (e.g. Ginsburg et al., 1990; Ivanov et al., 1998; Bohrmann et al., 2003), but no BSRs have been identified on seismic sections.

During Meteor cruise M52/1 in January 2002, a high resolution three dimensional seismic survey was carried out in the vicinity of the Sevastopol mud volcano in order to obtain the detailed spatial geometry of a collapsed structured mud volcano and its subsurface structures, which provide an evolution model directly related to gas/fluid migration along deep faults. The main objectives of this survey have been focused on following aims and questions:

- What is the 3 dimensional structure of the Sevastopol mud volcano?
- What kind of subsurface structures are associated with the mud volcano?
- What conclusions about the evolution and eruption style of the mud volcano can be drawn from the identified surface and subsurface structures?
- What are the main fluid/gas migration pathways controlling the formation of the mud volcano?
- Are there evidences for gas hydrates in the surrounding of the mud volcano?

3.3 Geological setting

The Black Sea, surrounded by Late Cenozoic mountain belts (the Pontides, the Caucasus, the Crimean Mountains and the Balkanides), is the world's largest anoxic intercontinental basin. The Black Sea presumably originated as a back-arc basin related to the subduction of the Thetyan Ocean in late Cretaceous time (Dewey et al., 1973; Finetti et al., 1988; Nikishin et al., 2003). Due to the collision between the Eurasian and the Arabian plates since the Eocene, the tectonic setting changed to a compressional regime (Nikishin et al., 2003). Structurally, the Black Sea is composed of two basins, the Western Black Sea Basin and the Eastern Black Sea Basin, which are separated by the Andrusov Ridge (Fig. 3.1) consisting of continental crust and overlain by 5-6 km of sediments (Tugolesov et al., 1985). The origin and the formation timing of the basins are still under debate (e.g., Okay et al., 1994; Rangin et al., 2002). Currently, it is widely accepted that the Western Black Sea Basin opened in Mid-Cretaceous, which is based on stratigraphic evidences from the northern Black Sea margin (e.g. Robinson et al., 1996). The age of the opening in the Eastern Black Sea is not as well documented and interpretations vary from Jurassic time (Golmshtok et al., 1992), to end-Cretaceous (Nikishin et al., 2003) and Paleocene/Eocene opening (Robinson et al., 1996; Spadini et al., 1996; Cloething et al., 2003).

The Western Basin is thought to be underlain by oceanic crust with a sediment cover of up to 19 km thickness (Tugolesov et al., 1985). The basement of the Eastern Basin

is thinned and it is still discussed whether it represents oceanic (Belousov et al., 1988; Finetti et al., 1988; Rangin et al., 2002) or continental crust (Tugolesov et al., 1985). The crust in the Eastern Basin, however, is overlain by up to 12 km thick post-rift sediments (Tugolesov et al., 1985; Rangin et al., 2002).

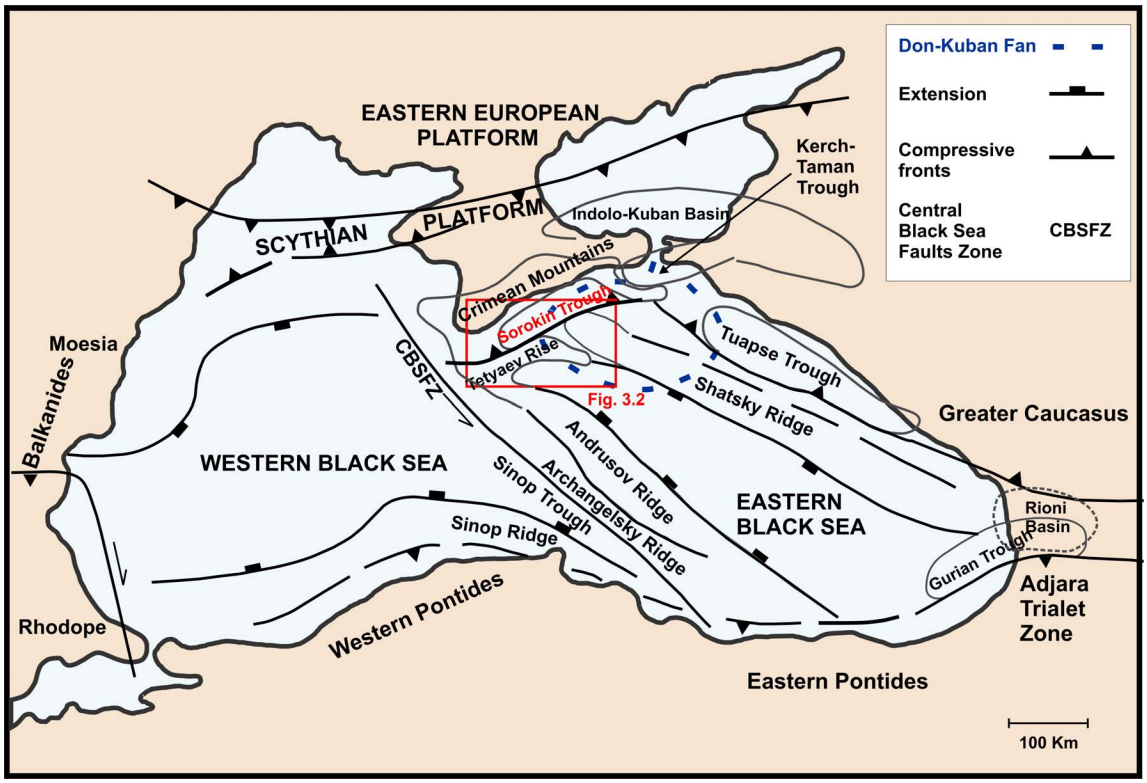

Figure 3.1: *Schematic map of the Black Sea showing the major tectonic units, morphological structures and the location of the study area (Sorokin Trough), highlighted in red (modified after Robinson et al., 1996). The grey lines mark the borders of the morphological structures.*

The Sorokin Trough (Figs. 3.1, 3.2) forms a 150 km long and 50 km wide structural depression along the south-eastern margin of the Crimean Peninsula in the Eastern Black Sea Basin at water depths of 800-2200 m (Tugolesov et al., 1985). The trough is considered to be a foredeep of the Crimean Mountains and belongs to a system of Oligocene-Miocene troughs, such as the Kerch-Taman and Indolo-Kuban Trough (Tugolesov et al., 1985). In the south and south-east, the Sorokin Trough is bordered by the Cretaceous-Eocene buried Shatsky Ridge and Tetyaev Rise (Figs. 3.1, 3.2). The formation of the Trough began in Oligocene time during Crimean-Alpine folding (Andreev, 1976).

Based on seismic data, two main units have been recognized in the sedimentary cover of the Sorokin Trough (Woodside et al., 1997): The lower unit consists of the upper part of the Maikopian Formation (Oligocene-lower Miocene) and Pliocene deposits. It is intensively folded and disturbed by numerous faults, which can be traced into the upper unit.

The thickness of the unit varies from 5 to 6 km. The upper unit consists of quaternary deposits, which are characterized by subparallel bedding (Limonov et al., 1997). The quaternary deposits can be laterally subdivided into fan deposits of the Pleistocene Palaeo Don-Kuban Fan and basinal deposits, consisting of hemipelagic sediments and turbidites with an origin in the Crimean Mountains (Limonov et al., 1997). The thickness of the unit is controlled by the underlying diapirs and varies from several 100 m up to 2 km, but generally increases towards the north-east. A compressional tectonic regime, produced by the northward movements of the Shatsky Ridge and the Tetyaev Rise, and the weight of the overburden affect the protrusion of the plastic and water-saturated clay of the Maikopian Formation and lead to the growth of diapiric structures (Limonov et al., 1997). The diapiric ridges mainly strike in the E-W-direction, but the strike direction changes east- and westward and follows the flanks of the buried Tetyaev Rise and Shatsky Ridge (Woodside et al., 1997). The compressive deformation facilitates fluid/gas migration towards the seafloor and over-pressured fluids lead to the formation of numerous mud volcanoes, which mostly evolve on the edges of the near-surface mud diapirs.

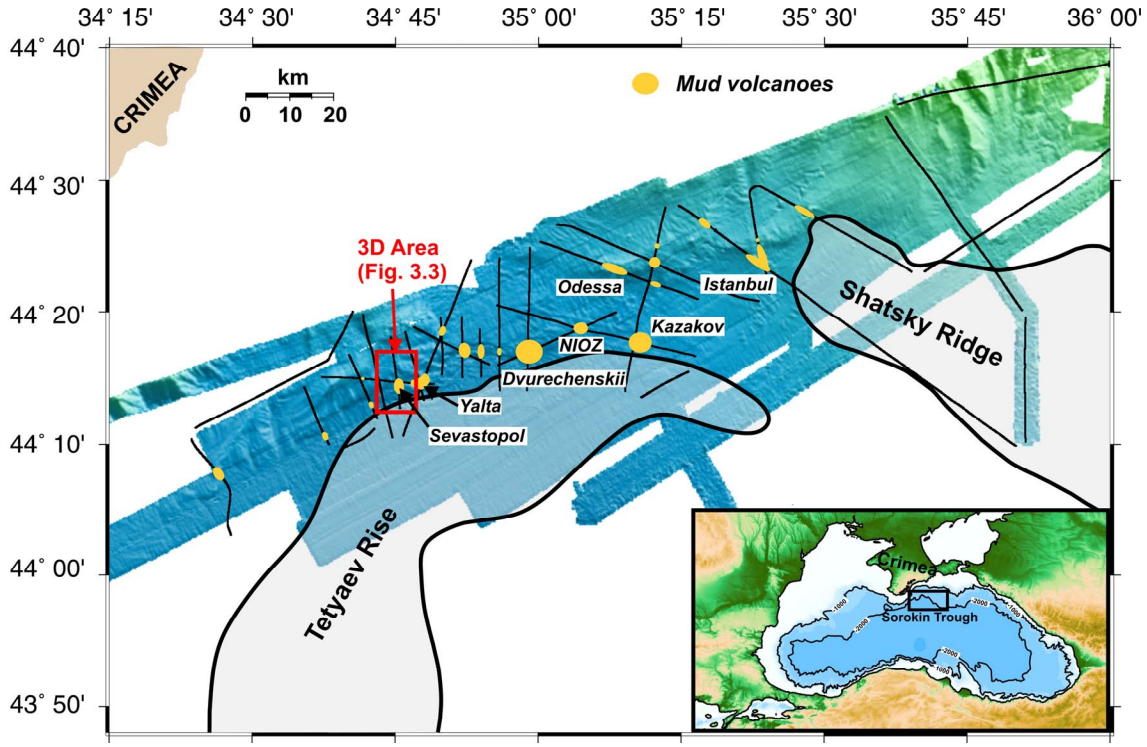

Figure 3.2: *Bathymetric map of the Sorokin Trough together with the location of the seismic overview profiles (continuous lines) and the area of the 3D survey (red rectangle). The yellow circles show the locations of the mud volcanoes observed during Meteor cruise M52/1.*

Based on seismic studies three types of mud volcanoes have been distinguished in the Sorokin Trough: most of the mud volcanoes are cone-shaped, some are collapsed structures (pockmarks), and one, the Dvurechenskii mud volcano, is flat-topped (Krastel et al., 2003). Most mud volcanoes are located at the northern edges of the Tetyaev Rise and Shatsky Ridge (Fig. 3.2). In the Sorokin Trough, gas hydrates were recovered from several mud volcanoes and above diapirs (Ginsburg et al., 1990; Bouriak & Akhmetjanov, 1998; Ivanov et al., 1998; Kenyon et al., 2002; Bohrmann et al., 2003). The gas hydrates are believed to form local accumulations, which are controlled by mud volcanoes and can be related to zones of intensive fluid flow towards the seafloor (Ginsburg et al., 1990; Bouriak & Akhmetjanov, 1998). In the Black Sea, gas hydrates are stable below a water depth of 700 m (Ginsburg et al., 1990).

3.4 Methods

The high resolution multichannel seismic data presented in this paper were collected during Meteor cruise M52/1 in early 2002. A GI-Gun with 0.4 l chambers (main frequency 100-500 Hz) towed in 1.4 m water depth was used along all seismic lines. Data were recorded by a 300 m long streamer section (SYNTRON) with 24 channels at a group distance of 12.5 m. The streamer was kept in a water depth of 3 m (+/- 0.5 m) by the attachment of 9 birds (cable levelers). Magnetic compass readings in the birds allow the determination of the position of each hydrophone group relative to the ship course. The data were digitally recorded at a sampling frequency of 4 kHz over an interval of 3 seconds. Positioning was based on GPS recordings. The seismic survey was divided into two parts. Initially, 44 seismic lines were shot as overview profiles to get information about the general structures and the distribution of the mud volcanoes in the survey area. Based on these results, first interpreted by Krastel et al. (2003), a 2.5 x 7.5 km large area around the Sevastopol mud volcano in the western Sorokin Trough was chosen for the three dimensional survey in order to resolve the structural variability observed in the overview lines (Fig. 3.2), which are characterized by a complex pattern of buried diapiric ridges and sedimentary basins.

Our 3D acquisition geometry consists of a series of 81 parallel 2D lines with a line spacing of 25 m (Fig. 3.3). The lines are oriented in the NNW-SSE direction perpendicular to the strike direction of the diapiric ridges. Additionally, 24 profiles with a line separation of 50-100 m increase the width of the survey region to ~6 km and 11 cross profiles were shot as connecting lines to the overview profiles.

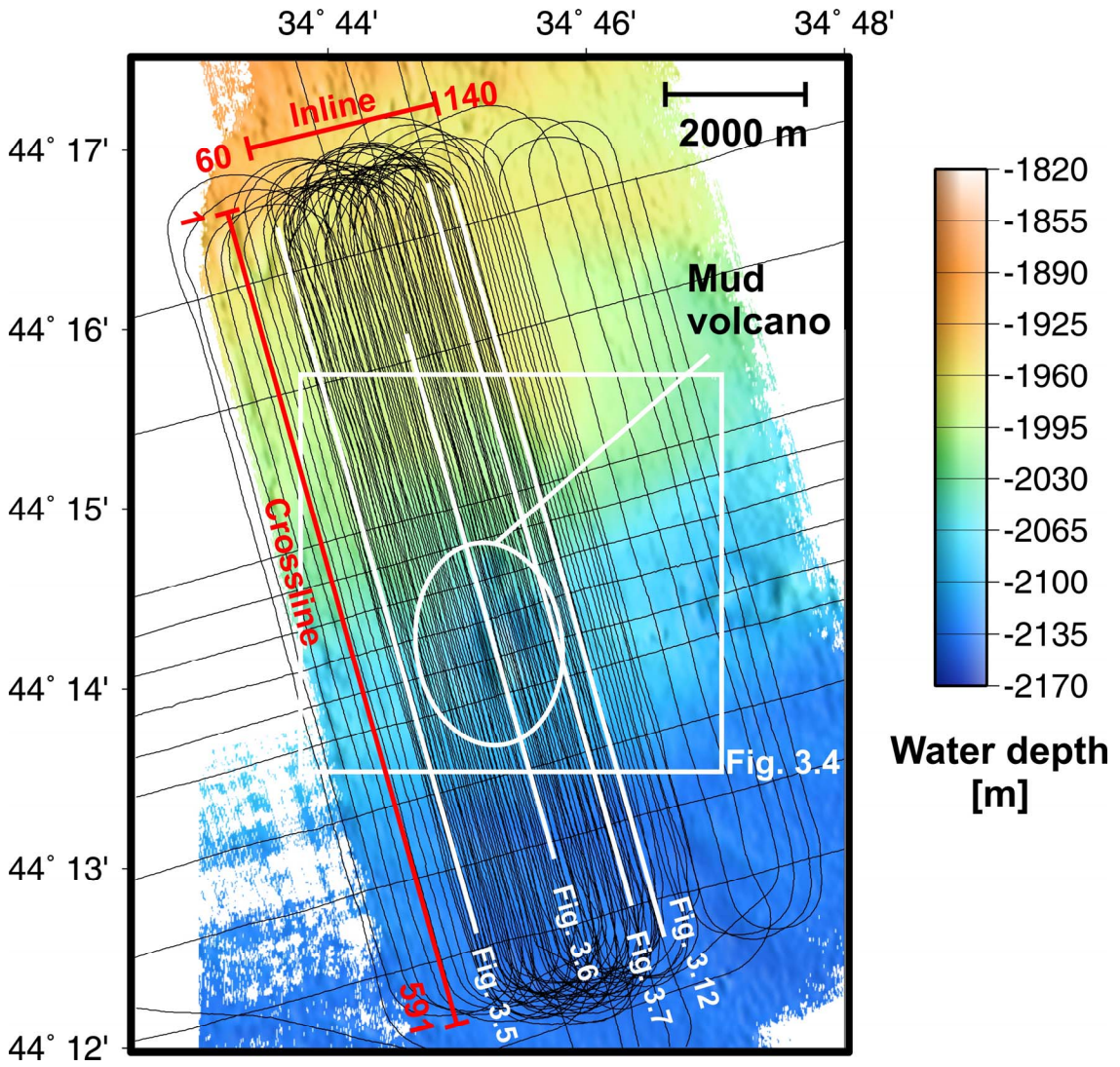

Figure 3.3: *Bathymetric map of the 3D survey area in the western Sorokin Trough based on 15.5 kHz Krupp Atlas Hydrosweep data together with the seismic tracks of the 3D grid. The white lines are shown in this paper.*

Geometry processing was done by custom software and includes the calculation of source and receiver positions, which was the basis for the calculations of offsets and the CMP binning. Residual lateral offsets between adjacent profiles binned on the same Inline were adjusted. Statics caused by vertical movements of the streamer were corrected with help of the depth information from the birds. Afterwards the 3D seismic data were NMO-corrected with a constant velocity of 1500 m/s, bandpass frequency filtered with a frequency content of 55/110 - 600/800 and stacked at a Common Cell Gather distance of 12.5 m in the Inline and 25 m in the Crossline direction. The average cell coverage was about 7. Finally, a FK-3D time migration at a constant velocity of 1500 m/s was applied. Due to the relatively short streamer (300 m maximal offset), and water depths of more than 2000 m no velocity

analysis was carried out. Locally low and irregular bin coverage along several Inlines, particularly at the margins of the grid, and the limited Crossline extension affect the quality of the 3D migration. Only the central grid area, comprising Inline 60-140, is unproblematic for the migration aperture and hence was used for interpretation. During the processing the amplitudes information were preserved and only spherical divergence was corrected.

Bathymetric data were continuously obtained with the Krupp Atlas Hydrosweep system, using a frequency of 15.5 kHz and 59 beams in a swath of 90°. Additionally, digital sediment echosounder data were permanently acquired by the Parasound/ParaDigMa System, which uses a pulse with a dominant frequency of 4 kHz.

3.5 Results

3.5.1 Bathymetry of the 3D seismic survey

The 3D study area is located at water depths of 1800 - 2150 m and characterized by a slope angle of about 0.5° towards the south-east. The relief is low in general, but three smooth ridge-like structures occur in the north (Fig. 3.4).

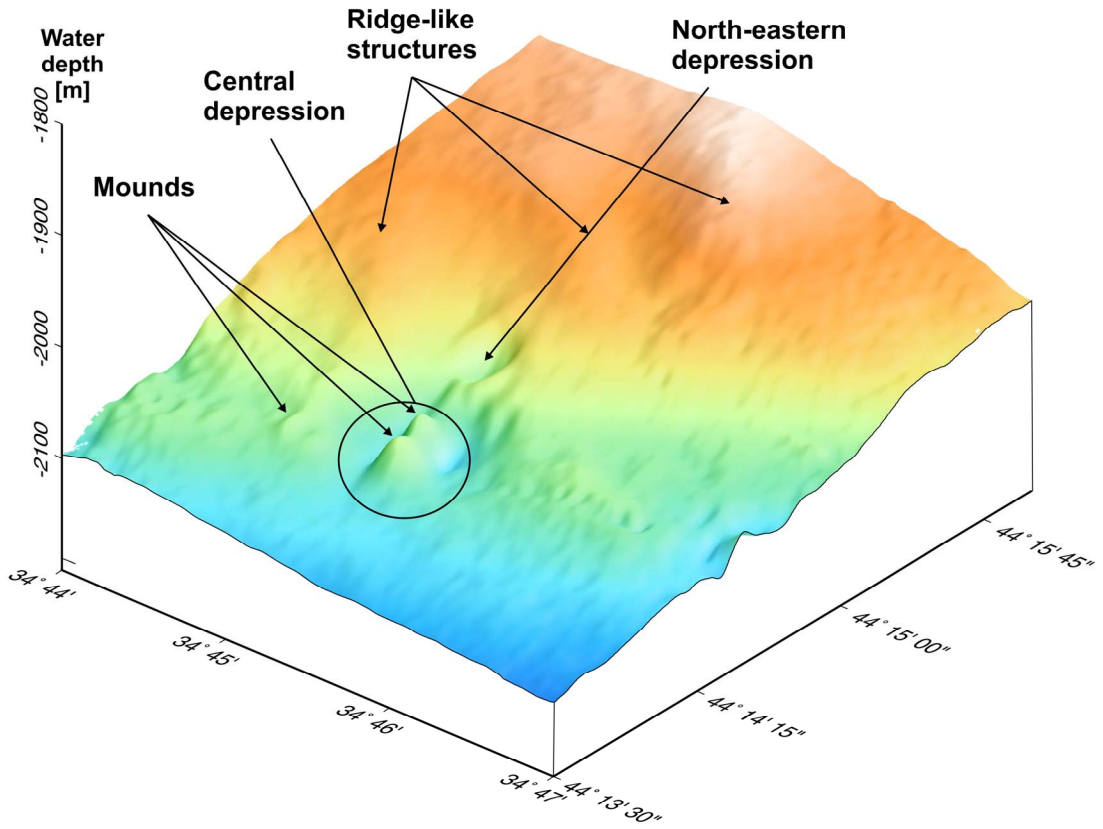

Figure 3.4: *Three dimensional bathymetric view of the slope within the 3D area. The depression structure and the mounds of the Sevastopol mud volcano are well pronounced within the smooth morphology of the slope.*

The elliptically shaped Sevastopol mud volcano comprises a ~1700 x 1100 m wide depression with a depth of about 25 m including two NNW-SSE trending cone-shaped mounds within its center. The southern cone has a height of 35 m and a diameter of about 500 m, while the northern cone rises 25 m and extends 500 m in the W-E direction and about 360 m in the N-S direction. The mounds show an asymmetrical shape with a maximal slope angle of 6.5° at their southern flanks, while the slope angle of the northern flanks is between 2.6°-4.5°. There is no significant relief within the depression except for the mounds. At the south-western rim of the depression a third mound rises about 10 m above the surrounding seafloor with a diameter of 300 x 200 m. A second circular depression with a radius of 330 m and a depth of 10-15 m is located at the north-eastern margin of the mud volcano.

3.5.2 Seismic structure of the 3D area

Based on four Inlines (Figs. 3.5-3.7) the main structural features, i.e. the diapiric structure, the Sevastopol mud volcano, and the sedimentary basins, and their variability within the study area are described below. On Fig. 3.8 a three dimensional block of the survey area is shown, and on Fig. 3.9 three time slices at depths of 2.95, 3.07 and 3.15 s TWT image the lateral changes of the subsurface structures.

Diapiric structure and Sevastopol mud volcano

The 3D area is characterized by a complex buried diapiric structure with two ENE-WSW striking diapiric ridges (Ridge 1 in the north and Ridge 2 in the south), separated by a small syncline (e.g. Fig. 3.5). The sediments in the western grid area are disrupted by a deep fault system with vertical offsets of several ms TWT (Fig. 3.5). The main fault trends E-W parallel to the diapiric ridges and can be traced for more than 1 km from the western edge of the grid area to the central part. The tops of the diapiric ridges are located at a depth of about 400 ms TWT below seafloor (bsf) (Figs. 3.5-3.7). With the exception of weak bulged reflections in the core of Ridge 2, the diapiric structure is generally characterized by acoustic transparency (Figs. 3.5-3.8).

High amplitude reflections (Bright Spots) were observed in two areas: In the range of Area 1 a package of Bright Spots occurs at about 300 ms TWT bsf just above and at the north-western edge of Ridge 1. The Bright Spots have a thickness decreasing from 150 ms TWT in the west to 40-50 ms TWT in the east (Figs. 3.5-3.7). The Bright Spots are characterized by chaotic reflection patches, so that it is unclear whether they are conformable or unconformable to the surrounding strata.

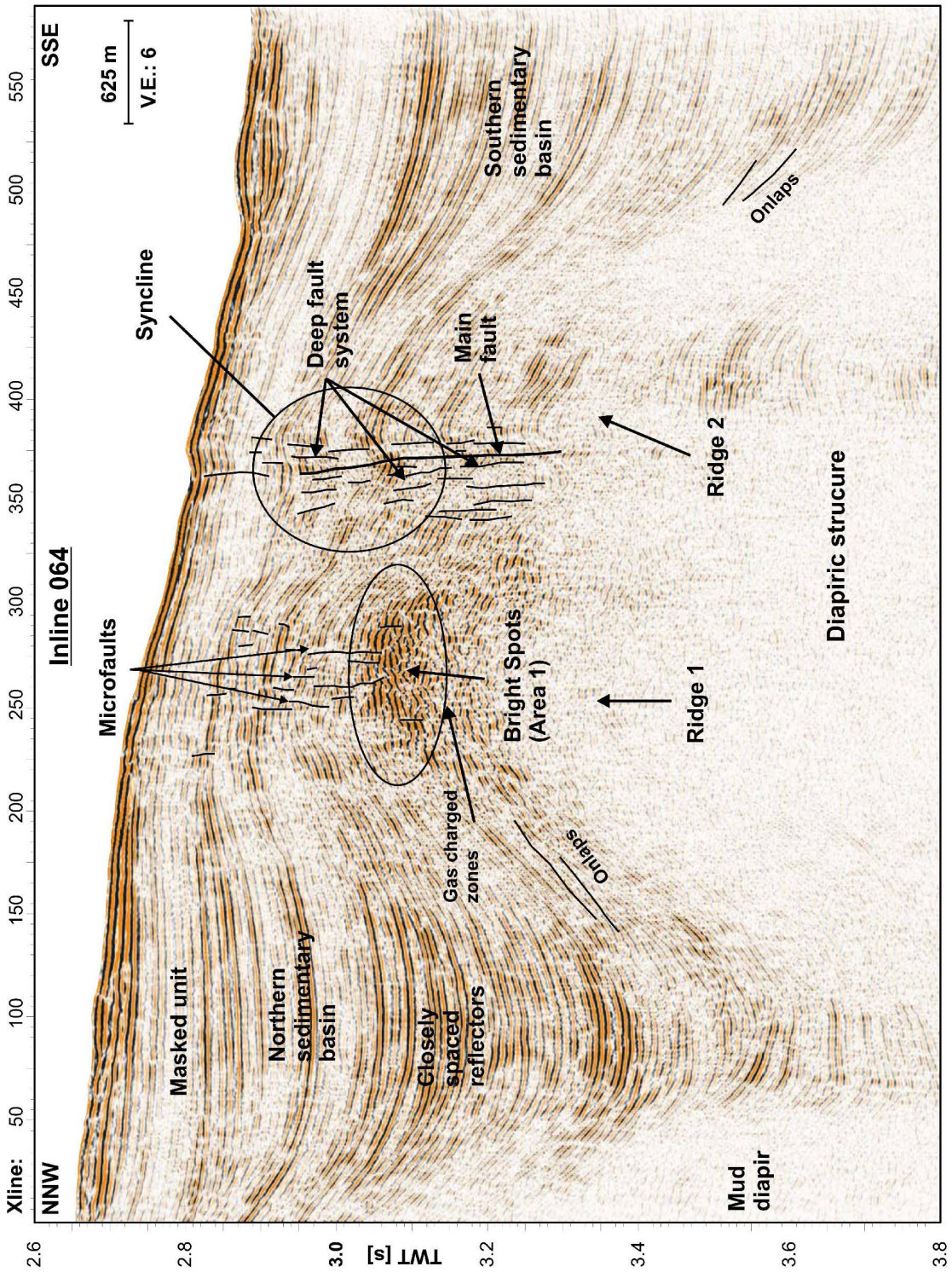

Figure 3.5: *Time migrated seismic inline 064 at the western periphery of the 3D grid (location is shown in Fig. 3.3). A deep fault system is developed between Ridge 1 and Ridge 2. Enhanced amplitude reflections (Bright Spots) are found above Ridge 1.*

On the top of Ridge 1, the Bright Spots are definitely conformable, but on the diapir flank the reflections seem to crosscut the stratigraphic units (Figs. 3.6, 3.7). In the outermost eastern portion of the grid area the Bright Spot reflections are less chaotic and conformable bedded into the strata at the onlap termination of the northern diapiric flank (Fig. 3.7). In the eastern grid area, Bright Spots additionally are imaged in the syncline between Ridge 1 and Ridge 2 (Area 2).

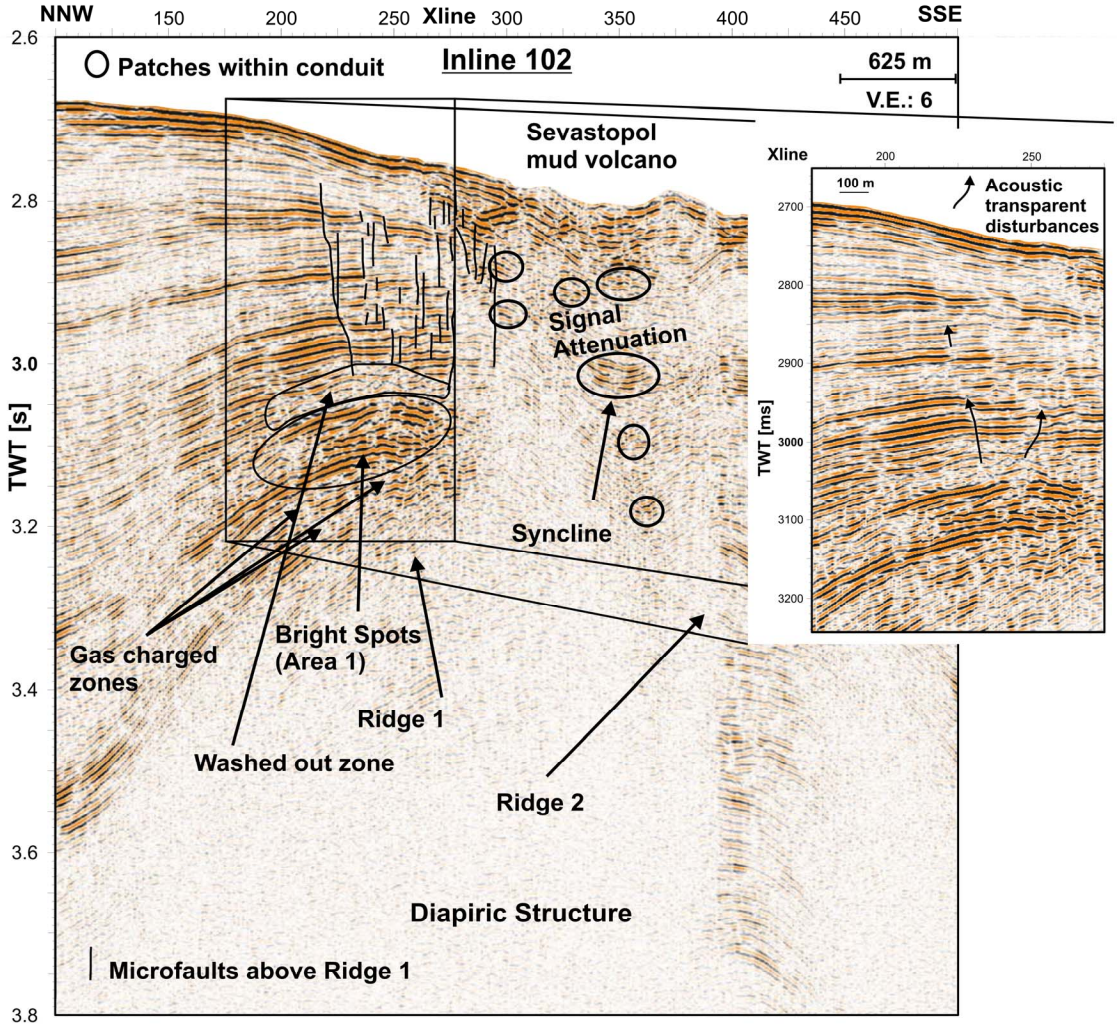

Figure 3.6: *Time migrated section of seismic inline 102 in the central grid area. The Sevastopol mud volcano is formed above the fault system, where it is characterized by a depression with two mounds inside the depression. Beneath the mud volcano, a zone of signal attenuation reaches down to the diapir. The Bright Spots are located on the northern edge of Ridge 1. The inset shows an interpreted portion of the seismic section. The location of the line is shown in Fig. 3.3.*

In the central 3D grid, the Sevastopol mud volcano is formed on the seafloor above the fault system developed between Ridge 1 and Ridge 2. The seafloor of the central depression structure of the mud volcano is represented by a package of diffuse and disrupted medium amplitude reflection patches (Fig. 3.6). The mounds located in the centre

of the depression are characterized by a weak seafloor reflection and short washed out inner reflections (Fig. 3.6). Beneath the mud volcano, a zone of signal attenuation with a width similar to the diameter of the mud volcano can be traced down to the diapir and reveals only few discontinuous reflection patches inside (Figs. 3.6, 3.8).

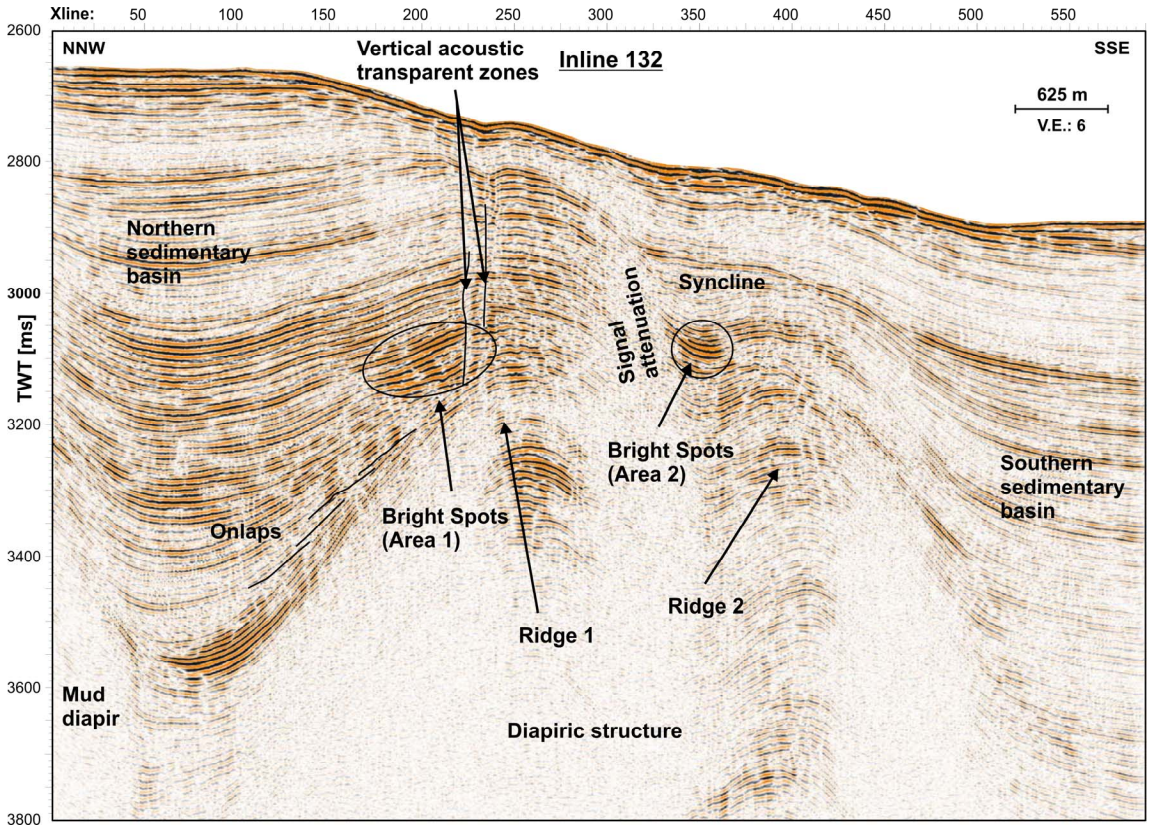

Figure 3.7: *Time migrated seismic inline 132 in the eastern part of the 3D grid. Bright Spots are observed at the northern flank of Ridge 1 and in the syncline between the ridges. The location of the line is shown in Fig. 3.3.*

Sedimentary basins

The two sedimentary basins separated by the diapiric structure are filled with well stratified parallel reflectors of laterally and vertically varying amplitudes (Figs. 3.5-3.8). The lower sedimentary layers are onlapping the flanks of the diapiric structure and the upper layers are bulged upward above the diapir. The sediments are generally characterized by units of weak amplitude reflections separated by closely spaced and continuous high amplitude reflectors. Signal penetration is down to 3.8 s TWT (Figs. 3.5, 3.7, 3.8). In the northern basin the units of weak amplitude reflections have a thickness of 80-100 ms TWT, decreasing above the diapiric structure and increasing with the water depth in the southern basin from 130 ms in the west to 200 ms TWT in the east (Figs. 3.5-3.8). Above Ridge 2 the reflection amplitudes are weakened (e.g. Figs. 3.5, 3.7), while there are enhanced amplitude reflections above Ridge 1, which are disrupted by numerous microfaults with a

vertical offset of 4-5 ms TWT (Figs. 3.5-3.8). Individual microfaults cannot be traced along Ridge 1, but represent local fractures laterally extending about 50-100 m and only a few faults can be traced for more than 200 m parallel to Ridge 1.

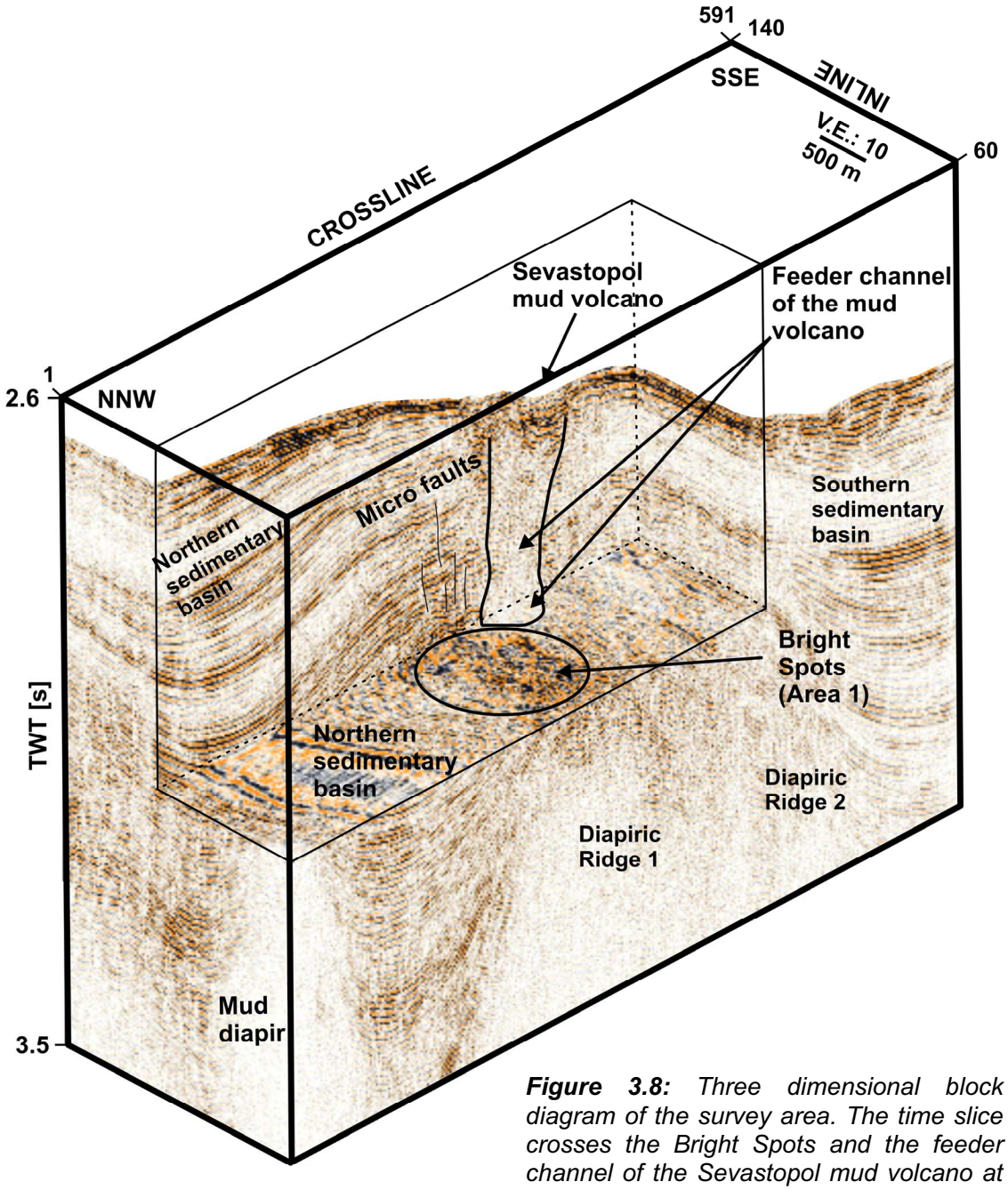

Figure 3.8: *Three dimensional block diagram of the survey area. The time slice crosses the Bright Spots and the feeder channel of the Sevastopol mud volcano at a depth of 3.09 s TWT. Two mud diapirs are imaged in the subsurface.*

The syncline between Ridge 1 and Ridge 2 extends about 250 m in the NNW-SSE direction with a steep northern and moderately dipping southern flank; the syncline can be traced down to the diapir (Figs. 3.5, 3.7). In the western and the central grid area the syncline is characterized by irregular weak reflection patches disturbed by the deep fault

system described above (Fig. 3.5). In the eastern grid area the syncline contains continuous horizontal reflectors onlapping the sediments bulged above Ridge 1 and continuing to the southern basin (Fig. 3.7).

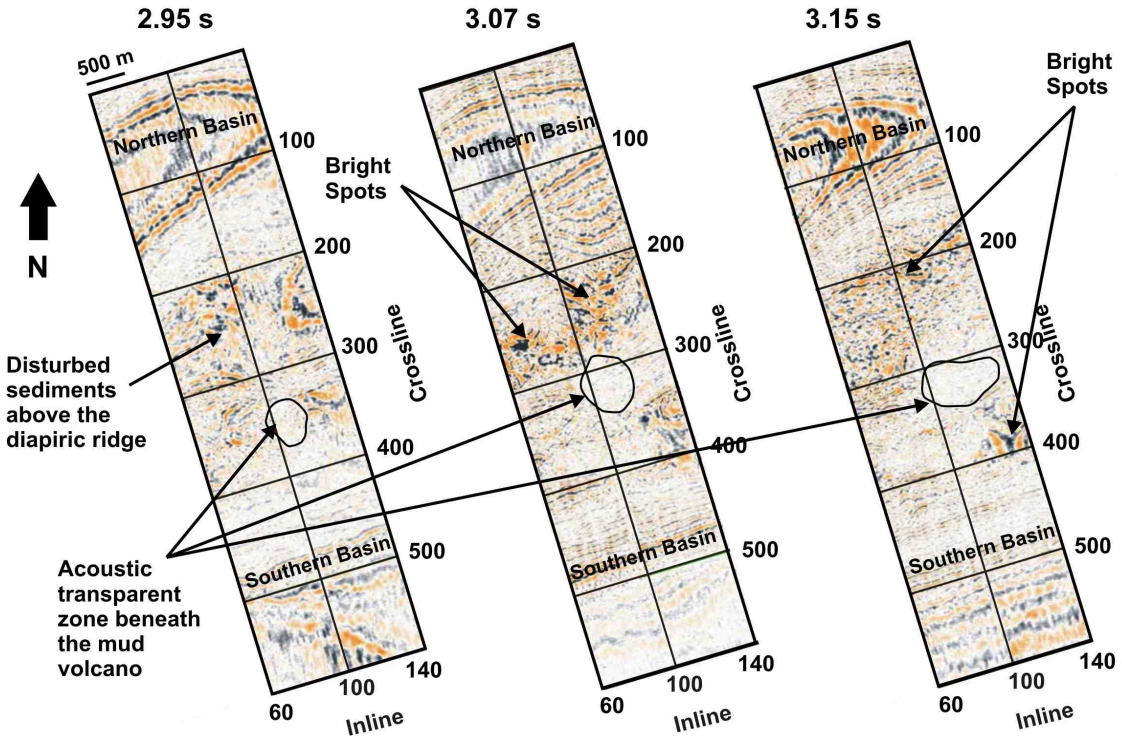

Figure 3.9: *Three time slices from the 3D seismic data cube calculated for the depths at 2.95 s, 3.07 s and 3.15 s TWT. Between the crosslines 200 and 300 chaotic reflections represent the sediments above Ridge 1 disturbed by the microfaults at depth shallower than 2.998 ms TWT, while at greater depths the Bright Spots are distinctly imaged. The zone of signal attenuation beneath the mud volcano has a circular shape with a diameter that increases with depth.*

3.5.3 Distribution of the subsurface structures

For a better understanding of the complex relationships between the structural features, the observed subsurface structures were mapped and are displayed together with the bathymetry collected during M52/1 cruise (Fig. 3.10). The depth bsf of the top of the Bright Spots varies from 0.266 to 0.486 s TWT in Area 1 and from 0.234 to 0.285 s TWT in Area 2 (Fig. 3.10). Most Bright Spots are located at a depth between 300 and 400 ms TWT bsf with an average depth of 337.5 ms TWT bsf. Within Area 1, the Bright Spots occur above the top of Ridge 1 in the western part of the study area, but occur mainly on its northern flank further to the east (Figs. 3.5-3.9). The Bright Spots of Area 1 occur at relatively constant depth along the trend of the diapir, but their depth increases from the top of Ridge 1 towards the northern basin. Two zones with anomalously shallow Bright Spots depth of less than 0.298 s TWT bsf are located above Ridge 1 at the south-western and

south-eastern edge of Area 1. The Bright Spots of Area 2 show fewer variations in depth, with greatest depth at the apex of the syncline. Above the Bright Spots within Area 1, acoustic anomalies were observed: Particularly in the east, several vertical acoustic transparent zones run vertically from the top of the Bright Spots up to 200 ms TWT along the microfaults, partly reaching through the Bright Spots down to the diapir (e.g. Fig. 3.7). These zones (blue zones in Fig. 3.10) are cylindrical-ellipsoidal shaped with lateral dimensions of 275 m x 250 m.

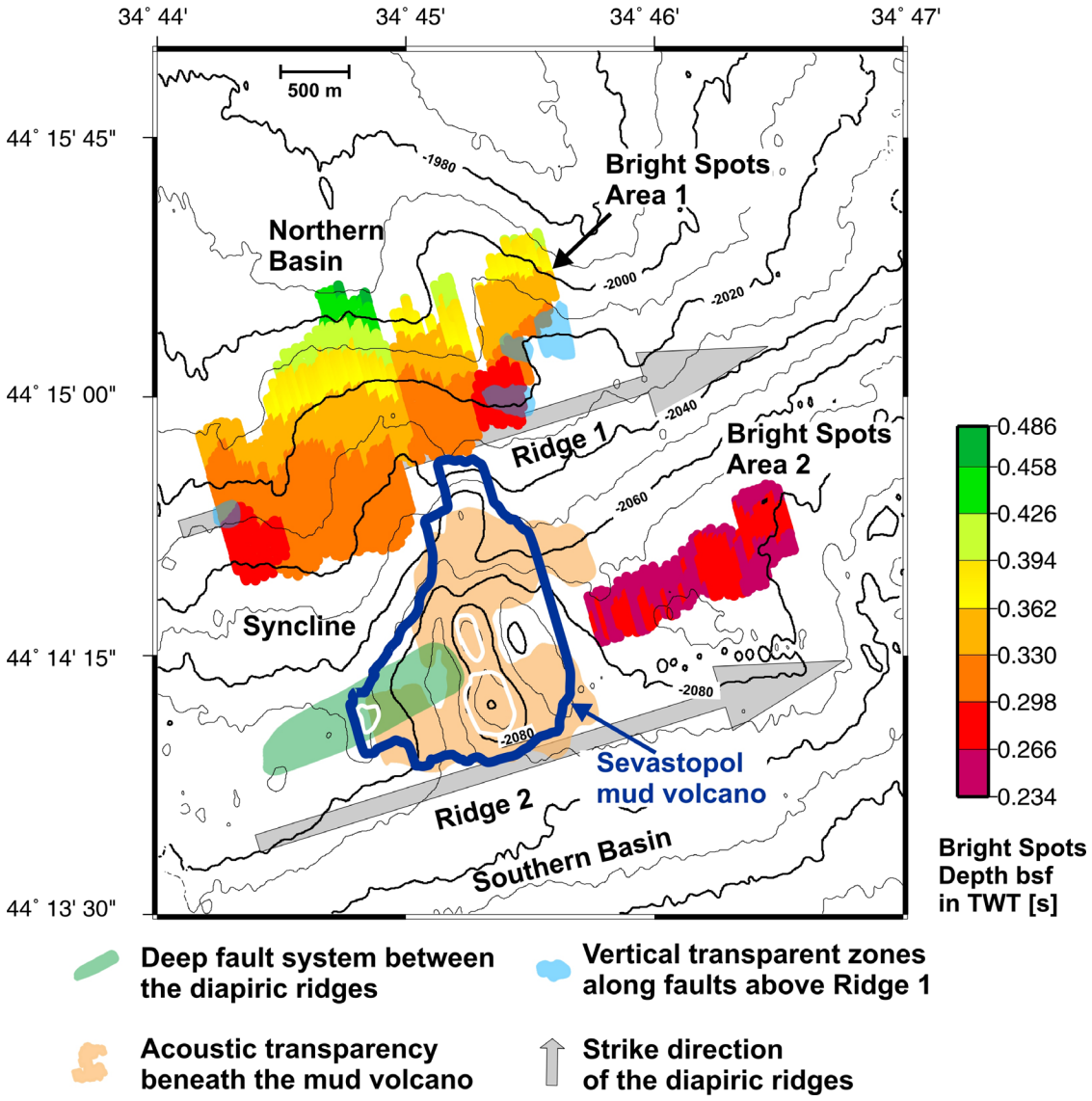

Figure 3.10: *Distribution of the main subsurface structures, i.e. the Bright Spots, the fault system and upward fluid migration pathways (transparent zones), mapped from the 3D seismic survey. The white lines in the range of the mud volcano mark the mounds of the mud volcano. The color contours represent the uppermost Bright Spot reflectors in TWT [s] bsf.*

The mud volcano is located between Ridge 1 and Ridge 2. The zone of signal attenuation observed beneath the mud volcano has similar lateral dimensions as the mud volcano (Figs. 3.6, 3.10). The fault system developed between the diapiric ridges forms a 180-200 m wide zone striking in the ENE-WSW direction and can be traced from the western edge of the 3D grid to the central part of the mud volcano, where the fault is lost due to the acoustic transparency beneath the Sevastopol mud volcano.

3.6 Interpretation and discussion

3.6.1 Evolution model of the Sevastopol mud volcano

Most mud volcanoes in the Sorokin Trough, including the Sevastopol mud volcano, are associated with near-surface mud diapirs (Woodside et al., 1997; Krastel et al., 2003), which are related to the clays of the Miocene Maikopian Formation. The convergence between the Crimean Peninsula in the north and the buried Tetyaev and Shatsky Ridges in the south in combination with a thick overburden on top of the Maikop clays led to the protrusion of diapirs and diapiric ridges (Limonov et al., 1997). Although our high resolution seismic data do not resolve the basis of the diapiric structures, we are convinced, that the diapirs observed in the 3D dataset are related to the Maikop Formation, because clasts recovered from mud breccia samples at the nearby Dvurechenskii mud volcano have been correlated to the Maikopian Formation (Bohrmann et al., 2003). The deep fault system developed between the diapiric ridges (Ridge 1 and Ridge 2) forming the complex near-surface diapiric structure located beneath the mud volcano acts as potential pathways for upward gas/fluid migration and controls the evolution of the Sevastopol mud volcano. The development of the fault system is controlled by the diapirism (see below). The zone of signal attenuation in the surrounding of the fault system indicates the presence of gas and fluid saturated material. Hence this zone is interpreted as the feeder channel connecting the mud volcano with the diapir (Fig. 3.6). Strong signal attenuation, however, might be caused by other factors as well, such as roughness or steepness of the seafloor or lithological issues. The high relief at the mud volcano and carbonate precipitations, often associated with mud volcanoes due to anaerobic oxidation of methane, could lead to the signal loss beneath the mud volcano. Seismic overview profiles collected across numerous mud volcanoes in the Sorokin Trough and the Central Black Sea all show a zone of strong signal attenuation beneath the mud volcanoes (Bohrmann and Schenk, 2002; Krastel et al., 2003). The zones of strong signal attenuation often are limited to a narrow zone beneath the top of the mud volcano and do not cover the entire width of the mud volcano. This observation strongly supports our interpretation that the zones of signal attenuation are related to gas and not to imaging or lithological effects. Reflection patches observed within the conduit

(e.g. Fig. 3.6) also contradicts strong signal loss due to the roughness or steepness of the flanks of the mud volcanoes. Thus, we propose that the Sevastopol mud volcano is fed from the diapir by fluidized mud rising with gas and fluids along the fault system to the seafloor.

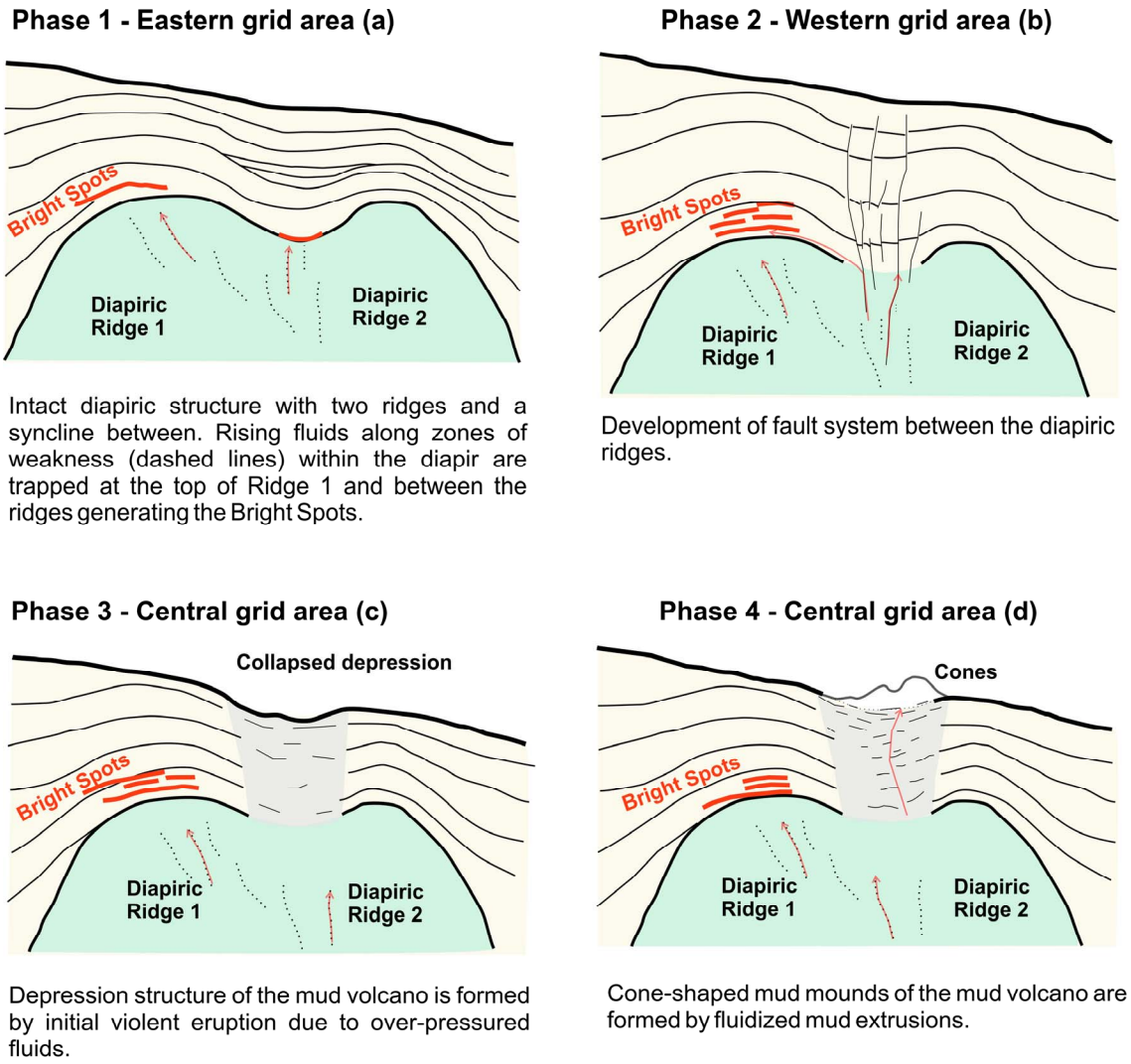

Figure 3.11: *Schematic illustration of the different phases of the evolution of the Sevastopol mud volcano and the subsurface structures as found in different areas of the 3D-grid. (a) The intact diapiric structure is observed in the eastern grid area. (b) The deep fault system developed in the western grid area acts as potential pathway for gas/fluids. (c) The depression structure of the mud volcano most likely was formed by an explosive eruption due to over-pressured fluids. (d) Fluids and fluidized mud arising along the fault system form the mud cones within the collapsed depression of the mud volcano. For detailed explanations see text. The red arrows indicate fluid migration.*

Based on the 3D images of the mud volcano we suggest a 4 phase evolution model for the Sevastopol mud volcano (Fig. 3.11). Phase 1 represents the intact diapiric structure: The two diapiric ridges are separated by a syncline filled with +/- horizontal reflections (Figs. 3.7, 3.11a). Bright Spots at the northern flank of Ridge 1 and between the diapiric ridges

indicate that upward gas and fluid migration occurs throughout the diapir into the strata generating the Bright Spots, where free gas accumulates. The development of the deep fault system between Ridge 1 and Ridge 2 during phase 2 is the first important stage in the evolution of the mud volcano and represents the incipient formation of the later feeder channel (Fig. 3.11b). The evolution of the faults is most likely associated with the diapirism and the compressional deformation. We suggest that the formation began along the steep southern flank of Ridge 1. Different protrusion rates of the diapiric ridges, presumably a rapid protrusion of Ridge 1, might have steepened its flank and lead to a vertical displacement of the ridges leading to the evolution of fractures. It remains unclear, why the fault system is only developed in the western and not yet in the eastern grid area. Phase 3 and 4 comprise two formation mechanisms of the mud volcano with different driving forces (Figs. 3.11c, 3.11d). The morphological shape of mud volcanoes reflects the eruption mechanism and the properties of the extrusion products (e.g. Brown, 1990; Ivanov et al., 1996; Kopf, 2002). Mud flows of low viscosity form large and flat bodies, and low porosity mud flow form steep mud domes or ridges. High pore-fluid pressure, e.g. caused by low permeability, might lead to violent eruptions (Kopf, 2002; Yusifov, 2004). The compressional tectonic deformation, the thick overburden and the low permeability of the mud diapir facilitate the generation of over-pressured fluids in the Sorokin Trough, thus we suggest that the Sevastopol mud volcano was initially formed by an explosive eruption due to seal failure leading to a collapsed depression structure (Phase 3, Fig. 3.11c). Disturbed sedimentary layers are represented by weak chaotic reflections within the conduit. Subsequent, quiet and effusive mud extrusions during phase 4 are believed to have formed the cones inside of the depression (Figs. 3.6, 3.11d).

3.6.2 Relationship between the Bright Spots and the base of the gas hydrate stability zone

The Black Sea is known for containing enormous concentrations of gas in the marine sediments (e.g. Hunt & Whelan, 1978; Ivanov et al., 1998). In the western Sorokin Trough numerous Bright Spots, observed either in the cores of anticlinal structures or at the updip terminations of strata with the diapirs at a relatively constant depth of ~ 300 ms TWT bsf (Krastel et al., 2003), indicate the presence of free gas. Similarly, in our 3D seismic survey area the high amplitude reflection packages identified just above or at the updip termination of the strata with the north-western flank of Ridge 1 and in the eastern grid area additionally in the syncline between Ridge 1 and Ridge 2 (Figs. 3.10, 3.12) are considered to represent Bright Spots related to free gas occurrences.

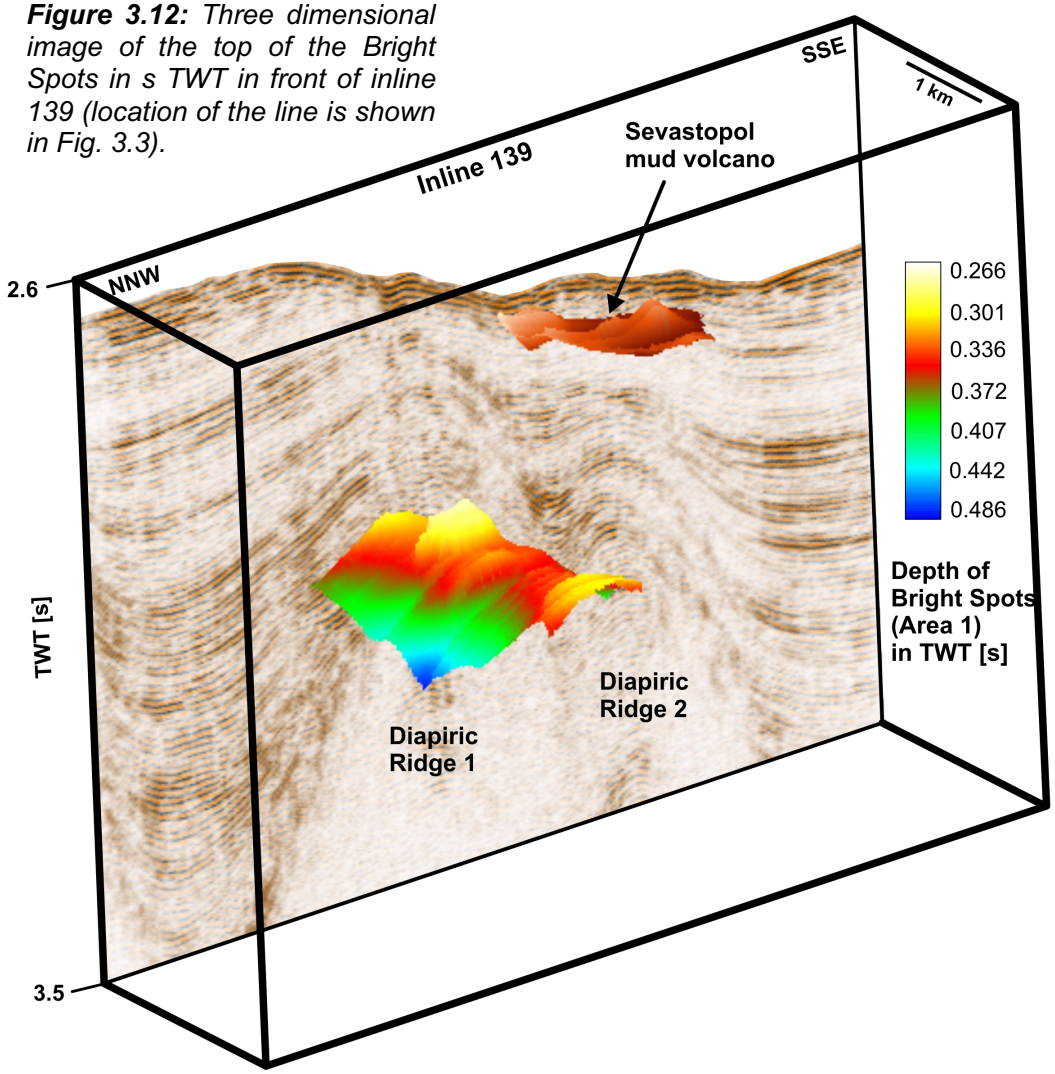

Figure 3.12: *Three dimensional image of the top of the Bright Spots in s TWT in front of inline 139 (location of the line is shown in Fig. 3.3).*

We identified further abundant lateral and vertical amplitudes variations in the dataset, but, the high amplitude reflections described as Bright Spots above differ significantly: The so-called Bright Spots form a thick package of diffuse high amplitude reflection patches and occur consistent above the diapir, while the other amplitude variations predominantly occur along one reflector. Apart from gas, there are numerous further factors affecting seismic amplitudes, such as changes of sediment properties, effects of topography, scattering and artifacts due to processing. The latter can be excluded, because true amplitudes are imaged. Analyzing the frequency content of seismic data can help to identify free gas in the sediments, because free gas absorbs the high frequency component of the seismic energy (Taylor et al., 2000). The decrease of the main frequencies from about 115 Hz above the Bright Spots to ~ 95 Hz beneath (Fig. 3.13) therefore supports the presence of free gas. Thus we attribute the Bright Spots to free gas occurrences.

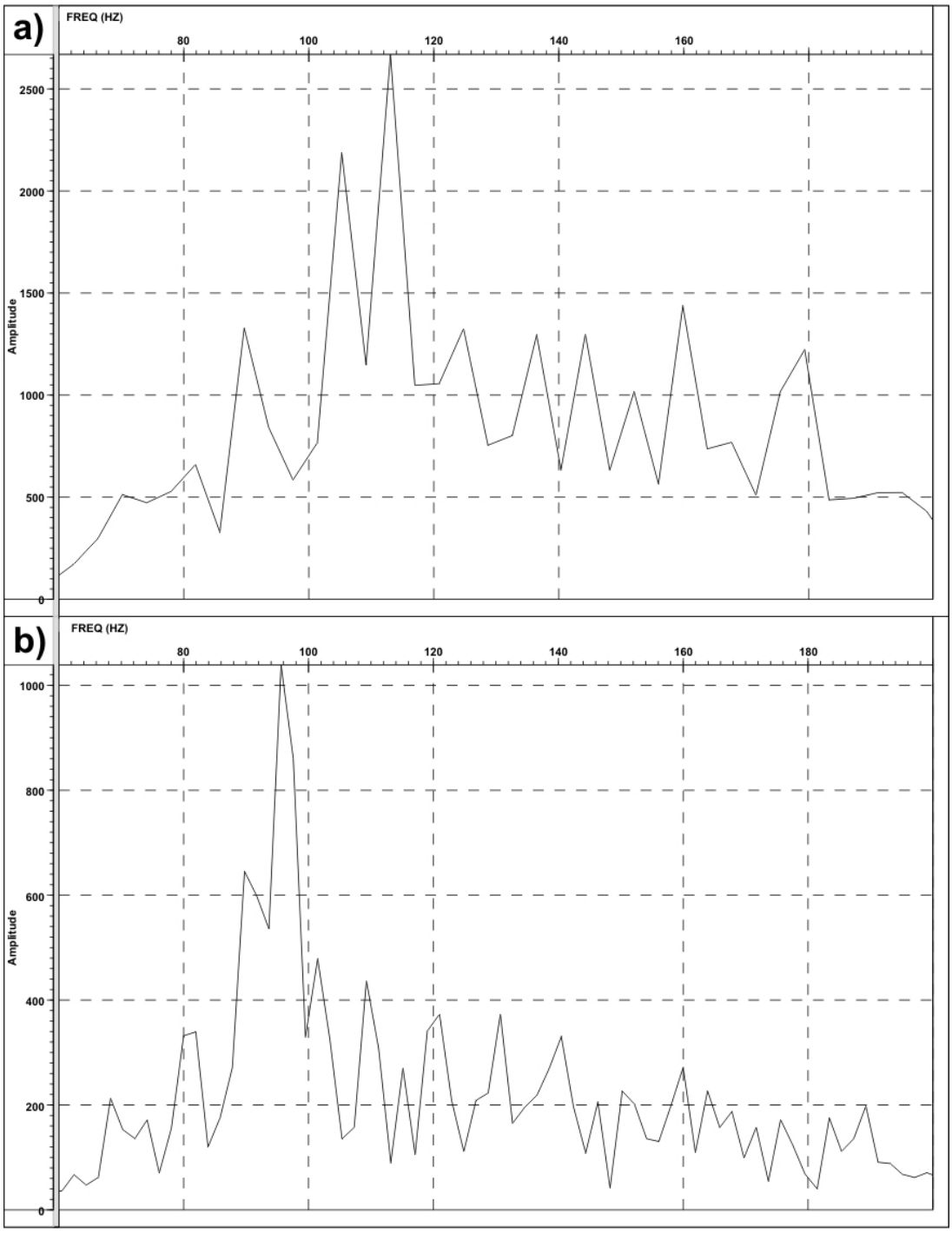

Figure 3.13: *Frequency Trace Graph for inline 102, a) above the Bright Spots, b) beneath the Bright Spots.*

A polarity change of the seismic signal would be an additional tool to identify free gas, because the velocity decrease caused by free gas leads to a negative reflection coefficient. Unfortunately, the chaotic and patchy reflection pattern prevents to determine the phase of the Bright Spot. We also need to keep in mind that no definite conclusions can

be drawn based on the reflection seismic methods alone, because interpretation is based on relative amplitude changes. Assuming that the Bright Spots are caused by free gas, it is worth to discuss the possible reasons for trapping of free gas. The flanks and the top of diapirs are typical locations for the trapping of gas and hence the observed Bright Spots could be interpreted as lithological or tectonic traps for free gas accumulation. The enhanced reflection patches beneath the Bright Spots, as in particular observed in the western grid area, might present gas charged zones (e.g. Figs. 3.5, 3.6), which is a well known phenomenon of Bright Spots (Holbrook, 2001). During Meteor cruise M52/1 gas hydrates were sampled at adjacent mud volcanoes, e.g. at the Dvurechenskii, Yalta and Odessa mud volcanoes (Fig. 3.2), though no gas hydrates were sampled at the Sevastopol mud volcano (Bohrmann et al., 2003). If gas hydrates are present, the base of the gas hydrate stability zone is often imaged as a bottom-simulating reflector (BSR), a high amplitude reflector with a negative reflection coefficient, marking the transition between the high velocity gas hydrates bearing sediments and the underlying low velocity sediments, mostly containing free gas (Shipley et al., 1979; Kvenvolden and Barnard, 1983; Minshull and White, 1989; Miller et al., 1991; Hyndman and Spence, 1992). Some studies suggest that the BSR is generated due to the contrast between the high velocity zone of gas hydrate cemented sediments above and water saturated sediments beneath (e.g. Hyndman and Davis, 1992). Most velocity-models, however, strongly suggest the presence of free gas beneath a BSR. Hence the widely accepted consensus is that a BSR reflection is caused by free gas trapped beneath the hydrate stability zone (Holbrook et al., 1996).

Despite the known presence of gas hydrates in the Sorokin Trough, a BSR is absent in all seismic sections. Our data show, that the depth range of the Bright Spots, varying from 235 to 485 ms TWT bsf (Figs. 3.10, 3.12), coincides with the approximate depth of the base of gas hydrate stability zone (BGHSZ), and hence the Bright Spots might be related to the stability field of gas hydrate. Assuming a sediment velocity of 1600 m/s, the Bright Spots are located at depths of 188-388 meter below seafloor (mbsf). We compared this measured depth with the theoretically calculated depth for the BGHSZ. The Bright Spots occur at a water depth of about 2020 m in Area 1 and about 2100 m in Area 2 (Fig. 3.10). Measured seafloor temperature is 9°C. Further we assume a constant temperature gradient of 29°C km^{-1}, a pure methane system and Black Sea water chlorinity. Based on these assumptions the calculated depth of the BGHSZ is located at about 380 mbsf in Area 1 and 400 mbsf in Area 2 (Fig. 3.14). Hence, most of the observed Bright Spots are located at shallower depths with a deviation of 10-210 m to the theoretical depth (Figs. 3.10, 3.12, 3.14). Only the deepest Bright Spots, observed at the northern flank of Ridge 1, coincide with the calculated depth. Changes of the factors controlling gas hydrate stability, i.e. temperature, pressure or salinity (e.g. Kvenvolden, 1993) can cause vertical movements of the BGHSZ.

Stability of hydrates is primarily controlled by changes in temperature. Heat flow measurements in the Sorokin Trough are very sparse, and the assumed temperature gradient of 29°C km^{-1} was measured in an area without mud volcanoes. Mud volcano areas are often characterized by increased heat flow values. As shown by Bohrmann et al. (2003), locally increased fluid flow in the Sorokin Trough does exist for the Dvurechenskii mud volcano (DMV) located at 2000 m water depth. Sediment temperatures of 16.5 °C at the DMV in close contact to the bottom water temperature of 9°C suggest high fluid flux within the mud volcano (Bohrmann et al., 2003). The high temperature measured at the DMV coincides with the maximum temperature for the methane hydrate stability at this depth (Bohrmann et al., 2003). No heat flow measurements exist for the Sevastopol mud volcano, but we expect higher heat flow values as well. Increased heat flow due to the rise of warm fluids, as expected in the surrounding of the Sevastopol mud volcano, leads to an uplift of the isotherms (e.g. von Huene and Pecher et al., 1999), and could have uplifted the BGHSZ to the depth of the Bright Spots. Assuming, that the Bright Spots represent the BGHSZ, an increased temperature gradient of 37°/km would explain the shallowing of the BGHSZ to 270 mbsf, representing the observed average depth of the Bright Spots (Fig. 3.14). The depth variations of the Bright Spots observed particularly in the NNW-SSE direction then also could be explained by variable fluid flow along the diapiric ridge. Considering the stability field of gas hydrates on Fig. 3.14, changes of the temperature gradient from 29°C to 52°C/km would effect the observed variations in depth bsf of the Bright Spots. If the Bright Spots represent the gas hydrate phase boundary, their depth bsf, which is constant along the trend of Ridge 1, but shallows from the flank towards the top (Figs. 3.10, 3.12), suggests high fluid flow along the top of Ridge 1 decreasing towards the northern basin. The points of shallowest Bright Spots, observed at the western and the eastern edges of Area 1 (Fig. 3.10), therefore might be related to locally focused fluid flow. Constant depth of the Bright Spots, as observed in the ENE-WSW direction, then means a constant depth of the gas hydrate phase boundary in the strike direction of the diapiric ridge.

Another aspect influencing the stability of gas hydrates is the salinity of pore waters, which often includes high salinity fluids in the range of mud volcanoes. Increased salinity would shift the gas hydrate stability field to lower temperatures (Kvenvolden, 1993; Taylor et al., 2000), and hence also would lead to a shallowing of the BGHSZ. Measured Cl^--concentrations of 810-900 mM at the Dvurechenskii mud volcano indicate the expulsion of high salinity fluids, which are considered to be formed during burial by diagenetic processes (Bohrmann et al., 2003; Aloisi et al., 2004). Salinity as high as measured at the DMV would uplift the theoretical BGHSZ into a depth of 300 m, which almost coincides with the average depth of the Bright Spots (270 m) (Fig. 3.14).

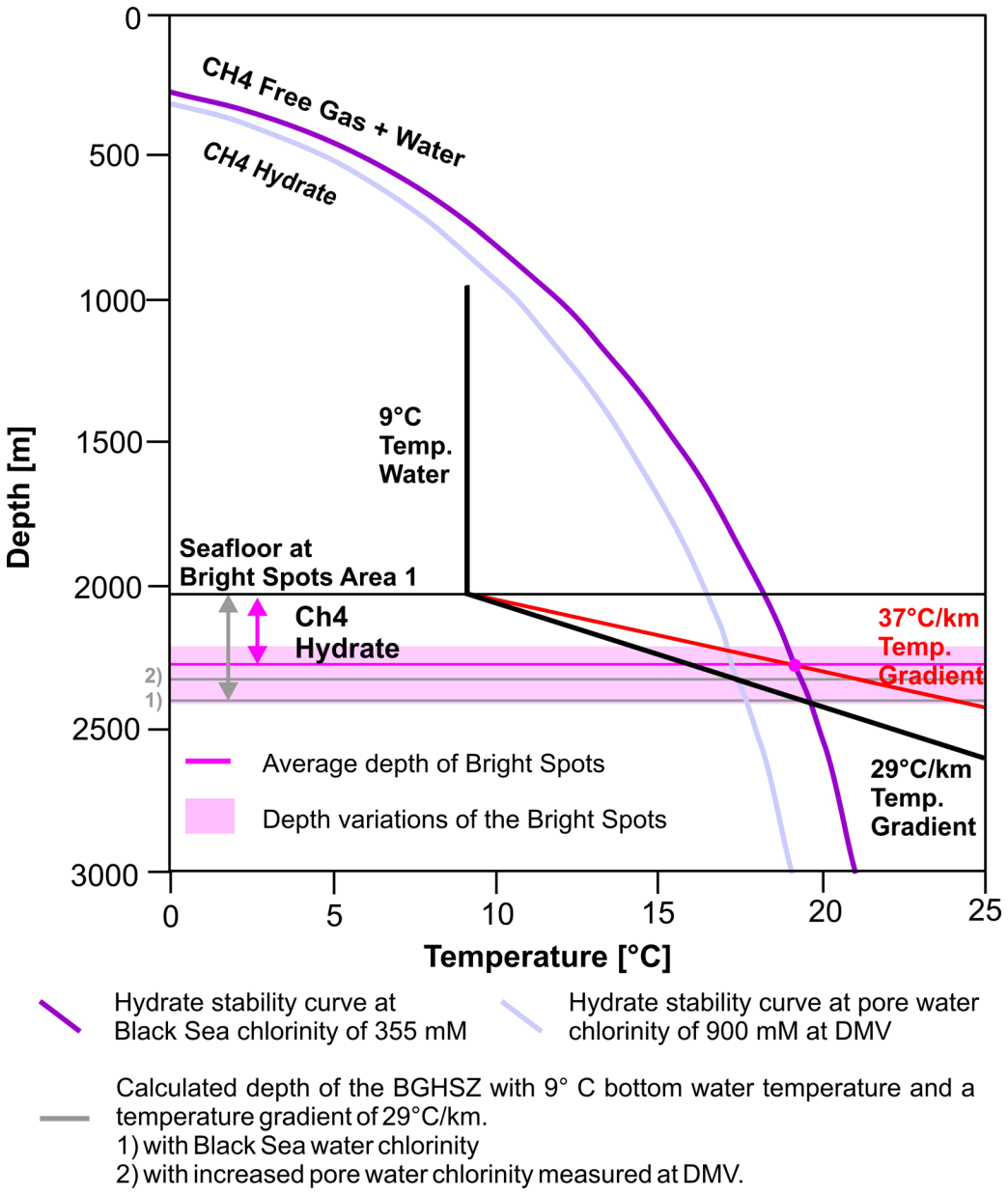

Figure 3.14: *Gas hydrate stability field for a pure methane system calculated with 1) Black Sea water chlorinity and 2) pore water chlorinity of 900 mM (measured in sediments at the Dvurechenskii mud volcano) (modified after Bohrmann et al., 2003). The depth of the theoretical BGHSZ is calculated with a bottom water temperature of 9°C and a constant temperature gradient of 29°C/km. Assuming, that the Bright Spots are related to the stability field of gas hydrates the change in temperature gradient was inferred from the depth of the Bright Spots.*

Although the Bright Spots correspond with the calculated depth of the BGHSZ and shallowing and depth variations could be explained by variable fluid flow or increased salinity fluids, it is not definite that the Bright Spots represent the BGHSZ. Due to the

stability field of gas hydrates BSRs follow isotherms and mimic the seafloor, typically crosscutting the strata (e.g. Shipley et al., 1979; Dillon & Paull, 1983; Max, 2000) The relationship of the Bright Spot reflections and the sedimentary strata, however, could not be determined in our data due to the chaotic and patchy reflection characteristics of the Bright Spots. Discordant layered reflection patches identified at the edges of Ridge 1 support that the Bright Spots might represent a BSR (Figs. 3.5-3.8). The Bright Spots are, however, not bound to a stratigraphic layer, as it would be expected for a lithological gas trap. On Inline 132 (Fig. 3.7) the reflections occur at different stratigraphic layers than on Inline 102 (Fig. 3.6). The Bright Spot reflections on Inline 064 (Fig. 3.5) can not be attributed to any reflector. Furthermore the occurrence of Bright Spots in the syncline between the diapiric ridges (Bright Spot Area 2) does not represent a typical stratigraphic trap. Thus, we speculate that the Bright Spots represent the base of the phase boundary of gas hydrates. In this scenario gas hydrates above the Bright Spots act as seal to trap the gas beneath due to the low permeability of hydrate layers (White, 1979; Bangs et al., 1993; Pecher et al., 1996; Holbrook, 2001).

The Bright Spots represent the shallowest depth of free gas in our data, and the sediments above are definitely located within the gas hydrate stability zone (GHSZ). Indications for the presence of gas hydrates above the Bright Spots of Area 1 might be given by zones of washed out reflections observed in the western grid area (Fig. 3.6), as sediments containing gas hydrates can reduce the impedance contrast across sedimentary interfaces (Lee & Dillon, 2001; Holbrook et al., 2002). This in particularly applies to low concentrations of gas hydrates. In contrast, layers with high gas hydrate saturations lead to a significant increase of the sediment velocity generating enhanced reflectance (e.g. Holbrook et al., 2002), thus concentrated gas hydrate layers could also explain the Bright Spot reflections. The sediment velocity of gas hydrate bearing sediments increases gradually with hydrate concentration, but even a low content of free gas in the pore space lead to a significant decrease of the velocity (Domenico, 1977). Therefore we assume that the Bright Spots are related rather to free gas than to gas hydrate. Alternatively to the occurrence of gas hydrates, disturbances in the sediments might also reduce sediment reflectivity.

As discussed above, we see local bright reflections at the depth of the BGHSZ, but why we do not see a BSR in the study area? An explanation for the absence of a BSR is that the concentration of free gas and gas hydrate is very low, as suggested e.g. for the Gulf of Mexico and portions of the Blake Ridge (Paull et al., 1996). Thus, the Bright Spots might represent fragments of a BSR, formed where fluid migration provides gas in sufficient amounts due to adequate fluid migration pathways, which are associated with the diapir and the mud volcano. This suggests that gas and gas hydrate occurrences in the Sorokin

Trough are not widespread, but controlled by local gas/fluid migration. Another explanation might be that fluid flow is episodic, so that the BSR does not have time to establish at a particular depth. Then, the depth of the BSR changes with time, thus the transition from gas hydrate to gas may occur over a large depth range and hence does not look like a sharp interface. Episodic fluid flow then would also control the activity of the mud volcano.

3.6.3 Fluid and gas migration

The distribution of the Bright Spots indicates local gas occurrences and gas hydrate occurrences above Ridge 1 and between the diapiric ridges, if the Bright Spots represent the BGHSZ as suggested above. A model of potential fluid migration pathways and the interactions of the mud volcano-diapir system and gas/gas hydrate occurrences are shown in Fig. 3.15. The source of the fluids is thought to be located within the Maikop clay diapirs released due to the transformation of smectite into illite under high temperature and pressure conditions. Kholodov (1983) determined the depth boundary between smectite and illite in the Eastern Kuban Trough at about 3.7 km. The low permeability of the Maikop clay and the sedimentary cover force over-pressured fluids, which are most likely released at zones of weakness, developed in the compressional tectonic regime, and migrate throughout the diapirs into the strata. Migration pathways within the diapir could not be identified due to the acoustic transparency of the homogeneous Maikop clays. The deep fault system between the diapiric ridges is considered to be the continuation of fractures within the diapir controlling the fluid migration towards the Sevastopol mud volcano. The well stratified hemipelagic sediments of the basins prohibit significant vertical upward fluid migration, but from the feeder channel gas/fluids might migrate laterally into the surrounding strata. The upward bulged sediments above Ridge 1 facilitate lateral gas/fluid migration along highly permeable stratigraphic layers towards the top of Ridge 1, where the gas accumulates generating the Bright Spots of Area 1 (Fig. 3.15). In the eastern grid area the fault system lacks and fluids rising through the diapir are trapped due to decreased vertical permeability and generate the Bright Spots of Area 2.

Besides the generation of bright reflections due to increased seismic impedance contrast, the occurrence of free gas in seismic sections is often characterized by acoustic transparency due to the attenuation of acoustic energy, which is especially pronounced in high resolution seismic data (Max, 1990; Taylor, 2000). Vertical acoustic void zones with a width of up to 225x200 m indicate upward gas/fluid migration along the microfaults above Ridge 1 into the GHSZ (Figs. 3.7, 3.10). The vertical transparent zones are located within the GHSZ and as mentioned above signal attenuation can also be due to the presence of gas hydrates, but the attenuation from gas hydrate bearing sediments is significantly lower than from free gas bearing sediments (Taylor et al., 2000). The interpretation of seismic

amplitudes, however, has to be handled carefully. Particularly in the eastern grid area such zones are observed (Fig. 3.10), although fewer microfaults occur, indicating that fluid flow is focused here, whereas in the western and central grid area fluid flow is evenly spread along numerous faults, but less focused. Acoustically transparent disturbances observed along numerous microfaults (e.g. Fig. 3.6) are interpreted as pathways for gas/fluid migration as well. The microfaults most likely have been developed during the diapiric growth and may allow sufficient amount of gas to migrate into the gas hydrate stability zone resulting in the formation of gas hydrate, if water is present. Based on the distribution of the fluid migration pathways and Bright Spots, gas hydrate formation is expected above and at the north-western flank of Ridge 1, as well as in the area surrounding the mud volcano and the feeder channel (Fig. 3.15).

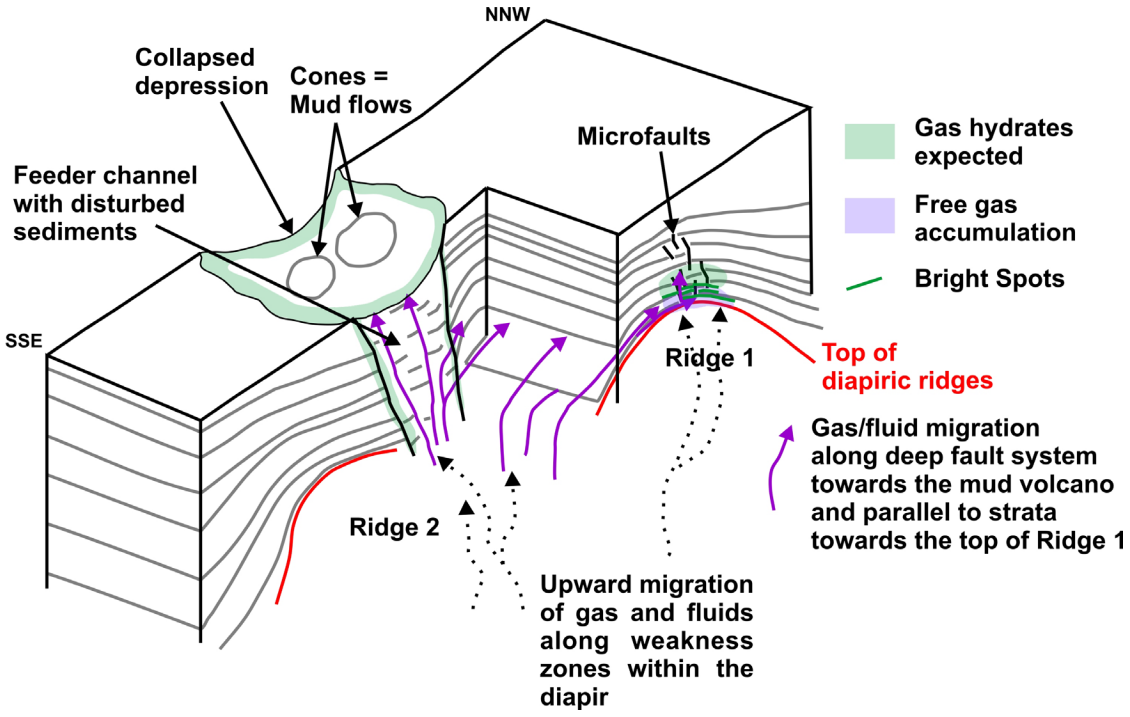

Figure 3.15: *Schematic model of the subsurface structures in the diapir-mud volcano system and suggested gas/fluid migration pathways. Gas hydrates are expected where focused fluid flow occurs, i.e. towards the top of Ridge 1 and in the surrounding of the mud volcano and its feeder channel.*

3.7 Conclusions

Few 3D seismic investigations of mud volcanoes have been documented yet, such as offshore Nigeria (Graue, 2000), in the Caspian Sea (Davies and Stewart, 2005), and in the Gulf of Cádiz (Masson and Berndt, 2006). We present a first 3D seismic dataset of a mud volcano (Sevastopol mud volcano) in the Sorokin Trough, Black Sea. Numerous mud volcanoes were identified in the Sorokin Trough, and the Sevastopol mud volcano is a representative for collapsed structures. Collapsed structures are known from other areas as well, such as the Central Black Sea and the Mediterranean Ridge (e.g. Ivanov et al., 1996), but have not been studied in 3D until now. The new 3D images give detailed information about the spatial geometry of the Sevastopol mud volcano and its subsurface structures. Based on the morphological features, an evolution model has been suggested for the Sevastopol mud volcano. In the Sorokin Trough compressive deformation affects the growth of diapiric ridges and facilitates fluid flow to the seafloor, expressed by the evolution of mud volcanoes above the diapirs. The 3D seismic data show that the depression structure of the Sevastopol mud volcano includes three cones. The Sevastopol mud volcano is formed above a complex diapiric structure with two diapiric ridges (Ridge 1 and Ridge 2) and is associated with a deep fault system developed between the ridges. The evolution of the fault system in the study area is most likely associated with the diapiric uplift, and the faults are thought to be the continuation of fractures and cracks within the mud diapir developed due to the compressional tectonic regime. The fault system and probably cracks/fractures within the diapir act as potential pathways for gas/fluid migration, feeding the mud volcano from the diapir. Presumably an initial explosive eruption due to over-pressured fluids formed the depression structure of the Sevastopol mud volcano and subsequently mud flows extruded at different locations where the faults disrupt the seafloor, forming the observed cones. Bright Spots indicate the accumulation of free gas at the top and the flanks of Ridge 1 and additionally between the diapiric ridges in the eastern grid area. The depth of the Bright Spots, which is constant along the trend of the diapiric ridge and only slightly increases at its flanks, is almost consistent with the approximate depth of the base of gas hydrate stability zone. The shallower location of the Bright Spots compared to the calculated theoretical depth of the BGHSZ could be explained by an increased temperature gradient of 37°C/km due to the rise of warm fluids next to the Sevastopol mud volcano. Gas hydrates are likely present above this depth and may act as a seal to trap the gas. The depth of the BGHSZ in the Sorokin Trough is strongly controlled by fluid flow and the variations in depth of the Bright Spots can be explained by variable fluid flow. Furthermore, threefold enhanced salinity pore fluids might shallow the BGHSZ into the depth of the Bright Spots, but chlorinity has not been measured at the Sevastopol mud volcano.

We observe gas migration into and within the GHSZ along microfaults located above Ridge 1, supplying the gas hydrate reservoir. The local distribution of the Bright Spots shows that gas and consequently gas hydrate occurrences are limited to local areas where strong fluid flow occurs along faults, providing sufficient concentrations of gas. Hence we suggest that gas hydrates occur above the Ridge 1 and near the mud volcano and the feeder channel. Fluid flow probably occurs episodic controlling the activity of the mud volcano and inhibiting the generation of a BSR. The distribution of gas hydrates is directly linked to the mud volcanism.

3.8 Acknowledgements

Our research was carried out within the MARGASCH project and funded by grants from the Deutsche Forschungsgemeinschaft (Kr2222/4). We thank the crew and the participating scientists of the Meteor cruise M52/1 for their hard work and assistance in data acquisition.

4 Gas seepage and gas/fluid migration associated with the canyon-ridge system offshore Batumi (Georgia, south-eastern Black Sea) inferred from multichannel seismic data

Michelle Wagner-Friedrichs, Elvan Bulgay, Hanno Keil, Sebastian Krastel, Gerhard Bohrmann, Michael Ivanov, Volkhard Spiess

To be submitted to International Journal of Earth Sciences

4.1 Abstract

Numerous gas seeps on the continental slope offshore Batumi (Georgia) occur in water depths at 850-1200 m on the top or flanks of ridge structures within the gas hydrate stability zone (GHSZ). High resolution multichannel seismic investigations carried out during the TTR-15 cruise (UNESCO Training Through Research Program) show that fluid migration towards the seafloor can be linked to the protrusion of buried diapiric structures, which controlled the development of the complex canyon-ridge system offshore Batumi. Depressions between growing diapirs guided the pathways for turbidity currents, primarily forming the canyon systems off Batumi by erosional processes. Over-steepening and faulting of canyon flanks due to diapiric uplift resulted in slope failures. Additionally, faults developed during the diapiric uplift particularly at the flanks and above the diapirs, as well as dipping reflectors at the steep flanks of the diapirs provide potential pathways for upward gas/fluid migration, which controls the distribution of the gas seeps off Batumi. A prominent gas seep of the survey area, the Batumi Seep, located on Kobuleti Ridge in the central study area, is characterized by high amplitude reflection patches beneath the seafloor, which indicate the presence of shallow gas hydrate and carbonate, most likely formed due to focused fluid flow. On several ridges additional potential seep sites were identified by acoustic disturbances in the strata. Although two diapiric mound structures have been identified, most seep sites offshore Batumi do not show upward material transport in diapirs. All seep sites are related to shallow gas accumulations, indicated by Bright Spots at different depths. Although gas hydrates have been sampled at different places, a bottom-simulating reflector (BSR) is limited to the Kobuleti Ridge, but Bright Spots at the depth of the BGHSZ (base of gas hydrate stability zone) might be related to the stability field of gas hydrate, generated where local fluid migration delivers sufficient gas to form gas hydrate. The depth of the BSR is located below the calculated theoretical depth of the BGHSZ for a methane-seawater system, which might be explained by low pore water salinity of 15‰.

4.2 Introduction

Gas seeps considerably contribute to hydrospheric and atmospheric methane concentrations by the release of significant amounts of methane. Methane emissions intensively impact the carbon cycle and the global warming, thus recently gas seeps get intensively studied (Hovland and Judd, 1988; Judd et al., 1997). Gas seepage occurs worldwide, particularly on continental margins, but also in deep waters with a thick sedimentary cover (Judd, 2003). Typically the methane is transported by focused fluid flow from sources at greater depth towards the seafloor along adequate permeable pathways (Greinert et al., 2002; Judd, 2003), e.g. along faults, parallel to permeable stratigraphic layers and at mud diapirs (Hovland and Curzi, 1989; Moore et al., 1991; Orange et al., 2002).

Gas emission at submarine gas seeps can be detected as flares of free gas bubbles in the water column by hydroacoustic methods (Greinert et al., 2006; Naudts et al., 2006) or by acoustic anomalies in unprocessed side-scan sonar data (Klaucke et al., 2005, 2006). Gas discharge is often related to morphological expressions on the seafloor, such as mud volcanoes and pockmarks, which are visible in hydroacoustic and seismic data (e.g. Hovland and Judd, 1988; Judd and Hovland, 1992). Indirect evidences for gas seeps are found in methane derived carbonates (Judd et al., 1997) and high backscatter anomalies in side-scan sonar data, which can indicate authigenic carbonate precipitations that are commonly associated with seeps, formed by anaerobic oxidation of methane (AOM) (e.g. Greinert et al., 2001; Bohrmann et al., 2003). Subsurface structures on seismic images provide information about potential pathways for fluid migration. As high gas content at seeps affects the seismic signal, amplitude anomalies, such as Bright Spots or acoustic transparency, indicate shallow gas accumulations and conduits of focused gas migration which might be related to seep sites (e.g. Judd and Hovland, 1992; Orange and Breen, 1992; Yun et al., 1999; Zühlsdorff and Spieß, 2004).

The anoxic environment of the Black Sea with enormous concentrations of methane in the marine sediments provides a high potential for methane emissions at cold vents. The Black Sea is the largest surface water reservoir of dissolved methane with a total methane concentration of 6×10^{12} mol (Reeburgh et al., 1991). The shelves and continental slopes of the Black Sea are well known for gas saturated sediments and gas seeps (Kruglyakova et al., 2004; Greinert et al., 2006; Naudts et al., 2006). Kessler et al. (2006) estimate that the gas emissions from cold vents to the hydrosphere and atmosphere in the whole Black Sea comprise about 3.6-5.65 Tg/y. Recently almost three thousand active methane seeps have been documented from the north-western Black Sea margin within the Dnepr paleo-delta (Naudts et al., 2006). The depth of these seeps is limited by the phase boundary of pure methane hydrate at 725 m (Naudts et al., 2006). Gas discharge associated with mud

volcanism is common in different regions of the Black Sea, as e.g. in the Central Black Sea and the Sorokin Trough (Limonov et al. 1994, 1997; Ivanov et al., 1996, 1998; Woodside et al., 1997; Bouriak and Akhmetjanov, 1998; Krastel et al., 2003). At three mud volcanoes in the Sorokin Trough hydroacoustic gas flares observed in echosounder data in water depth of about 2080 m were variable in time (Greinert et al., 2006). In the south-eastern Black Sea gas seeps created numerous pockmarks identified on the Turkish shelf (Ergün et al., 2002; Cifci et al., 2003). A thick sedimentary coverage and compressional deformation at the continental slopes of the Black Sea force over-pressured fluids and upward fluid migration along faults (Yun et al., 1999). Kruglyakova et al. (2004) suggest that gas seeps in the Black Sea are mainly related to tectonic faults, but Naudts et al. (2006) observed seeps controlled by stratigraphically controlled fluid migration in the Dnepr paleo-delta area.

Gas seeps off Georgia differ from the shallow water seeps in the north-western Black Sea and the mud volcanoes in the Central Black Sea and the Sorokin Trough, as most seeps off Georgia are not associated with upward transportation of sediments (e.g. mud breccia) and are located at water depths within the stability field of gas hydrate (Egorov et al., 2003; Klaucke et al., 2006). Gas hydrate destabilization might be an important factor supporting the seepage in this area and probably influence the slope stability. Several gas seeps recently have been identified on the continental slope off Batumi; the seeps are located on the tops or flanks of ridge structures, which are separated by deep incised canyons (Klaucke et al., 2006). Seismic investigations were carried out in the frame of the METRO project (Methane and methane hydrates within the Black Sea: Structural analyses, quantification and impact of a dynamic methane reservoir) within the TTR-15 cruise in order to study the subsurface structures controlling the distribution of the seeps off Batumi. The investigations were focused on the largest seep identified by Klaucke et al. (2006), which is named Batumi Seep, but further seeps have been identified and studied as well. The main objective of the seismic investigations is to study the evolution of the complex canyon-ridge system off Batumi. Specific question to be addressed are:

- What are the main processes controlling the development of the canyon-ridge system?
- What kind of subsurface structures control the distribution of the gas seeps?
- What are the fluid migration pathways?
- Is there a relationship between the seeps and the canyon-ridge structures?
- Are the seeps correlated to shallow gas accumulation?
- Are there evidences for gas hydrates associated with the seeps?

4.3 Geological setting of the south-eastern Black Sea

The Black Sea is a large intercontinental basin with anoxic conditions below 100-150 m water depth surrounded by Alpine orogenic belts: the Pontides in the south, the Caucasus in the north-east, the Balkanides in the west, and the Crimean Mountains in the north (Fig. 4.1). The Black Sea is believed to be of extensional origin, formed in the late Cretaceous as a backarc basin during the northward subduction of the Tethyan Ocean (Dewey et al., 1973; Robinson et al., 1995; Nikishin et al., 2003). During Eocene the tectonic setting changed to a compressional regime due to the collision between Eurasia and Arabia and the margins of the Black Sea are recently characterized by compressive deformation (Spadini et al., 1996; Nikishin et al., 2003). The Black Sea comprises two extensional subbasins, the Western and the Eastern Black Sea Basin, separated by the thinned continental Mid Black Sea Ridge. The Mid Black Sea Ridge is subdivided into the Andrusov and the Archangelsky Ridge (Fig. 4.1) (Tugolesov et al., 1985; Finetti et al., 1988; Robinson et al., 1996).

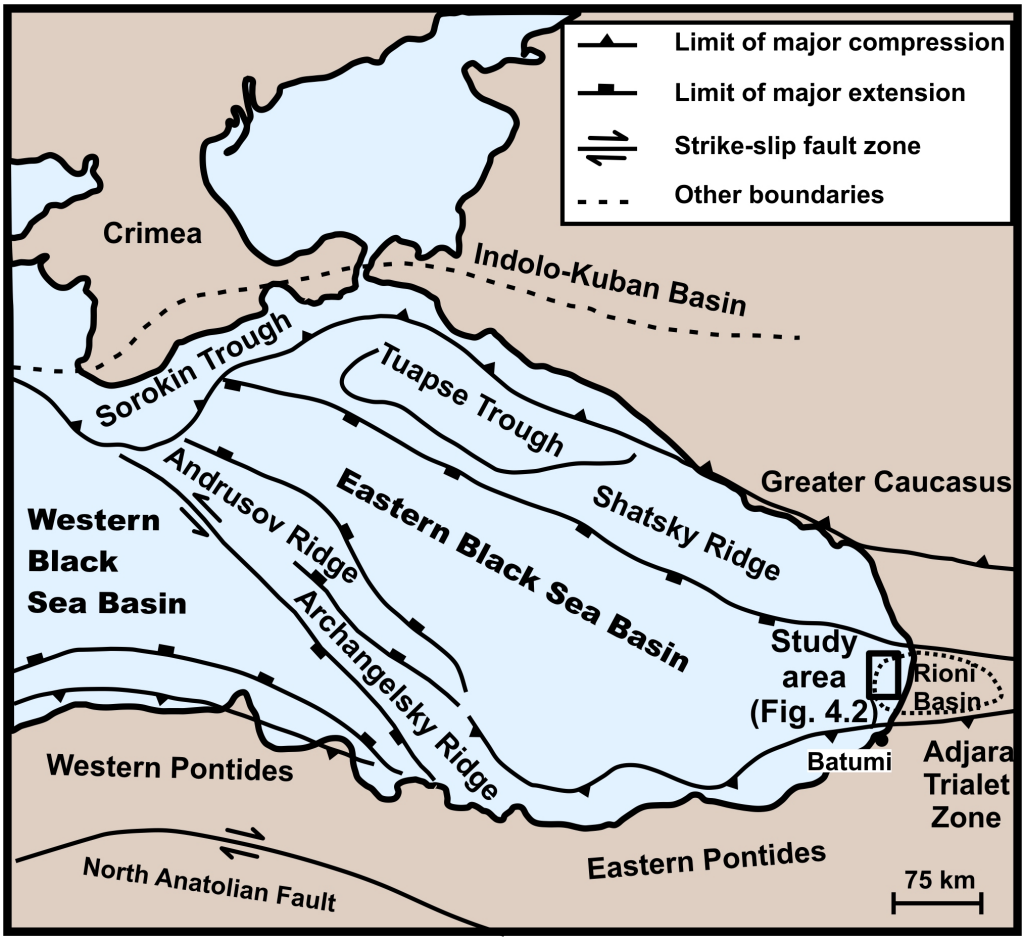

Figure 4.1: *Schematic map of the main tectonic zones within the Eastern Black Sea Basin (modified after Robinson et al., 1996). The study area is highlighted by a black rectangle.*

The Georgian Continental Slope at the south-eastern margin of the Eastern Black Sea Basin is bordered by the Shatskii Ridge in the north-east and the Eastern Pontides thrust belt in the south-east (Robinson et al., 1995; Robinson, 1996) (Fig. 4.1). The Eastern Black Sea Basin opened due to the separation of the Mid Black Sea High and the Shatsky Ridge by rotation about a pole west of Crimea (Spadini et al., 1996; Robinson et al., 1996), but the opening time is still uncertain and interpretations vary from Jurassic time (Golmshtok et al., 1992) to end-Cretaceous (Nikishin et al., 2003) and Paleocene/Eocene (Robinson et al., 1996; Spadini et al., 1996; Cloething et al., 2003). The Geology of Georgia is characterized by two major thrust belts: the ESE trending Greater Caucasus Thrust Belt in the north and the E-W trending Adjara Trialet Belt in the south (Fig. 4.1). The Adjara Trialet Belt appears to be a Palaeogene extensional basin closed during the Late Eocene or Oligocene (Robinson et al., 1997). The thrust belts are separated by two foreland basins, the Rioni Basin extending to the Black Sea in the west (Fig. 4.1) and the Kartli Basin in the east extending into the Caspian Sea (Banks et al., 1997). These basins are of flexural origin developed mainly during the Miocene through the loading of the Adjara Fold Belt (Banks et al., 1997; Robinson, 1997). A basement high, the Dziruli Massif, separates the basins and acts as the main source of the basinal sediments (Robinson et al., 1997). The Rioni Basin includes thick upper Miocene to Quarternary deposits, onlapping the Shatskii Ridge in the north and merging eastward with the post-rift fill of the Eastern Black Sea Basin (Banks et al. 1997; Robinson et al., 1997). The sequence is characterized by numerous unconformities related to the development of submarine canyons transferring sediments to the Black Sea (Banks et al., 1997).

The survey area off Batumi is located within the offshore extension of the Rioni Basin and characterized by a complex system of W-E striking canyon and ridge structures (Fig. 4.2). At the ridges numerous gas seeps were recorded as acoustic anomalies in unprocessed side-scan sonar data collected during the Poseidon cruise P317/4 in October/November 2004 (Klaucke et al., 2005, 2006). The seeps had been known from previous investigations in Russia (Meisner, pers. comm.). Most gas flares were observed on the Kobuleti Ridge at the so-called Batumi Seep Area in water depths of 850-900 m (Fig. 4.2).

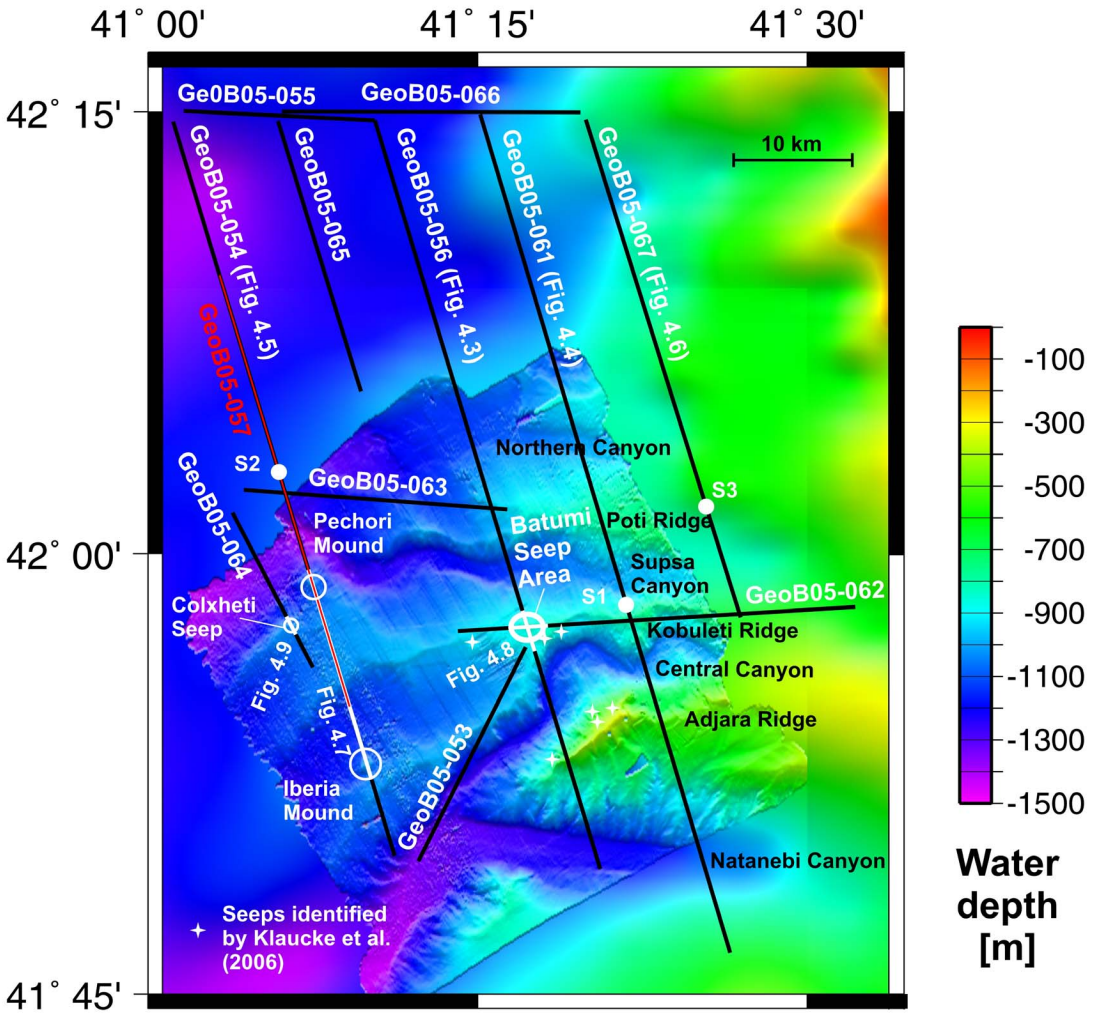

Figure 4.2: *Bathymetric map of the study area offshore Batumi (Georgia). The detailed bathymetric data in the southern study area were collected during the P317 cruise using a 50 kHz ELAC Bottomchart Mk-II multibeam system (Klaucke et al., 2005). Areas not covered by the multibeam data are filled with the GEBCO 1-min grid. The black lines represent the seismic profiles. The white stars show the locations of the seeps detected by Klaucke et al. (2006).*

4.4 Data

In the frame of the interdisciplinary METRO project, a multichannel seismic survey was carried out at the Georgian Continental Margin offshore Batumi using the TTR-15 cruise with the Russian research vessel Professor Logachev in June 2005. The main objective of this cruise was to study the distribution and characteristics of gas seeps, gas and gas hydrate occurrences in a complex canyon-ridge system. The main seismic source was a Sodera GI-Gun with 2 x 1.7 l chamber volume, but along one line (Geob05-057, location is shown in Fig. 4.2) a Mini GI-Gun was deployed with a chamber volume of 2 x 0.18 l to get a higher resolution image of the uppermost 500 ms TWT. Both guns were

operated with a mean air pressure of 140 bar supplied by two shipboard compressors. The data were acquired by a 100 m long streamer section with 16 channels of 6.25 m group length recorded at 4 kHz sampling frequency over an interval of 5 seconds. In total, 12 seismic lines were recorded with a total length of 324 km (Fig. 4.2).

After trace editing and geometry processing the seismic data were processed including NMO-corrections, bandpass frequency filtering with a frequency content of 20/40 - 200/400, FK-filtering with a wave number range between -0.25 and +0.25, CMP-sorting, stacking with a CMP distance of 10, 15 or 20 m, and final time migration. Other methods applied during the cruise include sediment sampling with gravity corer, multi corer, TV-grab and autoclave piston corer, ROV dives, as well as acoustic investigations with side-scan sonar and subbottom profiler.

4.5 Results

4.5.1 The canyon-ridge system offshore Batumi

The study area offshore Batumi is located at water depths of 600-1600 m and characterized by 6 W-E trending submarine canyons separated by 6 ridges of varying dimension and morphology (Figs. 4.2-4.6). In the southern part of the study area high resolution multibeam bathymetric data collected in 2004 (Klaucke et al., 2006) allow to trace the canyon-ridge system and give detailed information about their structures, which is not possible in the north due to the lack of high resolution bathymetry and low seismic coverage with a line spacing of 6-7 km. From south to north the canyons and ridges identified were named as follows: Natanebi Canyon, Adjara Ridge, Central Canyon, Kobuleti Ridge, Supsa Canyon, Poti Ridge, Northern Canyon (Klaucke et al., 2006), R1 Ridge, C1 Canyon, R2 Ridge, C2 Canyon and R3 Ridge (Fig. 4.2).

Most of the ridges, in particularly those in the south, are characterized by continuous well stratified reflectors with signal penetration down to about 800 ms TWT below seafloor (bsf). The sediments are partly tectonically disturbed by normal faults, as e.g. at the Kobuleti, Poti, R2 and R3 Ridge (Figs. 4.3-4.6). In the north, the ridges show a more irregular relief and the reflection characteristics become chaotic and change laterally, thus continuous reflectors alternate with chaotic reflection patterns and units of washed out reflections (Figs. 4.3-4.6). The steep flanks of the ridges are mainly characterized by erosion and often affected by slope failures (Figs. 4.3, 4.5, 4.6). At several ridge flanks blocks characterized by a chaotic to acoustic transparent seismic facies were observed, which are typical for slumps, imaged by homogeneous seismic pattern without internal structure (Figs. 4.3-4.5).

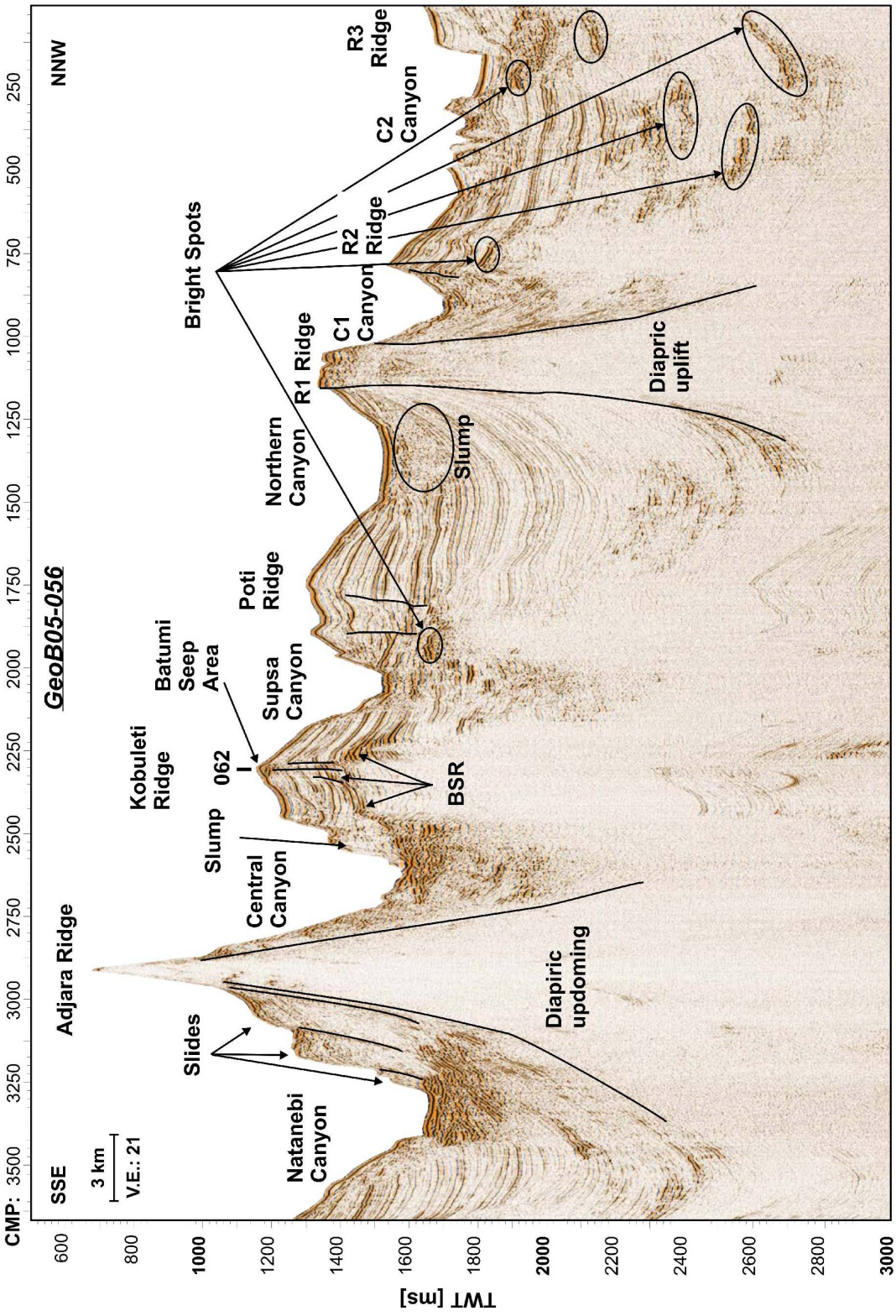

Figure 4.3: *Time migrated image of seismic line GeoB05-056 crossing the central study area and the Batumi Seep. The Batumi Seep is located above several near vertical faults reaching down to a BSR. Slump deposits with a thickness of 70 ms TWT at a depth of 60 ms TWT bsf at the Northern Canyon show sharp boundaries to the surrounding strata and are most likely originated from the flank of the R1 Ridge. See Fig. 4.2 for location of line.*

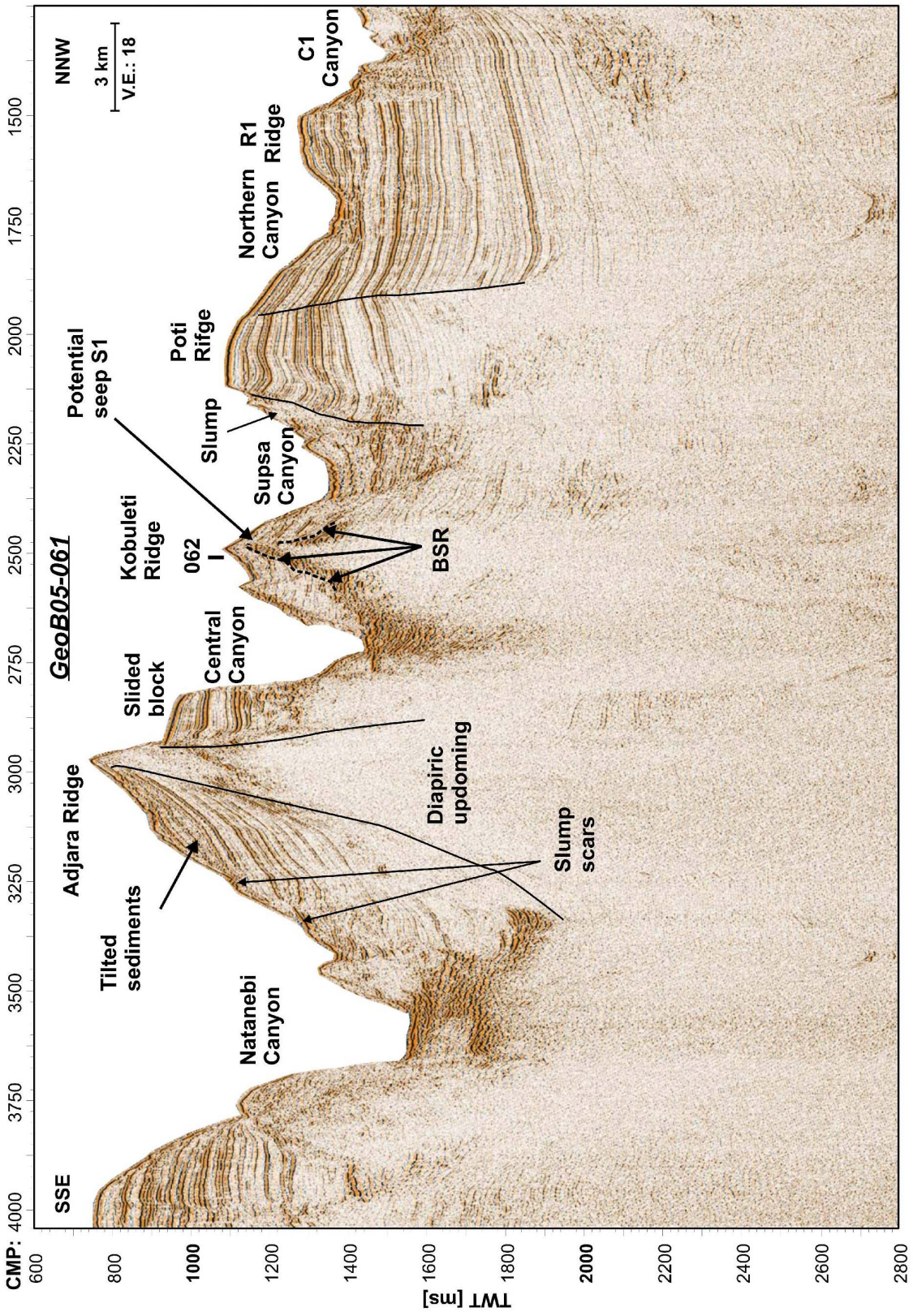

Figure 4.4: *Time migrated seismic profile GeoB05-061. The BSR below the Kobuleti Ridge is shifted upward in the vicinity of a fluid migration zone towards a potential seep site (S1) on the seafloor. The location of the line is shown in Fig. 4.2.*

Furthermore, we observed slides, which are characterized by downward moved blocks including continuous well stratified reflectors without internal deformation, as e.g. identified at the flanks of the Adjara Ridge (Figs. 4.3, 4.4). The flanks complicated by slumps and slides often show faults nearby, but faults were observed at flanks without slope failures as well (Figs. 4.3-4.5). The most noticeable ridge structure is the Adjara Ridge, rising up to 500 m above the canyon floor into water depths of 500 m. The Adjara Ridge has extremely steep flanks with slope angles of about 6° at the southern and 8-10° at the northern side. Diapiric structures characterized by acoustic transparency were observed beneath several ridges (Figs. 4.3-4.6). The Kobuleti Ridge, with a height of about 400 m above the canyon floor, significantly widens from about 4 km in the east to more than 20 km in the west and splits into 2 crests in about 1000 m water depth. These crests are separated by a 4200 m wide and 130 m deep channel (Fig. 4.5). The northern crest continues E-W trending, but the southern crest changes to the SW, which lead to increased width of the channel (Fig. 4.2). The sediments of the channel and the southern crest are characterized by transparent units, separated by some strong continuous reflectors becoming chaotic below 200 ms TWT bsf, while those of the northern crest are presented by closely spaced strong stratified reflectors down to 450 ms TWT bsf (Fig.4.5). The ridges in the north are characterized by an irregular relief, tend to asymmetric geometry and show less dimensions and heights (Figs. 4.3, 4.4, 4.6). For example, the Poti Ridge rises only 150-200 m above the canyon floor and has a steep southern, but smooth dipping northern flank (Figs. 4.3, 4.4, 4.6). The R1 Ridge has a flat southern flank with wavy relief (Fig. 4.6).

Beneath the canyons signal penetration varies from 200 to 800 ms TWT depending on the reflection characteristics, which can be divided into two typical seismic facies: (1) Discontinuous high amplitude reflectors with a thickness of 100-200 ms occur beneath the strong seafloor reflection at the southernmost Natanebi and Central Canyon, as well as in the eastern part of the C2 Canyon (Figs. 4.3. 4.4, 4.6). High amplitude reflection patches occur also at a depth of 160 ms TWT bsf beneath the axis and at 500 ms TWT bsf beneath the northern wall of the Natanebi Canyon (Fig. 4.4), as well as at depths of 280-900 ms TWT bsf at the C2 Canyon and its walls (Figs. 4.5, 4.6). (2) The central canyons are characterized by more or less well stratified, but lateral relatively limited parallel reflectors of varying amplitudes alternating with units of chaotic reflection patches and acoustic void zones (Figs. 4.3-4.6). The canyons in the south are deep and narrow with steep eroded walls. To the north, the morphology of the canyons changes showing irregular relief with indistinct incisions (Figs. 4.3-4.6). Several canyons show a meander pattern and changes of trend direction, e.g. the Central Canyon, which changes its trend direction from the E-W direction downslope to the south and connects with the straight W-E trending Central Canyon at about 1300 m water depth (Fig. 4.2).

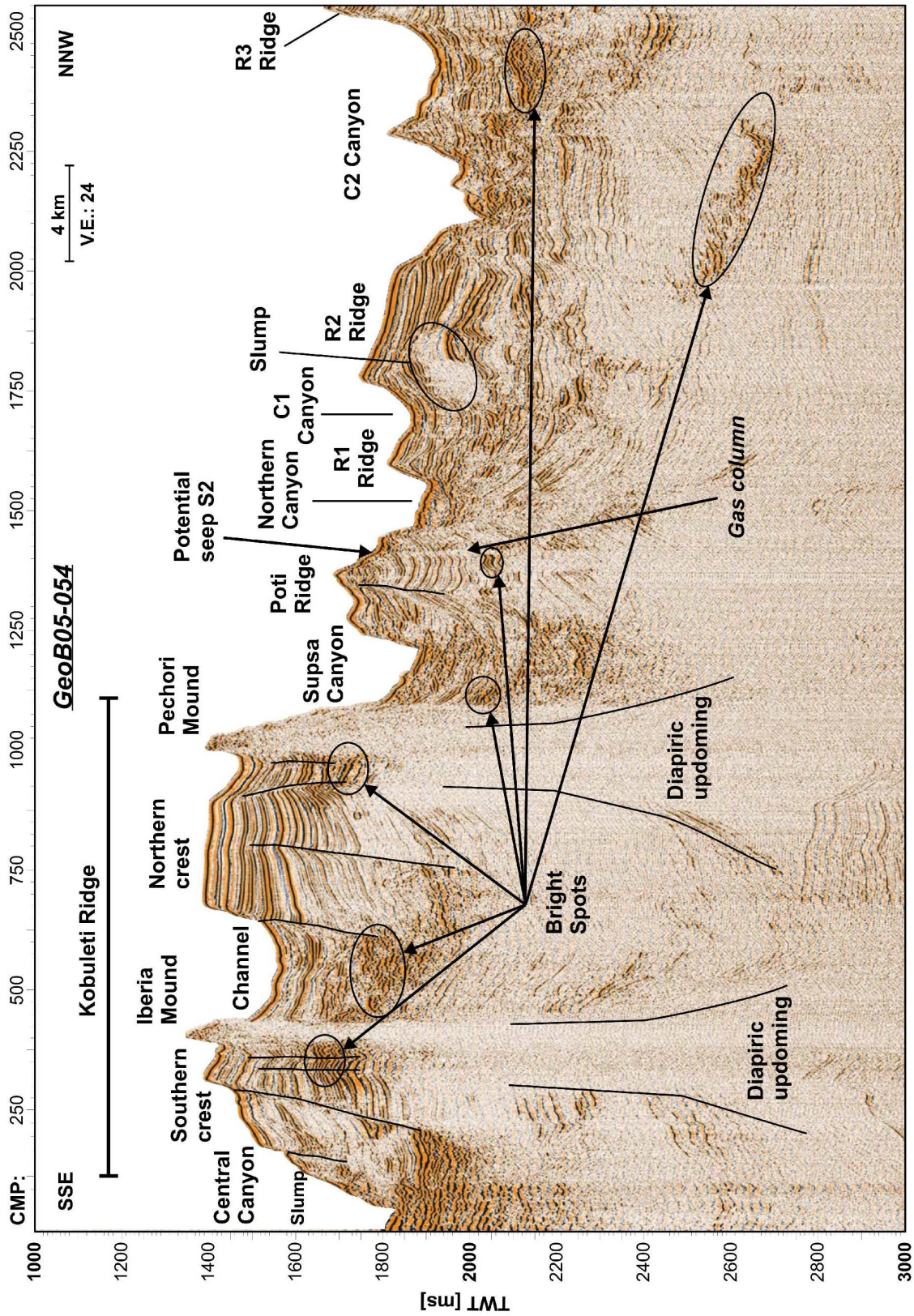

Figure 4.5: *Time migrated image of line GeoB05-054 crossing the western study area. The Kobuleti Ridge is subdivided into two crests showing two mound structures at its edges, underlain by diapiric structures. See Fig. 4.2 for location of line.*

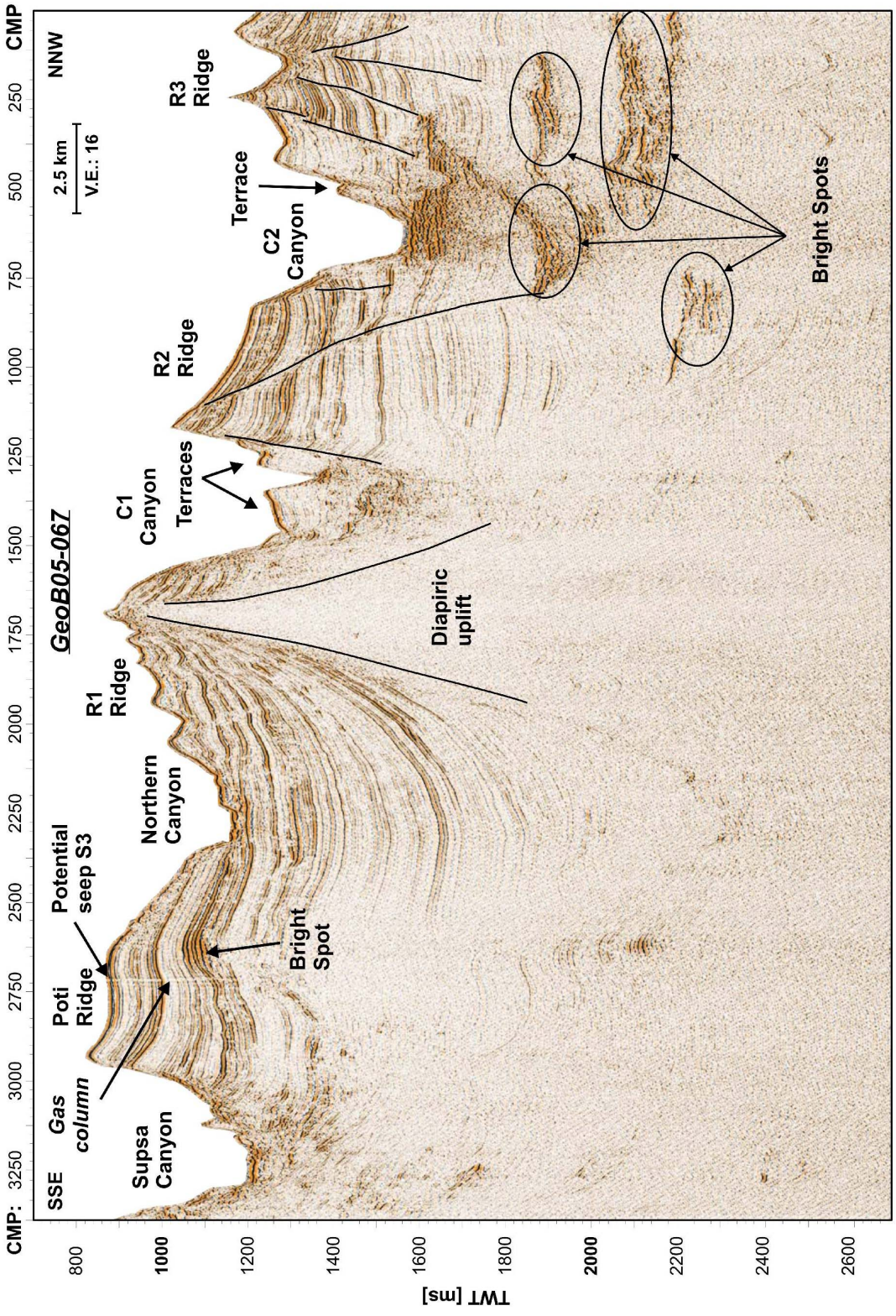

Figure 4.6: *The time migrated seismic profile GeoB05-067 in the north-eastern survey area. Thick parallel reflectors form a basin beneath the Northern Canyon. The walls of the C1 and C2 Canyons show terraces, which are characterized by acoustic transparency. Numerous Bright Spots occur at different depths beneath the C2 Canyon extending towards the R3 Ridge. The location of the line is shown in Fig. 4.2.*

4.5.2 Diapiric structures

Beneath the ridges several diapiric zones have been identified in the seismic data, characterized by acoustic transparent updoming structures onlapped by upward bulged reflectors (Figs. 4.3-4.6). Limited signal penetration of our high resolution data inhibits the observation of structures beneath 1 s TWT bsf, thus most diapirs could not be traced along the ridges. The central part of the Adjara Ridge is acoustically masked by a diapiric structure, which seems to pierce the seafloor as a steep ridge (Figs. 4.3, 4.4). In the subsurface of the Kobuleti Ridge upward bulged weak reflectors indicate the presence of two diapiric folds rising up to 500 ms TWT beneath the Iberia and Pechori Mound (Fig. 4.5). In the central and eastern portion of the study area no diapir could be observed at the Kobuleti Ridge due to the acoustic transparency below ~200 ms TWT (Figs. 4.3, 4.4), but Tugolesov et al. (1985) described a diapir trending along the Kobuleti Ridge at greater depth. The diapiric structure beneath the R1 Ridge has steep flanks and reaches almost up to the seafloor (Fig. 4.3), uplifting the sediments of the southern flank. Generally the sediments above the diapirs are fractured and disturbed. No diapirs are observed beneath the ridges further north.

4.5.3 Gas seeps

Offshore Batumi several gas seeps have been identified as acoustic anomalies in the water column and as high backscatter patches on the seafloor on side-scan sonar records collected during the P317 cruise in 2004 (Klaucke et al., 2005, 2006). The seeps are located either on the Kobuleti Ridge or at the northern flank of the Adjara Ridge (Klaucke et al., 2006) (Fig. 4.2). The largest seep area, named Batumi Seep Area, is located at about 850 m water depth on the Kobuleti Ridge (Fig. 4.2) (Klaucke et al., 2006) and was chosen for further detailed investigations within the TTR-15 cruise. During seismic profiling further structures most probably associated with gas discharge were observed, e.g. the so-called Colxheti Seep, the Pechori and Iberia Mounds, as well as three additional potential seep sites (Fig. 4.2).

The Batumi Seep Area

The Batumi Seep Area is imaged by two seismic profiles, shot along and perpendicular to the Kobuleti Ridge (Fig. 4.2). Two close-ups of the Batumi Seep Area are shown in Fig. 4.7. On the seismic data the seep area is characterized by a shallow buildup rising about 10 m with strong seafloor reflection and lateral dimensions of 1200 m in the ESE-WNW direction and 600 m in the SSE-NNW direction (Fig. 4.7). At the uppermost 60 ms TWT bsf chaotic strong reflection patches are imaged (Fig. 4.7).

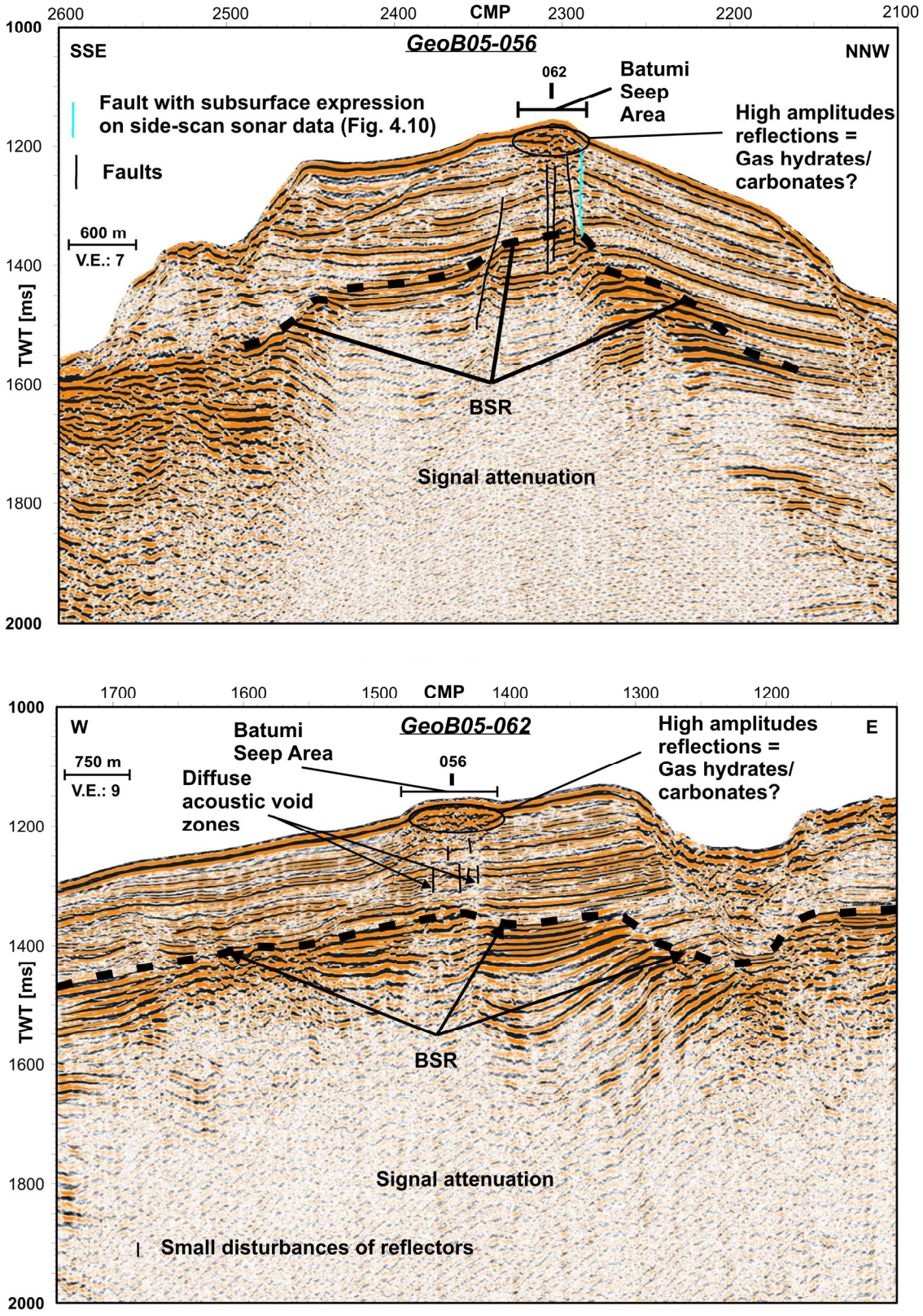

Figure 4.7: *Close-ups of seismic lines GeoB05-56 (top) and GeoB05-62 (bottom), crossing the Batumi Seep in the NW-SE and W-E direction, respectively. See Fig. 4.2 for location of the lines and the seep.*

Beneath and in the surrounding subsurface of the seep, the sediments are characterized by continuous parallel reflectors. At a depth of about 200 ms TWT bsf in average, a BSR can be traced along the Kobuleti Ridge (Fig. 4.7). Below the BSR, the seismic signal is significantly attenuated. On profile GeoB05-056, several near vertical faults with vertical offsets of up to 15 ms TWT are observed beneath and in the surrounding of the Batumi Seep probably striking in the E-W direction (Fig. 4.7). Few faults reach up to the seafloor; others trace through the BSR.

The Colxheti Seep Area

The Colxheti Seep Area is located at the flank of the northern crest on the westernmost Kobuleti Ridge at water depth of 1200 m (Fig. 4.8) and is characterized by a cone-shaped elevation with a height of 20 m and a width of 1400 m. The buildup is asymmetric with a steep southern flank with a dipping angle of 12°, but a smooth northern flank dipping with about 2° against the crest (Fig. 4.8). The seafloor reflection is indistinctly imaged at the southern flank, but the top and the northern side are characterized by weak discontinuous reflectors on the seafloor. Beneath the seep structure, weak reflection patches with a thickness of 170 ms TWT occur. Upward bulged sediments indicate the presence of a diapiric structure at 250 ms TWT bsf.

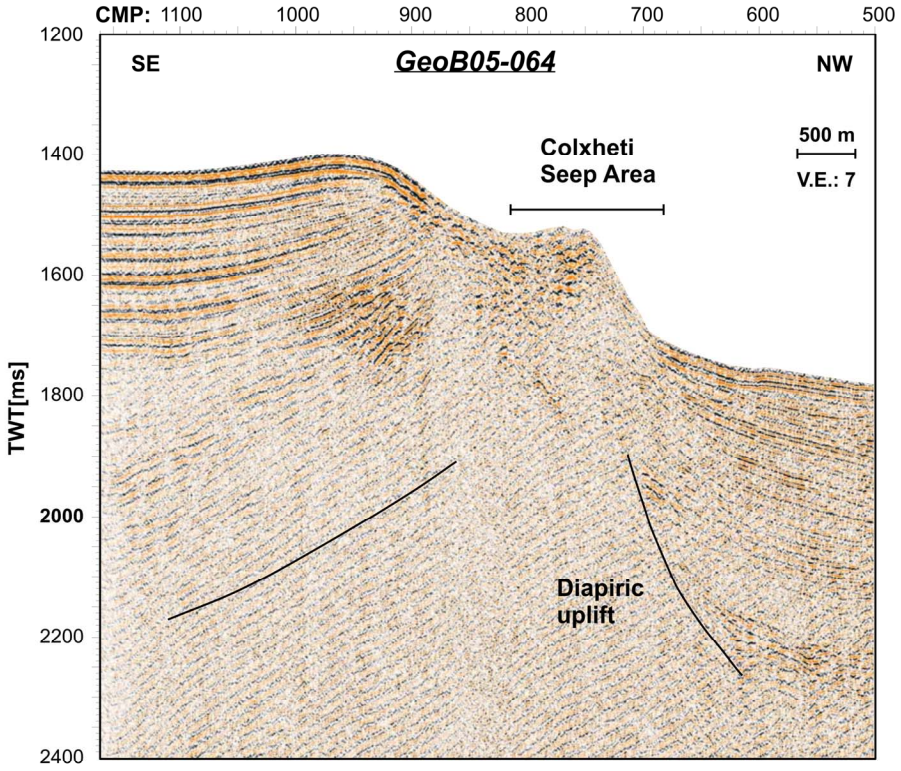

Figure 4.8: *Time migrated seismic section of line GeoB05-064 showing the Colxheti Seep. The location of the line is shown in Fig. 4.2.*

Potential seeps S1-S3

Three potential seep sites are observed on the eastern Kobuleti (S1) and on the western (S2) and eastern (S3) Poti Ridge (Figs. 4.4-4.6). The seeps are indicated by vertical acoustic transparent zones with widths of 60-180 m. The acoustic void zones almost reach up to the seafloor, but with exception of the S3 location the seafloor does not show weakened reflections or morphological irregularities as at the Batumi and Colxheti Seep. At the S3 potential seep site, the void zone traces through the seabed and a very small pinnacle with a height of about only 2 m is observed on the flat top of the Poti Ridge. The margins of the transparent zone are bordered by downward bended reflectors (Fig. 4.6). The potential seep S1 on the Kobuleti Ridge reaches through the BSR, which is significantly uplifted nearby to 75 ms TWT bsf (Fig. 4.4). The S2 and S3 potential seeps are flanked by a Bright Spot (Figs. 4.5, 4.6).

The Pechori and Iberia Mound

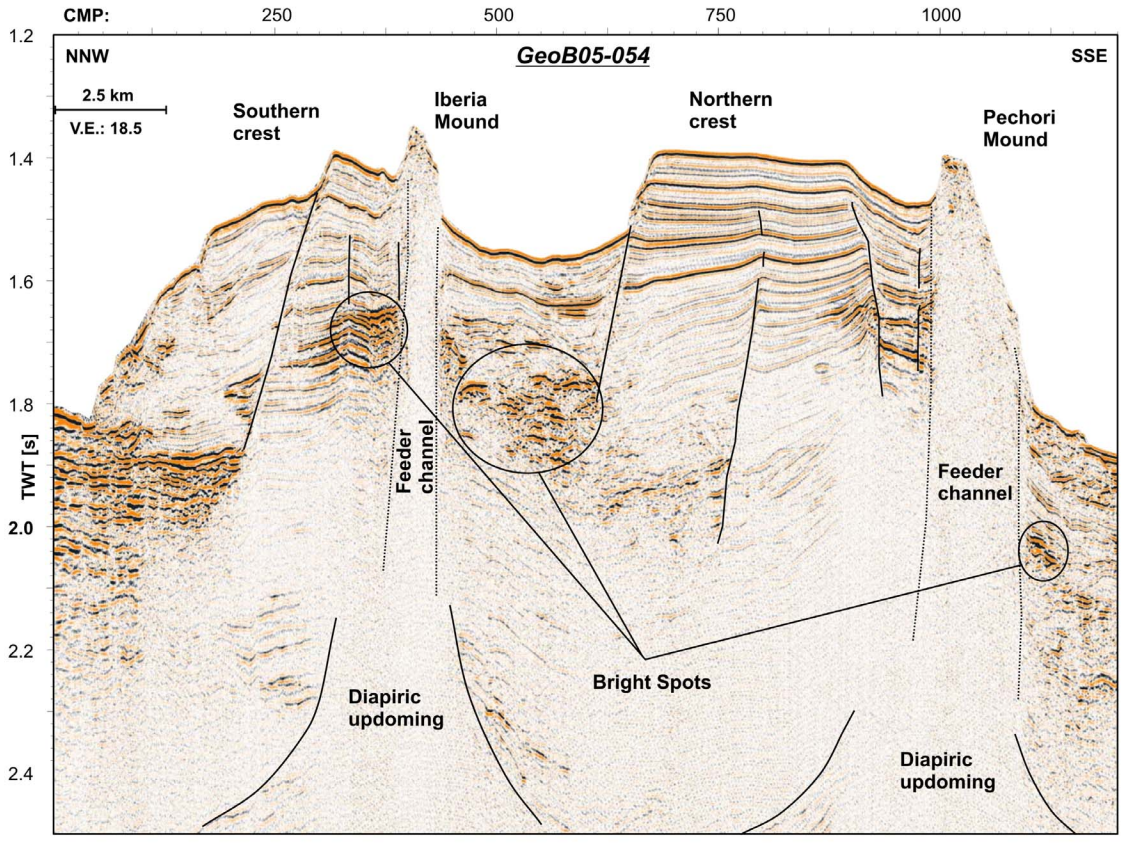

Figure 4.9: *Close-up of the Pechori and Iberia Mound located on the westernmost portion of the Kobuleti Ridge. Location is shown in Fig. 4.2.*

Two mounds were identified at the northern edges of the two crests forming the westernmost portion of the Kobuleti Ridge (Fig. 4.9). The mounds, named Iberia and Pechori Mound, are cone-shaped with heights of about 75 m and a diameter of 2000-2500 m with steep slope angles of 9-10° (Fig. 4.9). Both, in particularly the Pechori Mound, are characterized by a strong seafloor reflection on the top. In the subsurface the upper 50 ms TWT at the Iberia and 90 ms TWT at the Pechori Mound are represented by weak chaotic reflection pattern (Fig. 4.9). Beneath, a zone as wide as the diameter of the mounds characterized by acoustic transparency with sharp borders to the surrounding well stratified sediments can be traced down to the diapirs. The surrounding strata are partly disrupted by near vertical faults with vertical offsets of some 10 ms TWT (Fig. 4.9). Above and at the flanks of the diapirs small Bright Spots occur at a depth of 200-250 ms TWT bsf near the transparent zones.

4.6 Interpretation and Discussion

4.6.1 Gas seeps offshore Georgia

Gas seeps are common along the continental slopes of the Black Sea and have been intensively studied since the last decades, but seeps off Georgia are rarely documented yet. Recently, numerous gas seeps have been observed on the continental slope off Georgia in deep water of about 850-900 m within the gas hydrate stability field (Egorov et al., 2003; Klaucke et al., 2006). The Batumi Seep area covers an area of 0.5 km² on the Kobuleti Ridge and is the largest seepage area investigated offshore Georgia so far (Klaucke et al., 2006). Our multichannel seismic data show that the parallel reflectors of the subsurface sediments at the Batumi Seep are displaced by several near vertical faults, which partly pierce the seafloor in the range of the seep area (Fig. 4.7). With exception of narrow and diffuse acoustic void zones beneath the Batumi Seep on line GeoB05-062 (Fig. 4.7), no indications for gas migration could be identified in the seismic data, thus we can only presume that gas discharge at the seep is probably controlled by upward migration of fluids and gas along faults, although the void zones in line 062 could not be correlated to faults. The void zones on line 062 are located west and eastward of the faults imaged on line 056 (Fig. 4.7), and no direct relations to faults is possible. The presence of smaller faults, however, is indicated by small disturbances of seismic reflectors (2-3 ms TWT) beneath the Batumi Seep on line 062 (Fig. 4.7). The side-scan sonar image of the Batumi Seep on Fig. 4.10 shows, that the seafloor within the seep area is structured by numerous NW-SE trending faults (Klaucke et al., 2006). One of these faults coincides with a subsurface fault observed on the seismic line GeoB05-056 (location is shown in Fig. 4.10), suggesting that the faults on the seafloor represent the surface expression of the

subsurface faults observed in the seismic data. The surface faults crossing line GeoB05-062 could not be connected to subsurface faults on the seismic profile.

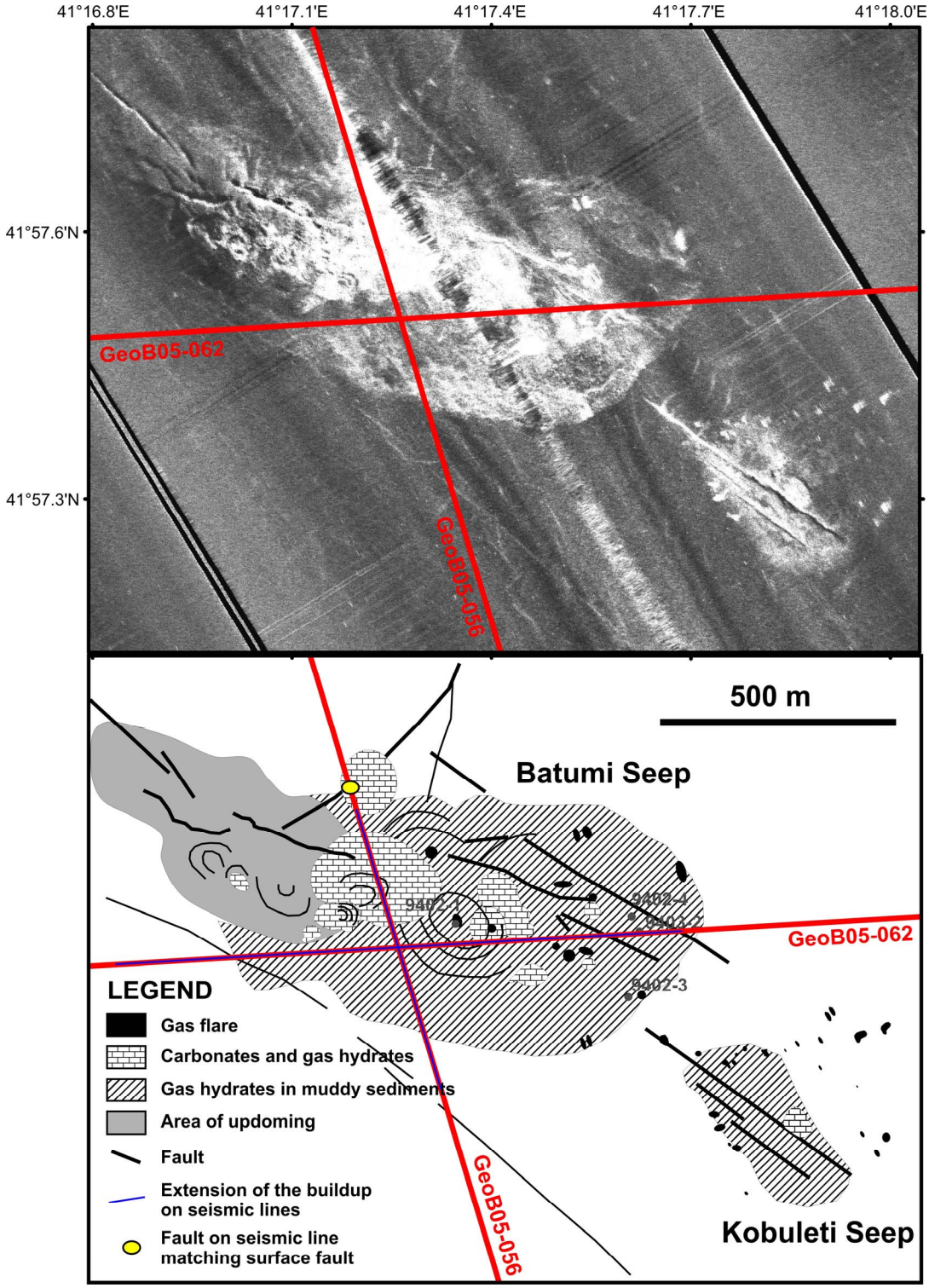

Figure 4.10: *75 kHz DTS-1 side-scan sonar image and interpretation of the Batumi Seep Area (Klaucke et al., 2006). The seismic profiles crossing the seep are imaged as red lines.*

Further potential seeps, named S1, S2 and S3, are indicated by narrow vertical acoustic transparent zones interpreted as conduits of focused upward gas/fluid migration, as gas/fluids affect seismic amplitudes leading to lost of seismic signal energy (e.g. Max, 1990). These so-called gas columns with a width up to 180 m (Figs. 4.4-4.6) were observed on the eastern Kobuleti, and the western and eastern Poti Ridge. At S1 and S2, the gas columns do not reach to the seafloor and no morphological expressions or seismic irregularities are observed on the seafloor. Thus, we suggest that these seeps are probably not active. Rising fluids might be trapped in the near subsurface, or flow might occur only episodically. At S3, the gas column can be traced through the seafloor and a small morphological irregularity (relief) indicates that this location is probably recently active. Gas discharge in the deep water of the Black Sea has been related to mud volcanoes at water depths down to 2200 m (Ivanov et al., 1996, 1998; Limonov et al., 1997; Woodside et al., 1997), but most gas seeps off Batumi are not associated with upward material transport (Klaucke et al., 2006). Our acoustic data (seismic, side-scan sonar and subbottom profiler) also do not show evidences for mud transport at the Batumi Seep as well as the potential seep sites, such as high morphological elevations and mud flows on the seafloor, and the cores collected during the TTR-15 cruise lack mud breccia. However, free gas bubbles are present above the Batumi Seep, identified as acoustic anomalies in the water column of unprocessed side-scan sonar records collected by Klaucke et al. (2006). Gas bubbles were also observed during the TTR-15 cruise by video observations with the ROV and in the water column while core retrieving.

In contrast to the Batumi Seep, the Pechori and Iberia Mounds observed at the western edge of the Kobuleti Ridge are large structures and characterized by wide acoustic transparent zones beneath, which we interpreted to represent the feeder channels. We suggest that the mounds are formed by upward rising gas saturated material along the acoustic transparent feeder channel. The feeder channel is connected to the diapirs beneath, which most probably represents the source of the material. Displaced reflectors north and south of the feeder channel beneath the Iberia Mound and several near vertical faults in the surrounding of the feeder channels indicate that upward migration is bound to faults, as the horizontal layered strata do not provide stratigraphic migration pathways. Mud volcanoes are characterized by the extrusion of mud (e.g. Dimitrov, 2002). As no mud flows have been identified on the side-scan sonar data, the Pechori and Iberia Mound probably do not represent mud volcanoes. Other positive morphological features related to gas escape might be carbonate or mud mounds as well as outcropping diapirs (e.g. Hovland and Judd, 1988). Sampled mud breccia at the Pechori Mound suggests that these structures might be mud mounds related to upward mud transport by fluid migration from the diapirs or might represent diapiric mounds due to diapiric upward mud transport. However, in contrast to the

Batumi Seep, the mounds show wide conduits beneath, indicating intensive transport of gassy material. The Colxheti Seep located 2500 m southwest of the Iberia Mound looks quite different compared to the Batumi Seep. While the Batumi Seep rises only about 10 m and no wide conduits for fluid migration are imaged in the subsurface, the cone-shaped Colxheti Seep is twice as large and is characterized by an extensive zone of acoustic transparency beneath, indicating transport of gassy material. Thus we suggest that the Colxheti Seep is rather a mound structure than a simple gas seep. Geochemical analyses show that the Batumi Seep is a simple pure gas system dominated by methane, while higher hydrocarbons occur at the Colxheti Seep and the Pechori Mound (Bohrmann, unpublished data). High hydrocarbons indicate a deeper source of portions of the gas, which at the mounds might be sourced in the diapirs and transported upward together with the mud. Several potential hydrocarbon source rocks occur in western Georgia, but their offshore extension is uncertain (Robinson et al., 1997). Most mud volcanoes in the Black Sea are sourced in the Maikop Formation (Ivanov et al., 1996), which most probably is the source of the seeps in our study area as well.

4.6.2 Gas and gas hydrate occurrences related to gas seeps

Most seeps off Batumi are located within the gas hydrate stability zone, meaning that free gas coexists with gas hydrate. Based on a pure methane system and sea water salinity of 33.5 ‰ (Dickens and Quinby-Hunt, 1994), the upper theoretical phase boundary of the gas hydrate stability zone in the study area is expected at water depths of about 720 m (calculated according to Sloan (1998) at typical Black Sea bottom water temperature of 9°C). Gas hydrates have been sampled at several locations in the study area, but a BSR was identified only at the Kobuleti Ridge in the surrounding of the Batumi Seep at water depths between 800 and 1000 m (Figs. 4.3, 4.4, 4.7, 4.11). The BSR trends along the ridge at depths ranging between 75 and 260 ms TWT bsf. With exception of the shallowest depth of 75 ms TWT bsf observed next to the potential seep site S1, the depth of the BSR shows only small variations in depth between 170 and 230 ms TWT bsf (Fig. 4.11).

As the gas composition at the Batumi Seep is dominated by methane with small amounts of ethane (unpublished data), we calculated a gas hydrate phase diagram for a two phase gas hydrate system with a composition of 99.9 % methane and 0.01% ethane at seawater salinity of 33.5 ‰ (after Sloan, 1998) (Fig. 4.12). Using the average water depth in the area of the BSR of 900 m, 9°C bottom water temperature and a geothermal gradient of 30°C/km, the lower limit of the gas hydrate stability zone (GHSZ) is expected at about 110 bsf (Fig. 4.12). The actual observed average depth of the BSR is located at 190 ms TWT bsf (~150 m with a sediment velocity of 1600 m/s), thus about 40 m beneath the calculated depth (Fig. 4.12).

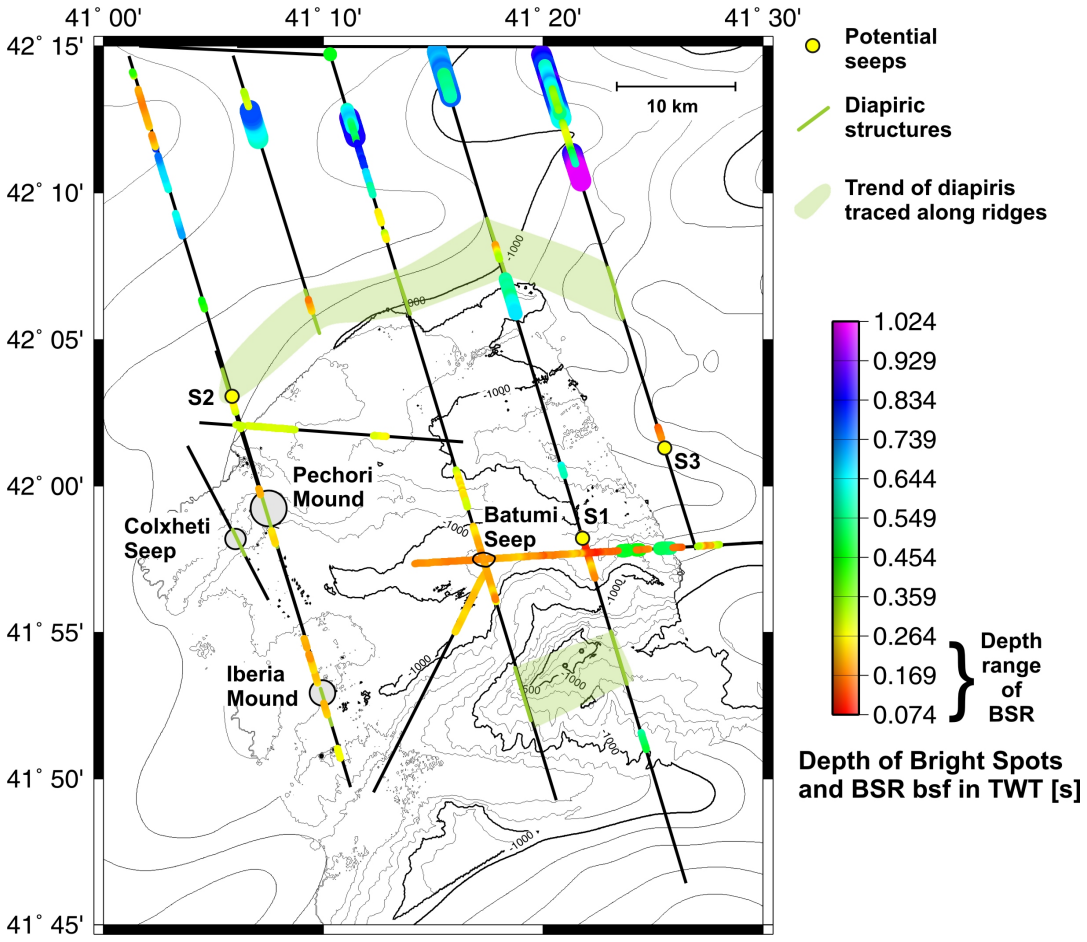

Figure 4.11: *Distribution and depth in s TWT bsf of the Bright Spots and the BSR, together with the location of the diapiric structures and the vent sites (mound structures, Batumi and Colxheti Seep, and the potential seep locations). The bathymetric contours are calculated from the bathymetric grid shown in Fig. 4.2.*

Downward shifts of the base of gas hydrate stability zone (BGHSZ) for example can be caused by reduced temperature or salinity (e.g. Kvenvolden, 1993). As the study area is located at an active seep site characterized by upward rising, probably warm, fluids, temperature would be expected rather to be increased than reduced. To prove the influence of salinity, we examined the gas hydrate stability phase diagrams for different salinities as well as for a pure water system without changing the other parameters. Three curves, calculated with salinities of 33.5‰, 15‰ and 0‰, are shown in Fig. 4.12. The calculations show, that changes in salinity significantly influence the phase boundary of the gas hydrate stability. The average depth of the BSR can be best adjusted with a salinity of about 15‰, which leads to a theoretical depth of the BGHSZ of about 150 m (Fig. 4.12).

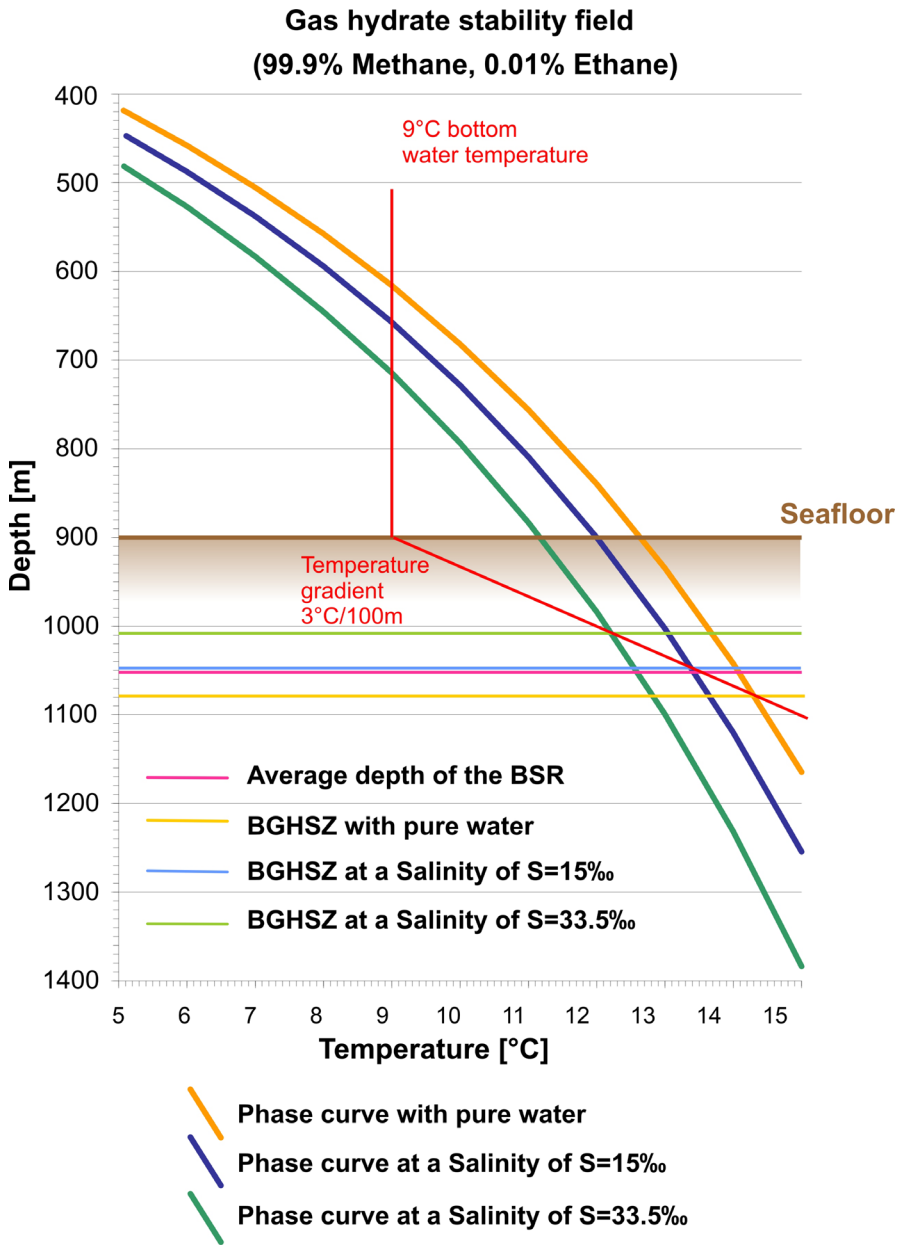

Figure 4.12: *Gas hydrate stability fields, calculated for methane dominated gas system with 99.9% methane and 0.01% ethane with salinities of 33.5‰, 15‰ and pure water (according to Sloan, 1998). The depth of the BGHSZ is calculated at 900 m water depth with a bottom water temperature of 9°C and a constant temperature gradient of 30°C/km. The average depth of the BSR is imaged as pink line.*

Pore water analyses show that chloride concentrations decline almost linearly from about 350 mM at the sediment-water interface to 250 mM in a sediment depth of 530 cm (Haeckel, pers. comm.), supporting that gas hydrates are probably formed at low salinity shifting the BGHSZ towards higher temperatures. Possible explanations for low salinity

values are a downward diffusion of Cl^- ions from sediments deposited under modern marine salinities into underlying limnic sediments with low salinities deposited during the last glacial periods (Manheim and Chan, 1974), or in the upflow of low salinity fluids in the range of the Batumi Seep. The Black Sea in general is characterized by low salinity due to restricted water exchange with the Mediterranean Sea. The brackish and oxic surface waters with a salinity of about 18‰ are separated by a stable halocline from the deep anoxic bottom waters with a salinity of about 22‰ (e.g. Murray et al., 1991).

Fig. 4.13 images a line drawing of the profile GeoB05-062 along the Kobuleti Ridge with the direct relationship between the BSR and the theoretical BGHSZ at salinity of 15‰. Although the average depth of the calculated BGHSZ fits with the average depth of the BSR, the direct relation along the profile shows significant variations and discrepancy between observed and calculated BGHSZ.

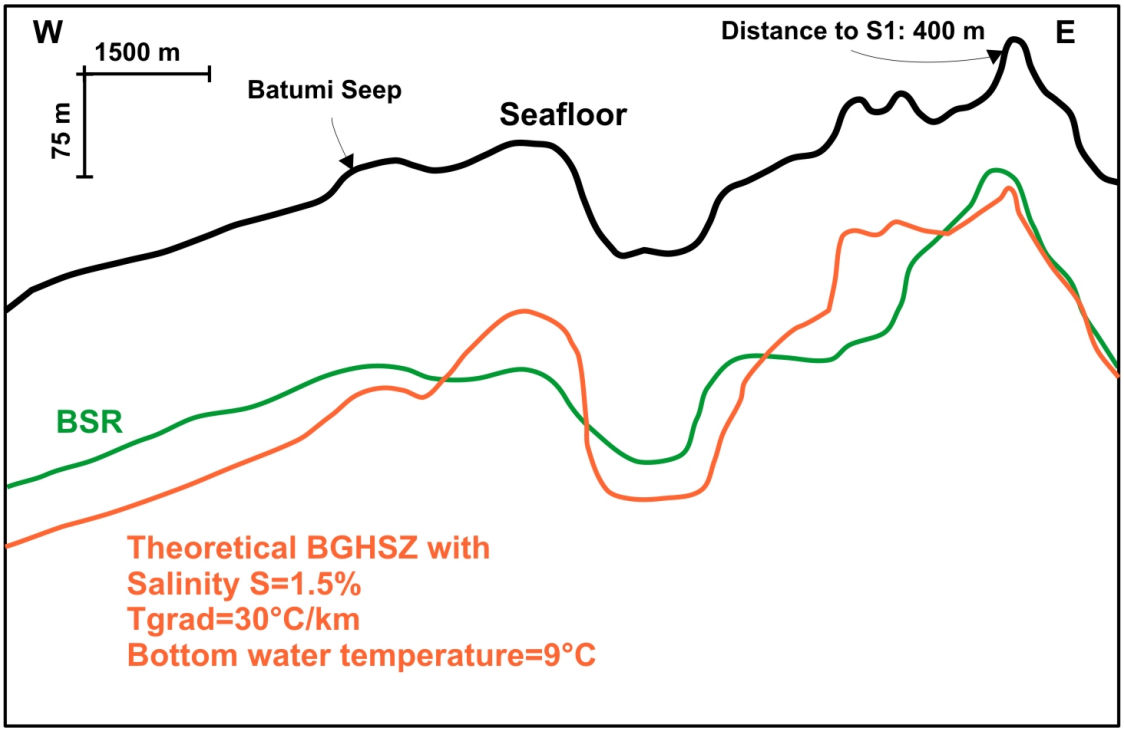

Figure 4.13: *Line drawing of line GeoB05-062 with the theoretical depth of the BGHSZ at a salinity of 15‰ and the depth of the BSR on the seismic section. The graph shows great depth variations between calculated and observed BGHSZ along the profile.*

The theoretical BGHSZ reflects the seafloor topography, but the BSR shows anomalies and does not exactly mimic the seafloor as expected. Thus, the BSR partly is located at shallower depth despite increased water depth. The BSR strongly fluctuates around the theoretical curve and partly the BSR is located above and partly beneath the theoretical BGHSZ. Only at the easternmost part of the line, the observed and calculated depths show

a good match (Fig. 4.13). This discrepancy indicates local variations of the factors influencing the BGHSZ, most probably in temperature and salinity, along the Kobuleti Ridge. The low average depth of the BSR in general suggests low salinity of about 15‰, but the profile suggests that the BSR is locally uplifted or shifted downward due to changes in salinity and/or temperature. However, we can only speculate about possible reasons for the BSR depth variations without heat flow measurements and a limited number of pore water analyses.

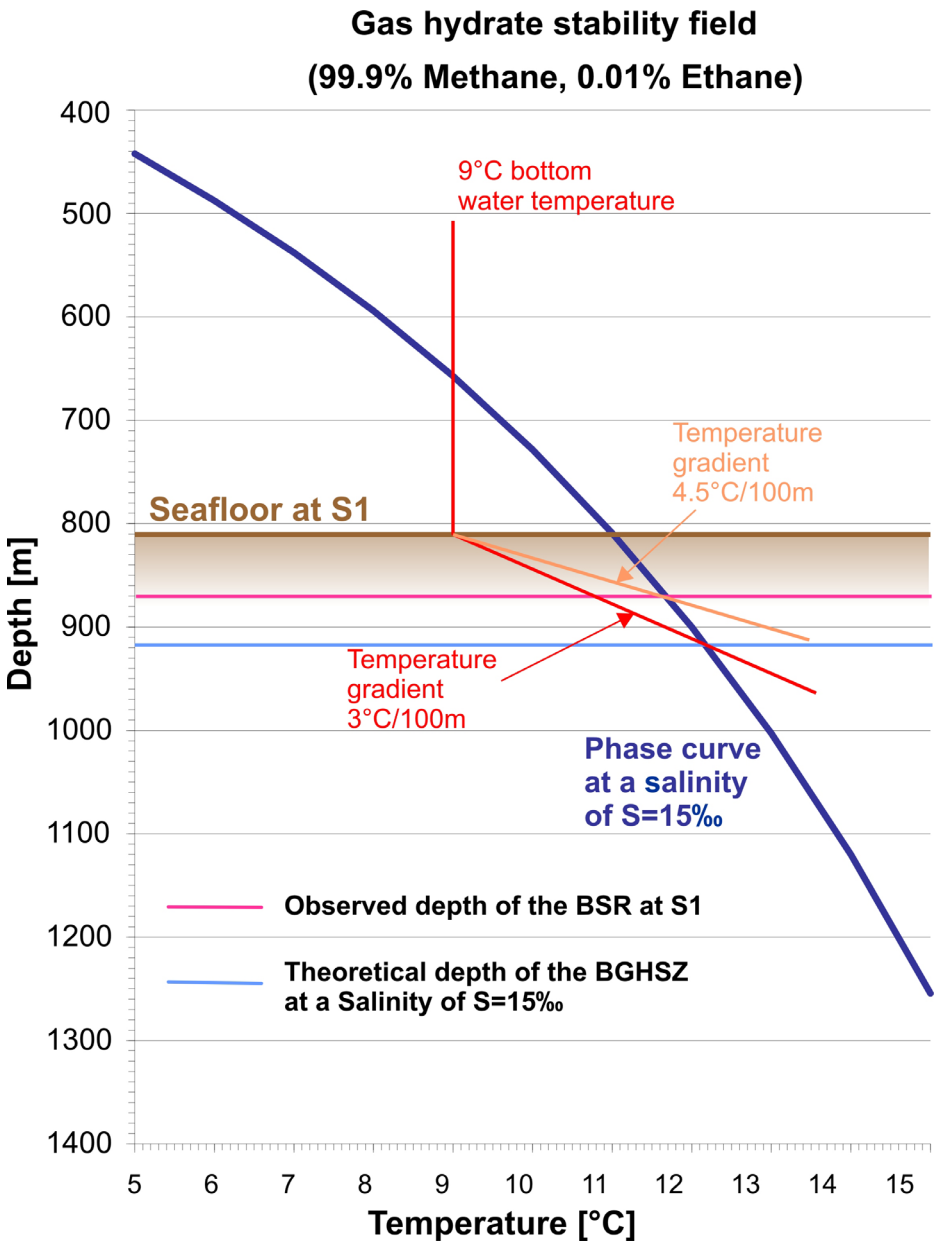

Figure 4.14: *Gas hydrate stability diagram with a salinity of 15‰ together with the calculated BGHSZ at a water depth of 810 m (=S1) (according to Sloan, 1998; with 9°C bottom water temperature and a geothermal gradient of 30°C/km). From the depth of the BSR at S1, the new temperature gradient of 45°C/km was calculated.*

The BSR is located shallower than the theoretical BGHSZ beneath the Batumi Seep and near the potential seep S1 (Fig. 4.13), which might indicate that increased temperature due to the rise of warm fluids uplifted the BGHSZ. North of the Batumi Seep and south of S1, the BSR is shifted downward to abnormally low depth with respect to the water depth, which may reflect reduced temperature at greater distance to the seeps. The most pronounced and abrupt uplift of the BSR to 74 ms TWT bsf (~60m) is found in direct vicinity to the potential S1 seep, which is located 7 km eastward of the Batumi Seep (Figs. 4.4, 4.11). This might reflect significantly increased heat flow leading to an upward shift of the BGHSZ. Assuming a salinity of 15‰, an increased temperature gradient of 45°C/km would uplift the BGHSZ from the expected 110 m for about 50 m to the observed depth of 60 m (Fig. 4.14). Although fluid flow is indicated by an acoustic void zone beneath the seafloor, no indications for gas discharge, such as irregularities or reduced reflection amplitudes, are observed on the seafloor, suggesting that most of the gas is probably trapped close to the subsurface below the BSR or within the GHSZ due to the absence of qualified migration pathways to the seafloor. Faults seem to act as migration pathways for the Batumi Seep Area, but such faults were not identified for the potential S1 seep site (Fig. 4.4).

Bright Spots are high amplitude reflections, which generally are interpreted to result from high-impedance contrasts between gas-poor strata and gas-rich sediments beneath. The presence of free gas in sediments significantly decreases the sediment velocity, thus Bright Spots usually are characterized by inverse polarity (e.g. Max, 1990). In the study area Bright Spots are widespread at different depths (Fig. 4.11), suggesting that gas accumulation is associated with fluid migration from greater depth. Bright Spots were found at and beneath the approximate depth of the BGHSZ (calculated with reduced salinity of 15‰) and can be distinguished into two depth zones. Numerous Bright Spots were observed at about 200 ms TWT bsf coinciding with the average depth of the BSR. These Bright Spots are related to the ridges and dominate at the westernmost part of the Kobuleti Ridge in the surrounding of the Iberia and Pechori Mound, as well as near the potential seeps S1-S3. Additionally some Bright Spots at similar depth level were observed at the northern Ridges and on the eastern Kobuleti Ridge in elongation to the BSR. The latter are interpreted to represent the fragmentary continuation of the BSR (Fig. 4.11). Thus, we speculate that all Bright Spots located in the depth range of the BSR probably represent the BGHSZ, but we are aware that gas could also be stratigraphically trapped by impermeable layers located near the depth of the BGHSZ. In this case we would expect that the Bright Spots are bound to a stratigraphic layer. The lateral variability of the reflection characteristics and disruption of strata by diapiric structures make it difficult to trace reflectors. On line 056 (Fig. 4.3) two Bright Spots located close together definitely occur within different stratigraphic units. Moreover, these Bright Spots are not related to a strong

reflector, which might indicate the boundary between different permeable horizons, but occur within a zone of low reflectance indicating homogeneous strata. This contradicts with the theory that the Bright Spots are lithologic gas traps. On the other hand, discordant layering of the Bright Spots would directly evidence that they are related to the stability field of gas hydrates, as the phase boundary of gas hydrate runs along isotherms (e.g. Shipley et al., 1979; Dillon & Paull, 1983). Most Bright Spots occur within chaotic reflection pattern and have small dimension, thus the relationship between the Bright Spots and the surrounding strata could not be clearly identified. Several Bright Spots seem to crosscut strata (Fig. 4.5), but on the eastern Poti Ridge a Bright Spot clearly is conform to strata (Fig. 4.6). Thus, with reflection seismic methods alone, the specific cause of the Bright Spots remains uncertain. As the Bright Spots are not bound to a stratigraphic layer and due to their constant depth at the average depth of the BSR with low depth variations of maximum 80 ms TWT, we suggest, that the Bright Spots reflect patches of a BSR, formed nearby seeps and mounds, where upward fluid migration provides enough gas to form gas hydrate. As intensively discussed for the BSR above, the depth variations of the Bright Spots might then be explained by variations in temperature or salinity as well. In the Sorokin Trough, Bright Spots, which have been related to the base of gas hydrate stability zone, are interpreted to be associated with locally fluid flow near mud volcanoes (Wagner-Friedrichs et al., in review). The Bright Spots off Batumi also are correlated to seeps associated with high fluid flow. The distribution of the Bright Spots and the BSR shows that all seeps are linked to shallow gas accumulation (Fig. 4.11).

Bright Spots located beneath the BGHSZ at depths between 300 and 1000 ms TWT bsf are most likely related to different gas charged horizons reflecting an alternation of porous sediments acting as potential gas reservoir and more impermeable sediments representing seals for the ascending gas. These Bright Spots have increased lateral dimension and are concentrated at the canyons and canyon walls while the upper Bright Spots are limited to the ridges (Fig. 4.11). This indicates that fluid migration pathways are associated with the ridges facilitating fluid upflow into the GHSZ. At the canyons, Bright Spots occur where strata is horizontal or onlaps diapirs, thus gas cannot migrate further upward along permeable layers and is trapped at greater depth (Figs. 4.4-4.6).

No Bright Spots occur within the gas hydrate stability zone, but additional strong reflection patches are observed directly beneath the seafloor at the Batumi Seep. High reflectance might be caused by free gas charged sediments alternating with gas poor impermeable horizons trapping gas charged zones (Holbrook, 2001); thus the reflection patches should be attributed to Bright Spots. But, high amplitude reflection anomalies within the GHSZ might also represent gas hydrate, which would lead to enhanced impedance contrast to the surrounding sediments, as sediments with high gas hydrate saturation are

characterized by significantly increased sediment velocity generating enhanced reflectance (e.g. Holbrook et al., 2002). Similar patchy reflections at seep sites were observed at the upper 40 m bsf on the southern summit of Hydrate Ridge (ODP Leg 204). The reflection patches could be attributed to massive gas hydrates with concentrations of up to 30% of the pore space, generated due to focused fluid flow (e.g. Tréhu et al., 2006). Torres et al. (2004) modeled that abundant supply of free gas is required to form such massive gas hydrates, which lead to the generation of brines when salts are excluded as hydrate forms. Another explanation for strength reflectance could be authigenic carbonate precipitations, which are common at gas seeps formed due to focused fluid flow by anaerobic oxidation of methane (e.g. Greinert et al., 2001). Observed gas bubbles at the Batumi Seep show the presence of free gas, but within the sediments free gas concentration probably is not high enough to generate Bright Spots, as gas trapped and accumulated within the GHSZ would be transformed into gas hydrate. Thus, we propose that the reflection patches beneath the buildup of the Batumi Seep directly reflect the presence of gas hydrates. Hence, the reflections have not been attributed to the Bright Spots. This is confirmed by coring and side-scan sonar data of the Batumi Seep: Samples at the Batumi Seep are significantly enriched in gas hydrates (unpublished data), and different high backscatter intensities observed at the Batumi Seep were interpreted by Klaucke et al. (2006) to reflect carbonate precipitations and concentrations of gas hydrate in the uppermost sediment coverage (Fig. 4.10). Thereby, gas hydrates cover the whole area of the buildup characterized by the reflection patches on the seismic data. Several small zones additionally contain carbonates. Gas hydrates and carbonates are characterized by different backscatter images on the side-scan data, but cannot be distinguished on our seismic data. The intensive gas hydrate concentrations may have been formed due to focused fluid flow towards the Batumi Seep.

The origin of the gas at the seeps off Batumi might be related to: (1) in situ gas generation, (2) dissociation of gas hydrates and (3) gas/fluid migration from greater depth. Assuming that in situ gas generation by microbial transformation of organic matter is constant within the study area, the local and patchy distribution of gas accumulation at different depths indicates that fluid/gas discharge predominantly is supplied by upward fluid migration from sources at greater depth. Gas geochemistry of the Batumi Seep show that the expelling fluids probably have a thermogenic source mixed with biogenic gas (Blinova et al., 2005; Klaucke et al., 2006). Gas seeps are usually related to focused fluid flow (Judd, 2003), which is bound to the ridges in the study area and might initiate the dissociation of gas hydrates, leading to further dewatering (Suess et al., 1999), which forces fluid venting (Greinert et al., 2001).

4.6.3 Role of diapirism for fluid migration pathways and for the evolution of the complex canyon-ridge system off Batumi

Compressional deformation in the south-eastern Black Sea due to the thrusting of the Greater Caucasus in the north and the Adjara Trialet Fold Belt in the south lead to the protrusion of several W-E trending diapiric structures within the clays of the Maikop Formation. The thick argillaceous Maikop Formation deposited in Oligocene-Lower Miocene time in the Black and Caspian Sea, as well as in the surroundings, is considered to be the main hydrocarbon source rock in this region. In the south-eastern Black Sea the Maikop Formation is located at a depth of 1-4 km (Tugolesov et al., 1985; Banks et al., 1997; Starostenko et al., 2004). Offshore Batumi, the diapirs are trending along the ridge structures (Tugolesov et al., 1985). On our seismic data several diapiric structures have been identified, namely at the R1, Kobuleti and Adjara Ridge (Figs. 4.3-4.6), but the limited signal penetration in general and the high gas content, as observed beneath the Kobuleti Ridge, inhibit to identify structures beneath 0.8-1 s TWT bsf.

The direct link between the diapirs and the ridge structures indicates that the diapirism significantly has influenced the development of the canyon-ridge system off Batumi. We think that the growth of the diapirs have guided the course of the canyons. The canyons off Batumi are dominated by erosive features, which indicate erosive down cutting by turbidity currents as found for many canyon systems (Stow and Myall, 2000). The protrusion of diapirs bulges the sediments above, which leads to subsidence nearby generating elongated depressions between the diapiric structures. The depressions act as preferred pathways for turbidity currents. The erosive power of turbidity currents formed proto canyons. Once these proto canyons were formed, subsequent turbidity currents deepen and widen the canyon. Due to missing bathymetric coverage close to the coast we cannot trace the canyons to sources on land (such as rivers) but high terrigeneous sediment input from land is the most likely source for frequent turbidity activity. Recently, there are no large river systems onshore in the range of the study area, but several smaller rivers in Georgia flow into the Black Sea between Poti and Batumi (Google Earth vs. 4.0.4416 beta, 2006), which might have been more dynamic and active at past periods of sea level low stand during last glacial periods, hence supplying large amounts of sediments to the slopes. The source provinces of the Georgian rivers are the glaciers of the Caucasus. Recently, the total volume of river sediment transport into the Black Sea represents 11100 m^3/a, of which 6700 m^3/a are transported on to the slope (Jaoshvili, 2000); thus sediment transport probably is sufficient to generate periodic turbidites on the slope.

The diapiric uplift and the resulting over-steepen of the canyon flanks directly affect their stability. Faults developed at the flanks of the ridges (Figs. 4.3-4.6) act as preferred gliding planes for slumps and slides towards the canyon floor, which is a common process

for canyon widening. Slumps and slides constitute an important component of the canyon deposition in addition to deposits from turbidity currents. Several slump/slide blocks and scars occur at the canyon walls, which partly could be associated with faults (Figs. 4.3-4.5). Due to the growth of a diapir the sediments at the southern flank of the Adjara Ridge have been tilted southward and at the northern side a large slide event occurred (Fig. 4.4). Faults observed at the flanks without slump scarps, e.g. at R2 Ridge (Figs. 4.3, 4.6) and at Pechori Mound (Fig. 4.5), indicate that faults were present first and were not caused by slump events, reflecting that fault-controlled processes play an important role in the development of the canyons. The erosion of the canyon flanks by the passage of large turbidity currents can also destabilize the wall sediments by over-steepening, leading to slumps, slides and debris flows (McCaffrey and Kneller, 1998). Gas hydrate dissociation due to slope failure might play an important role for gas seeps at the flanks of the ridges, such as the potential seep site S2, located at the flank of the Poti Ridge, and the Pechori and Iberia Mounds at the edges of the Kobuleti Ridge (Figs. 4.3, 4.5).

The Natanebi and Central Canyon, as well as the eastern part of the C2 Canyon are interpreted to represent recently active canyons, indicated by the high amplitude reflections at their floors (Figs. 4.3, 4.4, 4.6). These discontinuous reflectors most likely represent coarse grained sediments with increased content of terrigeneous material derived at the base of turbidity currents with origin on the shelf or the upper slope. Stratified reflections are absent, which indicates the lack of continuous hemipelagic sedimentation, most likely due to sediment transport through the canyons in the younger past. The central canyons are dominated by continuous reflectors, representing most probably hemipelagic sedimentation, partly disrupted by chaotic and acoustic transparent facies with thickness of about 30-40 m (Figs. 4.3-4.5), locally increasing to 90 m, e.g. at the slump at the Northern Canyon (Fig. 4.3). This seismic facies indicates homogeneous and hemipelagic sedimentation at long periods of canyon inactivity interrupted by slumps from the canyon walls or fine grained distal turbiditic deposits. At these canyons slope failures probably are the main processes for canyon deposition and widening. Only the C1 Canyon shows evidence for recent activity. At its landward potion, the C1 Canyon is characterized by a well pronounced axial v-shaped incision flanked by acoustically homogeneous terraces (Fig. 4.6). We suggest that the terraces represent a slump event, which blocked the active canyon. Ongoing turbidity activity incised the slump block, but turbidites appear not to be very dynamic as no evidences for recent turbidity activity is observed on the profiles further downslope. The sandy turbiditic deposits at the active canyons represent potential gas reservoirs and interbedded fine grained and hemipelagic sediments might act as a potential seal for gas. At active canyons with assumed coarse sediments, Bright Spots indicate the presence of free

gas, while at the inactive canyons with hemipelagic sediments Bright Spots are rare (Figs. 4.3, 4.4, 4.6).

Diapirism influences fluid migration pathways, as fractures and over-steepened flanks created during the growth of the diapirs represent potential fluid migration pathways controlling the distribution of the gas seeps associated with the ridge structures. Beneath the Batumi Seep no diapir has been observed in our seismic data, which probably is due to the limited signal penetration. However, as Tugolesov et al. (1985) described a diapiric ridge trending along the Kobuleti Ridge perpendicular to the slope, we assume that the diapiric structure observed at the westernmost Kobuleti Ridge continues beneath the Batumi Seep. Therefore, on the example of the Batumi Seep, we suggest a model, how the diapirism might control the canyon-ridge system and influence fluid migration pathways (Fig. 4.15).

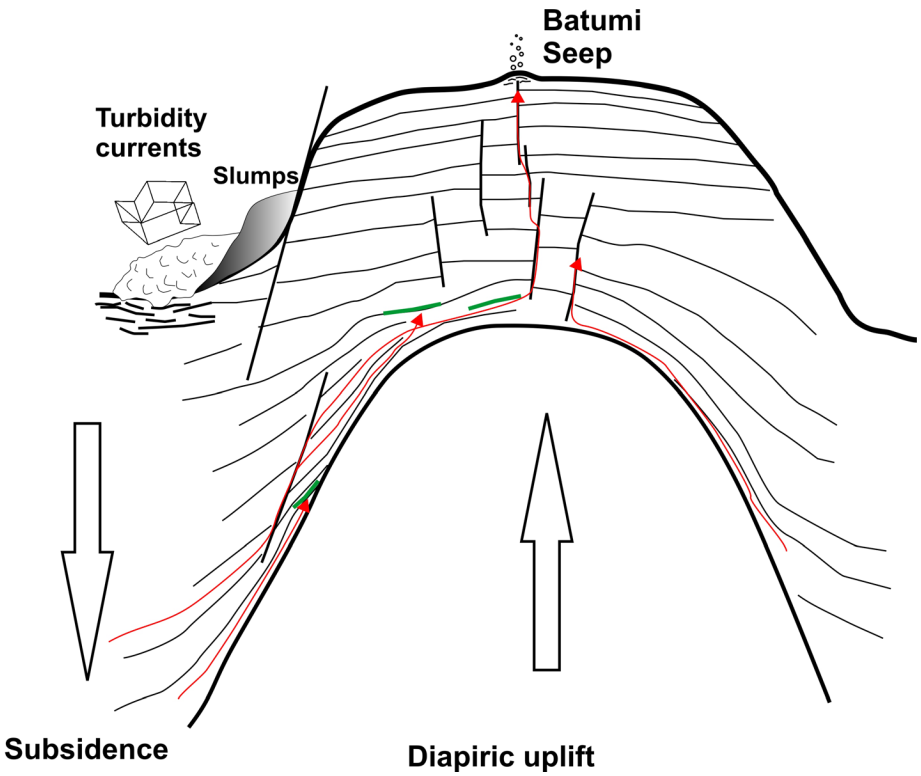

Figure 4.15: *Schematic sketch of the interactions between different geological processes within the study area, on the example of the Batumi Seep: the diapirism primarily controls the evolution of fluid migration pathways at the flanks and tops of the grown diapirs. Depressions between growing diapirs guide the courses of the canyons by generating weakness zones and synclines acting as preferred pathways for turbidity currents. Faults are potential glide planes for slides and slumps.*
The green lines represent Bright Spots; the red arrows mark potential fluid migration pathways.

Upward bulged sediments at the flanks of the diapirs allow fluid migration parallel to strata along more permeable horizons towards the top of the diapirs. Faults develop at the flanks of the diapirs due to over-steepened sediments; these faults are potential pathways for focused upward fluid migration. The parallel bulged layered sediments above the diapir generally inhibit upward fluid migration, thus upflow of fluids/gas occurs where faults developed during the diapiric growth above. Additionally, the evolution of faults and upward fluid migration probably are forced by the N-S oriented tectonic loading of the thrust belts. Bright Spots often observed nearby diapirs support that fluid migration is linked to the diapirism. Simultaneously faults at the canyon flanks control the slope stability and may induce slope failures filling and widening the canyons. Turbidity currents are considered to be the main erosional process forming the canyons. The course of the currents is guided by depressions evolved between the growing diapirs.

4.7 Conclusions

The canyon-ridge system offshore Batumi is directly controlled by the growth of diapiric structures, which are located beneath the ridges. Depressions evolved due to subsidence between the diapirs guided turbidity currents, which cut the canyons deeply into pre-existing strata. Faults develop at the canyon flanks during the diapiric uplift. The faults directly impact the slope stability as they act as gliding planes for slope failures.

Faults developed at the flanks and above the diapirs as well as upward bulged strata present potential fluid migration pathways, hence controlling the distribution of fluid migration towards the seafloor and discharge offshore Batumi. Seeps are therefore associated with the ridges. The tectonic loading of the thrust belts in the north and the south is believed to be the main driving force for upward fluid migration. Our seismic data reveal four seeps and three potential seeps. The largest and most active seep is the Batumi Seep, which is located in 870 m water depth on the Kobuleti Ridge. The Batumi Seep is characterized by a small buildup with a height of 10 m and high amplitude reflection patches directly beneath the seafloor, interpreted to represent either gas hydrates or carbonate precipitates. Gas emissions at the Batumi Seep are related to fluid migration along near vertical faults. Fluid migration is imaged as narrow vertical acoustically void zones in the seismic data. Based on so-called gas columns towards the seafloor, three potential seep sites have been determined at two ridges, but only one of these sites probably is active. Bright Spots are widely distributed in the study area, indicating local gas accumulation at different depth. Gas accumulations are probably related to upward fluid migration from greater depth. Coarse grained canyon fill facies from turbidites, dominating at the northern and southern canyon floors, might act as near surface gas reservoirs as well. A BSR trends along the Kobuleti Ridge, but BSRs lack in the remaining study area, indicating the

presence of high permeable gas/fluid migration pathways towards the Kobuleti Ridge. The low average depth of the BSR could be explained by low salinity of only 15‰ due to either the limnic period of the Black Sea in glacial time or the upflow of low salinity fluids. Discrepancy between the depth of the BSR with respect to the theoretical BGHSZ indicate local variations of temperature or/and salinity. Numerous Bright Spots could be attributed to the depth of the BGHSZ and thus are interpreted to represent patches of the BSR. Potential vents are related to these Bright Spots, indicating that shallow gas reservoirs control seepage off Batumi. Only the Pechori and Iberia Mound as well as the Colxheti Seep are interpreted to be formed by upward transport of mud, most likely sourced in the diapiric structures beneath. The material flux at the other seeps, i.e. Batumi, and the potential seeps S1, S2, and S3, is probably low.

4.8 Acknowledgements

We thank the participants of the TTR-15 cruise as well as the captain and the crew members of RV Professor Logachev for the great assistance and cooperation in data acquisition. This cruise was carried out within the METRO project, funded by the Federal Ministry of Education and Research (BMBF) in the frame of the Geotechnologien Program (03G0604A).

5 Summary and outlook

The Black Sea contains thick gas rich sediments in an anoxic environment providing best conditions to study seafloor seepage, which is widely distributed along the continental slopes of the Black Sea. In two areas of the Black Sea, the Sorokin Trough off Crimea and the continental slope off Batumi (Georgia), the distribution, structure and evolution of two different vent systems and their relationship to near-subsurface structures have been investigated by means of high resolution multichannel seismic and additional acoustic data. The interpretation of the seismic data shows that the distribution of seafloor seepage in both regions is controlled by fluid migration along permeable pathways associated with diapiric uplift in the subsurface. However, morphological structures, types and evolution styles of the seepage systems in these areas significantly vary. In the Sorokin Trough, seepage is expressed by intensive material upflow and the formation of mud volcanoes; at the continental slope off Batumi gas seeps with low material flux dominate. This thesis provides new insights into the distribution and structure of different mud volcano types in the Sorokin Trough and seep structures off Batumi. The evolution of the mud volcanoes in the Sorokin Trough and the seeps off Batumi is directly linked to faults, controlling fluid migration; faults are well imaged on the seismic data below and in the direct vicinity of the seepage sites. Faults primarily occur above and at the flanks of the diapirs. Hence, the development of the faults is considered to be related to the diapirism. The evolution of the mud volcanoes is directly bound to the near-surface diapirs; seismic data show that the mud volcanoes are located directly above or at the edges of E-W- trending diapiric ridges associated with the Maikop Formation. The link between mud volcanoes, diapirs and fault systems well imaged on the seismic data suggests that the mud volcanoes are fed from the diapirs by fluid migration along faults. The fluids probably are sourced within the Maikop Formation, released at great depth during smectite-illite transformation. Different depositional environments in the Sorokin Trough influence the sediment permeability and hence affect the evolution mechanism of the mud volcanoes in the Sorokin Trough, which is reflected in the high morphological variability of the mud volcanoes.

In the Sorokin Trough, 25 mud volcanoes have been analyzed and characterized based on high resolution multichannel seismic and Parasound sediment echosounder data collected during the Meteor cruise M52/1. With exception of the Kazakov mud volcano, all mud volcanoes are associated with near-subsurface mud diapirs. The protrusion of the diapiric ridges, mainly striking in the W-E direction, resulted from the N-S oriented convergence between the Crimean Mountains in the North and the buried Tetyaev and Shatsky Ridges in the South. Deep single channel seismic data collected by the SSC “Yuzhmorgeologia” of Gelendzhik in 1979 reveal that the diapirs are related to the Maikop Formation, a prominent thick clayey Oligocene-Miocene series with great hydrocarbon

source potential deposited in the Black Sea and surrounding areas. The mud volcanoes are clustered north of the buried Tetyaev Rise and Shatsky Ridge, as the ridges act as barrier for lateral fluid migration resulting in over-pressured fluids, preferentially released at faults. The deep seismic data reveal numerous faults within and beneath the Maikop Formation reaching into the Pliocene and Quaternary sediments. Near-surface faults develop during the diapiric uplift primarily above and at the over-steepened flanks of the diapirs. Fluid migration from great depth along deep and near-surface faults controls the evolution of the mud volcanoes. The mud volcanoes highly vary in morphology and size, and could be catalogued into four morphological types: (1) cone-shaped structures, (2) collapsed depression structures, (3) collapsed depression structures with one or more cones inside, and (4) one flat-topped structure. The great morphological variability reflects different driving mechanisms depending on the availability of permeable fluid migration pathways and the depositional environment. Three areas with different sedimentologic and structural environments could be distinguished, which are dominated by specific morphological types of mud volcanoes. The data show a change of violent eruptions creating collapsed depression structures in the west where hemipelagic sediments dominate to quite mud extrusions forming cone-shaped mud volcanoes in the East, which are intensively influenced by homogeneous fan deposits of the Palaeo Don-Kuban Fan. In Area 1, located in the western Sorokin Trough, collapsed depression structures predominate, which are formed by explosive eruptions due to over-pressured fluids. Low permeable horizons within the hemipelagic sediments act as traps for rising fluids leading to increased pore pressure and over-pressured fluids. Seal failure results in violent eruptions and sudden release of fluids/gas, forming the collapsed structures. Bright Spots widely distributed in this area nearby mud volcanoes indicate the presence of trapped gas. The homogeneous Palaeo Don-Kuban Fan sediments at the central plain (Area 2) and the eastern portion of the Sorokin Trough (Area 3) are characterized by increased permeability leading to reduced pore fluid pressure. This setting results in more quiet mud extrusions reflected by cone-shaped structures. In Area 2, high mud flow rates along faults with great offsets of about 20 m lead to the largest mud volcano structures in the Sorokin Trough: the Nioz and Kazakov mud volcano with dimensions of up to 2000 m in width and about 100 m in height. The small cone-shaped mud volcanoes observed in Area 3 indicate less frequent mud extrusions or low mud flow rates. In the easternmost Sorokin Trough, the mud volcanoes are concentrated above a morphological high, which is underlain by a diapiric ridge. Stratigraphically controlled fluid migration along dipping strata towards the high might supply mud extrusions, which results in moussy and fluid rich eruption products.

A new 3D seismic dataset across the Sevastopol mud volcano in the western Sorokin Trough provides detailed information about the three dimensional structure of a

collapsed mud volcano structure and its spatial relationship to the subsurface structures in the Black Sea for the first time. The analyses show that faults acting as potential fluid migration pathways play an important role for the evolution of the mud volcano. The Sevastopol mud volcano is characterized by an 1100 x 1700 m large depression with a depth of about 25 m, including three NNW-SSE trending mounds of asymmetrical shape with heights up to 35 m. The Sevastopol mud volcano is located above a syncline developed between two diapiric ridges. The interpretation of the data shows that fluid migration along the deep fault system developed during the growth of the diapirs between the ridges feds the mud volcano from the diapiric ridges. The well bedded hemipelagic sediments of the basins surrounding the mud volcano inhibit significant vertical fluid migration and provide suitable traps for gas/fluids. An evolution model established for the Sevastopol mud volcano suggests that trapped over-pressured fluids induced a violent explosion after seal failure, leading to sudden release of gas and mud, and creating the collapsed depression of the Sevastopol mud volcano. The destroyed sediments fell back into the depression. Permeability of these sediments is increased allowing subsequent effusive fluid and mud flow extrusion, which formed the cones inside of the depression. High amplitude reflections (Bright Spots) indicate the accumulation of free gas above and at the flanks of the diapiric structure. The depth of the Bright Spots almost coincides with the approximate calculated depth of the BGHSZ. As the depth of the Bright Spots is constant along the trend of the diapiric ridge and only slightly increases at its northern flank, we suggest that the Bright Spots represent the BGHSZ. Warm fluids rising towards the mud volcano might explain the shallower depth of the Bright Spots with respect to the BGHSZ. Increased temperatures then might have uplifted the BGHSZ into the depth of the Bright Spots. Assuming that the Bright Spots represent the BGHSZ, the average depth of the Bright Spots (270 mbsf) suggest an increased temperature gradient of 37°C/km. The depth variations of the Bright Spots indicate that the BGHSZ is strongly controlled by fluid flow. Changes of the temperature gradient from 29°C to 52°C/km would explain the observed variations in depth. Gas and gas hydrates are suggested to occur locally where strong fluid flow occurs directly linked to the mud volcanism. We propose that gas hydrates are present above one of the diapric ridges and in the surrounding of the mud volcano and its feeder channel. Gas/fluids might migrate laterally from the feeder channel into the surrounding strata. Permeable upward bulged layers act as pathways to the diapiric top where gas/fluids are trapped and imaged as Bright Spots. Microfaults above the diapiric ridges act as fluid migration pathways into the GHSZ. The activity of the mud volcano probably is controlled by episodic fluid flow, which inhibits the generation of a BSR.

A new high resolution seismic dataset off Batumi (Georgia), acquired during the TTR-15 cruise in June 2005, reveal numerous deep water gas seeps in a complex canyon-

ridge system. The development of the canyon-ridge system off Batumi is attributed to the protrusion of diapiric structures associated with the ridges. Depressions developed between growing diapirs and guided turbidity currents, which preferentially used pre-existing morphological depressions. These depressions were deepened by the erosive power of the turbidity currents. Faulting and over-steepening of the canyon flanks is forced by the diapiric uplift. Both, faulting and over-steepening, directly affects slope stability and induces slope failures, such as slumps and slides, which are a common process of canyon widening. Numerous gas seeps occur at water depths of 850-1200 m on the top or flanks of the ridges. The distribution of the seeps is controlled by fluid migration along pathways associated with the diapiric uplift beneath the ridges. Faults at the flanks and above the diapirs, as well as over-steepened strata at the diapir flanks provide potential fluid migration pathways towards the seafloor. Thus, fluid migration and seepage is focused towards the ridges. Four seepage sites and three potential seep locations were identified on the seismic data. The Batumi Seep, the largest and most active seep, is located in 870 m water depth on the Kobuleti Ridge. It has only a low seafloor expression with a height of 10 m. High amplitude reflection patches directly beneath the seafloor are interpreted to represent either gas hydrate deposits or carbonate precipitates, most likely formed due to focused fluid flow towards the vent site. Fluid migration beneath the Batumi Seep is fault-controlled. The potential seep sites were assigned by near-subsurface gas columns reaching towards the seafloor on the Kobuleti and Poti Ridge. Only one of these sites is believed to be active, as the gas column distorts the seafloor reflection and a small pinnacle is built. Widely distributed Bright Spots at different depth levels indicate local gas accumulation related to upward fluid migration from greater depth. All seeps are related to shallow gas accumulation trapped near diapiric structures. Gas/fluid migration appears to be focused towards the Kobuleti Ridge, as high gas and gas hydrate occurrences are indicated by a BSR trending along the Kobuleti Ridge. The depth of the BSR is located 40 m below the theoretical depth of the BGHSZ for a methane-seawater system. The discrepancy in depth could be explained by abnormal low salinity pore fluids of only 15‰ shifting the BGHSZ downward to the observed depth of the BSR. The low salinity may reflect the limnic period of the Black Sea in glacial time or the upflow of low salinity fluids. Reduced temperature would downward shift the BGHSZ as well, but nearby vent sites, we rather would expect high than reduced temperatures. Thus, we calculated with a given temperature gradient of 30°C/km. The depth variations of the BSR with respect to the theoretical BGHSZ observed along the Ridge might be explained by local changes in temperature or salinity. BSRs lack in the remaining study area, but Bright Spots at same depth are suggested to represent patches of the BSR formed where sufficient gas is supplied by local fluid flow.

This thesis provides new insights into morphology, distribution and evolution of seafloor seepage structures at two different vent systems of the Black Sea. The investigations show that seepage is related primarily to fluid migration along faults developed during the growth of diapiric structures. However, several questions remain unsolved. Although seepage in both areas is associated with near-subsurface diapiric ridges, only the Sorokin Trough is characterized by high material flux resulted in the formation of numerous mud volcanoes. In contrast, vent sites off Batumi are dominated by gas seeps with low material flux and no mud volcanoes are known up to now. It can only be speculated about the differences concerning the driving mechanism for material upward transport, such as the lack of extensive fault zones in the area off Batumi. Another explanation might be that the mobilization of mud in the Sorokin Trough is supported by intensive faulting at great depth within the Maikop Formation, hence facilitating fluid migration through the diapirs into the sediments above and to the seafloor. Offshore Batumi, fluid migration rather appears to occur along strata and faults in the surrounding of the diapirs than through the diapirs. Moreover, the diapirs off Batumi are located at greater depth, suggesting that stronger driving forces would be required to transport the mud towards the seafloor. As only few seismic profiles exist offshore Georgia further data coverage is needed to obtain the detailed distribution of the subsurface structures and to investigate the direct link between fluid migration pathways, diapiric structures and distribution of seeps in this area. In the Sorokin Trough different deposition regimes affect the eruption style and the morphological shape of mud volcanoes. It remains unclear, whether this can be contributed to the seeps off Batumi as well, as data coverage is too low. The seeps of Batumi are characterized by low morphological expression and there might be furthermore seeps not yet identified. Hence, further profiling with hydroacoustic methods is needed to identify possible seep locations by the detection of flares, seafloor backscatter anomalies and/or amplitude anomalies in the subsurface indicating vent sites. Although gas hydrates have been sampled in both areas, a BSR has only been identified on the Kobuleti Ridge off Batumi. Bright Spots at the depth of the BGHSZ are attributed to the stability field of gas hydrates. This suggests that local gas and gas hydrate accumulation related to focused fluid migration at vent sites and mud volcanoes, although gas hydrate can be present, even when a BSR lacks. The depth bsf of the BSR off Batumi is exceptionally high, but possible explanations remain speculative. Further investigations should include intensive temperature and pore water measurements and analyses to prove whether changes in temperature or salinity fit with the depth of the BSR.

Studies in the Sorokin Trough show a great morphological variability of mud volcanoes and different evolution models are presented in this thesis. A remaining question is weather the mud volcanoes are recently active, which could not be concluded from our

seismic data. The Dvurechenskii mud volcano is well known to be an active seep, but what is about the other mud volcanoes? Intensive flare imaging by side-scan sonar and echosounder profiling across mud volcanoes, as e.g. collected across the Batumi Seep off Georgia, would show release of free gas bubbles and evidence active sites. Additionally, exact coring at mud volcanoes would be necessary, as well as video observation to observe free gas bubbles. Furthermore, heatflow measurements as at the DMV might indicate active seeps. All mud volcanoes are related to near subsurface faults, but closely spaced parallel seismic lines are needed to identify the spatial distribution and detailed relation of fault systems, diapirs and mud volcanoes. The fault system beneath the Sevastopol mud volcano is absent east of the mud volcano, but continues to the West. Due to the limited extension of the 3D survey it remains open how far the fault can be traced westward, and whether the faults at the M3 and M4 mud volcano belong to the same fault system. Based on the 3D seismic studies Bright Spots near the Sevastopol mud volcano are interpreted to represent the upward shifted BGHSZ due to rise of warm fluids and gas hydrate deposits were suggested to be present above. Only few cores exist for the Sevastopol mud volcano, which did not contain gas hydrates but presence of gas hydrate might be overlooked. Locations of expected gas hydrate occurrences could be selected from our seismic data, as e.g. above the Bright Spots north of the Sevastopol mud volcano and at the margin of the depression. Nothing is known about the heat flow values at and in the surrounding of the Sevastopol mud volcano. Hence, well directed sedimentological, geochemical, and geophysical investigations of Sevastopol mud volcano would allow to prove the results presented in this thesis.

The Sevastopol mud volcano is the first mud volcano in the Black Sea detailed imaged by a three dimensional seismic survey. The 3D investigations give detailed information about the three dimensional spatial geometry of a collapsed mud volcano and its subsurface structures, such as faults acting as fluid migration pathways. The studies allowed drawing conclusions on the evolution of such type of mud volcano. For a better understanding of the factors influencing the distribution and evolution of the different mud volcano types leading to the great morphological variability observed, as well as to obtain the geometrical relationships to subsurface structures, e.g. diapirs and fluid migration pathways, additional 3D surveys across other mud volcano types in the Sorokin Trough would be useful. Interesting mud volcano structures would be the cone-shaped Istanbul mud volcano, the DMV, which is a very active mud volcano with flat top, and an additional collapsed structure. Additionally to the multichannel reflection seismic data, in the 3D area across the Sevastopol mud volcano, an OBS/OBH dataset was recorded simultaneously. From this data, a velocity model will be calculated at the Leibniz Institute of Marine Sciences (Kiel). A combination of the amplitude analyses from the multichannel seismic data and the

velocity information from the OBS/OBH data would enable precise detection of gas and gas hydrates, and would allow quantifying the gas hydrate content.

Presently, during the Meteor-cruise M72/3B proceeding in April 2007 in the frame of the METRO project, new data for a better understanding of the distribution and driving mechanisms of seep sites, as well as to investigate how the character of a vent system is related to fluid migration pathways and sedimentary and tectonic structures, will be collected in different areas of the Black Sea (Shatsky Ridge and Tuapse Trough offshore Russia, Batumi Seep Area offshore Batumi (Georgia), and Archangelsky Ridge offshore Samsun (Turkey)). Additionally to side-scan sonar and multichannel seismic profiling, sediment sampling with multi corer, TV grab and autoclave piston corer will complete the investigations. During this cruise, also shallow seeps will be investigated in order to study seeps at the transition zone of the GHSZ.

References

Akhmetzhanov, A.M., Ivanov, M.K. and Volkonskaya, A.V., 2002. The character of recent turbiditic sedimentation on the south-eastern Crimean slope and the Pallas Uplift. In: Mediterranean and Black Sea Turbidite Systems and Deep-Sea Fans - Bucharest 5-8 June 2002. CIESM Workshop Series n°17: 69-72.

Aloisi, G., Drews, M., Wallmann, K., and Bohrmann, G., 2004. Fluid expulsion from the Dvurechenskii mud volcano (Black Sea) Part I. Fluid sources and relevance to Li, B, Sr, I and dissolved inorganic nitrogen cycles. EPSL, 225: 347-363.

Aloisi, G., Pierre, C., Rouchy, J.M., Foucher, J.P., Woddside, J.M., and the Medinaut Scientific Party, 2000. Methane-related authigenic carbonates of eastern Mediterranean Sea mud volcanoes and their possible relation to gas hydrate destabilization. EPSL, 184: 321-338.

Anderson, A.L., and Bryant, W.R., 1990. Gassy sediment occurrence and properties: Northern Gulf of Mexico. Geo-Marine Letters, 10: 209-220.

Andreev, V., 1976. The Crimean and Caucasian foredeeps in the Sea (in Russian). Izvestiya Akad Nauk SSSR Ser Geol, 11: 130-133.

Ansted, D.T., 1866. On the mud volcanoes of the Crimea, and on the relation of these and similar phenomena to deposits of petroleum. Proc. R. Inst. G.B., IV: 628-640.

Bagirov, E., Nadirov, R., and Lerche, I., 1996. Flaming eruptions and ejections from mud volcanoes in Azerbaijan: Statistical risk assessment from the historical records. Ener. Expl. Exploit., 14: 535-583.

Bangs, N.L.B., Sawyer, D.S., and Golovchenko, X., 1993. Free gas at the base of the gas hydrate zone in the vicinity of the Chile triple junction. Geology, 21: 905-908.

Banks, C.J., Robinson, A.G., and Williams, A.P., 1997. Structure and regional tectonic of the Achara-Trialet Fold Belt and the adjacent Rioni and Kartli Foreland Basins, Republic of Georgia. In: Robinson, A.G. (ed) Regional and petroleum geology of the Black Sea and surrounding region: AAPG Memoir, 68: 331-345.

Behrmann, J.H., 1991. Conditions for hydrofracture and the fluid permeability of accretionary wedges. EPSL, 107: 550-558.

Belousov, V.V., Volvovsky, B.S., Arkhipov, I.V., Buryanova, B.V., Evsyukov, Y.D., Goncharov, V.P., Gordienko, V.V., Ismagilov, D.F., Kislov, G.K., Kogan, L.I., Kondyurin, A.V., Kozlov, V.N., Lebedev, L.I., Lokholatnikov, V.M., Malovitsky, Y.P., Moskalenko, V.N., Neprochnov, Y.P., Otisty, B.K., Rusakov, O.M., Shimkus, K.M., Shlezinger, A.E., Sochelnikov, V.V., Sollogub, V.B., Solovyev, V.D., Starostenko, V.I., Starovoitov, A.F., Terekhov, A.A., Volvovsky, I.S., Zhigunov, A.S., and Zolotarev, V.G., 1988. Structure and evolution of the erath's crust and upper mantle of the Black Sea. Bolletino di Geofisica Teorica ed Applicata, 30: 109-196.

Blinova, V., Ivanov, M., Sahling, H., and Bohrmann, G., 2005. Geochemical characteristics and origin of the hydrocarbon gases from seepage areas offshore Georgia and Turkey in the Black Sea (P317/4-cruise). International workshop on "Methane in sediments and water column of the Black Sea: Formation, transport pathways and the role within the carbon cycle". Sevastopol, Ukraine, May 17-22, 2005.

Blinova, V.N., Ivanov, M.K., and Bohrmann, G., 2003. Hydrocarbon gases in deposits from mud volcanoes in the Sorokin Trough, north-eastern Black Sea. Geo-Marine Letters, 23: 250-257.

Boetius, A., Revenschlag, K., Schubert, C.J., Rickert, D., Widdel, F., Gieseke, A., Armann, R., Jorgensen, B.B., Witte, U., and Pfannkuche, O., 2000. A marine microbial consortium apparently mediating anaerobic oxidation of methane. Nature, 407: 623-626.

Bohrmann, G., and Schenck, S., 2002. GEOMAR Cruise Report M52/1, MARGARSCH, RV Meteor, marine gas hydrates of the Black Sea. GEOMAR, Kiel.

Bohrmann, G., and Torres, M.E., 2006. Gas hydrates in marine sediments. In: Schulz, H.D., and Zabel, M.: Marine Geochemistry. Springer, GEOTECH-194: 481-512.

Bohrmann, G., Ivanov, M., Foucher, J.-P., Spiess, V., Bialas, J., Greinert, J., Weinrebe, W., Abegg, F., Aloisi, G., Artemov, Y., Blinova, V., Drews, M., Heidersdorf, F., Krabbenhöft, A., Klaucke, I., Krastel, S., Leder, T., Polikarpov, I., Saburova, M., Schmale, O., Seifert, R., Volkonskaya, A. and Zillmer, M., 2003. Mud volcanoes and gas hydrates in the Black Sea: new data from Dvurechenskii and Odessa mud volcanoes. Geo-Marine Letters, 23: 239-249.

Bouriak, S., Vanneste, M., and Saoutkine, A., 2000. Inferred gas hydrates and clay diapirs near the storegga Slide on the southern edge of the Voring Plateau, offshore Norway. Marine Geology, 163: 125-148.

Bouriak, S.V., and Akhmetjanov, A.M., 1998. Origin of the gas hydrate accumulations on the continental slope of the Crimea from geophysical studies. In: Henriet, J.-P. and Mienert, J. (eds) Gas Hydrates: Relevance to world margin stability and climate change. Geological Society, London, Special Publications, 137: 215-222.

Bray, C.J., and Karig, D.E., 1985. Porosity of sediments in accretionary prisms and some implications for dewatering processes. J Geophys Res, 90: 768-778.

Brooks, J.M., Kennicutt, I.I. M.C., Fay, R.R., MacDonald, T.J., and Sassen, R., 1984. Thermogenic gas hydrates in the Gulf of Mexico. Science, 225: 409-411.

Brown, K.M., (1990). Nature and hydrogeologic significance of mud diapirs and diatremes for accretionary systems. J Geophys Res, 95: 8969-8982.

Brown, K.M., Bekins, B., Clennell, B., Dewhurst, D., and Westbrook, G., 1994. Heterogeneous hydrofracture development and accretionary fault dynamics. Geology, 22: 259-262.

Buffet, B.A., 2000. Clathrate hydrates, annual review of earth planetary sciences. Annual Review of Earth Planetary Sciences, 28: 477-507.

Bünz, S., Mienert J., Bryn, P., and Berg, K., 2005. Fluid flow impact on slope failure from 3D seismic data: a case study in Storegga Slide. Basin Res., 17: 109-122.

Caress, D.W., and Chayes, D.N., 1996. Improved Processing of Hydrosweep Multibeam Data on the R/V Maurice Ewing. Marine Geophysical Researches, 18: 631-650.

Cavagna, S., Clari, P., and Martire, L., 1998. Methane-derived carbonates as an evidence of fossil mud volcanoes: A case history from the Cenozoic of northern Italy. Paper presented at Fifth International Conference on Gas in Marine Sediment, Shallow Gas Group, Bologna, Italy, 1998.

Cifci, G., Dondurur, D., and Ergün, M., 2003. Deep and shallow structures of large pockmarks in the Turkish shelf, Eastern Black Sea. Geo-Marine Letters, 23: 311-322.

Cifci, G., Dondurur, D., Ergün, M., 2002. Sonar and high resolution seismic studies in the Eastern Black Sea. Turkish Journal of Earth Sciences, 11(1): 61-81.

Claypool, G.E., and Kaplan, I.R., 1974. The origin and distribution of methane in marine sediments. Natural Gases in Marine Sediments. Plenum Press, New York: 99-139.

Clennell, M.B., Hovland, M., Booth, J.S., Henry, P., and Winters, W.J., 1999. Formation of natural gas hydrates in marine sediments: 1. Conceptual model of gas hydrate growth conditioned by host sediment properties. J Geophys Res, 104: 22985-23003.

Cloething, S., Spadini, G., Van Wees, J.D., and Beekman, F., 2003. Thermo-mechanical modeling of Black Sea Basin (de)formation. Sedimentary Geology, 156: 169-184.

Collett, T.S., 1998. Well log evaluation of gas hydrate saturation. Transactions of the Society of Professional Well Log Analysts, Thirty-Ninth Annual Logging Symposium, Paper MM. Washington, DC: Library of Congress.

Davies, R.J., and Stewart, S.A., 2005. Emplacement of giant mud volcanoes in the South Caspian Basin: 3D seismic reflection imaging of their root zones. Journal of the Geological Society, 162: 1-4.

De Batist, M., Klerkx, J., Van Rensbergen, P., Vanneste, M., Poort, J., Golmshtok, A.Y., Kremlev, A.A., Khlystov, O.M., and Krinitsky, P., 2002. Active hydrae destabilization in Lake Baikal, Sibiria? Terra Nova, 14(6): 436-442.

De Lange, G., and Brumsack, H.J., 1998. Pore water indications for the occurrence of gas hydrates in eastern Mediterranean mud dome structures. In: Proceedings ODP, Scientific Results, Leg 160. Ocean Drilling Program, College Station, Tex: 569-574.

Dewey, J.F., Pitman, W.C., Ryan, W.B.F., and Bonnin, J., 1973. Plate Tectonics and the Evolution of the Alpine System. Geological Society of America Bulletin, 84: 3137-3180.

Dickens, G. R., and Quinby-Hunt, M.S., 1994. "Methane hydrate stability in seawater." Geophys Res Lett 21(19): 2115-2118.

Dickens, G.R., Paull, C.K., Wallace, P., and ODP Leg 164 Scientific Party, 1997. Direct measurement of in situ methane quantities in a large gas-hydrate reservoir. Nature (London), 385(6615): 426-428.

Dillon, W.P., and Paull, C.K., 1983. Marine gas hydrates II. Geophysical evidences. In: Cox JL 8ed) Natural gas hydrates, properties, occurrence and recovery. Butterworth, Woburn, MA: 73-90.

Dillon, W.P., Lee, M.W., Fehlhaber, K., and Coleman, D.F., 1994. Gas hydrates on the Atlantic continental margin of the United States controls on concentration. In: Howell D (Ed.), US Geological Survey Professional Paper, 1570: 313-330.

Dimitrov, L.I., 2002. Mud volcanoes - the most important pathway for degassing deeply buried sediments. Earth-Science Reviews, 59: 49-76.

Dimitrov, L.I., 2003. Mud volcanoes - a significant source of atmospheric methane. Geo-Marine Letters, 23:

Domenico, S.N., 1977. Elastic properties of unconsolidated porous sand reservoirs. Geophysics, 42: 1339-1368.

Duman, M., Duman, S., Lyons, T.W., Avci, M., Izdar, E., and Demirkurt, E., 2006. Geochemistry and sedimentology of shelf and upper slope sediments of the south-central Black Sea. Marine Geology, 227: 51-65.

Ecker, C., Dvorkin, J., and Nur, A., 1998. Sediments with gas hydrates: internal structure from seismic AVO. Geophysics, 63: 1659-1669.

Egorov, V.N., Polikarpov, G.G., Guli, S.B., Artemov, Yu.G., Stokozov, N.A., and Kostova, S.K., 2003. Present-day views on the environment-forming and ecological role of the Black Sea methane gas seeps. Mar. Ecol. J., 2: 5-26 (in Russian).

Eichhubl, P., Greene, H.G., Naehr, T., and Maher, N., 2000. Structural control of fluid flow: offshore fluid seepage in the Santa Barbara Basin, California. J. Geochem. Explor., 69/70: 545-549.

Ergün, M., Dondurur, D., and Cifci, G., 2002. Acoustic evidence for shallow gas accumulations in the sediments of the eastern Black Sea. Terra Nova, 14: 313-320.

Finetti, I., Bricchi, G., Del Ben, A., Pipan, M., and Xuan, Z., 1988. Geophysical study of the Black Sea. Bolletino di Geofisica Teorica ed Applicata, 30: 197-324.

Flemings, P.B., Liu, X., and Winters, W., 2003. Critical pressure and multiphase fluid flow in Blake Ridge gas hydrates. Geology, 31: 1057-1060.

Floodgate, G.D., and Judd, A.G., 1992. The origins of shallow gas. Cont. Shelf Res., 12: 1145-1156.

Gay, A., Lopez, M., Cochonat, P., Sultan, N., Cauquil, E., and Brigaud, F., 2003. Sinuous pockmark belt as indicator of a shallow burieed turbiditic channel on the lower slope of the Congo Basin, West African Margin. In: Van Rensbergen, P., Hillis, R.R., Maltmann, A.J., and Morley, C.K. (Eds.), Subsurface Sediment Mobilization. Geological Society of London Special Publications, 216: 173-189.

Ginsburg, G.D., and Soloviev, V.A., 1994. Mud volcanoes and gas hydrates in the Caspian Sea. Bull. Geol. Soc. Denmark, 41: 95-100.

Ginsburg, G.D., and Soloviev, V.A., 1997. Methane migration within the submarine gas-hydrate stability zone under deep-water conditions. Marine Geology, 137: 49-57.

Ginsburg, G.D., Ivanov, V.L., and Soloviev, V.A., 1984. Natural gas hydrates of the World's Oceans. PGO Sevmorgeologica: 141-158 (in Russian).

Ginsburg, G.D., Kremlev, A.N., Grigor, M.N., Larkin, G.V., Pavlenkin, A.D. and Saltykova, N.A., 1990. Filtrogenic gas hydrates in the Black Sea (21st voyage of the research vessel Evpatoriya). Soviet Geol Geophys, 31: 101-152.

Ginsburg, G.D., Milkov, A.V., Cherkashov, G.A., Egorov, A.V., Vogt, P.R., and Crane, K., 1997. Gas Hydrates at the Haakon Mosby mud volcano. AGU Spr. Meet, S187.

Ginsburg, G.D., Milkov, A.V., Soloviev, V.A., Egorov, A.V. Cherkashev, G.A., Vogt, P.R., Crane, K., Lorenson, T.D., and Khutorskoy, M.D., 1999. Gas hydrate accumulation at the Haakon Mosby mud volcano. Geo-Marine Letters, 19: 57-67.

Golmshtok, A.Y., Zonenshain, L.P., Terekhov, A.A., and Shainurov, R.V., 1992. Age, thermal evolution and history of the Black Sea Basin based on heat flow and multichannel reflection data. Tectonophysics, 210: 273-293.

Golubnichaya, L.M., 1969. Oligocene and Low Miocene. In: Geology of the USSR, V. VIII. Krymea, Moscow: 224-232.

Google Earth vs. 4.0.4416 beta. 2006. http://dl.google.com/earth/GE4/GoogleEarthWin.exe.

Gorkun, V.N., and Siryk, I.M., 1968. Calculating depth of deposition and volume of gas expelled during eruptions of mud volcanoes in southern Sakhalin. Int. Geol. Rev., 10((1)): 4-12.

Gorman, A.R., Holbrook, W.S., Hornbach, M.J., Hackwith, K.L., Lizarralde, D., and Pecher, I., 2002. Migration of methane gas through the hydrate stability zone in a low-flux hydrate province. Geology, 30(4): 327-330.

Grant, J.A., and Schreiber, R., 1990. Modern Swathe Sounding and Sub-Bottom Profiling Technology for Research Applications: The Atlas Hydrosweep and Parasound Systems. Marine Geophys Researches, 12: 9-19.

Graue, K., 2000. Mud volcanoes in deepwater Nigeria. Marine and Petroleum Geology, 17: 959-974.

Greinert, J., Artemov, Y, Egorov, V., De Batist, M., and McGinnis, D, 2006. 1300-m-high rising bubbles from mud volcanoes at 2080m in the Black Sea: Hydroacoustic characteristics and temporal variability. EPSL, 244: 1-15.

Greinert, J., Bohrmann, G., and Suess, E., 2001. Methane-venting and gas hydrate-related carbonates at the Hydrate Ridge: their classification, distribution and origin. In: Paull, C.K., and Dillon, W.P. (Eds.), Natural Gas Hydrates: Occurrence, Distribution, and Detection. Geophysical Monograph, 124: 99-113.

Greinert, J., Bollwerk, S.M., Derkachev, A., Bohrmann, G., and Suess, E., 2002. Massive barite deposits and carbonate mineralization in the Derugin Basin, Seaof Okhotsk: precipitation process at cold vent sites. EPSL, 203: 165-180.

Griboulard, R., Bobier, C., Faugères, J.C., Huyghe, P., Gontier, E., Odonne, F., and Welsh, R., 1998. Recent tectonic activity in the south Barbados prism: Deep-towed side-scan sonar imagery. Tectonophysics, 284: 79-99.

Guliyev, I.S., and Feizullayev, A.A., 1997. All About Mud Volcanoes. Nafta Press, Baku.

Hedberg, H.D., 1974. Relation of methane generation to under compensated shales, shale diapirs and mud volcanoes. Am. Assoc. Pet. Geol. Bull., 58: 661-673.

Heggland, R., 1998. Gas seepage as an indicator of deeper prospective reservoirs. A study based on 3D seismic data. Marine and Petroleum Geology, 15: 1-9.

Henry, P.H., Pichon, X.L., Lallemant, S., Lance, S., Martin, J.B., Foucher, J.-P., Fiala-Medioni, A., Rostek, F., Guilhaumou, N., Pranal, V., and Castrec, M., 1996. Fluid flow in and around a mud volcano field seaward of the Barbados accretionary wedge: results from Manon Cruise. J Geophys Res, 101((B9)): 20297-20323.

Holbrook, W.S., 2001. Seismic Studies of the Blake Ridge: Implications for Hydrate Distribution, Methane Expulsion, and Free Gas Dynamics. In: Natural Gas Hydrates: Occurrences, Distribution, and Detection. Geophysical Monograph, 124: 235-256.

Holbrook, W.S., Gorman, A.R., Hornbach, M., Hackwith, K.L., Nealon, D., Lizarralde, D., and Pecher, I.A., 2002. Seismic detection of marine methane hydrate. The Leading Edge, 21(7): 686-689.

Holbrook, W.S., Hoskins, H., Wood, W.T., Stephen, R.A., and Lizarralde, D., 1996. Methane Hydrate and Free Gas on the Blake Ridge from Vertical Seismic Profiling. Science, 273: 1840-1843.

Holland, C.W., Etiope, G., Milkov, A.V., Michelozzi, E., and Favali, P., 2003. Mud volcanoes discovered offshore Sicily. Marine Geology, 199: 1-6.

Hovland, M., and Curzi, P., 1989. Gas seepage and assumed mud diapirism in the Italian Central Adriatic Sea. Marine and Petroleum Geology, 6: 161-169.

Hovland, M., and Judd, A., 1988. Seabed Pockmarks and Seepages: Impact on Geology, Biology and the Marine Environment. Graham and Trotman, London: 293 pp.

Hovland, M., Hill, A., and Stokes, D., 1997. The structure and geomorphology of the Dashgil mud volcano, Azerbaijan. Geomorphology, 21: 1-15.

Hunt, I.M., 1990. Generation and migration of petroleum from abnormally pressured fluid compartments. AAPG Bulletin, 74: 1-12.

Hunt, J., and Whelan, J., 1978. Dissolved gases in the Black Sea sediments. Initial Reports of the Deep Sea Drilling Project, 42: 661-665.

Hyndman, R.D., and Davies, E.E., 1992. A mechanism for the formation of methane hydrate and seafloor bottom simulating reflectors by vertical fluid expulsion. J Geophys Res, 97: 7025-7041.

Hyndman, R.D., and Spence, G.D., 1992. A seismic study of methane hydrate marine bottom simulating reflectors. J Geophys Res, 95, No. B5: 6683-6698.

Ivanov, M.K., Konyukhov, A.U., Kulnitskii, L.M., and Musatov, A.A., 1989. Mud volcanoes in deep part of the Black Sea. Vestnik MGU Serie de Geologia, 3: 21-31 (in Russian).

Ivanov, M.K., Limonov, A.M. and van Weering, T.C.E., 1996. Comparative characteristics of the Black Sea and Mediterranean Ridge mud volcanoes. Marine Geology, 132: 253-271.

Ivanov, M.K., Limonov, A.M. and Woodside, J.M., 1998. Extensive deep fluid flux through the sea floor on the Crimean continental margin (Black Sea). In: Henriet, J.-P. and Mienert, J. (eds) Gas Hydrates: Relevance to world margin stability and climate change. Geological Society, London, Special Publications, 137: 195-213.

Iversen, N., and Jörgensen, B.B.,, 1985. Anaerobic methane oxidation rates at the sulfate-methane transition in marine sediments from Kattegat and Skagerrak (Denmark). Limnol. Oceanogr., 30(5): 944-955.

Jakubov, A.A., Alizade, A.A., and Zeinalov, M.M., 1971. Mud volcanoes of Azerbaijan. SSR: Atlas. Elm-Azerbaijan Acad. of Sci. Pub. House, Baku (in Russian).

Jaoshvili, S., 2000. River runoff and sediment discharges into the Black Sea. IOC Workshop Report, 145: 29-38.

Judd, A., 2003. The global importance and context of methane escape from the seabed. Geo-Marine Letters, 23: 147-154.

Judd, A., Davies, G., Wilson, J., Holmes, R., Baron, G., and Bryden, J., 1997. Contributions to atmospheric methane by natural seepages on the UK continental shelf. Marine Geology, 137: 165-189.

Judd, A., Hovland, M., Dimitrov, L.I., Garcia-Gil, S., and Jukes, V., 2002. The geological budget at Continental Margins and its influence on climate change. Geofluids, 2: 109-126.

Judd, A.G., 2000. Geological source of methane. In: Atmospheric Methane: Its role in the Global Environment, edited by M.A.K. Khalili. Springer, New York: 280-303.

Katzmann, R., Holbrook., W.S., and Paull, C.K., 1994. A combined vertical -incidence and wide-angle seismic study of a gas hydrate zone, Blake Ridge. Journal of Geophysical Research, 99: 17975-17995.

Kenyon, N.H., Ivanov, M.K., Akhmetzhanov, A.M., Akhmanov, G.G., 2002. Geological Processes in the Mediterranean and Black Seas and North East Atlantic. Preliminary results of investigations during the TTR-11 cruise of RV Professor Logachev. Intergovernmental Oceanographic Commission technical series, 62: 89pp.

Kessler, J.D., Reeburgh, W.S., Southon, J., Seifert, R., Michaelis, W., and Tyler, S.C., 2006. Basin-wide estimates of the input of methane from seeps and clathrates to the Black Sea. EPSL, 243: 366-375.

Kholodov, V.N., 1983. Post-sedimentation Transformations in Elisional Basins (on example of the East Near Caucasus) (in Russian). Nauka, Moscow, 152.

Klaucke, I., Sahling, H., Bürk, D., Weinrebe, W., and Bohrmann, G., 2005. Mapping Deep-Water Gas Emissions With Sidescan Sonar. EOS, 86(38): 341-343.

Klaucke, I., Sahling, H., Weinrebe, W., Blinova, V., Bürk, D., Lursmanashvili, N., and Bohrmann, G, 2006. Acoustic investigation of cold seeps offshore Georgia, eastern Black Sea. Marine Geology, 231: 51-67.

Kohl, B., and Roberts, H.H., 1994. Fossil foraminifera from four active mud volcanoes in the Gulf of Mexico. Geo-Marine Letters, 14: 126-134.

Kopf, A., and Behrmann., J.H., 2000. Extrusion dynamics of mud volcanoes on the Mediterranean Ridge accretionary complex. In: from the Arctic to the Mediterranean: Salt, Shale, and Igneous Diapirs in and around Europe, edited by B. Vendeville, Y. Mart, and J.-L. Vigneresse, Geol. Soc. Spec. Publ., 174: 169-204.

Kopf, A.J., 2002. Significance of mud volcanism. Reviews of Geophysics, 40: 1-52.

Krastel, S., Spiess, V., Ivanov, M.K., Weinrebe, W., Bohrmann, G. and Shashkin, P., 2003. Acoustic images of mud volcanoes in the Sorokin Trough, Black Sea. Geo-Marine Letters, 23: 230-238.

Kruglyakova, R., Gubanov, Y, Kruglyakov, G., and Prokoptsev, G., 2002. Assessment of technogenic and natural hydrocarbon supply into the Black Sea and seabed sediments. Cont. Shelf Res., 22: 2395-2407.

Kruglyakova, R.P., Byakov, Y.A., Kruglyakova, M.V., Chalenko, L.A., and Shevtsova, N.T., 2004. Natural oil and gas seeps on the Black Sea floor. Geo-Marine Letters, 24: 150-162.

Kruglyakova, R.P., Prokoptzev, G.P., and Berlizeva, N.N., 1993. Gas-hydrates in the Black Sea as potential hydrocarbon source. Razvedka I Ohrana Nedr, 12: 7-19 (in Russian).

Kutas, R.I., Kobolev, V.P., and Tsvyashchenko, V.A., 1998. Heat flow and geothermal model of the Black Sea depression. Tectonophysics, 291: 91-100.

Kvenvolden, K.A., 1988. Methane hydrate - A major reservoir of carbon in the shallow geosphere? Chemical Geology, 71: 41-51.

Kvenvolden, K.A., 1993. Gas Hydrates - Geological Perspective and Global Change. Reviews of Geophysics, 31: 173-187.

Kvenvolden, K.A., and Barnard, L.A., 1983. Gas hydrates of the Blake Outer Ridge, Site 533, Deep Sea Drilling Project Leg 76. Initial Reports of the Deep Sea Drilling Project, 76: 353-365.

Kvenvolden, K.A., and Lorenson, T.D., 2001. The Global Occurrence of Natural Gas Hydrate. Geophysical Monograph, 124: 3-16.

Kvenvolden, K.A., and McDonald, T.J., 1985. Gas hydrates of the Middle America Trench. Deep Sea Drilling Project Leg 84. Initial Reports of the Deep Sea Drilling Project, 84: 667-682.

Kvenvolden, K.A., Reeburgh, W.S., and Lorenson, T.D., 2001. Naturally occurring methane seepage as a factor in global climate change. paper presented at USGS Workshop, U.S. Geol. Soc., Portland, Oregon.

Kvenvolden, K.A., and Rogers, B.W., 2005. Gaia's breath - global methane exhalations. Marine and Petroleum Geology, 22: 579-590.

Lebedinsky, V.I., 1969. Crymean Magmatism. In: Geology of the USSR, V. VIII. Krymea, Moscow(301-340).

Lee, M.W., and Dillon, W.P., 2001. Amplitude blanking related to the pore-filling of gas hydrates in sediments. Marine Geophys Researches, 22: 101-109.

Lee, M.W., Hutchinson, W.F., Agena, W.F., Dillon, W.P., Miller, J.J., and Swift, B.A., 1994. Seismic character of gas hydrates on the south-eastern US continental margin. Marine Geophysical Researches, 16: 163-184.

Leifer, I., and Patro, R.K., 2002. A bubble mechanism for methane transport from the shallow seabed to the surface: a review and sensitivity study. Cont. Shelf Res., 22: 2409-2428.

Lelieveld, J., Crutzen, P.J., and Brühl, C., 1993. Climate effects of atmospheric methane. Chemosphere, 26: 739-768.

Lelieveld, J., Crutzen, P.J., and Dentener, F.J., 1998. Changing concentration, lifetime and climate forcing of atmospheric methane. Tellus, Ser. B, 50: 128-150.

Lerche, I., 2000. Estimates of worldwide gas hydrate resource. Energy Exploration & Exploitation, 18: 329-337.

Ligtenberg, J.H., 2005. Detection of fluid migration pathways in seismic data: implications for fault seal analysis. Basin Res., 17: 141-153.

Limonov, A.F., van Weering, Tj.C.E., Kenyon, N.H., Ivanov, M.K., and Meisner, L.B., 1997. Seabed morphology and gas venting in the Black Sea mud volcano area: Observation with the MAK-1 deep-tow side scan sonar and bottom profiler. Marine Geology, 137: 121-136.

Limonov, A.F., Woodside, J.M., and Ivanov, M.K. (Eds.), 1994. Mud volcanism in the Mediterranean and Black Seas and shallow structure of the Eratostenes Seamount. Initial results of the geological and geophysical investigations during the third UNESCO-ESF 'Training Through Research' Cruise of RV Gelendzhik, June-July 1993. UNESCO Rep. Mar. Sci., 64. 173 pp.

Luff, R., Wallmann, K., and Aloisi, G., 2004. Numerical modeling of carbonate crust formation at cold vent sites: significance for fluid and methane budgets and chemosynthetic biological communities. EPSL, 221: 337-353.

Luo, X., and Vasseur, G., 2002. Natural hydraulic cracking: Numerical model and sensitivity study. EPSL, 201: 431-446.

MacDonald, G.T., 1990. Role of methane clathrates in past and future climates. Clim. Change, 16: 247-281.

MacDonald, I.R., Guinasso, Jr. N.L., Sassen, R., Brooks, J.M., Lee, L., and Scott, K.T., 1994. Gas hydrate that breaches the seafloor on the continental slope of the Gulf of Mexico. Geology, 22: 699-702.

Makogon, Y.F., 1997. Hydrates of Hydrocarbons. PennWell, Tulsa, Oklahoma: 482 pp.

Manheim, F.T., and Chan, K.M., 1974. Interstitial waters of Black Sea sediments: New data and review. In: The Black Sea - Geology, Chemistry and Biology, Vol. 20 (ed. Degens, E.T., Ross, D.A.): 155-180.

Masson, D.G., and Berndt, C., 2006. 3D acquisition over mud volcanoes in the Gulf of Cádiz and submarine landslides in the Eivissa Channel, western Mediterranean Sea. National Oceanography Centre, Southampton, Cruise Report No. 3. RRS Charles Darwin Cruise 178: 39 pp.

Mathews, M.A., and von Huene, R., 1985. Site 570 methane hydrate zone. Initial Reports of the Deep Sea Drilling Project, 84: 773-790.

Max, M.D., 1990. Gas hydrate and acoustically laminated sediments: probable environmental cause of anomalously low acoustic-interaction bottom loss in deep ocean sediments. Naval Research Laboratory report, 9235: 68pp.

Max, M.D., 2000. Natural Gas Hydrate: In Oceanic and Permafrost environments. Kluwer Academic Publishers, London, Boston, Dordrecht: 414.

Mazzini, A., Ivanov, M.K., Parnell, J., Stadnitskaya, A., Cronin, B.T., Poludetkina, E., Mazurenko, L., and van Weering, T.C.E., 2004. Methane-related authigenic carbonates from the Black Sea: geochemical characterisation and relation to seeping fluids. Marine Geology, 212: 153-181.

McCaffrey, B., and Kneller, B., 1998. Mechanics of submarine debris flow initiation. Geoscience, Abstracts Volume, 98: 9.

Meisner, L.B., Tugolesov, D.A., and Khakhalev, E.M., 1996. Western Black Sea Mud Volcano Province (in Russian). Okeanologia, 36(N1): 119-127.

Michaelis, W., Seifert, R., Nauhaus, K., Treude, T., Thiel, V., Blumenberg, M., Knittel, K., Gieseke, A., Peterknecht, K., Pape, T., Boetius, A., Amann, R., Jörgensen, B.B., Widdel, F., Peckmann, J., Pimenov, N.V., and Guli, M.B., 2002. Microbial reefs in the Black Sea fuelled by anaerobic oxidation of methane. Science, 297: 1013-1015.

Milkov, A.V., 1998. Gas hydrates of the Haakon Mosby mud volcano. M.Sc. thesis, St. Petersburg State University, St. Petersburg (in Russian).

Milkov, A.V., 2000. Worldwide distribution of submarine mud volcanoes and associated gas hydrates. Marine Geology, 167: 29-42.

Milkov, A.V., Claypool, G.E., Lee, Y.-J., Xu, W., Dickens, G.R., Borowski, W.S, and the ODP Scientific Party, 2003b. In situ methane concentrations at Hydrate Ridge, offshore Oregon: New constraints on the global gas hydrate inventory from an active margin. Geology, 31(10): 833-836.

Milkov, A.V., Dickens, G.R., Claypool, G.E., Lee, Y.-J., Borowski, W.S., Torres, M.E., Xu, W., Tomaru, H., Tréhu, A.M., and Schultheiss, P., 2004. Co-existence of gas hydrate, free gas, and brine within the regional gas hydrate stability zone at Hydrate Ridge (Oregon margin): evidence from prolonged degassing of a pressurized core. EPSL, 222: 829-843.

Milkov, a.V., Sassen, R., Apanasovich, T.V., and Dadashev, F.G., 2003a. Global gas flux from mud volcanoes: A significant source of fossil methane in the atmosphere and the ocean. Geophysical Research Letters, 30(2): 1037. doi:10.1029/2002GL016358.

Miller, J.J., Lee, M.W., and von Huene, R., 1991. An analysis of a seismic reflection from the base of a gas hydrate zone, offshore Peru. AAPG Bulletin, 75: 910-924.

Minshull, T., and White, R.S., 1989. Sediment compaction and fluid migration in the Makran accretionary prism. J Geophys Res, 94: 7387-7402.

Minshull, T.A., Singh, S.C., and Westerbrook, G.K., 1994. Seismic velocity structure at a gas hydrate reflector, offshore western Colombia, from full waveform inversion. Journal of Geophysical Research, 99: 4715-4734.

Moore, J.C., Brown, K.M., Horath, F., Cochrane, G., MacKay, M., and Moore, G., 1991. plumbing accretionary prisms. In: Tarney, J., Pickering, K.T., Knipe, R.J., and Dewey, J.F. (Eds.). The Behavior and Influence of Fluids in Subduction Zones. The Royal Society, London: 49-62.

Moore, J.C., Orange, D., Kulm, L.D., 1990. Interrelationship of fluid venting and structural evolution: Alvin observations from the frontal accretionary prism, Oregon. J Geophys Res, 95: 8795-8808.

Motyka, R.J., Poreda, R.J., and Jeffrey, A.W.A., 1989. Geochemistry, isotopic composition, and origin of fluids emanating from mud volcanoes in the Copper River basin Alaska. Geochim. Cosmochim. Acta, 53: 29-41.

Murray, J.W., Top, Z., and Özsoy, E., 1991. Hydrographic properties and ventilation of the Black Sea. Deep-Sea Res., 38 (Suppl. 2): 663-689.

Naudts, L., Greinert, J., Artemov, Y., Staelens, P., Poort, J., Van Rensbergen, P., and De Batist, M., 2006. Geological and morphological setting of 2778 methane seeps in the Dnepr paleo-delta, northwestern Black Sea. Marine Geology, 227: 177-199.

Nikishin, A.M., Korotaev, M.V., Ershov, A.V., and Brunet, M.-F., 2003. The Black Sea basin: tectonic history and Neogene-Quaternary rapid subsidence modeling. Sedimentary Geology, 156: 149-168.

Okay, A.I., Celal Sengor, A.M., and Görür, N., 1994. Kinematic history of the opening of the Black Sea and its effect on the surrounding regions. Geology, 22: 267-270.

Orange, D.L., and Breen, N.A., 1992. The effects of fluid escape on accretionary wedges: 2. Seepage force, slope failure, headless submarine canyons, and vents. J Geophys Res, 97: 9277-9295.

Orange, D.L., Yun, J.W., Maher, N., Barry, J., and Green, G., 2002. Tracking California seafloor seeps with bathymetry, backscatter and ROV's. Cont. Shelf Res., 22: 2273-2290.

Pascoe, E.H., 1912. The oilfields of Burma. Mem. Geol. Surv. India, 40((1)).

Paull, C.K., Matsumoto, R., Wallace, P. et al., 1996. Proc Ocean Drilling Program, Initial Reports 164. Ocean Drilling Program, College Station, TX: 623 pp.

Paull, C.K., Usller, W., and Borowski, E.S., 1994. Sources of biogenic methane to form marine gas hydrates. In: Sloan, E.D., Happel, J., and Hnatow, M.A. (eds.), International Conference on Natural Gas Hydrates. Ann. N.Y. Acad. Sci., 715: 392-409.

Pecher, I.A., Minshull, T.A., Singh, S.C., and von Huene, R., 1996. Velocity structure of a bottom simulating reflector offshore Peru: Results from full waveform inversion. EPSL, 139: 459-469.

Peckmann, J., Reimer, A., Luth, U., Luth, C., Hansen, B.T., Heinicke, C., Hoefs, J., and Reitner, J., 2001. Methane-derived carbonates and authigenic pyrite from the northwestern Black Sea. Marine Geology, 177: 129-150.

Perez-Belzuz, F.B., Alonso, B., and Ercilla, G., 1997. History of mud diapirism and trigger mechanisms in the western Alboran Sea. Tectonophysics, 282: 399-422.

Rangin, C., Bader, A.G., Pascal, G., Ecevitoglu, B., and Görür, N., 2002. Deep structure of the Mid Black Sea High (offshore Turkey) imaged by multi-channel seismic survey (BLACKSIS cruise). Marine Geology, 182: 265-278.

Reeburgh, W.S., Ward, B.S., Whalen, S.C., Sandbeck, K.A., Kilpatrick, K.A., and Kerkhof, L.J., 1991. Black Sea methane geochemistry. Deep-Sea Res., 38: S1189-S1210.

Reeburgh, W.S., Whalen, S.C., and Alperin, A.J., 1993. The role of methylotrophy in the global methane budget. In: Murrel, J.A., Kelly, D.P. (Eds.), Microbial Growth on C-1 Compounds. Intercept, Andover, UK: 1-14.

Reed, D.L., Silver, E.A., Tagudin, J.E., Shipley, T.H., and Vrolijk, P., 1990. Relations between mud volcanoes, thrust deformation, slope sedimentation and gas hydrate, offshore north Panama. Marine and Petroleum Geology, 7: 44-54.

Rehder, G., Brewer, P.W., Peltzer, E.T., and Friedrich, G., 2002. Enhanced lifetime of methane bubble streams within the deep ocean. Geophys Res Lett, 29: 21-24.

Riedel, M., Collett, T.S., Malone, M.J., and the Expedition 311 Scientists, 2006. Proc. IODP, 311: Washington, DC (Integrated Ocean Drilling Program Management International, Inc.). doi:10.2204/iodp.proc.311.2006.

Roberts, S., and Nunn, J.A., 1995. Episodic fluid expulsion from geopressured sediments. Marine and Petroleum Geology, 12: 195-204.

Robinson, A.G., 1997. Introduction: Tectonic Elements of the Black Sea Region. In: Robinson, A.G. (ed) Regional and petroleum geology of the Black Sea and surrounding region: AAPG Memoir, 68: 1-6.

Robinson, A.G., Griffith, E.T., Gardiner, A.R. and Home, A.K., 1997. Petroleum Geology of the Georgian fold and thrust belts and foreland basins. In: Robinson, A.G. (ed) Regional and petroleum geology of the Black Sea and surrounding region: AAPG Memoir, 68: 347-367.

Robinson, A.G., Rudat, J.H., Banks, C.J. and Wiles, R.L.F., 1996. Petroleum Geology of the Black Sea. Marine and Petroleum Geology, 13(No. 2): 195-223.

Robinson, A.G., Spadini, G., Cloetingh S., and Rudat, J., 1995. Stratigraphic evolution of the Black Sea: inferences from basin modelling. Marine and Petroleum Geology, 12(8): 821-835.

Ross, D.A., and Degens, E.T., 1974. Recent sediments of the Black Sea. In: Degens, E.T., Ross, D.A. (Eds.), The Black Sea - Geology, Chemistry and Biology. AAPG Memoir, 20. AAPG, Tulsa: 183-199.

Ross, D.A., Uchupi, E., Prada, K.E., and MacIlvaine, J.C., 1974. Bathymetry and Microtopography of Black Sea. In: Degens, E.T., Ross, D.A. (Eds.), The Black Sea - Geology, Chemistry and Biology. AAPG Memoir, 20. AAPG, Tulsa: 1-10.

Sager, W.W., MacDonald, I.R., and Rousheng, H., 2003. Geophysical signatures of mud mounds at hydrocarbon seeps on Louisiana continental slope, northern Gulf of Mexico. Marine Geology, 198: 97-132.

Sain, K., Minshull, T.A., Singh, S.C., and Hobbs, R.W., 2000. Evidence for thick free gas layer beneath the bottom simulating reflector in the Macran accretionary prism. Marine Geology, 164: 3-12.

Sassen, R., Losh, S., Cathles, L., Roberts. H., Whelan, J.K., Milkov, A.V., Sweet, S.T., and De Freitas, D.A., 2001. Massive vein-filling gas hydrate: Relation to ongoing gas migration from the deep subsurface Gulf of Mexico. Marine and Petroleum Geology, 18: 551-560.

Schmale, O., Greinert, J., and Rehder, G., 2005. Methane emission from high-intensity marine gas seeps in the Black Sea into the atmosphere. Geophysical Research Letters, 32(L07609): doi: 10.1029/2004GL021138.

Schmuck, E.A., and Paull, C.K., 1993. Evidence for gas accumulation associated with diapirism and gas hydrates at the head of the Cape Fear Slide. Geo-Marine Letters, 13: 145-152.

Schoell, M., 1988. Multiple origins of methane in the Earth. Chemical Geology, 71: 1-10.

Shipley, T., Houston, M., and Buffer, R., 1979. Seismic reflection evidence for the widespread occurrence of possible gas hydrate horizons on continental slopes and rises. AAPG Bulletin, 63: 2204-2213.

Shnukov, E.F., Sobolevskiy, Y.V., and Kutniy, V.A., 1995. Unusual carbonate buildups at continental slope of the north-western Black Sea: an apparent consequence of the degassing of sediments. Lithology and Minerals, 5: 461-541.

Sibuet, M., and Olu, K., 1998. Biogeography, biodiversity and fluid dependence of deep-sea cold-seep communities at active and passive margins. Deep-Sea Research II, 45: 517-567.

Singh, S.C., Minshull, T.A., and Spence, G.D., 1993. Velocity structure of a gas hydrate reflector. Science, 260: 204-207.

Sloan, E.D., 1990. Clathrate Hydrates of natural gas. Marcel Deker, New York: 641 pp.

Sloan, E.D., 1998. Physical/chemical properties of gas hydrates and applications to world margin stability and climatic change. In: Henriet, J.-P. and Mienert, J. (eds) Gas Hydrates: Relevance to world margin stability and climate change. Geological Society, London, Special Publications, 137: 31-50.

Spadini, G., Robinson, A. and Cloetingh, S., 1996. Western versus Eastern Black Sea tectonic evolution: pre-rift lithospheric controls on basin formation. Tectonophysics, 266: 139-154.

Spiess, V., 1993. Digitale Sedimentechographie - Neue Wege zu einer hochauflösenden Akustostratigraphie. Berichte Fachbereich Geowissenschaften. Universität Bremen, 35: 1-199.

Stadnitskaya, A.N., 1997. Distribution and Composition of Hydrocarbon Gas in the Seabed Sediments of the Sorokin Trough (South-Eastern Part of the Crimean Margin). In: Gas and Fluids in Marine Sediments: gas hydrates, mud volcanoes, tectonics, sedimentology and geochemistry in Mediterranean and Black Seas. Fifth Post-Cruise Meeting of the Training Through Research Program and International Congress Amsterdam, The Netherlands. 27-29 January 1997. IOC Workshop Report, 129: 10.

Stamatakis, M.G., Baltatzis, E.G., and Skounakis, S.B., 1987. Sulfate minerals from a mud volcano in the Katakolo area, western Peloponnesus, Greece. Am. Mineral., 72: 839-841.

Starostenko, V., Buryanov, I., Makarenko, I., Rusakov, O., Stephenson, R. Nikishin, A., Georgiev, G., Gerasimov, M., Dimitriu, R., Legostaeva, O., Pchelarov, V., and Sava, C., 2004. Topography of the crust-mantle boundary beneath the Black sea Basin. Tectonophysics, 381: 211-233.

Stoll, R.D., Ewing, J., and Bryan, G.M., 1971. Anomalous velocities in sediments containing gas hydrates. Journal of Geophysical Research, 76: 2090-2094.

Stow, D. A. V., and Myall, M., 2000. Deep-water sedimentary systems: New models for the 21st Century. Marine and Petroleum Geology, 17: 125-135.

Sturz, A.A., Kamps, R.L., and Earley, P.J., 1992. Temporal changes in mud volcanoes, Salton Sea geothermal area. In: Water-Rock Interactions, edited by Kharaka, Y.K., and Maest, A.S.. Balkema, Brookfield, Vt., 2: 1363-1366.

Suess, E., Carson, B., Ritger, S.D., Morre, J.C., Jones, M.L., Kulm, L.D., and Cochrane, G.R., 1985. Biological communities at vent sites along the subduction zone off Oregon. Biol. SOc. Wash. Bull., 6: 475-484.

Suess, E., Torres, M., Bohrmann, G., Collier, R.W., Greinert, J., Linke, P., Rehder, G., Trehu, A., Wallmann, K., Winckler, G., and Zuleger, E., 1999. Gs hydrate destabilization: enhanced dewatering, benthic material turnover and large methane plumes at the Cascadia convergent margin. EPSL, 170: 1-15.

Suess, E., Torres, M.E., Bohrmann, G., Collier, R.W., Ricken, D., Goldfinger, C., Linke, P., Heuser, A., Sahling, H., Heeschen, K., Jung, C., Nakamura, K., Greinert, J., Pfannkuche, O., Tréhu, A., Klinkhammer, G., Whiticar, M.J., Eisenhauer, A., Teichert, B., and Elvert, M., 2001. Seafloor methane hydrates at Hydrate Ridge, Cascadia Margin. In: Paull, C.K., and Dillon, W.P. (Eds.), Natural Gas Hydrates: Occurrence, Distribution, and Detection. Geophysical Monograph, 124: 87-98.

Taylor, M.H., Dillon, W.P., and Pecher, I.A., 2000. Trapping and migration of methane associated with the gas hydrate stability zone at the Blake Ridge Diapir: new insights from seismic data. Marine Geology, 164: 79-89.

Topham, D.R., 1984. The formation of gas hydrates on bubbles of hydrocarbon gases rising in seawater. Chem. Eng. Sci., 39: 821-828.

Torres, M.E., Wallmann, K., Tréhu, A.M., Bohrmann, G., Borowski, W.S., and Tomaru, H., 2004. Gas hydrate growth, methane transport, and chloride enrichment at the southern summit of Hydrate Ridge, Cascadia margin off Oregon. EPSL, 226: 225-241.

Tréhu, A.M., Bohrmann, G., Rack, F.R., Torres, M.E. et al., 2003. Proc. ODP, Init. Repts., 204. College Station, TX (Ocean Drilling Program): doi: 10.2973/odp.proc.ir.204.2003.

Tréhu, A.M., Flemings, P.B., Bangs, N.L., Chevallier, J., Gràcia, E., Johnson, J.E., Liu, C.-S., Liu, X., Riedel, M., and Torres, M.E., 2004b. Feeding methane vents and gas hydrate deposits at sout Hydrate Ridge. Geophys Res Lett, 31(L23310): doi:10.1029/2004GL021286.

Tréhu, A.M., Long, P.E., Torres, M. E., Bohrmann, G., Rack, F.R., Collett, T.S., Goldberg, D.S., Milkov, A.V., Riedel, M., Schultheiss, P., Bangs, N.L., Barr, S.R., Borowski, W.S., Claypool, G.E., Delwiche, M.E., Dickens, G.R., Gracia, E., Guerin, G., Holland, M., Johnson, J.E., Lee, Y.-J., Liu, C.-S., Su, X., Teichert, B., Tomaru, H., Vanneste, M., Watanabe, M., and Weinberger, J.L., 2004a. Three-dimensional distribution of gas hydrate beneath southern Hydrate Ridge: constraints from ODP Leg 204. EPSL, 222: 845-862.

Tréhu, A.M., Torres, M.E., Bohrmann, G., Colwell, F.S., 2006. Leg 204 Synthesis: Gas hydrate distribution and dynamics in the Central Cascadia Accretionary Complex. In: Tréhu, A.M., Bohrmann, G., Torres, M.E., and Colwell, F.S. (Eds.): Proceedings of the Ocean Drilling Program, Scientific Results, 204: College Station, TX (Ocean Drilling Program): 1-40.

Tugolesov, D.A., Gorshkov, A.S., Meisner, L.B., Soloviev, V. and Khakhalev, E.M., 1985. Tectonics of the Mesozoic-Cenozoic deposits of the Black Sea (in Russian). Nedra, Moscow.

Ussler, W., and Paull, C:K., 2001. Ion exclusion associated with marine gas hydrate deposits. In: Paull, C.K., and Dillon, W.P. (Eds.), Natural Gas Hydrates: Occurrence, Distribution, and Detection. Geophysical Monograph, 124: 41-51.

Van Rensbergen, P., De Batist, M., Klerkx, J., Hus, R., Poort, J., Vanneste, M., Granin, N., Khlystov, O., and Krinitsky, P., 2002. Sublacrustine mud volcanoes and methane seeps caused by dissociation of gas hydrates in Lake Baikal. Geology, 30: 631-634.

Van Rensbergen, P., Morley, C.K., Ang, D.W., Hoan, T.Q., and Lam, N.T., 1999. Structural evolution of shale diapirs from reactive rise to mud volcanism: 3D seismic data from the Baram delta, offshore Brunei Darussalam. Journal of the Geological Society, London, 156: 633-650.

Volkonskaya, A., 1997. Geological Features of the Paleo- Don/Kuban Deep-Sea Fan according to the results of the seismic study on the Pallas Uplift (north-eastern Black Sea). In: Gas and Fluids in Marine Sediments: gas hydrates, mud volcanoes, tectonics, sedimentology and geochemistry in Mediterranean and Black Seas. Fifth Post-Cruise Meeting of the Training Through Research Program and International Congress Amsterdam, The Netherlands. 27-29 January 1997. IOC Workshop Report, 129: 5.

von Huene, R., and Pecher, I.A., 1999. Neotectonics and the origins of BSRs along the Peru margin. EPSL, 166: 47-55.

Wagner-Friedrichs, M., Krastel S., Spiess, V., Ivanov, M., Bohrmann, G., and Meisner, L., in review. 3D seismic investigation of the Sevastopol mud volcano in correlation to gas/fluid migration pathways and gas hydrate occurrences in the Sorokin Trough (Black Sea).

Wallmann, K., Drews, M., Aloisi, G., and Bohrmann, G., 2006. Methane discharge into the Black Sea and the global ocean via fluid flow through submarine mud volcanoes. EPSL, 248: 545-560.

Wessel, P., and Smith, W.H.F., 1998. New, improved version of the Generic Mapping Tools Released. EOS, Transactions, AGU, 79: 579.

Wever, T.F., Abegg, F., Fiedler, H.M., Fechner, G., and Stender, I.H., 1998. Shallow gas in the muddy sediments of Eckernförde Bay, Germany. Cont. Shelf Res., 18: 1715-1739.

White, R.S., 1979. Gas hydrate layer trapping free gas in Gulf of Oman. EPSL, 42: 114-120.

Wilson, R.D., Monaghan, P.H., Osanik, A., Price, L.C., and Rogers, M.A., 1974. Natural marine oil seepage. Science, 184(4139): 857-865.

Wood, W.T., Gettrust, J.F., Chapman, N.R., Spence, G.D., and Hyndman, R.D:, 2002. Decreased stability of methane hydrates in marine sediments owing to phase boundary roughness. Nature, 420: 656-659.

Woodside, J.M., Ivanov, M.K., and Limonov, A.F., 1997. Neotectonics and fluid flow through seafloor sediments in the Eastern Mediterranean and Black Seas. Parts I and II. UNESCO IOC Tech Ser, no 48: 224 pp.

Woodside, J.M., Ivanov, M.K., Limonov, A.F., and Shipboard Scientists of the Anaxiprobe Expiditions, 1998. Shallow gas and gas hydrates in the Anaximander Mountains regions, eastern Mediterranean Sea. In: Henriet, J.-P. and Mienert, J. (eds) Gas Hydrates: Relevance to world margin stability and climate change. Geological Society, London, Special Publications, 137: 177-193.

www.ifm-geomar.de/index.php?id=gh_struktur&L=0

Yamano, M., Uyeda, S., Aoki, Y., and Shipley, T.H., 1982. Estimates of heat flow derived from gas hydrates. Geology, 10: 339-343.

Yassir, N.A., 1989. Mud volcanoes and the behaviour of overpressured clays and silts. Ph.D. thesis. Univ. Coll. London, London, UK: 249 pp.

Yefremova, A.G., and Zhizhchenko, B.P., 1974. Occurrence of crystalline hydrates from gases in precipitates of present-day oceanic regions (in Russian). Dokl Akad Nauk SSSR, 214: 1179-1181.

Yun, J.W., Orange, D.L., and Field, M.E., 1999. Subsurface gas offshore of northern California and its link to submarine geomorphology. Marine Geology, 154: 357-368.

Yusifov, M., and Rabinowitz, P.D., 2004. Classification of mud volcanoes in the South Caspian Basin, offshore Azerbaijan. Marine and Petroleum Geology, 21: 965-975.

Zaridze, G.V., and Tatrishvili, N.F., 1964. Intrusions. In: Geology of the USSR, v. X. Georgian SSR, Moscow(353-386).

Zonenshain, L.P., and Le Pichon, X., 1986. eep Basins of the Black Sea and Caspian Sea as Remnants of Mesozoic back-arc basins. Tectonophysics, 123: 181-211.

Zühlsdorff, L., 1999. High resolution multi-frequency surveys at the eastern Juan de Fuca Ridge flank and Cascadia Margin - Evidence from thermally and tectonically driven upflow in marine sediments. Berichte Fachbereich Geowissenschaften. Universität Bremen: pp. 118.

Zühlsdorff, L., and Spieß, V., 2004. Three-dimensional seismic characterization of a venting site reveals compelling indications of natural hydraulic fracturing. Geology, 32: 101-104.

General acknowledgements

I am very thankful to Prof. Dr. Volkhard Spieß for giving me the opportunity to work on this PhD study, for his support and helpful ideas, and for being the advisor to this thesis. I would also like to thank Prof. Dr. Gerhard Bohrmann for accepting to be the secondary referee to this work and for supporting this research with helpful suggestions and comments. The research was funded by the DFG (Deutsche Forschungsgemeinschaft (Kr2222/4)).

I am very grateful to Dr. Sebastian Krastel-Gudegast who contributed greatly to the success of this work with supportive tips and ideas for the manuscripts, as well as helpful discussions about data. I am also very thankful to him for pre-reading my thesis, which was quite a great effort, especially during the last weeks.

Many thanks go to Leonid Meisner from the SSC “Yuzhmorgeologia” of Gelendzhik (Russia) for constructive and successful cooperation on the first manuscript. Thanks for enabling the combination of the high resolution and the deep seismic data to realize this manuscript. I thank Leonid for detailed insights into the geology of the Black Sea and discussions on the data of the first manuscript when he stayed 4 weeks in Bremen in 2004.

I wish to thank all colleagues from the working group MTU (AG Spieß) for the nice and cooperative atmosphere. I am especially thankful to Lars Zühlsdorff for assistance on the 3D seismic processing and his helpful comments and answers on all questions about 3D seismic methods for the second manuscript. Thanks to Elvan Bulgay for processing of the multichannel data for the third manuscript. Many thanks go to Feliz Demirel-Schlüter for pleasant coffee breaks and also many thanks to my room mate Noémi Fekete for kindly working days, and especially for the encouragements during the evenings of the last weeks.

I thank Ingo Klaucke from the Leibniz Institute of Marine Sciences for giving access to the bathymetric grid off Batumi, which I used for imaging and interpretation in the third manuscript. The maps in this work were created by using the public domain software Generic Mapping Tools (GMT). Seismic processing was applied by using the VISTA software (Seismic Image Software Ltd.). Seismic data was interpreted by using the software package Kingdom Suite (Seismic Micro Technology, Inc.).

I am grateful to my parents for support of many kinds during all the years of my life, and I would also like to thank my friends.

Finally, my very special thanks go to my husband, Oliver, for his mental and technical support during my whole PhD work, for his patience and sympathy, for the loneliness he tolerated during times of being grass widower when I have been on cruise or conference, and last but not least for controlling the reference list of my thesis.